Interference Management in Wireless Cellular Networks

Harald Burchardt

A thesis submitted for the degree of Doctor of Philosophy.
The University of Edinburgh.
May 6, 2013

Abstract

In wireless networks, there is an ever-increasing demand for higher system throughputs, along with growing expectation for all users to be available to multimedia and Internet services. This is especially difficult to maintain at the cell-edge. Therefore, a key challenge for future orthogonal frequency division multiple access (OFDMA)-based networks is inter-cell interference coordination (ICIC). With full frequency reuse, small inter-site distances (ISDs), and heterogeneous architectures, coping with co-channel interference (CCI) in such networks has become paramount. Further, the needs for more energy efficient, or "green," technologies is growing.

In this light, Uplink Interference Protection (ULIP), a technique to combat CCI via power reduction, is investigated. By reducing the transmit power on a subset of resource blocks (RBs), the uplink interference to neighbouring cells can be controlled. Utilisation of existing reference signals limits additional signalling. Furthermore, cell-edge performance can be significantly improved through a priority class scheduler, enhancing the throughput fairness of the system. Finally, analytic derivations reveal ULIP guarantees enhanced energy efficiency for all mobile stations (MSs), with the added benefit that overall system throughput gains are also achievable.

Following this, a novel scheduler that enhances both network spectral and energy efficiency is proposed. In order to facilitate the application of Pareto optimal power control (POPC) in cellular networks, a simple feasibility condition based on path gains and signal-to-noise-plus-interference ratio (SINR) targets is derived. Power Control Scheduling (PCS) maximises the number of concurrently transmitting MSs and minimises their transmit powers. In addition, cell/link removal is extended to OFDMA operation. Subsequently, an SINR variation technique, Power SINR Scheduling (PSS), is employed in femto-cell networks where full bandwidth users prohibit orthogonal resource allocation. Extensive simulation results show substantial gains in system throughput and energy efficiency over conventional power control schemes.

Finally, the evolution of future systems to heterogeneous networks (HetNets), and the consequently enhanced network management difficulties necessitate the need for a distributed and autonomous ICIC approach. Using a fuzzy logic system, locally available information is utilised to allocate time-frequency resources and transmit powers such that requested rates are satisfied. An empirical investigation indicates close-to-optimal system performance at significantly reduced complexity (and signalling). Additionally, base station (BS) reference signals are appropriated to provide autonomous cell association amongst multiple co-located BSs. Detailed analytical signal modelling of the femto-cell and macro/pico-cell layouts reveal high correlation to experimentally gathered statistics. Further, superior performance to benchmarks in terms of system throughput, energy efficiency, availability and fairness indicate enormous potential for future wireless networks.

Declaration of originality

I hereby declare that the research recorded in this thesis and the thesis itself was composed and originated entirely by myself in the Department of Electronics and Electrical Engineering at The University of Edinburgh.

The exceptions to the above are as follows:

- The MATLAB code used as a basis for the simulation setup in Chapter 4 was developed by Zubin Bharucha in his PhD thesis [1], "*Ad Hoc* Wireless Networks with Femto-Cell Deployment: A Study."

Harald Burchardt

Acknowledgements

First of all, I would like to extend my undying gratitude to my family, who have always supported me, and facilitated my pursuit for any aspirations that I have/had. Without their reinforcement, I would never have arrived at this point, and achieved what I have so far in my life. This thesis is also your creation. Furthermore, a massive acknowledgement goes out to all my friends scattered across the globe, which kept my spirits high throughout these past years. In this breath, I would like to specifically thank the party corner, Nik, Stefan, Bogo and Dobro, for making this PhD bearable even in times of great stress and frustration.

I owe my undying gratitude to Prof. Harald Haas, my supervisor, who has guided me throughout the course of my studies, and continuously pushed me to improve and perfect not only my research, but also my professional attitude and working efficiency. I only hope that I can repay you for your extensive loyalty and trust. In addition, special thanks go out to Zubin and Sinan, for not only being great friends, but also aiding and supporting my research throughout this thesis. I would also like to thank DoCoMo Euro-Labs for their close cooperation, especially Gunther and, towards the end, Taoka, who were always available for questions and improvement suggestions.

Finally, I would like to acknowledge the financial support of DoCoMo Euro-Labs for this PhD, without which the past three years would not have been possible.

Contents

List of figures

List of tables

Acronyms and Abbreviations

1G	1st Generation
2G	2nd Generation
3G	3rd Generation
3GPP	3rd Generation Partnership Project
4G	4th Generation
AP	access point
AMC	adaptive modulation and coding
AMPS	Advanced Mobile Phone Service
ABS	Almost-blank subframe
BS	base station
CAPEX	capital expenditure
CSMA	carrier sense multiple access
CLT	central limit theorem
CSI	channel state information
CDMA	code division multiple access
CN	core network
CoMP	coordinated multi-point transmission
CCI	co-channel interference
CDF	cumulative distribution function
DRB	Data Radio Bearer
DSL	Digital Subscriber Line
DFT	discrete Fourier transform
DL-SCH	Downlink Shared Channel
DFR	dynamic frequency reuse
EDGE	Enhanced Data Rates for GSM Evolution
ETSI	European Telecommunications Standards Institute
FFT	fast Fourier transform
FBS	femto-BS
FMS	femto-MS
FPC	fractional power control

FFR	fractional frequency reuse
FDD	frequency division duplex
FDM	frequency division multiplexing
FDMA	frequency division multiple access
GPRS	General Packet Radio Services
GSM	Global System for Mobile Communications
HetNet	heterogeneous network
ICT	information and communication technology
IMT-2000	International Mobile Telecommunications-2000
ITU	International Telecommunication Union
ICD	inter-cell distance
ICIC	inter-cell interference coordination
ICI	inter-channel interference
ISD	inter-site distance
ISI	inter-symbol interference
IFFT	inverse fast Fourier transform
J-TDMA	joint TDMA
J-ZF	joint zero-forcing
J-MMSE	joint minimum mean-square error
LA	link adaptation
LTE	Long-Term Evolution
LTE-A	LTE-Advanced
MBS	macro-BS
MMS	macro-MS
MR	maximum rate
MINLP	mixed-integer non-linear programming
MS	mobile station
MME	Mobility Management Entity
MCS	modulation and coding scheme
MC	multi-carrier
NE	Nash Equilibrium
NAS	non-access stratum
NMT	Nordic Mobile Telephony
OPEX	operational expenditure

OFDM	orthogonal frequency division multiplexing
OFDMA	orthogonal frequency division multiple access
PBCH	Physical Broadcast Channel
PDSCH	Physical Downlink Shared Channel
PBS	pico-BS
PCS	Power Control Scheduling
PSS	Power SINR Scheduling
PDF	probability distribution function
PMF	probability mass function
PF	proportional fair
PFS	proportional fair scheduler
POPC	Pareto optimal power control
QAM	quadrature amplitude modulation
QPSK	quadrature phase shift keying
RRC	Radio Resource Control
RTM	Radio Telefono Mobile
r.v.t	random variable transformation
RSRP	reference signal received power
RNTP	relative narrowband transmit power
RRH	remote radio head
RB	resource block
SON	Self-Organising Network
S-GW	Serving Gateway
SMS	Short-Message System
SRB	Signalling Radio Bearer
SIR	signal-to-interference ratio
SINR	signal-to-interference-plus-noise ratio
SNR	signal-to-noise ratio
SC	single carrier
SC-FDMA	single carrier frequency division multiple access
SFR	soft frequency reuse
SDMA	space division multiple access
SR	Stepwise Removal
TDD	time division duplex

TDMA	time division multiple access
TACS	Total Access Communications System
TPC	transmitter power control
UMTS	Universal Mobile Telecommunications System
UMA	Unlicensed Mobile Access
UTRA	UMTS Terrestrial Radio Access
ULIP	Uplink Interference Protection
WCDMA	wideband code division multiple access

List of Symbols

a	placeholder variable
a_i	constant in polynomial for i^{th}power
A	placeholder constant
A_{m}	maximum angular attenuation loss
$A_{i,j,k}$	PSS feasibility condition constant
$\mathcal{A}$	set of PSS feasibility condition constants
b	placeholder variable
$\hat{b}$	BS-type variable
B	placeholder constant
B_{sys}	system bandwidth
B_{RB}	RB bandwidth
B_u	nominal bandwidth assigned to MS$_u$
c	placeholder variable
c_i	chord i
$c(\cdot)$	chord length
C	placeholder constant
C_{IA}	interference alignment capacity
C^*	nominal desired rate
C_u^*	desired rate of MS$_u$
$\hat{C}$	desired rate Rayleigh parameter
$\bar{C}$	average desired rate
$\bar{C}_{\text{m}}$	MMS average desired rate
$\bar{C}_{\text{f}}$	FMS average desired rate
C_u	throughput of MS$_u$
C_u^{BM}	nominal benchmark throughput of MS$_u$
C_u^{ULIP}	nominal ULIP throughput of MS$_u$
C_{sys}	system throughput
$C_{\text{sys}}^{\text{BM}}$	nominal benchmark system capacity
$C_{\text{sys}}^{\text{ULIP}}$	nominal ULIP system capacity

$\mathbf{C}$	vector of user throughputs
$\mathbf{C}^*$	vector of user desired rates
D	BS separation parameter
d	distance in m
d_i	distance from interfering PBS inside macro-cell
d_o	distance from interfering PBS outside macro-cell
$\hat{d}$	distance of PBS from HetNet macro-cell centre
$d_i(t)$	total transmitted data at MS_i at time t
$\mathbf{E}[\cdot]$	expectation operator
$f(\cdot)$	nominal function
$f(\mathbf{F})$	feasibility condition for PCS/PSS based on $\mathbf{F}$
$f(\mathbf{\Gamma})$	feasibility condition for PCS/PSS based on $\mathbf{\Gamma}$
$f_{\bar{\gamma}}(\cdot)$	ordering function of average SINRs
$f_{\mathbf{F}_x}(\cdot)$	characteristic function of $\mathbf{F}$ of size x
$f_W(\cdot)$	nominal PDF of random variable W
$f_{C^*}(C^*)$	PDF of desired rates
$f_d(\cdot; D)$	PDF of Tx-Rx distance parametrised by D
$f_{d,\text{mac}}(\cdot; R)$	PDF of distance to MBS parametrised by R
$f_{d,\text{pic}}(\cdot; R, D)$	PDF of distance to PBS parametrised by R and D
$f_{\theta,\text{mac}}(\cdot)$	PDF of angle from central lobe of MBS
$f_\theta(\cdot)$	PDF of angle from interfering MBS
$f_\phi(\cdot)$	PDF of uniformly distributed angle ϕ
$f_\varphi(\cdot)$	PDF of converted angle φ
$f_D(\cdot; R)$	PDF of interfering PBS distance to macro-cell centre parametrised by R
$f_{I,\text{dB}}(\cdot; D)$	PDF of nominal logarithmic interfering signal parametrised by D
$f_{I_{s,\text{oc}}}(\cdot; R, D)$	PDF of linear own-cell interference parametrised by R and D
$f_{I_{s,\text{oc}},\text{dB}}(\cdot; R, D)$	PDF of logarithmic own-cell interference parametrised by R and D
$f_{\sum I_s}(\cdot; R)$	PDF of linear sum interference in HetNet macro-cell parametrised by R
$f_{\sum I_s,\text{dB}}(\cdot; R)$	PDF of logarithmic sum interference in HetNet macro-cell parametrised by R
$f_{L,\text{dB}}(\cdot; D)$	PDF of nominal logarithmic link path loss parametrised by D
$f_{L_d,\text{dB}}(\cdot; D)$	PDF of logarithmic distance-dependent path loss parametrised by D
$f_{L_{d,\text{mac}},\text{dB}}(\cdot; R)$	PDF of logarithmic distance-dependent path loss from MBS parametrised by R

$f_{L_d,I_{\mathrm{mac}},\mathrm{dB}}(\cdot;R)$	PDF of logarithmic distance-dependent path loss from interfering MBS parametrised by R
$f_{L_{s,\mathrm{mac}},\mathrm{dB}}(\cdot;R)$	PDF of logarithmic signal path loss from MBS parametrised by R
$f_{L_{s,\mathrm{pic}},\mathrm{dB}}(\cdot;R,D)$	PDF of logarithmic signal path loss from PBS parametrised by R and D
$f_{L_s,I_{\mathrm{mac}}}(\cdot;R)$	PDF of linear signal path loss from interfering MBS parametrised by R
$f_{L_s,I_{\mathrm{mac}},\mathrm{dB}}(\cdot;R)$	PDF of logarithmic signal path loss from interfering MBS parametrised by R
$f_{L_s,I_{\mathrm{pic}}}(\cdot;R)$	PDF of linear signal path loss from interfering PBS parametrised by R
$f_{L_s,I_{\mathrm{pic}},\mathrm{dB}}(\cdot\|D;R)$	PDF of logarithmic signal path loss from interfering PBS dependent on D and parametrised by R
$f_{L_s,I_{\mathrm{pic}},\mathrm{dB}}(l;R)$	PDF of logarithmic signal path loss from interfering PBS parametrised by R
$f_{L_s,\sum I_{\mathrm{mac}}}(\cdot;R)$	PDF of linear signal path losses from multiple interfering MBSs parametrised by R
$f_{L_s,\sum I_{\mathrm{mac}},\mathrm{dB}}(\cdot;R)$	PDF of logarithmic signal path losses from multiple interfering MBSs parametrised by R
$f_{L_s,\sum I_{\mathrm{pic}}}(l;R)$	PDF of logarithmic signal path losses from multiple interfering PBSs parametrised by R
$f_{L_{\theta,\mathrm{mac}},\mathrm{dB}}(\cdot)$	PDF of logarithmic angular attenuation from MBS
$f_{L_\theta,I_{\mathrm{mac}},\mathrm{dB}}(\cdot)$	PDF of logarithmic angular attenuation from interfering MBS
f_{L_d}	nominal PDF of linear distance-dependent path loss
f_{L_θ}	nominal PDF of linear angular attenuation
$f_{L_{\theta\|d}}(\cdot)$	nominal PDF of linear angular attenuation dependent on Tx-Rx distance d
$f_{L_{d\|\theta}}(\cdot)$	nominal PDF of linear distance-dependent path loss dependent on angle from central lobe θ
$f_{P_r,\mathrm{dB}}(\cdot)$	PDF of nominal logarithmic received power
$f_{P_t}(\cdot)$	PDF of nominal linear transmitted power
$f_{P_t,\mathrm{dB}}(\cdot)$	PDF of nominal logarithmic transmitted power
$f_{S,\mathrm{dB}}(\cdot;D)$	PDF of nominal logarithmic desired received signal parametrised by D
$f_{S,\mathrm{dB}}(\cdot;R,D)$	PDF of nominal logarithmic desired received signal parametrised by R and D
$f_{X_\sigma,\mathrm{dB}}(\cdot)$	PDF of lognormal shadowing value
$F_{i,j}$	i^{th}row and j^{th}column entry of $\mathbf{F}$

$F_{C^*}(\cdot)$	CDF of desired rates
$F_{P_t}(\cdot)$	CDF of nominal linear transmitted power
$F_W(\cdot)$	nominal CDF of random variable W
$\mathbf{F}$	interference matrix
$g_{\hat{b}}$	BS-type $\hat{b}$ transmit power minus path loss
G	nominal channel gain
G_{dB}	nominal logarithmic channel gain
$G_{k,l}^m$	channel gain from transmitter l to receiver k on RB$_m$
$G_{\min,v_i}$	minimum channel gain to interfering MBS$_i$
$h(\cdot,\cdot)$	function of maximum of two PDFs
$H_{k,l}^m$	channel transfer function from transmitter l to receiver k on RB$_m$
$\mathbf{H}$	nominal channel matrix
i	nominal index
$i_{R^*[k]}$	index i of MS$_i$ of k^{th}entry in R^*
I	nominal interference
$\sum I$	nominal sum interference
$I_{k,l}$	interference caused at FMS$_k$ caused from FMS$_l$'s FBS
I_u^m	interfering signal at MS$_u$ on RB$_m$
$I_{\mathrm{avg,\,dBm}}^m$	logarithmic time-averaged interference on RB$_m$ in dBm
$I_v^{m,\mathrm{tol}}$	interference tolerance of MS$_v$ for RB$_m$
$\mathcal{I}_m$	set of interferers on RB$_m$
$\mathbf{I}$	identity matrix
j	nominal index
k	nominal index
k_{B}	Boltzmann constant
k_{sc}	number of subcarriers per RB
K	placeholder variable
l_{p}	number of ULIP priority bands
L_{dB}	nominal link path loss in dB
$L_d(\cdot)$	distance-dependent path loss
L_s	signal path loss
$L_\theta(\cdot)$	angular attenuation loss
$L_{s,\mathrm{dB}}$	logarithmic signal path loss
$L_{d,\mathrm{mac,dB}}$	logarithmic distance-dependent path loss from MBS

$L_{\theta,\mathrm{mac,dB}}$	logarithmic angular attenuation from MBS
$L_{\theta_I,\mathrm{dB}}$	logarithmic angular attenuation from interfering MBS
$L_{s,I_{\mathrm{pic}}}$	logarithmic signal path loss from interfering PBS
$L_{\mathrm{des,\,dB}}$	FPC logarithmic desired path loss
$L_{\mathrm{int,\,dB}}$	FPC logarithmic interfering path loss
m	nominal index
$\tilde{m}$	CQI index
$\hat{m}$	MS-type variable
$m(\cdot,\cdot)$	function of minimum of two PDFs
M	number of system RBs
$\mathcal{M}$	set of system RBs
$\mathbf{M}$	nominal CoMP pre-processing matrix
n_{r}	number of target-reducing MSs in PSS group
n^{RB}	nominal number of RBs
n_u^{RB}	number of RBs assigned to MS_u
$n(u)$	number of users in a femto-cell
$n_c(u)$	number of users in femto-cell c
n_{usr}	random variable of number of MSs in system
N	nominal thermal noise
N_j	number of MSs in cell j
N_I	nominal number of interfering PBSs
N_{p}	number of PBSs per HetNet macro-cell
$\bar{N}$	average number of users per macro-cell
N_{sc}	number of OFDM subcarriers
N_{sf}	number of subframes for convergence
N_{step}	number of steps for convergence
N_{app}	number of apartment blocks per HetNet macro-cell
N_{cdma}	potential number of users in CDMA system
N_{fdma}	number of users in FDMA system
N_{tdma}	number of users in TDMA system
$\mathcal{N}(\mu,\sigma^2)$	normal random variable of mean μ and variance σ^2
$O(\cdot)$	in the order of
p	placeholder variable
p_{act}	active femto-cell probability

p_{ABS}	probability of ABS transmission
$p_{n(u)=i}$	probability for i users in a femto-cell
$p_d(\cdot)$	distance probability distribution
$p_\theta(\cdot)$	angular probability distribution
P_r	nominal received power
$P_{r,\mathrm{dB}}$	nominal logarithmic received power
P_r	nominal transmitted power
$P_{r,\mathrm{dB}}$	nominal logarithmic transmitted power
P_u	transmission power of MS$_u$
$P_{u,j}$	nominal transmission power of MS$_u$ on jthsystem RB
$P_{\hat{b},\mathrm{dB}}$	nominal logarithmic BS transmission power
$P_i(k)$	transmission power of MS$_i$ at iteration k
P_u^{BM}	nominal benchmark transmission power for MS$_u$
P_u^{ULIP}	nominal ULIP transmission power for MS$_u$
P_u^m	transmission power of MS$_u$ on RB$_m$
$P_{\max}$	maximum transmission power
$P_{\max,\mathrm{dBm}}$	maximum logarithmic transmission power in dBm
$P_{\max,\mathrm{FBS}}$	maximum FBS transmission power
$P_{\max,\mathrm{MBS}}$	maximum MBS transmission power
$P_{\max,\mathrm{PBS}}$	maximum PBS transmission power
$P_{\max,\mathrm{FMS}}$	maximum FMS transmission power
$P_{\max,\mathrm{MMS}}$	maximum MMS transmission power
$\tilde{P}^m_{\max,\,i}$	maximum ULIP transmission power for MS$_i$ on RB$_m$
$\mathbf{P}$	power allocation vector
$\mathbf{P}(k)$	power allocation vector at iteration k
$\mathbf{P}^*$	optimal power allocation vector
$\mathbf{P}[\cdot]$	probability operator
r	placeholder variable
r_{gr}	PSS SINR target reduction factor
r_{o}	r_{gr} rounding factor
$r_i(t)$	instantaneous rate of MS$_i$ at time t
$r_i^c(t)$	instantaneous rate of MS$_i$ on RB$_c$ at time t
R	nominal cell radius
R_H	hexagonal cell radius

R^*	sorted list of R_i's
$R^*[k]$	k^{th}entry in R^*
R_i	long-term service rate of MS$_i$
R_{a}	femto-cell scenario apartment dimension
$\mathcal{R}_j$	N_j-tuple of average MS SINRs in cell j
$\mathcal{R}_j^*$	ordered N_j-tuple of average MS SINRs in cell j
$\text{Rayl}(\sigma_{\text{R}})$	Rayleigh distribution with parameter σ_{R}
s	placeholder variable
s_{sc}	symbol rate per subcarrier
S_k	desired signal strength by MS$_k$
S_H	set of high-priority RBs
S_L	set of low-priority RBs
S_M	set of mid-priority RBs
S	nominal desired received signal power
S_{dB}	nominal logarithmic desired received signal power
S_u^m	desired received signal by MS$_u$ on RB$_m$
$\mathcal{S}_{\text{users},j}$	set of MSs in cell j
$\mathcal{S}_{\text{hp},j}$	set of high-priority MSs in cell j
$\mathcal{S}_{\text{lp},j}$	set of low-priority MSs in cell j
$\mathcal{S}_{\text{mp},j}$	set of mid-priority MSs in cell j
t	nominal time
t_{sf}	subframe duration
T	nominal temperature
U_H	set of high-priority MSs
U_L	set of low-priority MSs
U_M	set of mid-priority MSs
$\mathcal{U}_j^*$	N_j-tuple of order positions of average SINRs in cell j
$\mathbf{u}$	scaled SINR vector
V_H	set of sorted λ_i^c's on high-priority RBs
V_L	set of sorted λ_i^c's on low-priority RBs
V_M	set of sorted λ_i^c's on mid-priority RBs
w	placeholder variable
w_{lf}	cell association BS load weighting factor; $\in[0,1]$
W	placeholder random variable

$\mathcal{W}_k$	interference graph removed interferers
x	placeholder variable
$x_i^c(t)$	indicator RB_c is allocated MS_i at time t; $\in\{0,1\}$
X	placeholder random variable
X_σ	lognormal shadowing random variable
Y	placeholder random variable
Y_u^m	composite received signal by MS_u on RB_m
z	simulation time slots per run
z_p	number of previous time slots of considered SINR values
α	general channel parameter
α_i	indoor channel parameter
α_o	outdoor channel parameter
β	general channel parameter
β_i	indoor channel parameter
β_o	outdoor channel parameter
β_u	energy efficiency of MS_u
β_u^BM	nominal benchmark energy efficiency of MS_u
β_u^ULIP	nominal ULIP energy efficiency of MS_u
$\beta_\text{sys}^\text{BM}$	nominal benchmark system energy efficiency
$\beta_\text{sys}^\text{ULIP}$	nominal ULIP system energy efficiency
$\hat{\beta}_u$	energy consumption of MS_u
γ	SINR
γ_u	SINR of MS_u
$\gamma_u(k)$	SINR of MS_u at iteration k
γ^th	SINR threshold
γ^*	nominal SINR target
γ_u^*	SINR target of MS_u
$\gamma_{(i),\text{up}}^*$	SR updated SINR target of i^thremaining link
$\gamma_i^{*,\text{up}}$	PSS updated SINR target of MS_i
$\gamma_i^{*,(m)}$	SINR target of MS_i at iteration m
γ_u^m	SINR of MS_u on RB_m
$\bar{\gamma}_{j,i}$	average SINR of MS_i in cell j
$\hat{\gamma}$	SIR
$\hat{\gamma}^*$	interference graph SIR target

$\hat{\gamma}_u^*$	SIR target of MS_u
$\hat{\gamma}^{\mathrm{th}}$	SIR threshold
Γ_{dB}	nominal FPC logarithmic SINR target
$\mathbf{\Gamma}$	vector of PSS group SINR targets
$\mathbf{\Gamma}_{\min}$	minimum vector of PSS group SINR targets
δ	placeholder factor
$\hat{\delta}$	ULIP interference tolerance signalling margin
Δf	OFDM subcarrier frequency spacing
Δ_γ	difference between user's average SINR and SINR target
ε_{s}	symbol efficiency
η	thermal noise
η_0	noise spectral density
θ	placeholder angle
θ_I	angle from central lobe of interfering MBS
$\theta_{3\mathrm{dB}}$	half antenna gain angle from central lobe
λ	eigenvalue
$\lambda_i^c(t)$	PF metric of MS_i on RB_c at time t
$\lambda_{\mathrm{arc}}(\cdot)$	arc length
$\tilde{\mu}(u)$	maximum number of users per femto-cell
$\mu_{I_{\mathrm{pic}}}$	average PBS interference
ν	FPC parameter
ξ	placeholder variable
$\hat{\xi}$	placeholder factor $\in(0,1]$
π	pi
$\Pi(\cdot)$	system fairness (Jain's index)
ρ_F	Perron-Frobenius eigenvalue of $\mathbf{F}$
$\rho(\cdot)$	general inverse function
$\rho_d(\cdot)$	inverse function of distance to path loss
$\rho_D(\cdot)$	inverse function of interfering PBS distance
$\rho_p(\cdot)$	inverse function of linear power to logarithmic domain
$\rho_{\mathrm{dB}}(\cdot)$	inverse function of logarithmic power to linear domain
$\rho_\theta(\cdot)$	inverse function of angle to attenuation
$\rho_{\theta_I}(\cdot)$	inverse function of interfering angle to attenuation
σ	general lognormal shadowing standard deviation

σ_{i}	indoor lognormal shadowing standard deviation
σ_{o}	outdoor lognormal shadowing standard deviation
$\sigma_{I_{\mathrm{pic}}}$	PBS interference standard deviation
σ_{R}	Rayleigh distribution parameter
ϕ	placeholder angle
$\hat{\phi}$	angle of PBS from central lobe of MBS in HetNet macro-cell
φ	placeholder variable
χ	system availability (*i.e.*, proportion of MSs achieving desired rate)
ψ	placeholder variable
Ω_{BS}	cell association BS score
Ω_{load}	cell association BS load score
Ω_{RSRP}	cell association RSRP score
$\mathbf{0}$	zero vector
$\mathbf{1}_{\mathbf{A}}$	indicator function on vector $\mathbf{A}$
$\circledast$	convolution operator
$\lvert\cdot\rvert$	cardinality operator
$(\cdot)^{H}$	Hermitian operator
$(\cdot)^{\dagger}$	transpose operator

Chapter 1
Introduction

1.1 About this Thesis

The issue of inter-cell interference coordination (ICIC) for high-capacity next generation wireless networks is addressed in this thesis. With the ever-increasing uptake of mobile users, wireless communication has evolved into a utility similar to water and electricity, needed by almost all people of today's modern society. Furthermore, the large demands for multimedia services such as Internet, TV, etc., are fast rendering state-of-the-art cellular systems incapable of supporting the requested traffic in the network [2, 3]. Thus, smaller cell sizes, micro-cells and full frequency reuse are implemented to increase the spatial reuse of wireless resources over a geographical area. However, while this inherently increases the signal-to-noise ratio (SNR) in the network, the high interference caused by the dense cellular structure harms the achievable spectral efficiency. Furthermore, the additional power consumption from the multitude of base stations (BSs) indicates the necessity for more energy efficient ICIC techniques for modern networks.

On the other hand, recent studies indicate that a substantial portion of wireless traffic originates indoors [4]. Poor signal reception through walls severely inhibits the operation of indoor data services, attracting considerable interest in the concept of femto-cells [5]. Thus, femto-BSs (FBSs), which are low-cost, low-power, short range, plug-and-play BSs, aim to enhance indoor coverage, alleviating this burden from the macro-cell sites. Furthermore, macro-cell coverage is extended through pico-cells, which provide micro-cells within a macro-cell in order to further augment the availability of wireless resources. Hence, future wireless networks are moving towards heterogeneous architectures, with multiple access points (APs) available in each macro-cell [6].

This work focuses primarily on the development of novel ICIC techniques to manage the upcoming challenges of future heterogeneous networks (HetNets). The coordination of the dense macro-cellular environment, femto-cell deployment and additional micro-cells is addressed, with special attention paid to spectrally and energy efficient operation of these systems.

1.2 Growth of Wireless Technology

Since the introduction of mobile technologies over two decades ago, wireless communication has penetrated to almost all people in the developed world, and is tremendously increasing in developing countries, thus making the mobile phone the most widespread information and communication technology (ICT) to date. Furthermore, due to the continuous growth and expansion of mobile technologies and applications, the requested traffic is increasing at a tremendous rate. This is evident in Fig. 1.1, where it is estimated that the global demand for mobile communications will increase almost six-fold within the next three years [7]. Clearly, this is a challenging rate for mobile operators to maintain.

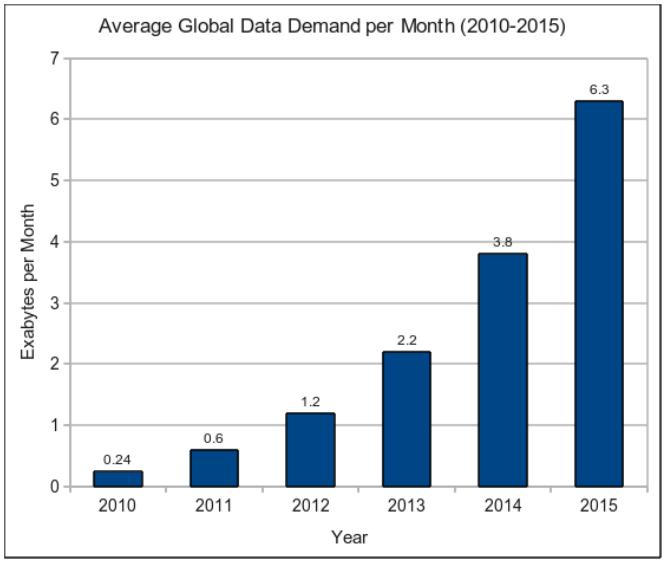

Figure 1.1: *The predicted, almost exponential, increase in demand of mobile communications services over the next years [7].*

This trend is further supported by the graphs shown in Fig. 1.2, where it is evident that from its humble beginnings as a worldwide service (Global System for Mobile Communications (GSM)) approximately thirty years ago, in 2011 over 85% of the Earth's inhabitants made use of mobile devices for communication [2]. This is even more astonishing when considering that at the turn of the millennium, only approximately 15% possessed mobile phone subscriptions, and this almost solely in the developed world [2]. Furthermore, just eleven years ago did the number of fixed-telephone line subscriptions (which now, as can be seen in Fig. 1.2, has been on the decline since 2005) still exceed that of mobile devices, indicating mobile technology is quickly (or, has succeeded in) replacing landlines as the principal tool for point-to-point

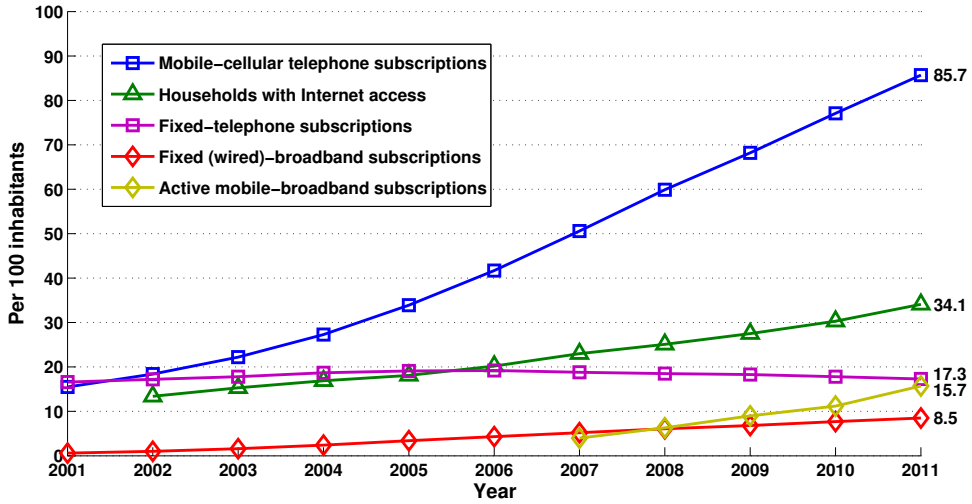

Figure 1.2: *Global development of ICT in terms of percentage penetration for: mobile subscriptions, Internet access, users of internet, fixed-line subscriptions, mobile broadband subscriptions, and wired-broadband subscriptions [2].*

communications. Moreover, it is evident that the number of mobile broadband subscriptions has received significant uptake in the developed world in recent years [2], further contributing to the growing traffic demands on mobile networks.

Numerous studies (*e.g.*, [8]) indicate that the availability of Internet services can be instrumental for the development of a nation. However, fixed broadband access is often scarcely, or not at all, available in developing nations. In 2011, only 24% of the population of developing countries had access to the Internet, compared with less than 10% before 2007 [2]. Clearly, establishing high-speed Internet access over the growing mobile networks in such countries is of paramount importance [1].

In this light, femto-cells offer a unique opportunity to provide not only indoor coverage in developed nations, but further expand coverage in developing countries for greater wireless and Internet penetration. However, the introduction of femto-cells into existing architectures may severely complicate the operation of a network. Therefore, the development of more advanced ICIC techniques for not only established but also growing wireless networks is essential to their successful employment. Moreover, in this time of heightening environmental concerns, practical ICIC approaches which limit the complexity and energy consumption of a network are elementary in the implementation of wireless technologies.

1.3 Contributions

To support the ever-growing data rates, Long-Term Evolution (LTE) networks and beyond are moving towards full frequency reuse and smaller cell sizes [6, 9], consequently enhancing the inter-cell interference in the network, especially detrimental in the uplink. To this end, transmitter power control (TPC) is utilised in the wireless uplink to balance the SNRs of the mobile stations (MSs) in a cell at the BS, and hence ease simultaneous reception. In TPC, each MS transmits at a power level that is large enough to compensate the signal attenuation from itself to its serving BS, and further to overcome interference from other cells. It has been shown, however, that in many cases this may lead to transmit power explosions [10, 11], rendering the TPC operation itself ineffective. Furthermore, in general cell-edge performance becomes highly limited. Utilising the interfering link to a neighbouring macro-BS (MBS) in order to mitigate the interference caused to that cell, on the other hand, can prevent such a breakdown. Additional signalling in the network can be limited by utilising the reference signal received powers (RSRPs) from neighbouring MBSs to estimate the interfering path gains. Furthermore, a fair scheduler employing a priority class reuse scheme provides protection to cell-edge users, and creates an essentially even distribution of throughput throughout the macro-cell. Through this, an adaptive *soft frequency reuse* scheme is induced, which inherently provides interference protection and uplink throughput gains for the majority of macro-MSs (MMSs). Moreover, guaranteed energy efficiency gains for all MMSs in the network are achieved.

As mentioned above, conventional power control methods can result in extremely large transmit powers under high interference conditions. Furthermore, most centralised control schemes are based on optimisation techniques [12–14], which *a)* generally split the subcarrier and power allocation problems yielding suboptimal solutions, and *b)* are highly computationally complex. In this thesis, a simple feasibility criterion, based on path gains and signal-to-noise-plus-interference ratio (SINR) targets, is derived enabling the simultaneous scheduling of interfering macro-users such that Pareto optimal power control (POPC) [15] can be performed. Hence, the scheduling and power control problems have been united at reduced operational complexity. In addition, randomly deployed femto-cell environments are considered, where full bandwidth users cause extreme interference to neighbouring cells in both downlink/uplink, once again complicating the TPC procedure(s). Through extension of the feasibility condition enabling femto-MS (FMS) SINR variation, the application of POPC is facilitated in such dense, high interference scenarios. As a result, system throughput and energy efficiency improvements for

both the macro- and femto-cellular environments over TPC and fractional power control (FPC) techniques can be achieved.

However, because the backhaul of FBSs is ideally performed through the user's Digital Subscriber Line (DSL) connection, there may be cases where the connection is slow or even non-existent due to lack of inter-operability [6]. Thus, centralised schemes might break down. Furthermore, the resource and power allocation problem in multicellular networks belongs to the class of mixed-integer non-linear programming (MINLP) problems, for which the solutions are known to be $\mathcal{NP}$-hard [16, 17]. Therefore, the final contribution of this project presents a methodology for distributed and autonomous resource and power allocation through the use of a fuzzy logic system. In fuzzy logic, human expertise/knowledge about a given problem or challenge can be implemented for autonomous decision-making based on fuzzified input variables. Furthermore, $\mathcal{NP}$-hard solutions are inherently avoided. In the femto-cell case, by utilising locally available information at the MS/BS, each cell can perform autonomous resource and power allocation in order to best serve the users in the system. It has been shown through experimental comparison that fuzzy logic is able to provide *close-to-optimal* system performance at significantly reduced complexity, and with the complete elimination of inter-BS signalling.

Finally, future wireless networks are evolving towards HetNets, where power control and interference coordination is performed via extensive cross-tier communication [6, 18, 19]. As in such networks many types of APs are available to a MS within a small geographical area, the spatial reuse of resources is dramatically enhanced (*i.e.*, improving available data rates) however the interference environment is significantly complicated. Distributed and autonomous ICIC is highly beneficial here, in order to all but eliminate inter-tier signalling and induce a Self-Organising Network (SON). Additionally, autonomous cell association for MSs entering the system is enabled. Ultimately, extensive simulation analyses verify significant system performance enhancements in terms of throughput, availability, energy efficiency and fairness. On a final note, in order to support the fuzzy logic ICIC scheme, a unique signal analysis of a typical HetNet is performed. The cumulative distribution functions (CDFs) of received signals in both the macro-layer (*i.e.*, including pico-BSs (PBSs)) and femto-cell layer are derived, thus providing a basis model for further research in such networks.

1.4 Thesis Layout

Chapter 2 provides a comprehensive basis for the research presented in the following chapters. In this chapter, an overview of the history and evolution of wireless communication networks is presented. As multiple access presents a key functionality in the evolution of wireless systems, its roadmap to modern cellular systems is presented. A few key concepts in the areas of frequency reuse and power control will be introduced, as the ICIC techniques introduced in this thesis are based on and attempt to improve on these. In addition, an overview of recent research in network interference management techniques is provided. Finally, the upcoming challenges in future HetNets will be presented, and the femto-cellular overlay will be discussed.

The reseach in this project considers future, 4th Generation (4G) systems and network architectures, and therefore a common system model is utilised throughout this thesis. Chapter 3 gives a detailed description of the system model applied, and the corresponding channel models. Furthermore, a common LTE-centric simulator is appropriated throughout the thesis, which will also be described in this chapter. Within this, the simulation scenarios, time evolution, and performance benchmark techniques are presented.

In Chapter 4, the traditional uplink power control challenge is reevaluated for dense, macro-cellular deployments and investigated from the viewpoint of interference mitigation rather than power minimisation. The first contribution of this thesis presents a methodology to balance the areal distribution of SINR over a cell by creating a cell-interdependent soft frequency reuse scheme. In Uplink Interference Protection (ULIP), MS transmit powers are controlled by accounting for the interference caused to neighbouring BSs. Analytic derivations guarantee performance benefits for users and the system as a whole. In addition, SINR and frequency selective schedulers are implemented in collaboration with ULIP, providing contrasting benefits to the wireless systems.

Chapter 5 suggests a more centralised approach to the ICIC challenge, where MSs are scheduled according to path gains and SINR targets in order to maintain the individual and system spectral efficiencies. A practical and simple feasibility criterion for simultaneous transmission of interfering users is derived. In the dense, macro-cell environment Power Control Scheduling (PCS) creates groupings of MSs between which interference can be mitigated through Pareto optimal transmit powers. Furthermore, Power SINR Scheduling (PSS) provides a mechanism to modify the SINRs of interfering MSs in dense, random femto-cell deployments, such that strongly

interfering femto-cells do not lose coverage.

Solutions for the efficient management of future HetNets and their inherent challenges are considered in Chapter 6. More specifically, a distributed and autonomous technique utilising a direct implementation of fuzzy logic for ICIC is presented, yielding significant performance gains in both femto-cellular deployments and larger HetNets, while completely eliminated inter-BS signalling. A comprehensive signal analysis is performed, where the desired and interfering signal CDFs are derived for the typical deployment environments in such networks. Extensive simulations yield encouraging performance results both in comparison to the system optimum, and versus state-of-the-art benchmark techniques.

Finally, conclusions of the previous chapters, a discussion of the limitations of the research in its current state and ideas/paths for future work in these areas are presented in Chapter 7.

Chapter 2
Background

2.1 Historical Overview: The Path to Long-Term Evolution (LTE)

Mobile communications have evolved immensely since the introduction of the first mobile telephone systems in the 1950s. In the early days, each geographical area was allocated a specific frequency band with the BS radiating at the maximum legal transmission power. On the one hand, this clearly limited the number of concurrently active connections, and on the other meant that a MS moving from one geographical area to another would necessarily have to drop its call and reinitiate in the new area. Evidently, these primitive services restricted the number of simultaneously servable users to the number of channels assigned to each particular BS. Furthermore, aside from MSs being bulky, power-hungry, and therefore car-borne, the lack of a commonly agreed standard made roaming between different networks impossible [1]. However, it would be a few decades before such a development began.

In the early 1980s, the generational phase of mobile communications began with the introduction of the, aptly named, 1st Generation (1G) of mobile telecommunications standards. Introduced in 1981, the Nordic Mobile Telephony (NMT) system was the first international mobile telecommunication system, and was adopted in the Nordic countries, the Netherlands, Switzerland, Russia and eastern Europe [20]. Around the same time, Total Access Communications System (TACS) was rolled out in the U.K., RC2000 in France, Radio Telefono Mobile (RTM) in Italy, C-450 was utilised in West Germany, Portugal and South Africa, and Advanced Mobile Phone Service (AMPS) systems were adopted in the U.S.A. and Australia [21]. Simultaneously, several systems were competing in Japan. Through these large-scale deployments of wireless networks a standardised service over large geographical areas was created, allowing for the origination of *roaming*, where users could leave their home network and still be served by neighbouring operators. Clearly, this development was able to attract a much greater and extensive range of customers, and hence the large revenues generated by the growing number of subscriptions captivated the opportunities for new businesses in the market [1].

Unfortunately, due to the analogue nature of 1G deployments, the only opportunities for com-

munication over these networks was voice traffic, albeit with some related supplementary services. However, with the foundation laid, a new direction to continue the development of mobile telecommunications was begun: digitising the existing networks. This would allow operators to increase the system capacity such that the growing rate of new subscriptions could be met, and further to enhance the reliability of the networks, as analogue networks often suffered from *cross-talk* and inconsistent call quality. Ultimately, however, it allowed the network operators to provide mobile services beyond voice. In Europe, the planning for a region-wide system to encompass multiple nations had begun as early as 1982, when the well-known GSM (originally named Groupe Spécial Mobile) was created to develop a standardised telecommunications system that would be available across Europe. In 1989, the European Telecommunications Standards Institute (ETSI) was handed the responsibility for the continued development and eventual standardisation of GSM, and subsequently the first specifications of GSM networks were published in 1990. The rollout of this network across Europe is referred to as the 2nd Generation (2G) of mobile communications. Through the digital nature of these networks, services in addition to traditional voice could be provided, including data services such as Short-Message System (SMS), email, web-browsing and location-based mobile services [21]. Moreover, by this time mobile devices had become increasingly handy, further enhancing the growth rate of mobile subscriptions.

In the latter stages of the 1990s, "2.5G" systems began to be introduced that enabled packet data services across the network, such as General Packet Radio Services (GPRS) and Enhanced Data Rates for GSM Evolution (EDGE). Despite their relatively low rates, they were considered to be pre-3rd Generation (3G) technologies and hinted at the possible applications in future packet-based systems. Ultimately, through its success in Europe, the rollout of GSM quickly gained momentum and was adopted in nearly all countries across the globe. With a worldwide basis to build on, the next generation of wireless networks was around the corner, and united the world to develop and evolve this technology together.

During the expansion of 2G networks around the world in the 1990s, research was already underway into 3G technologies. In fact, the International Telecommunication Union (ITU) had began research on 3G mobile communications in the 1980s on the International Mobile Telecommunications-2000 (IMT-2000) project, which was supposed to deliver rates of over 2000 kbps by the start of the new millennium. While GSM networks were providing circuit-switched data services at downlink rates of up to 14.4 kbps, the rapidly increasing demand

for Internet connectivity and multimedia application on the mobile devices made it evident that the next generation of wireless networks needed to provide far superior data rates [2]. In Europe, Universal Mobile Telecommunications System (UMTS) was established as the 3G technology, and simultaneously in other parts of the world similar systems were being developed such as wideband code division multiple access (wCDMA) in Japan and cdma2000 in the U.S.A. To this end, 3rd Generation Partnership Project (3GPP), an internation consortium comprised of several international standardisation bodies based in Europe, U.S.A and Asia, was constructed as the standardisation and development group for worldwide 3G UMTS Terrestrial Radio Access (UTRA) systems. The first 3G networks began deployment after the turn of the millennium with the goal of providing data rates up to 348 kbps for mobile users, whereas (quasi-)stationary MSs could achieve over 2 Mbps [21]. As can be inferred by the names for the Japanese and American 3G technologies, code division multiple access (CDMA) was chosen as the platform upon which 3G systems were to be designed, mainly due to its ability to support a theoretically infinite number of users at very large bandwidth, while being essentially immune to interference [22]. However, implementations of CDMA networks have been unable to verify these theoretical benefits [23]. Nonetheless, the continued demands for higher and higher data rates drove the further development and deployment of 3G systems, and new releases have continuously facilitated their evolution [9].

Following this, in order to keep up with the ever-increasing demands in terms of user data rate, and by extension, enhanced system capacity, LTE-Advanced (LTE-A) is the 3GPP initiative for 4G communications systems (which is based on LTE, considered 3.9G). These systems are designed to be competitive for the next decade, by providing technological enhancements to meet the spectral efficiency targets of 5 bps/Hz and 2.5 bps/Hz in the downlink and uplink, respectively, as defined in [24]. For the 20 MHz bandwidths envisioned for LTE/LTE-A, this translates to peak speeds of 100 Mbps in the downlink and 50 Mbps in the uplink, comfortably competing with fixed-line home broadband rates. Moreover, one of the key goals of LTE and LTE-A is to provide adequate cell-edge performance in the networks, an area that was rather neglected in previous generations. The key enabling technology for 4G networks is orthogonal frequency division multiplexing (OFDM), a multi-carrier (MC) transmission technique that splits the available spectrum into hundreds of orthogonal subcarriers, each transmitting data proportional to the subcarrier bandwidth. Not only does OFDM provide a more efficient utilisation of spectrum [25], the extension to multiple access is quite convenient.

Finally, due to the extensive propagation of wireless resource utilisation, it has become increasingly difficult to procure large portions of spectrum for future networks [1]. Therefore, by exploiting the key features of OFDM, LTE-A is designed to utilise spectrum allocations between 1.4 and 20 MHz (*i.e.*, up to 100 MHz when utilising multiple carriers), and can operate on all frequency bands specified by the ITU for IMT-2000 systems [9, 26]. Furthermore, 4G systems are required to operate in both paired and unpaired spectra, necessitating seamless functionality in either time division duplex (TDD) or frequency division duplex (FDD) mode, imposing the development of multi-mode terminals, and evolving wireless networks to truly global systems [9].

2.2 Overview of Concepts

In this section, a description of the concepts and technologies that this thesis bases upon is given. Furthermore, the evolution of these concepts to today's state-of-the-art is presented.

2.2.1 Multiple Access

In a cell where multiple MSs are attempting to share the available resources, the manner in which these resources are accessed by the MSs is called *multiple access*. The two most basic types of multiple access are frequency division multiple access (FDMA) and time division multiple access (TDMA), performing access in the frequency and time domain, respectively. In CDMA, codes are used to differentiate between MSs. Finally, recent attention has been given to orthogonal frequency division multiple access (OFDMA), which provides, effectively, a combination of TDMA and FDMA to more efficiently use the available spectrum. This technique has gained considerable interest for 4G systems, and is utilised as the basis for LTE [9]. Thus, this is a key technology for the research in this thesis.

2.2.1.1 FDMA

As the name suggests, FDMA splits the available spectrum into multiple (for instance, N_{fdma}), non-overlapping narrowband channels, and assigns individual channels to individual users [27]. Each user is allocated the spectrum portion for as long as needed, and no other user can share the same channel for the duration of the call. This is shown in Fig. 2.1(a). Due to the large

symbol time of the narrowband signals, the amount of intersymbol interference is low and, thus, little or no equalisation is required in FDMA systems [27].

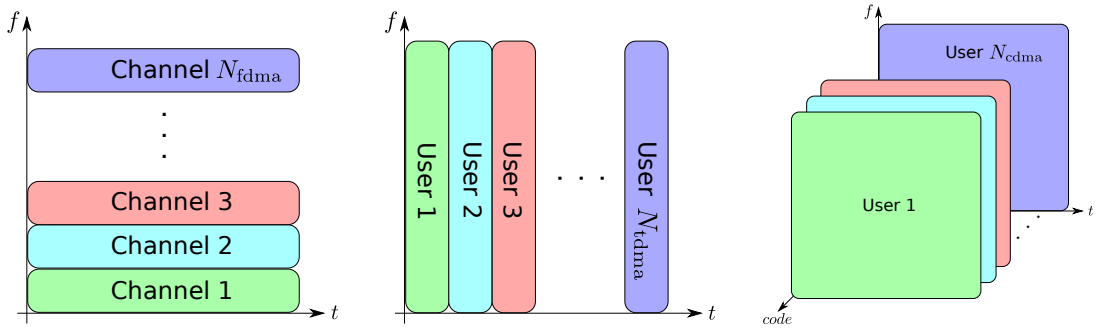

(a) FDMA (b) TDMA (c) CDMA

Figure 2.1: *In FDMA operation, each user is uniquely allocated a portion of the available bandwidth, which no other user may access, for the duration of the intended call. In TDMA operation, each user is allocated all the available bandwidth for the duration of a single time slot. In CDMA operation, users are allocated the full bandwidth for the entire time duration. Users are separated using orthogonal codes unique to each user.*

2.2.1.2 TDMA

TDMA can be seen as the complement to FDMA, where users are multiplexed in time such that at any one time instant only a single user is granted access to the entire bandwidth. This is shown in Fig. 2.1(b). Each user then occupies a cyclically repeating time slot, so a channel may be described as a particular time slot that reoccurs every *frame*, where N_{tdma} time slots constitute a single frame [27]. In general, TDMA systems necessitate larger overheads as compared to FDMA, due to time slot synchronisation and *guard slots* necessary to separate users and prevent intra-cell interference.

2.2.1.3 CDMA

The main drawback of FDMA and TDMA is that it limits the number of servable users in a cell to the N_{fdma} narrowband channels or N_{tdma} time slots per frame allocated in the system, respectively. In CDMA, all users are granted simultaneous access to the total available bandwidth for the entire time duration, and the separation between the users is performed in a third dimension: the *code domain*. Here, each user's signal is spread with an (approximately) or-

thogonal pseudo-noise *spreading signal* or *code* over the entire bandwidth [27]. This can be seen in Fig. 2.1(c). Due to this, the utilisation of the same resource by all other users in a cell is seen as noise by the single user; thus, CDMA is known as a spread-spectrum technique.

Clearly, increasing the number of users in the system raises the noise floor in a linear manner [27], this is known as the *cell breathing* effect. Therefore, CDMA systems can be classified as interference-limited [28]. Furthermore, power control is highly important for efficient CDMA operation in order to provide constant received power levels for all users. However, due to the lack of perfect power control, the *near-far effect* is identified as a key issue in CDMA systems, as a stronger interfering link than a desired link will lead to very low SNR values. However, the potential for high data rates and a large number of servable users is the key factor behind the use of CDMA for 3G technologies.

2.2.1.4 OFDMA

OFDMA is a multiple access technique that bases on the concept of OFDM, which dates back to the 1960s [29, 30], and divides the available frequency spectrum into multiple orthogonal subcarriers. However, it was not until the design of the discrete Fourier transform (DFT) and fast Fourier transform (FFT) that OFDM became implementable in practical systems [31, 32]. OFDM and OFDMA are classified as MC transmission techniques, which are able to perform exceptionally in wireless communications systems as mobile radio channels are typically highly frequency- and time-variant [9]. MC operation, as opposed to single carrier (SC) techniques, is well-equipped to handle such environments.

In general, MC transmission techniques parallelise a fast serial data stream into several slower data streams, *i.e.*, by dividing the channel bandwidth into multiple parallel subchannels of significantly smaller bandwidth. In OFDM, this is performed such that the bandwidth of each subcarrier is less than the channel coherence bandwidth, and hence non-frequency-selective, or *spectrally flat* [9]. Furthermore, in OFDM, these non-frequency-selective subcarriers are shaped in such a manner to be orthogonal to one another, eliminating the need for guard intervals between them, as is the case in frequency division multiplexing (FDM). This orthogonality induces a more efficient utilisation of spectrum in comparison to classical SC transmission or FDM, as shown in Fig. 2.2.

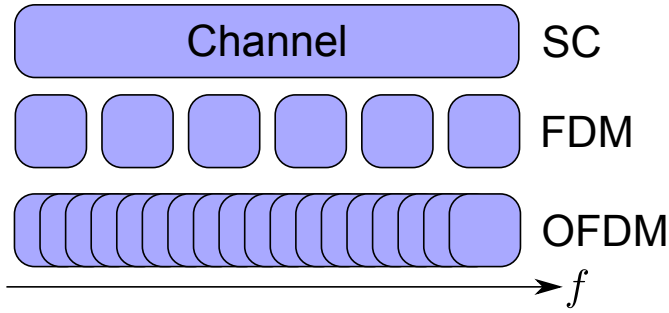

Figure 2.2: *A graphical illustration of how OFDM makes more efficient use of the spectrum than SC or FDM schemes [1].*

OFDM combines the distinct advantages of flexibility to operate independently of the available spectrum, *i.e.*, in different channel bandwidths, and with low complexity at the receiver-side. The application of spectrally flat subcarriers in MC transmission is first proposed for cellular mobile radio networks [33]. This was in 1985, almost thirty years ago. With the advances in digital signal processing techniques, hardware development and the multitude of research since then, OFDM and, more specifically, OFDMA has become a uniquely suitable candidate for LTE and 4G systems [1].

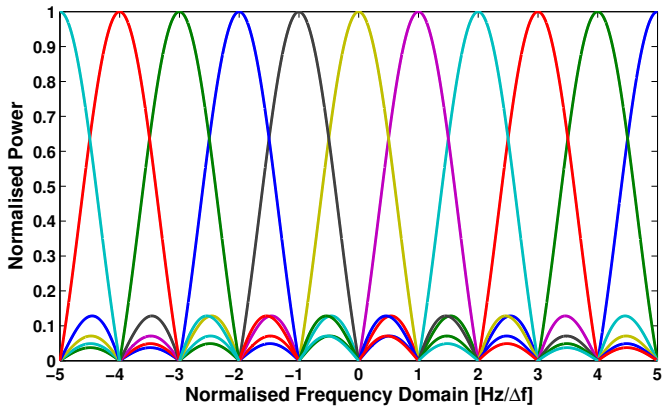

Figure 2.3: *Sinc-shaped-subcarrier spacing in OFDM. Assuming perfect synchronisation, all subcarriers are orthogonal to one another. Here, Δf is the subcarrier spacing.*

OFDM System The OFDM modulator comprises N_{SC} complex modulators, each modulator corresponding to a single OFDM subcarrier. By utilising a sinc-shaped subcarrier, these become orthogonal to one another in frequency and, hence, avoid inter-carrier interference. This is shown in Fig. 2.3, where at the peak of each subcarrier, the other subcarriers form an aggregate of zero; this is where OFDM gets its name. The OFDM modulator is shown in

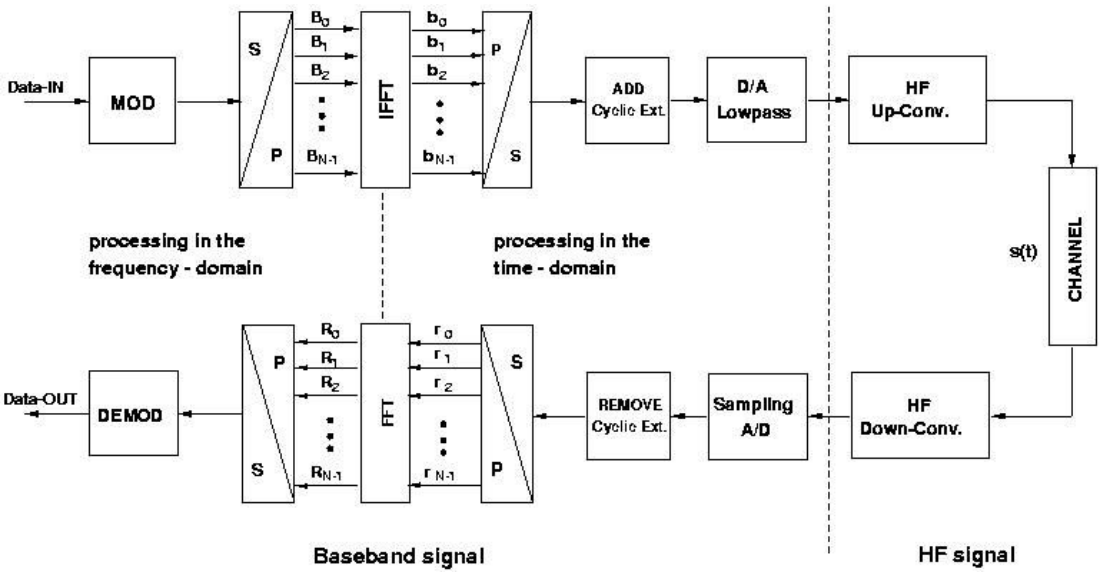

Figure 2.4: *OFDM operation: A serial data stream is converted to parallel, multiplexed onto orthogonal subcarriers using the IFFT, and aggregated to form the transmitted signal. After transmission through the wireless channel and reception, the received stream is separated into the components of each subcarrier using the FFT, and then re-serialised and demodulated [34].*

Fig. 2.4, where it is clear that the input serial stream of modulation symbols (these symbols can be from any modulation alphabet, in LTE specifically quadrature phase shift keying (QPSK), 16 quadrature amplitude modulation (QAM) and 64QAM are utilised [9]) is parallelised, the individual symbols are mapped onto subcarriers using the IFFT, and then the parallel streams are re-serialised and the signal is transmitted.

Fig. 2.4 also depicts the basic operation of the OFDM demodulator. As expected, this is essentially the reverse operation of the modulator. Again, the incoming serial stream is parallelised, and now is fed through an FFT in order to separate the information into the components of each subcarrier. Following this, the symbols are again serialised, and then detected and demodulated in the final stage of the receiver. Due to their orthogonality, the OFDM subcarriers do not interfere with each other after separation, assuming perfect frequency synchronisation. If this fails, however, a loss of subcarrier orthogonality can lead to inter-channel interference (ICI), a phenomenon usually prevented in classic MC transmission via allocation of physical frequency guard intervals. In order to improve the robustness of OFDM against channel frequency selectivity, a *cyclic prefix* is inserted during modulation. This, in essence, provides a guard against both ICI and inter-symbol interference (ISI) [31, 35].

OFDMA Structure The typical structure of OFDM transmission is shown in Fig. 2.5, where N_{sc} modulation symbols are transmitted simultaneously on all subcarriers, forming an OFDM symbol. On the next OFDM symbol, the following N_{sc} modulation symbols of the incoming data stream are transmitted, and so on. From this structure, it is clear that a very simple extension can be made to provide multiple access, or OFDMA. Here, multiple users can be scheduled simultaneously by assigning each a distinct subset of orthogonal subcarriers. Thus, each user can transmit its information without interference from users sharing the available spectrum. This is similar to FDMA, however the overlapping subcarriers allow for a denser and more efficient utilisation of the bandwidth. Furthermore, users may also be scheduled in time (*i.e.*, OFDM symbols). Multiple users may share the same subcarrier over different symbols, similar to a TDMA scheme. Thus, it is clear that OFDMA combines both FDMA and TDMA, and concurrently reduces complexity.

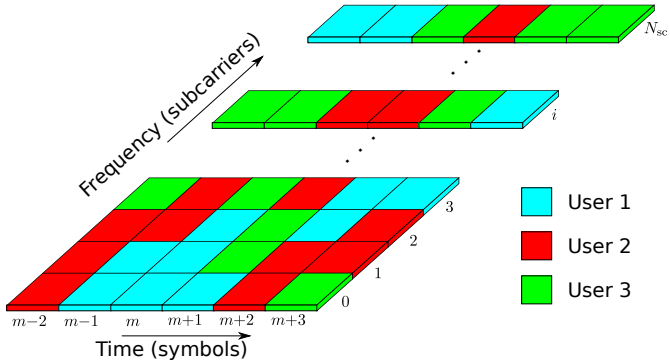

Figure 2.5: *In OFDMA, the time-frequency spectrum is split into subcarriers and time slots, such that in each time slot, each user may be allocated numerous frequency resources.*

Usually, subcarriers are allocated to users in contiguous groups in order to minimise the signalling overhead required for resource assignment. However, a distributed user multiplexing with non-contiguous subcarrier allocation is also possible. It is shown in [36–38], that for a multi-user system, a significant increase in the achievable throughput in a cell can be achieved when transmitting over a fading channel, rather than a flat channel, for the same average received signal power. This is called *multi-user diversity*. One of the major benefits of OFDMA is that it may exploit the (differing) frequency-selective fading characteristics of multiple MSs in the available spectrum, in order to optimise the allocation of subcarriers (or resource blocks (RBs), where a RB is a collection of subcarriers, and a more coarse resource allocation) to the users in the cell. Fig. 2.6 demonstrates such an allocation, where the average channel gain can be maintained at above 0 dB, therefore enhancing the potential throughputs

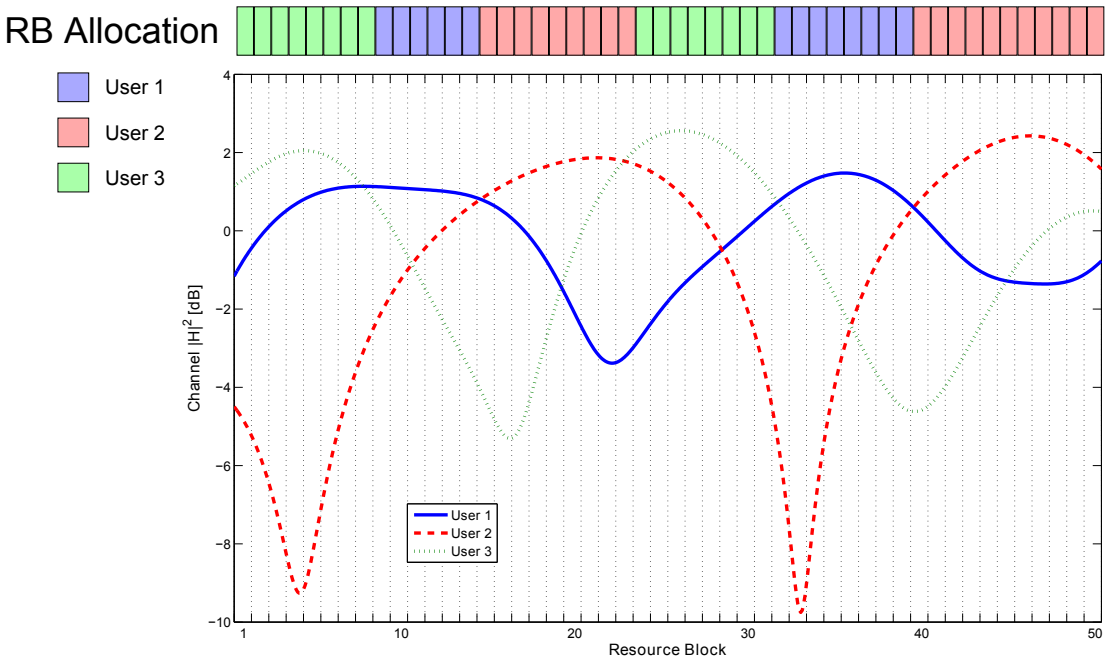

Figure 2.6: *An example of how multi-user diversity can benefit the capacity of an OFDMA system [1]. Each RB is allocated to the MS with the superior channel response on that particular resource. Thus, allocations in deep fades are avoided.*

over a flat, non-frequency selective channel. Furthermore, this is the key enabler for scheduling mechanisms such as the proportional fair scheduler (PFS), which utilises the potential instantaneous rates amongst competing users to optimise their resource allocations [39].

It should be mentioned that other forms of multiple access exist such as space division multiple access (SDMA) and contention-based multiple access (*e.g.*, Aloha, carrier sense multiple access (CSMA)); however are not discussed here as they do not relate to the work in this thesis.

2.2.2 Frequency Reuse

As was mentioned at the beginning of Section 2.1, the original mobile communications systems consisted of a high power BS that was meant to serve a large geographical area. However, this not only severely limited the number of concurrently served users [40], but also greatly restricted, or did not allow, for roaming of users outside this area. Therefore, a mechanism was developed to not only expand the coverage area of mobile networks, but also to increase the number of accessible channels (and hence, users); this is called the *cellular concept* [41, 42]. In this concept, rather than a single BS, many lower-power BSs, each allocated a set of radio

channels, are utilised that each cover a smaller geographic area called a *cell*.

However, it is clear that if two neighbouring BSs were to utilise a similar set of radio resources, these would interfere with each other and, consequently, degrade the performance in each cell. Thus, cells were formed into *clusters*, where in each cluster every cell is allocated a different set of channels than any of its neighbours. Moreover, these clusters can then be repeated over much larger geographical areas, such that the system bandwidth is reused several times within the system. This orthogonal allocation of radio resources within clusters of BSs in a system is known as *frequency reuse* [41]. Fig. 2.7 shows the most primitive form of frequency reuse,

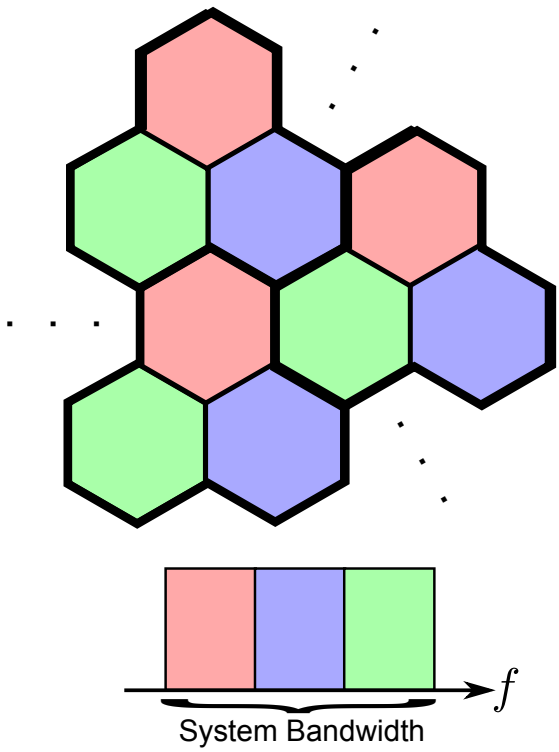

Figure 2.7: *The most basic form of frequency reuse, where the available bandwidth is divided into three (can be increased for higher interference mitigation,* e.g.*, 4, 7, 9,. . .) equally-sized orthogonal bands, and distributed such that no neighbouring cells utilise the same band. Here, three clusters are shown.*

where the system bandwidth is divided into three orthogonal subbands (corresponding to a "frequency reuse of three") and each cluster is formed by three neighbouring cells. Therefore, due to the geographical separation between cells hosting the same frequencies, the co-channel interference (CCI) is mitigated.

Unfortunately, there is a clear drawback to this scheme: the diminished *spatial reuse* of re-

sources over the network area. Evidently, reusing more channels in each cell would increase the number of servable users. However, this reuse is limited by the interference that is tolerable in each cell, and thus cluster sizes, and hence the physical separation of channels, can be increased in order to protect co-channel cells from each others interference. Therefore, there exists a clear tradeoff between bandwidth utilisation and interference limitation.

2.2.2.1 Fractional Frequency Reuse (FFR)

In conjunction with growing demands for mobile services, the necessity arose for enhanced system capacity. According to Shannon [43], the most effective method for improving capacity is increasing the available bandwidth. Without adding to the already expensive system bandwidth, this is performed by improving the spatial reuse of resources, and can be easily achieved given two realisations:

- MSs near the cell-centre not only experience high signal quality due to their close proximity to the serving BS, but are also shielded from other-cell interference due to physical separation.

- On the other hand, it is clear that cell-edge users will receive stronger interference from other cells, simply due to proximity. Furthermore, these MSs will experience degraded performance due to the large distance to their BS.

Thus, it is clear that while cell-centre users do not necessitate excessive interference protection, cell-edge MSs are still highly vulnerable to CCI. Through this, FFR is born.

In FFR, all cell centres in the system employ a frequency reuse of one, where as the cell-edges in a cluster still employ classical frequency reuse [44, 45]. This is portrayed in Fig. 2.8. When comparing this channel allocation to that in Fig. 2.7, it is clear that the number of radio resources that are available in each cell are twice that of classical frequency reuse, hence doubling the system capacity (for higher cluster orders, this gain is even greater). Of course, additional CCI is now present in the system, somewhat degrading performance [43], however the gained bandwidth greatly outweighs this (minor) performance reduction.

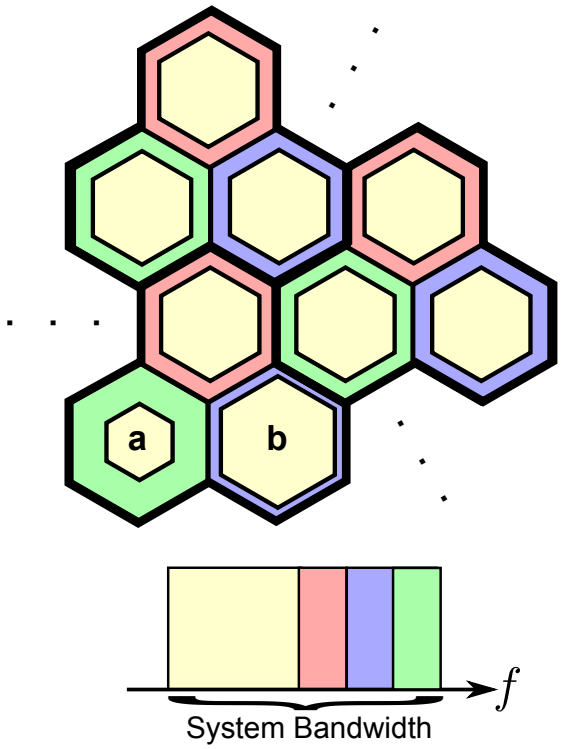

Figure 2.8: *FFR improves the spatial reuse of resources by reusing the same band in the centre of the cell, and protecting the edges through standard frequency reuse.*

2.2.2.2 Dynamic Frequency Reuse (DFR)

It is clear that, while FFR greatly enhances the available resources in the network, there is still room for further improved spatial reuse, and hence capacity. Of course, with this progression of higher channel utilisation, the original ideal of frequency reuse, interference reduction, is continuously diminishing. Therefore, the necessity for ICIC mechanisms arises to substitute this interference mitigation.

A very basic example of DFR is given in [44], where the FFR sizes are modified based on cell load. This is shown in Fig. 2.8, where cell "b" exhibits a larger than average load, whereas cell "a" is serving a lower number of users. Therefore, the central frequencies are extended in cell "b" to improve the spatial reuse, whereas interference protection is enhanced in cell "a" by a smaller area of reuse one. A similar form of DFR is suggested in [46], where the available resources in each cell are partitioned into two groups: fully reused and dynamically reused subcarriers. While the fully reused resources experience interference from all cells, the dynamically reused subcarriers are allocated in a sectorised manner in order to reduce interference. In theory, this scheme is able to achieve a frequency reuse of one in the whole cell.

Another method for DFR is proposed in [47], which partitions the available system bandwidth into multiple subbands which are dynamically accessible in each cell. Through feedback from MSs of interference on each of the subbands, the algorithm dynamically allocates these resources in each cell based on the immediate interference environment. Depending on the traffic loads, certain cells can achieve full frequency reuse (Section 2.2.2.3). Finally, recent research investigates distributed DFR techniques [48–50] where BSs may individually access a predefined number of subbands. However, these approaches greatly restrict subband reassignment when the interference conditions change.

2.2.2.3 Full Frequency Reuse

If interference is ignored, then it is clear that the capacity of mobile cellular network would be maximised when all cells share the entire system bandwidth; this is called *full frequency reuse*, and will be utilised in LTE deployments [9]. In keeping with the previous figures, such channel

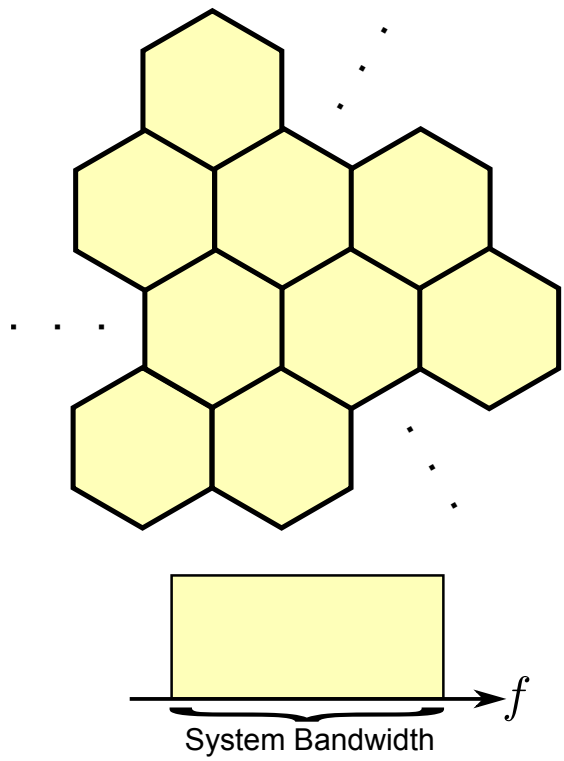

Figure 2.9: *Full frequency reuse employs a frequency reuse of one, maximising the available resources by utilising the full bandwidth in all cells of the network.*

allocation is depicted in Fig. 2.9, where it is clear that all BSs can transmit on the full available bandwidth. Clearly, this results in very high CCI in all cells from their immediate neighbours.

Since a further goal of LTE is acceptable cell-edge performance [9], it is clear that ICIC is vital to the performance of these networks. Among others, the main techniques necessary for LTE ICIC are:

- Interference mitigation/alignment,
- Power control for interference reduction,
- Frequency domain scheduling for interference coordination, and
- Partial/dynamic frequency reuse at cell-edges,

to name a few. This thesis proposes ICIC methodologies that implement a combination of the above mechanisms in order to maintain full frequency reuse, and further supply adequate performance to cell-edge users.

2.2.2.4 Soft Frequency Reuse (SFR)

One such group of techniques already proposed is that of SFR, or adaptive FFR [45]. In SFR, the full bandwidth is utilised in all cells, however transmit power control (*i.e.*, reduction) is performed on a subset of the resources in each cell, where the full power resources are reused in a similar manner to frequency subbands in FFR. In fact, a methodology for SFR has already been standardised for LTE [51].

An implementation of SFR is shown in Fig. 2.10, in which fixed power masks [45, 52] are implemented in the cell-centres where, similar to the motivation for FFR, users are in need of less power to achieve their SINR requirements (due to BS proximity). Furthermore, the diminished transmit power provides interference reduction for neighbouring cells. At the cell-edges, full power transmission is allocated to enable MSs to maintain sufficient SNR. Finally, research is conducted in [53] into adaptive SFR techniques, where the power masks on the individual subbands may be tuned to the immediate interference environment. As mentioned previously, this thesis investigates exactly such methods, by which full frequency reuse is maintained through interference mitigation via intelligent scheduling and power control.

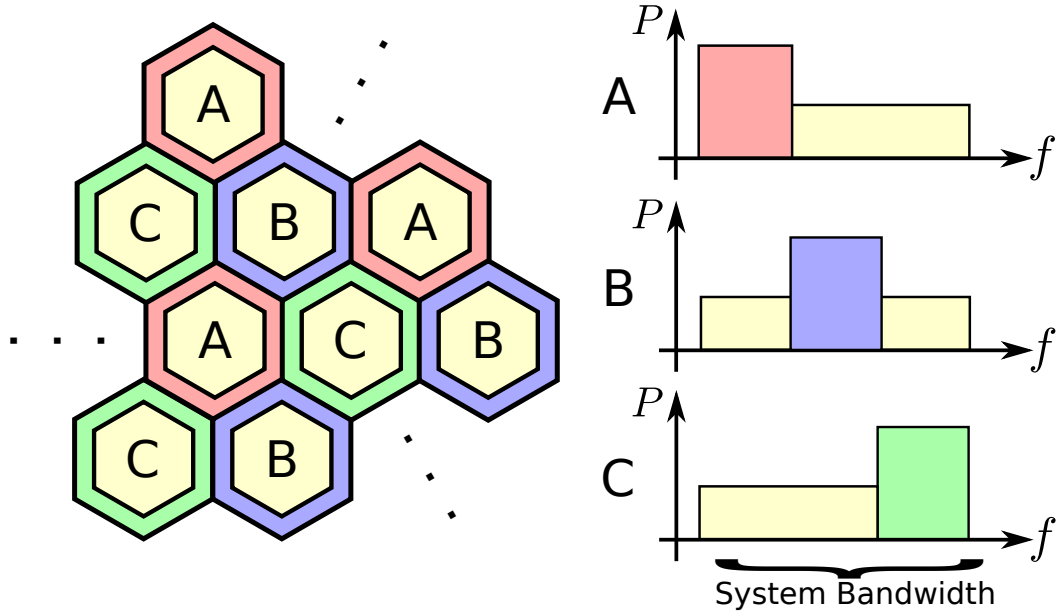

Figure 2.10: *SFR optimises the full frequency reuse of resources by providing interference mitigation to neighbouring cells through transmit power reduction on certain frequency bands.*

2.2.3 Power Control

Transmit power control is one of the most important radio resource management techniques for mobile networks, because it limits the repercussions of two fundamental challenges in wireless networks [54]:

- The limited, and often under-utilised radio spectrum resources make interference mitigation and management crucially paramount to the operation of wireless networks.
- Mobile wireless devices, such as smart-phones, have significant limitations in terms of battery life, hence limiting the *talk time* available before necessarily recharging. Particularly for uplink transmission, the slower development of battery technology in terms of lifetime in comparison to advances in communications continues the substantial impact this constraint has on wireless networks.

Therefore, the application of TPC, *i.e.*, controlling the transmission power to achieve high performance, is common practice in wireless communication networks [54].

In general, power control is utilised to achieve at least one of the following goals:

- Interference mitigation for system capacity enhancement.
- Creating "greener" Internet and mobile networks and prolonging mobile handset battery life by conserving energy.
- Providing QoS by adapting to channel variations.

It is clear that the above goals are all, at least partially, correlated with the SINR [54]. The better the SINR on a link, the higher the quality of the signal. By increasing the transmission power, the received signal power and, consequently, the SINR can be improved. However, this may be a waste of power if the particular application requested does not require such a substantial link quality. Hence, ideally a transmitter would utilise just enough power to meet the necessary SINR *target*; this is the idea of power control. Finally, it should be mentioned that increasing transmit power may not necessarily improve SINR. If the power on other, concurrently transmitting, links is also augmented, a diminishing of the local SINR may arise.

To briefly highlight the benefits of power control for such networks, a few examples are given here. First of all, in [55] it was shown that the application of power control in CDMA systems can double the capacity compared to the non-power control case. Moreover, suitably modifying the rate of power adaptation in the TPC algorithm can induce up to 50% additional gains [56]. In [57], the amalgamation of power control with BS assignment is shown to provide 2–4 times the capacity of a standard CDMA network using power control alone. Furthermore, studies indicate that TPC offers substantial (*i.e.*, orders of magnitude) improvements in terms of energy consumption and device battery lifetime compared to a constant power approach [58]. The exact gains are highly dependent on the utilised transmission rates.

It is clear that power control is an important operation in wireless communication networks. In the following, a more detailed overview of TPC techniques for voice and data applications will be given, along with a description of the proposed LTE FPC scheme.

2.2.3.1 Power Control for Voice Applications

In voice networks, the target of TPC is the maximisation of simultaneously transmitting links achieving a specific SINR [54]. In the early nineties, some of the first research of power control schemes for interference-limited (*i.e.*, noiseless) cellular networks was introduced by Zander in [11]. In this paper, a TDMA/FDMA system with a common signal-to-interference ratio

(SIR) threshold $\hat{\gamma}^{\mathrm{th}}$ for successful communication for all users sharing the same channel is considered. In a centralised scheme, the TPC algorithm attempts to find a transmit power vector $\mathbf{P}^*$ that maximises the minimum SIR of the links. This can be implemented in both downlink and uplink, however without the consideration of a maximum power. It is shown that a unique, feasible solution is always reachable where all links converge to the same SIR, $\hat{\gamma}$.

However, there is no guarantee that this $\hat{\gamma}$ is greater than the $\hat{\gamma}^{\mathrm{th}}$ necessary for successful communication. Furthermore, since these approaches lead to SIR-balancing, this means that all links would be subject to unacceptable performance. Thus, the concept of *cell removal* is introduced in [11], where ideally an optimal combination of cells (*i.e.*, interferers) is removed from the power control problem to find a remaining set of links that achieves $\hat{\gamma}\geq\hat{\gamma}^{\mathrm{th}}$. In [59], a partially distributed technique based on [11] is proposed, where each link updates it power by considering the values of its previous transmit power, SIR and a positive normalisation parameter. In this iterative scheme, cell removal is applied if a solution is not found after a predefined number of iterations. The cell with the worst initial SIR is removed, and the method is reapplied for the remaining links, and then the next worse cell, and so on. Ultimately, both schemes [11, 59] improve the network capacity by decreasing the user outage probability.

In [60], a fully distributed power control technique that necessitates no inter-link communication to achieve $\mathbf{P}^*$ is presented. A significant advantage of this technique is the inclusion of a maximum power, $P_{\max}$, limitation such that transmit powers cannot explode. This scheme is shown to be faster than the distributed scheme proposed in [59], however it should be mentioned that also here some cooperation is necessary during cell removal. Finally, in [61], the scenarios where SIR targets may be both heterogeneous and variable (*e.g.*, due to fading or mobility) are studied. The goal of the power control algorithm is to maximise the possible SIR on each link provided knowledge of the individual targets $\hat{\gamma}_u^*$. It can be shown that there always exists a unique transmit power vector that gives an SIR for each link that is $\delta\hat{\gamma}_u^*$. However, when $\delta<1$, link (cell) removal must again be utilised to find an acceptable solution.

So far, interference-limited, noiseless systems were discussed. In [62], the above described methodology is extended to noisy environments, where a fully distributed algorithm is presented that can achieve the SINR targets, $\hat{\gamma}^{\mathrm{th}}$, of a group of interfering users at minimal power, given such a power allocation is feasible. In [63], a further simplified version of this algorithm is presented. Unfortunately, these algorithms diverge to infinity if no feasible solution is possible. This shortcoming was addressed in [64], where a necessary and sufficient condition for

convergence of the algorithm(s) was provided. Moreover, it was shown in [64] that if such a feasible $\mathbf{P}^*$ vector could be found, that it is Pareto optimal. It should be noted that one of the main differences to the techniques proposed in [11, 59–61] is that here the goal is to find a minimum power vector which satisfies the SINR target on each link, rather than maximising the minimum achievable SIR in the system [54]. Furthermore, it is important to distinguish $\mathbf{P}^*$ as the *smallest component-wise* power vector [64], rather than the vector that minimises the system power.

A distinguished disadvantage of the aforementioned power control techniques is that there is no guarantee that when a link becomes active (*i.e.*, SINR$\geq\gamma^{\mathrm{th}}$), it will remain active in further iterations of the algorithm [54]. If a new link desires to enter the system, or already existing links modify their transmission requirements, some active links may not be able to cope with the additional interference. Hence, a new link may be admitted to the system even though it is not safe to admit it. This issue was dealt with extensively in [65], where the authors join the power and *admission control* problems. Thus, MSs not achieving their SINR targets and, hence, causing unrewarded interference in the network, would be dropped after a number of iterations in order to prevent further harm to other users. While this technique is fully distributed, some cooperation is necessary when the $P_{\max}$ constraint is implemented.

2.2.3.2 Power Control in Data Networks

In general, a data link does not necessitate a specific performance level for transmission, but instead utilises a tradeoff between the achieved SINR and the cost needed to achieve it [54]. Thus, the target of power control in data networks is not, as in voice, to provide a minimum signal level, but rather to maximise certain utilities that define the performance of a mobile data link. Loosely, the goal is the minimisation of transmission errors on each data link. Hence, there is never the question of whether a link should be removed or not. In this case, the active links may exhibit selfish behaviour, *i.e.*, maximising their own metrics, or take the performance of competing links into account and maximising a system metric, for example.

Note that for data-centric networks, a change of perspective is needed. In voice networks, individual link consideration is practically non-existent. All links desire to be transmitting, and from a system viewpoint, given a feasible power vector can be found for the specific set of links, this is the optimal solution. Even when a solution where all links are active is infeasible, the traditional approach is to still maximise the number of concurrently transmitting links.

However, since data links are capable of operating at any SINR level and the removal of links is no longer necessary for user satisfaction, individual user and system performance metrics can be utilised for coordination [54], *e.g.*, from the perspective of the operator, profit maximisation. On the other hand, game theoretic methods seem appropriate when MSs independently vary their transmission powers, with the various users competing amongst each other. In order to express such power control mechanisms, utilities, value and cost functions are considered.

In [66], a utility function is proposed that is based on the number of successfully transmitted information bits per Joule of energy spent. The problem is modelled as a non-cooperative game, where each link attempts to selfishly maximise its own utility. By posing the game as a collection of maximisation problems, the solution shows that if similar SINR-dependent performance metrics are used, the system converges to an SINR-balancing result. While desirable for voice networks, this Nash Equilibrium (NE) is suboptimal for data applications [54]. In essence, it may be preferable for a given link to achieve a lower SINR while improving its utility function. Thus, the SINR-balancing result can be seen as a local optimum to the problem, but not the global one. Furthermore, in [62], the higher the interference on a link, the higher the necessary transmit power to overcome it. However, this does not take into account the interference caused to other links, which is a vital parameter in data networks to achieve the target of minimising the number of transmission errors. Thus, in [66] a net utility function is developed which weighs the achievement of a user's SINR with the cost of increasing the transmit power. This NE leads to a more efficient network than the previously mentioned one, though proves rather unfair as different SINRs are allocated to each MS.

Finally, in [67] the concept of opportunistic power control is proposed. Here, SINR targets are decreased when channel conditions worsen and, consequently, so too are the associated transmit powers. The iterative algorithm is shown to converge for any initial power vector, as long as the game is feasible. Furthermore, this scheme can seamlessly integrate minimum SINR voice links into the system without risking their outage.

2.2.3.3 LTE Power Control

To conclude, the uplink power control mechanism that is envisioned for utilisation in LTE systems is discussed here. This bases on a form of FPC, which is given in [68] by

$$P^m_{\mathrm{dBm}} = \min\left\{\Gamma_{\mathrm{dB}} + I^m_{\mathrm{avg,\,dBm}} + \nu L_{\mathrm{des,\,dB}} + (1-\nu)L_{\mathrm{int,\,dB}},\ P_{\mathrm{max,dBm}}\right\}\ , \tag{2.1}$$

where

- P^m_{dBm} is the uplink power assigned to RB$_m$;
- Γ_{dB} is the nominal SINR target, which may be set as the user's target or the target at the cell-edge, depending on ν;
- $I^m_{\mathrm{avg,\,dBm}}$ is the (time-)average interference incident on RB$_m$. This is necessary in order to overcome CCI from neighbouring cells;
- $L_{\mathrm{des,\,dB}}$ is the desired link path loss, utilised to achieve the target SINR at the serving BS;
- $L_{\mathrm{int,\,dB}}$ is the interfering link path loss. This can be activated in order to take into account the interference to neighbouring cells; and
- $P_{\mathrm{max,dBm}}$ is the maximum transmission power allocatable to the RB.

Furthermore, the parameter ν allows to tune the power control equation between own-cell satisfaction and interference limitation. In general, however, depending on ν, (2.1) achieves a balance between conventional TPC (ν=1) and maximum power transmission (ν=0).

2.3 Recent Interference Coordination Research

In this section, an overview of more recent research into the topic of interference coordination is provided. While the techniques presented here are not yet practically implementable into wireless systems, they indicate promising directions for future research and implementation.

2.3.1 Stochastic Geometry

Stochastic geometry approaches attempt to model telecommunications network architectures for the purposes of strategic planning and economic analysis [69, 70]. In general, stochastic geometric models consist of representing the structural components of a network as realisations of stochastic processes. Other network characteristics such as BS placement and consequent cell sizes, traffic demand, and mobility are formulated as functionals of these processes and therefore are dependent solely on their distributions and parameters. Hence, stochastic models

avoid a detailed description of the network [70]. Overall, the goals of stochastic geometric modelling can be summarised as [69]

- the limitation of parameters solely to those necessary to determine the network optimal architecture;
- the provision of analytical expressions for performance metrics based on these parameters, thus allowing more effective comparisons to strategic alternatives; and
- the integration of natural constraints on the modelling of the physical network structure.

As mentioned before, the essential principle is the stochastic modelling of the spatial characteristics of the network. For example, a model of a typical cellular network should include stochastic descriptions for [70]

- BS locations;
- the road system;
- vehicle traffic on these roads; and
- the network management protocols such as resource allocation and handover.

Essentially, the modelling of these four areas can describe the operation of the entire network, reducing the need for a large number of parameters for the same description.

The utilisation of stochastic geometry for the specific modelling of mobile wireless networks has recently gained significant interest due to the necessity for more accurate and dynamic modelling techniques. In [71], the authors present an overview of the theory of stochastic geometry in collaboration with random graphs for the analysis and design of wireless networks. Where stochastic geometry enables to study the average behaviour over many spatial realisations of a network, random (geometric) graphs collar the distance-dependence and inherent randomness in node connectivity. On the other hand, in [72] the stochastic geometry tools are utilised to design a mathematical model of the coexistence of narrowband and ultrawideband users in HetNets. Cross-tier single- and aggregate-interferer error probability expressions are derived, indicating that classic spectral regulations based on individual transmit power budgets may not be sufficient for the management of interference in future HetNets. However, many of

the interdependencies between interfering users are not considered in the model, and hence the dynamics of the network are not accurately captured.

On the other hand, recent research has shown the emergence of stochastic geometric applications for network management and optimisation. Stochastic geometric modelling is utilised in [73] to optimise the number of transmitting elements in multicellular cooperative systems. In collaboration with inter-cell interference nulling, cluster formations and sizes can be tuned to provide capacity gains. In [74], sum rate maximisation through stochastic modelling is proposed, where the optimum number of concurrently transmitting links that achieves the maximum sum throughput is derived. The authors further suggest the application of such techniques to HetNets, although models for such networks may become highly complex and intractable. In general, however, it is clear that stochastic geometry can play a key role in the characterisation of the long-standing open problem of wireless system capacity [71], and further may provide significant assistance in the management of future mobile telecommunications networks.

2.3.2 Interference Alignment (IA)

In its simplest form, IA can be considered as a pre-coding technique for the *interference channel*. It is a cooperative transmission strategy that encodes signals linearly over multiple dimensions such as time and/or frequency resources, or antennas. The coding over multiple dimensions designs transmissions to align the interfering signals observed at each receiver into a lower dimensional subspace [75]. Through this procedure, interference alignment maximises the multiplexing gain (also known as degrees of freedom) over the K-user interference channel, *i.e.*, the number of non-interfering symbols that can be transmitted simultaneously. Interestingly, where orthogonal multiplexing techniques such as time division multiplexing (TDM) and FDM divide the spectrum (and, consequently, the achievable capacity per user) into K parts, the implementation of interference alignment allows for each of the K users to appropriate half of the total spectrum, and hence the sum rate can be described by

$$C_{\mathrm{IA}} = \frac{K}{2} \log_2 \left(1 + 2P_t\eta^{-1}\right) , \tag{2.2}$$

where $P_t\eta^{-1}$ represents the average link SNR. This, incidentally, is also the sum capacity of the symmetric interference channel: IA is capacity-optimal for this channel [76]. Furthermore, it is clear from (2.2) that C_{IA} scales linearly with the number of users K, whereas standard multiplexing schemes generally create a hard limit on capacity based on their resource division.

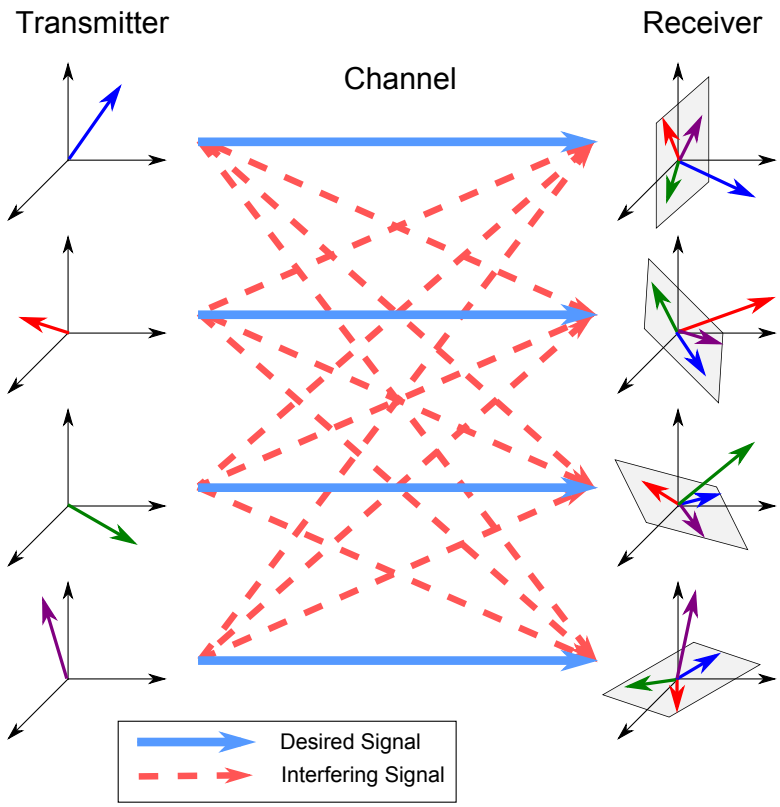

Figure 2.11: *An illustration of the IA concept. The transmitted signals are pre-coded in such a manner that the interference signals at each receiver align in a lower dimensional space. This leaves a free dimension for the user to decode its desired signal interference-free [77].*

As an example of the IA concept, consider the four user scenario in Fig. 2.11, where the coding of the real valued signals is performed over three dimensions and transmitted over real valued channels. In this system, each receiver observes three interfering signals from the other users, where each signal is represented by a vector in real three dimensional space. Without specific structuring, the three interference signals would not favourably align, and hence may occupy all three signal dimensions at the receiver [76, 78]. IA cooperatively pre-codes the user transmissions such that each set of three interfering signals becomes fully contained within a two dimensional space. Thus, by projecting the desired received signal onto the subspace orthogonal to the interference subspace, users can decode their messages free from interference.

While IA theoretically provides substantial benefits for wireless systems, it is based on some impractical assumptions that make its implementation difficult. Some of these challenges are discussed below [77]:

- **Dimensionality**: As IA functions on coding over multiple dimensions (see Fig. 2.11 for a three-dimensional example), it is clear that the more interferers that need to be mitigated, *i.e.*, the larger K, the more dimensions will be necessary to align the interfering signals. It has been shown in [75] that alignment in the frequency domain incurs a growth in the number of signaling dimensions that is *faster than exponential* with increasing K. This clearly poses a significant restriction on the applicability of IA to modern networks.

- **Channel Estimation**: Since IA bases on pre-coding, channel state information (CSI) estimation at the transmitter/receiver(s) is key to its performance. Hence, a sufficient portion of resources must be allocated for pilot transmission, and in some cases CSI feedback. This can cause substantial signalling burdens on the network, as an IA precoder must be modified whenever the channel conditions change appreciably.

- **Synchronisation**: Linear precoding in IA necessitates tight synchronisation between cooperating nodes, and hence can become susceptible to minor timing or carrier frequency offsets. In the presence of insufficient synchronisation, additional interference is induced in the system, rendering the IA solution ineffective.

- **Network Management**: In IA, cooperating nodes must not only synchronise, but also share CSI, negotiate physical layer parameters and potentially self-organise into smaller alignment clusters when full network alignment becomes too complex. Such coordination can prove difficult even in a centralised system, whereas distributed network protocols must be modified to function within this more cooperative physical layer.

Therefore, it can be concluded that while IA has great potential for future wireless systems, there are many impractical assumptions necessary for its functionality that need to be overcome.

2.3.3 Coordinated Multipoint Transmission (CoMP)

One of the most fervently discussed topics for cooperative multicellular communication in future networks is that of CoMP [79], where neighbouring BSs transmit together to multiple users in their cells. In CoMP, MSs in neighbouring cells are grouped based on the received pilot signal strength from the surrounding BSs, *i.e.*, users are grouped if the strongest BSs they see are identical. Once these groups are formed, each of the MSs in each group is served simultaneously by these BSs. (see Fig. 2.12). Consequently, the BSs jointly pre-code their transmissions

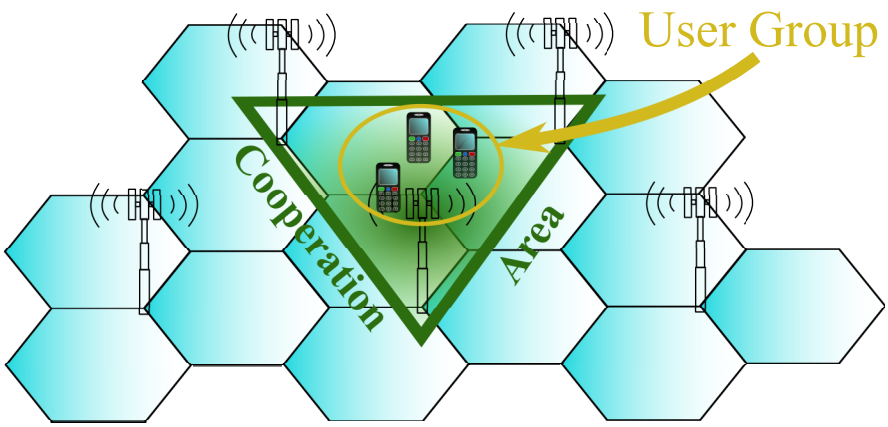

Figure 2.12: *A visualisation of CoMP, where the users within neighbouring cells, that experience identical sets of strongest BSs, can be served simultaneously and cooperatively by this set of BSs, eliminating interference from what would be the strongest interfering cells [80].*

to the user group such that the combined received signal from the set of BSs at each MS provides the user with its desired signal (*i.e.*, that would have been transmitted from its serving BS), without receiving any interference from the other cells in its set of strongest BSs. In [81], the combination mechanisms of such pre-processing techniques are described and compared:

- **Joint TDMA (J-TDMA)** - Only one MS in the user group is served in each time slot. Thus, transmission is automatically CCI-free, at the cost of reduced spectral efficiency.
- **Joint zero-forcing (J-ZF)** - The joint pre-coding matrix $\mathbf{M}=\mathbf{H}^H\left(\mathbf{H}\mathbf{H}^H\right)^{-1}$ is the pseudo-inverse of the aggregate channel matrix $\mathbf{H}$, where H denotes the hermitian operator, such that each user only receives a noisy version of its intended data. However, just as ZF receivers amplify noise, J-ZF pre-coding generally increases the average transmit power.
- **Joint minimum mean-square error (J-MMSE)** - This pre-processing achieves a compromise between CCI cancellation and transmitter power efficiency. Based on the MMSE criterion, the pre-coding matrix is given by $\mathbf{M}=\mathbf{H}^H\left(\mathbf{H}\mathbf{H}^H+\eta\mathbf{I}\right)^{-1}$.

Essentially, CoMP eliminates the interference from what would normally be the most strongly interfering BSs, consequently enhancing SINR and thus throughput at each MS.

A common problem in the CoMP concept is that the gain strongly relies on ideal "user centric" clustering and assignment, meaning all MSs should be served by their individual set of strongest cells. In a large network with irregularly distributed MSs in the cells, the difficulty is to find

sufficient users with these sets being identical, since due to shadowing the signal strength of BSs might be widely distributed. Thus, the typical penetration rate of MSs that might be served by such a single specific set of cells is often very small, causing many users to be denied service. In [80] partial CoMP, where shifted coverage areas increase the probability of MSs sharing a set of strongest cells, is suggested to alleviate this problem. While the performance gains of partial CoMP can surpass those achievable via full CoMP, the additional signalling and complexity must be compensated by limiting transmission of reference signals by the MSs. Nonetheless, large SINR and throughput gains are achieved by both schemes.

While CoMP does not achieve the performance of system optimisation (*i.e.*, albeit at significantly reduced complexity), it is able to provide large gains over user-based cooperation schemes. Unfortunately, a substantial increase in signalling over traditional inter-cell cooperation techniques is necessary to facilitate CoMP. Nevertheless, this is true for most of the recent multi-cell cooperation techniques, as the "simple" solutions are no longer sufficient to provide the large throughput demands of today's networks. Moreover, it is evident that user clustering techniques will need to be optimised to enhance CoMP performance. In general, however, it is clear that multicellular cooperation will be paramount to the performance and development of future wireless communications networks.

2.3.4 Fuzzy Logic Control

Most recently, the utilisation of *fuzzy logic* for network optimisation and operation has attracted considerable interest among researchers. In fuzzy logic, an input range is divided into multiple "membership functions" which give a coarse evaluation of the variable rather than a continuous measurement [82]. In addition, multiple inputs (*i.e.*, specifically, their membership functions) may be combined via simple AND and OR operations describing the relationship between the variables in order to produce the needed output decision. Through this, combining multiple (sometimes interdependent) input variables can be performed at significantly reduced complexity, and furthermore the direct application of "human expertise" to machine decision-making entities can be achieved. Whereas classical control methods necessitate analytical task models, fuzzy controllers are usually designed by expressing the way that experts make decisions in the rule base [83].

An example of a fuzzy logic controller is shown in Fig. 2.13, where the temperature and pressure information from a steam turbine are combined to control its throttle setting. In the figure,

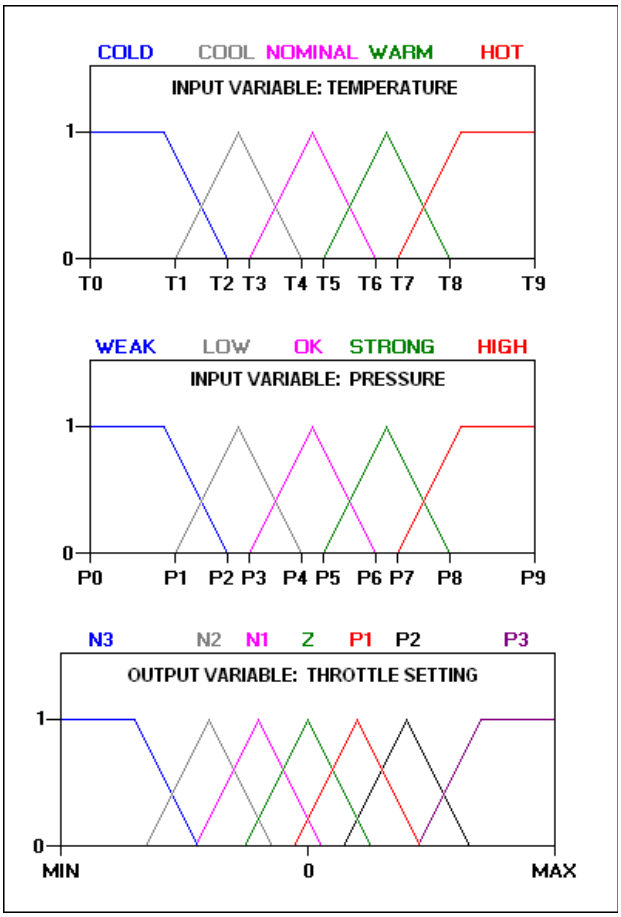

Figure 2.13: *Example of a fuzzy logic control system designed to regulate the driving of a steam turbine. The temperature and pressure inputs are combined to determine turbine throttle setting.*

it is clear that rather than utilising continuous variable inputs, both the temperature and pressure ranges are subdivided into multiple membership functions coarsely describing the state of the variable. This allows rules combining the variables to be designed such as, *e.g.*, "if temperature is HOT and pressure is HIGH then set throttle to N3," reflecting the actions that would be taken if a human was driving the turbine. By extension, a multitude of input variables can be compounded to determine multiple outputs, and hence control much larger systems. A detailed description of the fuzzy logic theory can be found in [82].

The application of fuzzy logic in collaboration with reinforcement learning techniques is comprehensively studied in [83], in order to tune the outputs of fuzzy inference systems. In general, fuzzy learning techniques are split into two phases: the first phase to optimise the number of membership functions and rules for each input, and second to tune the actual positions of the

input and output fuzzy sets. On the other hand, the application to wireless network coordination is investigated in [84–86], where fuzzy logic reduces the complexity of the learning algorithms by providing coarse evaluations of the network state. On a cell-individual basis, by adapting subband transmission powers [84], adjusting the antenna downtilt [85], or modifying the downlink relative narrowband transmit power (RNTP) thresholds [86] the interference on specific resources can be controlled or removed completely. However, QoS requirements of individual users are neglected, a perspective that is addressed in Chapter 6 of this thesis.

Finally, the application of fuzzy logic in this thesis is seen as a step towards the utilisation of machine learning to resolve the multidimensional optimisation problem that is a mobile wireless network. While some research in this direction has been performed for wireless sensor networks [87–89], such approaches have been scarcely investigated for cellular communications [90]. However, the ability of fuzzy logic and machine learning techniques to amalgamate a multitude of variables and parameters to perform multidimensional decision-making implies great potential for their utilisation in future wireless networks.

2.4 Heterogeneous Networks

Future wireless communications systems are moving towards heterogeneous architectures, where within a cell a user may connect to over four different types of APs (*e.g.*, macro-, pico-, femto-cells, relays and/or remote radio heads (RRHs)) [6]. Intuitively, this has many positive effects for a MS, which can now choose among several connections to find the most suitable one. Furthermore, users benefit from an even greater spatial reuse of resources, in effect the frequency reuse factor can be said to much less than one. The types of nodes considered in HetNet deployment and their specification are shown in Table 2.1 [6, 91]. Although, it should be mentioned that in this thesis, HetNets employing only pico- and femto-cells are considered.

Node/AP	Transmit Power	Coverage	Backhaul
Macro-cell	46 dBm	Few km	S1 Interface
Pico-cell	30(37) dBm	300(500) m	X2 Interface
Femto-cell	< 23 dBm	< 50 m	DSL/Broadband
Relay	30 dBm	300 m	Wireless
RRH	46 dBm	Few km	Fiber

Table 2.1: *HetNet AP Specifications*

Through the various types, locations and dense deployment of APs, and the different transmission powers/ranges associated with them, numerous technical challenges are posed by femto/pico-cell overlays [6, 18, 19], *e.g.*, cell-organisation/optimisation, resource assignment to users, and especially interference coordination between APs within the same and neighbouring cells. Furthermore, it is clear standard frequency reuse and/or ICIC techniques only go so far in dealing with these new challenges. These mainly fall into the following areas:

- *Network self-organisation* - Self-configuration, -healing, and -optimisation are required of all cells. These tasks become increasingly difficult given the additional number of network parameters that need to be considered.
- *Backhauling* - The connection of the different BSs to the core network (CN) necessitates extra infrastructure. For femto-cells in particular, the long delay via wired backhauls complicates macro-femto ICIC [19].
- *Handover* - The higher number of APs clearly increases the amount of handover decisions in the network, imposing further additional signalling on the CN.
- *Interference* - Cross-tier interference created to/from the overlaid cells (*e.g.*, pico-/femto-cells) must be mitigated to maintain performance, especially if access to these cells is restricted. High intra-tier interference due to dense deployment is also of concern.

Especially the handling of interference within and across tiers is paramount to the performance of such future wireless networks. The main sources of interference in HetNets [6] can be categorised and broken down as follows:

- Unplanned deployment
  - Low-power nodes such as femto-cells are deployed by end-users at “random” locations, and can be active/inactive at any time, further randomising their interference.
  - Due to backhauling difficulties (such as a non-operator DSL connection), interference coordination with femto-cells may not be possible.
  - Continuous sensing and monitoring is required by cells to dynamically/adaptively mitigate interference from the other tiers.
  - Intra-tier interference is of major concern mainly within densely deployed femto-cells.

- Closed-subscriber access
  - Restricted access control of pico- and femto-cells may lead to strong interference scenarios in both the downlink and uplink if users cannot handover.
  - This will cause large interference at MSs that are near femto-, pico-cells but cannot access them.
- Node transmission power differences
  - The lower power of nodes such as pico- and femto-cells can cause association issues, and also downlink/uplink interference problems, *e.g.*, a mobile near a pico-cell connected (in the downlink) to a high-power macro-BS may cause large uplink interference at the pico-cell.

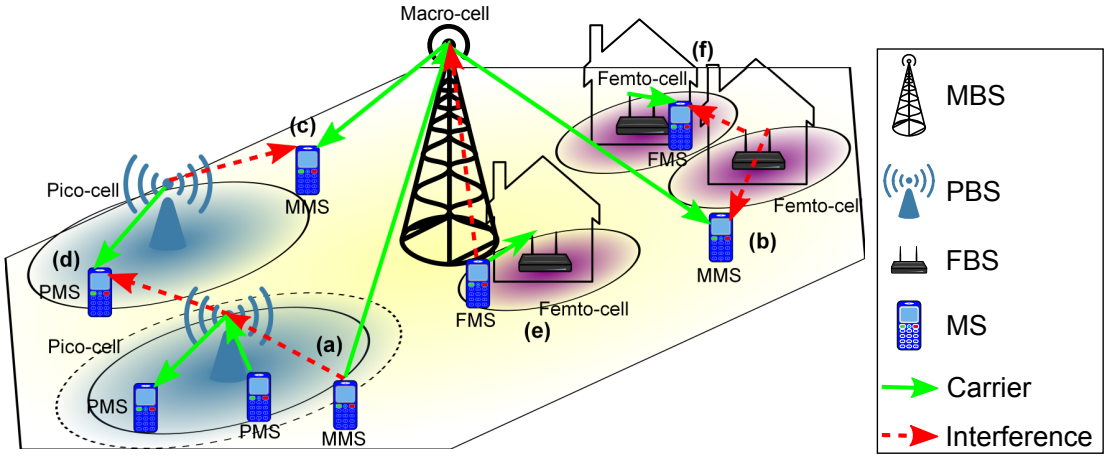

Figure 2.14: *Typical deployment in HetNet cell: cross-tier and intra-tier interference can lead to undesired performance degradation, user outage, and cell association issues [6].*

A detailed illustration of the interference environment in a HetNet cell containing PBSs and femto-cells is portrayed in Fig. 2.14. The interference scenarios depicted can be described as follows:

(a) Uplink interference caused at a PBS by a nearby MMS transmitting to the MBS. The range expansion is not large enough to connect the MS to the pico-cell.

(b) Downlink interference at a MMS, which is located close to a building containing FBS(s). Due to closed subscriber access, the MMS cannot connect to the femto-cell.

(c) A MMS with close proximity to a pico-cell receives downlink interference from the PBS.

(d) A MS connected to the pico-cell receives downlink interference from the neighbouring PBS. This situation is rather unavoidable, as connecting to the other PBS would simply swap the carrier and interference signals.

(e) A FMS being served in the uplink by a femto-cell located near the MBS can cause severe interference to MMSs requesting co-channel uplink resources.

(f) Finally, co-located femto-cells may significantly interfere with each other in both the downlink (shown here) and uplink. Even open access FBSs may not be able to alleviate this scenario.

These are just a few of the many cross-tier ((a), (b), (c), and (e)) and intra-tier ((d) and (f)) interference scenarios that arise in such densely deployed HetNets. Thus, this calls for more sophisticated and efficient ICIC techniques that should, ideally, limit the additional signalling in an already highly burdened CN.

2.4.1 The Almost-Blank Subframe (ABS)

The state-of-the-art interference coordination for LTE HetNets is the ABS: a time-domain ICIC technique where an aggressor BS creates "protected" subframes for a victim BS by reducing its transmission activity on these [92]; the occurrences of the ABSs are known *a priori* at the coordinating BSs. Thus, throughput improvements are induced via the provided interference protection [93]. However, the omitted transmission frames may have adverse affects on the data rates at the aggressor BS. Fig. 2.15 depicts a typical ABS slot [6].

In general, ABSs are utilised to prevent high interference to a nearby MS between different tiers in the HetNet, *e.g.*, a macro-user in the downlink situated in close proximity to a closed-access femto-cell (scenario (b) in Fig. 2.14), or also for smaller cell MSs experiencing high interference from a nearby MMS (scenario (a) in Fig. 2.14). However, intra-tier interference may also be mitigated through ABS transmission.

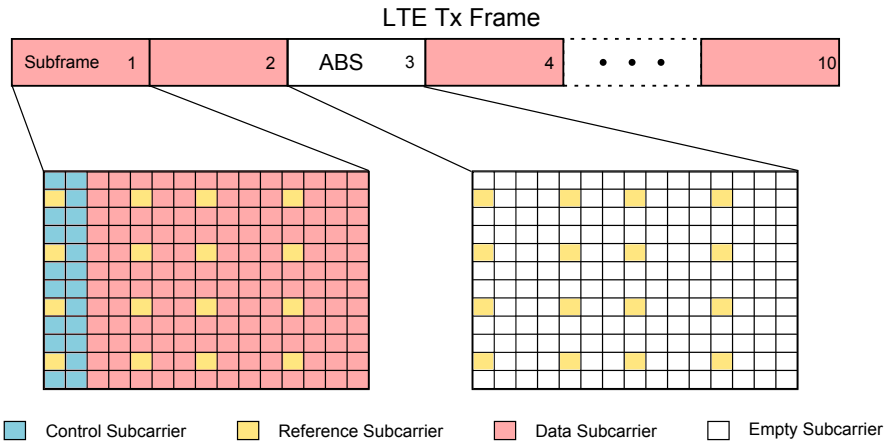

Figure 2.15: *ABS transmission for interference protection in HetNets. The position(s) of the ABS slot(s) are communicated between BSs via the network backbone.*

2.4.2 Femto-Cell Deployment

FBSs are defined in this context as low-cost, low-power, short range, plug-and-play BSs that operate in the licensed spectrum and aim to extend and enhance macro-cell indoor coverage. They utilise cable Internet or broadband DSL connections to backhaul to the CN of the operator [94], and exhibit a range typically in the tens of meters. Femto-cells were initially designed to provide improved and personalised indoor coverage in residential settings. However, recent research extends the applicability of these BSs to office, metropolitan and even campus deployments [95].

It can be argued that the utilisation of femto-cells, and smaller cells in general, is paramount to providing the near infinite bandwidth requirements for future wireless networks [96]. Furthermore, femto-cells are in a unique position to offer ubiquitous high-speed data access by providing a localisation of radio resources, where the shared use of bandwidth in macro-cellular networks can be replaced with a more personal utilisation of frequencies. Moreover, this personalisation of mobile access creates the potential for new consumer-based products that can target the extensive tail distribution of consumer desires [97], thus enhancing consumer reach and reducing complexity at the operator-side. Finally, femto-cells may be able to utilise higher frequency bands (due to low coverage requirements) which are more suited for high data rate services and can isolate the femto-cells from the main mobile network. Through this, small/femto-cell deployment can be developed as a complementary driver to standard mobile cellular networks [95].

From the standpoint of network operators, femto-cell deployments offer a multitude of benefits. Primarily, large portions of mobile traffic can be offloaded from the macro-network to personal [98], home BSs as a significant amount of calls made within cellular networks originate from the home or workplace. Research in [99] indicates that operators' network costs may be reduced by up to 70% by shifting traffic to FBSs. This is especially the case when high rate services such as Internet or multimedia applications are concerned. Finally, the fact that femto-cells operate with unmodified mobile devices is an important advantage over competing technologies such as Unlicensed Mobile Access (UMA), which requires terminals to cooperate with a variety of multiple access techniques [95, 100]. These multimode devices can become very expensive and present higher rates of battery drain due to increased complexity.

In summary, the key advantages of femto-cell deployment for future networks are as follows [4]:

- **Enhanced capacity and coverage**: Through femto-cell deployment, the spatial reuse of resources is greatly enhanced. Furthermore, due to their short link-distances, femto-cells can provide high SINRs at greatly diminished transmit powers [101], prolonging handset battery life. The lower transmit powers generate significantly less interference to neighbouring wireless users, and femto-cells themselves are protected by wall penetration losses and outdoor propagation. Finally, as each FBS generally only serves a handful of users, significantly larger portions of both transmit power and bandwidth can be allocated to FMSs in comparison to MSs in the macro-layer.

- **Benefits to the macro-cell**: Due to the origination of a significant portion of traffic indoors, this can now be served by femto-cells, substantially reducing the burden on the macro-cell, which would anyhow suffer from penetration losses to indoor users. This allows the macro-cell to rededicate the additional resources towards providing better performance for mobile MMSs, especially at the cell-edge [102].

- **Operator cost reduction**: Finally, the deployment of femto-cells will reduce the operational expenditure (OPEX) and capital expenditure (CAPEX) of network operators [94], as in general FBSs are installed at the customer-side. Therefore, not only will operators be alleviated of the burden of installing additional BSs for enhanced wireless coverage, but also the operational costs including additional electricity, maintenance and service. A recent study [103] concludes that the OPEX per macrocell (typically $\$60,000$ per year) is reduced to just $\$200$ per year per femto-cell, a more than significant saving.

2.5 Motivation

The evolution of mobile telecommunications services from 3G technologies (*e.g.*, UMTS, wCDMA, cdma2000) to LTE and beyond (*i.e.*, 4G) marks the next significant progression of ICT. The higher rates and enhanced coverage envisioned in LTE and LTE-A are facilitated through further cell size reduction, full frequency reuse, and intelligent interference management and power control techniques [9]. Furthermore, the goals for increased spectral efficiency are compounded with a vision for more energy efficient networks. In this thesis, three areas of research for these future (it should be mentioned that LTE networks have already been rolled out in Europe and Asia, along with the U.S.A. [2]) networks are identified, and more specifically, three network scenarios. The consideration, and mainly, development of ICIC for these three scenarios is described below.

The **dense, urban macro-cellular** deployment projected in LTE networks, coupled with the intent of full frequency reuse, induces high CCI and energy consumption in localised areas. This can be extremely detrimental for mobile service, especially in the uplink. The development of traditional power control techniques [68, 104] only goes so far in dealing with such high interference scenarios. While TPC has evolved from the conventional SNR-driven techniques to additionally considering interference to other cells, it has been shown that in many cases such techniques can simply converge to full power transmission [15], and break down. Therefore, interference protection in the uplink for mainly cell-edge MSs, but theoretically for all users in each cell, is investigated in Chapter 4. On the other hand, generic power control for CDMA systems (which can easily be extended to OFDMA due to orthogonality of subcarriers), where interfering users' SINR targets are met with minimum power [15], is suggested, however also breaks down in high interference environments. In [105], various techniques to enhance the functionality of this power control are proposed, although mainly base on optimisation in *ad hoc* networks, reducing their relevance for LTE cellular communication. However, it is clear target fulfilment combined with minimum power is highly desirable for future networks, and thus Chapter 5 addresses the adaptation of POPC [15] to the aforementioned scenario, presenting a centralised technique applicable for both the uplink and downlink.

The second scenario of interest is depicted in Fig. 2.14, point (f), the matter of interference coordination for **dense, random femto-cellular** deployments. While abundant research on femto-to-macro interference has been carried out [106, 107], few techniques have been considered to manage the intra-tier interference between several densely deployed FBSs. Furthermore, due

to full frequency utilisation, high interference is present in such scenarios, and hence efficient power control is necessary to combat these undesirable effects. In the second part of Chapter 5, the macro-cell technique presented earlier in the chapter is modified and, hence, extended to the femto-cell scenario for power and interference management in such dense deployments. Another potential challenge in femto-cell networks originates from the backhaul connection through a subscriber's DSL connection. Due to inter-operator communication or high traffic loads, such a backhaul connection can become highly latent and unreliable [6], which may complicate both cross- and intra-tier interference coordination. For this reason (and the general complexity of HetNets), the final chapter of this thesis investigates distributed and autonomous resource and power allocation for femto-cellular networks. While research in this field has begun to grow in recent times [108, 109], most of these methods still rely on inter-BS signalling, an assumption that is removed in Chapter 6.

Finally, the evolution towards the **HetNet** scenario is examined in the second part of Chapter 6, which can be viewed essentially as an amalgamation of the two previously considered scenarios. The compressed deployment of BSs, consequent aggregated spatial reuse of resources, and the resulting complication of the interference environment greatly enhance the difficulty for efficient performance of ICIC techniques [6, 18, 19]. Furthermore, it is clear from Section 2.4 that decentralisation will be key in maintaining the effectiveness of such networks [110]. Thus, the final part of Chapter 6 culminates in the extension of the distributed and autonomous resource management methodology, introduced earlier in the chapter, to application in HetNets. Through the analysis and investigation of the three aforementioned scenarios, this thesis provides significant bases for ICIC utilisation and further development in 4G mobile communication networks and beyond.

2.6 Summary

In this chapter, the history of mobile communications was reviewed and the evolution of mobile networks from 1G to LTE and beyond was presented. Following this, a detailed overview of the key concepts upon which this thesis bases is given. The relevant multiple access techniques are discussed, the evolution of frequency reuse is presented, along with a description of power control methodology. In addition, a brief overview of more recent research topics is presented. Moreover, the deployment and challenges of HetNets and femto-cells were highlighted. Finally, the motivation for the following chapters in this thesis is portrayed.

Chapter 3
Investigated System and Simulation Environment

3.1 Overview

This chapter provides an in-depth description of the system environment and performance metrics utilised throughout this thesis. Furthermore, the simulation(s) and benchmarks utilised for performance evaluation in each of the technical chapters in this thesis are described.

The work in this thesis concentrates on LTE and LTE-A networks. Therefore, an OFDMA network is considered, where the system bandwidth B_{sys} is divided into M RBs. A RB defines one basic time-frequency unit of bandwidth $B_{\text{RB}}{=}{}^{B_{\text{sys}}}/_{M}$. Each BS-type (*i.e.*, MBS, PBS, FBS) transmits at a fixed maximum downlink power $P_{\text{max},\hat{b}}$, where $\hat{b} \in \{\text{MBS, PBS, FBS}\}$. Further, each MS-type (*i.e.*, MMS or FMS) is allocated a maximum uplink power $P_{\text{max},\hat{m}}$, where $\hat{m} \in \{\text{MMS, FMS}\}$. Perfect time and frequency synchronisation is assumed.

3.2 System and Channel Model

Universal (*i.e.*, full) frequency reuse and FDD is considered, such that each cell utilises the entire system bandwidth B_{sys}. The set of RBs $\mathcal{M}$, where $|\mathcal{M}| = M$, is distributed by each BS to its associated MSs. Throughout this work, u defines an MS, and v_u the BS with which this MS is associated. The received signal observed by MS$_u$ from BS$_{v_u}$ on RB$_m$ is given by

$$Y_u^m = \underbrace{P_u^m G_{u,v_u}^m}_{S_u^m} + I_u^m + \eta\,, \tag{3.1}$$

where G_{u,v_u}^m signifies the channel gain (including fading and shadowing effects) between the MS$_u$ and its serving BS$_{v_u}$, observed on RB$_m$. Furthermore, P_u^m denotes the transmit power allocated to MS$_u$ on RB$_m$, S_u^m the desired received power, $\eta{=}\eta_0 B_{\text{RB}}$ the thermal noise, η_0 is the noise spectral density, and I_u^m is the co-channel interference received on RB$_m$ from MSs in

neighbouring cells, defined by

$$I_u^m = \sum_{i \in \mathcal{I}_m} P_i^m G_{u,v_i}^m \,, \tag{3.2}$$

where $\mathcal{I}_m$ represents the set of co-channel interferers (*i.e.*, set of MSs in neighbouring cells that are also assigned RB$_m$). Hence, the SINR observed at the MS$_u$ on RB$_m$ is calculated by

$$\gamma_u^m = \frac{S_u^m}{I_u^m + \eta} = \frac{P_u^m G_{u,v_u}^m}{\sum\limits_{i \in \mathcal{I}} P_i^m G_{u,v_i}^m + \eta} \,. \tag{3.3}$$

It should be mentioned that (3.1)-(3.3) are given for the downlink, however are equivalent in the uplink when $G_{v_u,i}^m$ is utilised. Following this, the *user throughput* C_u is calculated as the data transmitted on the RBs assigned to MS$_u$

$$C_u = \sum_m^{n_u^{\mathrm{RB}}} k_{\mathrm{sc}} s_{\mathrm{sc}} \varepsilon_{\mathrm{s}}(\gamma_u^m) \,, \tag{3.4}$$

where n_u^{RB} is the total number of RBs allocated to MS$_u$, k_{sc} the number of subcarriers per RB, s_{sc} the symbol rate per subcarrier, and $\varepsilon_{\mathrm{s}}(\gamma)$ the symbol efficiency (*i.e.*, modulation and coding order), dependent on the achieved SINR γ, given in Table 3.1[1]. Finally, the system throughput is the sum rate of all MSs in the network

$$C_{\mathrm{sys}} = \sum_u C_u \,. \tag{3.5}$$

The *energy efficiency* β_u measures the data rate per unit of transmit power (or, alternatively, the data sent per unit of energy) of MS$_u$. This is defined as follows:

$$\beta_u = \frac{C_u}{P_u} = \frac{\sum_m^{n_u^{\mathrm{RB}}} k_{\mathrm{sc}} s_{\mathrm{sc}} \varepsilon_{\mathrm{s}}(\gamma_u^m)}{\sum_m^{n_u^{\mathrm{RB}}} P_u^m} \quad \left[\frac{\mathrm{bits/s}}{\mathrm{W}}\right] \equiv \left[\frac{\mathrm{bits}}{\mathrm{J}}\right] , \tag{3.6}$$

where P_u is the transmit power, and C_u the achievable capacity from (3.4).

Lastly, Jain's Fairness Index [112] is used to calculate the *throughput fairness* of the system in each time slot

$$\Pi(\mathbf{C}) = \frac{\left[\sum_u C_u\right]^2}{|\mathbf{C}| \sum_u C_u^2} \,, \tag{3.7}$$

[1] In Table 3.1, the modulation and coding schemes (MCSs) are taken from LTE [9], and the SINR ranges from [111]. In general, these values are operator specific, and hence are not standardised.

where $\mathbf{C}$ denotes the throughputs of all MSs in the system, and $|\cdot|$ is the cardinality operation. While other fairness measures exist such as statistical variance, the coefficient of variance, max-min fairness [113], or normalised distance from the optimum; in this thesis Jain's index is utilised due to its independence of scale and vector size, range between zero and one, and intuitive relation to user perception [114].

As an example, consider a multi-link system, where each user exhibits different channel conditions. It would be capacity-optimal to give the entire bandwidth to the MS closest to the BS, however this would be highly unfair and result in a very low $\Pi \rightarrow 0$. On the other hand, allocating bandwidth and power by the inverse of the path gains would allow the users to achieve similar performance, and result in $\Pi \rightarrow 1$.

CQI index	min. SINR [dB]	Modulation	Code rate	Efficiency ε_{s} [bits/sym]
0	-	None	-	0
1	-6	QPSK	0.076	0.1523
2	-5	QPSK	0.12	0.2344
3	-3	QPSK	0.19	0.3770
4	-1	QPSK	0.3	0.6016
5	1	QPSK	0.44	0.8770
6	3	QPSK	0.59	1.1758
7	5	16QAM	0.37	1.4766
8	8	16QAM	0.48	1.9141
9	9	16QAM	0.6	2.4063
10	11	64QAM	0.45	2.7305
11	12	64QAM	0.55	3.3223
12	14	64QAM	0.65	3.9023
13	16	64QAM	0.75	4.5234
14	18	64QAM	0.85	5.1152
15	20	64QAM	0.93	5.5547

Table 3.1: *Adaptive Modulation and Coding Table*

Channel Model In general, the channel gain, $G_{k,l}^{m}$, between a transmitter l and receiver k, observed on RB$_m$ is determined by the path loss, log-normal shadowing, and channel variations caused by frequency-selective fading:

$$G_{k,l}^{m} = \left|H_{k,l}^{m}\right|^2 10^{\frac{-L_s+X_\sigma}{10}}, \tag{3.8}$$

where $H_{k,l}^{m}$ describes the channel transfer function between transmitter l and receiver k on RB$_m$, L_s=$L_d(d)$+$L_\theta(\theta)$ is the path loss (in dB), $L_d(d)$ is the distance dependent path loss, $L_\theta(\theta)$ is attenuation due to angular separation, and X_σ is the log-normal shadowing value (in dB) with standard deviation σ, as described in [115]. The channel response exhibits time and frequency dispersions, however channel fluctuations within a RB are not considered as the RB dimensions are significantly smaller than the coherence time and bandwidth of the channel [116]. Furthermore, the path loss $L_d(d)$ is identical on all RBs assigned to the MS. Finally, the delay profiles used to generate the frequency-selective fading channel transfer factor $H_{k,l}^{m}$ are taken from suitable propagation scenarios in [115], [117].

The path loss model used to calculate $L_d(d)$ is for indoor and outdoor links [118] and calculates the path loss as

$$L_d(d) = \alpha + \beta \log_{10}(d) \quad [\text{dB}]\,, \tag{3.9}$$

where d is the distance between transmitter and receiver, and α, β are the channel parameters. Furthermore, the signal attenuation from a macro-BS due to horizontal angular separation from the central lobe, $L_\theta(\theta)$, is given by

$$L_\theta(\theta) = \min\left(12\left(\frac{\theta}{\theta_{3\text{dB}}}\right)^2, A_\text{m}\right) \quad [\text{dB}]\,, \tag{3.10}$$

where θ is the angle the MS-BS link deviates from the central lobe, $\theta_{3\text{dB}}$ is the angle at which the gain is half that of at the centre of the lobe, and A_m=20 dB is the maximum possible attenuation [118].

Finally, log-normal shadowing is added to all links through correlated shadowing maps. These are generated such that the correlation in shadowing values of two points is distance-dependent.

3.3 Simulation

Monte Carlo simulations are used to provide performance statistics of the proposed ICIC techniques. The simulator is built following LTE specifications. It should be mentioned that while the general simulation composition is described here, each chapter will provide a brief summary of its specific environment, and all relevent simulation parameters employed.

For each simulation, 2000 scenarios are generated to remove the random effects from MS/BS

placement, lognormal shadowing and frequency selective fading. These results are then combined to acquire statistically relevant performance measurements of the system.

3.3.1 Network Construction and User Distribution

Three scenarios are investigated in the course of this project, and ICIC techniques are developed and evolved for each. Initially, a dense, small cell, and therefore high-interference **macro-cellular** environment is examined, followed by a transition to **femto-cellular** deployment. Finally, a **HetNet** served by macro-, pico- and femto-cells is considered. These scenarios are selected based on the forecast for future wireless networks, where smaller cell sizes and femto-cell deployment are envisioned to improve network throughput and energy efficiency [101, 119], and finally evolving to heterogeneous architectures with multiple types of APs available to users [6]. The constructions of these three scenarios are discussed in detail below.

3.3.1.1 Macro-cellular Network

The simulation area is comprised of a single-tier, *tessellated hexagonal cell* distribution. Each cell is served by a sector of a MBS, where a MBS has three $120°$ sectors. Each MBS is placed at the junction of the three hexagonal cells it serves. The size of the macro-cells is parametrised by the inter-cell distance (ICD), which is equivalent to $1/\sqrt{3}$ of the inter-site distance (ISD).

To eliminate border effects with regards to interference, an additional two tiers are simulated. However, statistics are only taken from the first tier (and centre cell). Users are distributed uniformly over the simulation area such that each cell hosts, on average, $\bar{N}$ MMSs. Further, MBS-MMS allocation is done based on path loss, such that each MMS is assigned to the MBS with the most favourable channel conditions.

3.3.1.2 Femto-cellular Network

A 5×5 apartment grid is considered for the femto-cell scenario, where the probability p_{act} describes the likelihood of an active FBS in a given apartment. It is assumed that multiple FMSs may be present in an apartment. As it is unlikely all cells will have the same number of FMSs, the user generation is implemented via probability table, where depending on the maximum number of users $\tilde{\mu}(u)$ allowed per cell, the number of FMSs $n_c(u)\in\{1,\ldots,\tilde{\mu}(u)\}$ present in

cell c is randomly chosen. Table 3.2 gives two examples of probability tables[2], where *a)* equal probabilities are given to all $n(u)$, or *b)* the probability reduces with each additional MS. An

$\tilde{\mu}(u)$	1	2	3	4
$p_{n(u)=1}$	1	1/2	1/3	1/4
$p_{n(u)=2}$	0	1/2	1/3	1/4
$p_{n(u)=3}$	0	0	1/3	1/4
$p_{n(u)=4}$	0	0	0	1/4

or

$\tilde{\mu}(u)$	1	2	3	4
$p_{n(u)=1}$	1	2/3	4/7	8/15
$p_{n(u)=2}$	0	1/3	2/7	4/15
$p_{n(u)=3}$	0	0	1/7	2/15
$p_{n(u)=4}$	0	0	0	1/15

Table 3.2: *Probability tables for the number of users allocated in a single femto-cell.*

example of such a scenario is shown in Fig. 3.1. In each active femto-cell, both the FMSs and

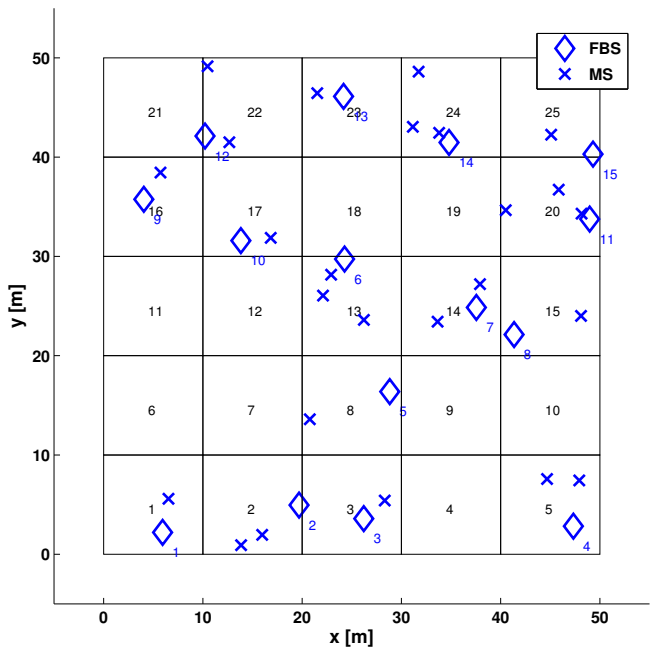

Figure 3.1: *Apartment block scenario with* $p_{\mathrm{act}} = 0.5$*, where each apartment is* $R_{\mathrm{a}} \times R_{\mathrm{a}}$ *with* R_{a}=10 *m, with* $\tilde{\mu}(u)$=3 *and equal user number probabilities.*

FBS are uniformly distributed in the apartment. Due to the private deployment of femto-cells a closed-access system is assumed, so each FMS is assigned to the FBS in its apartment, even if a foreign cell exhibits superior link conditions.

[2]In general, a femto-cell is assumed to contain only a single user for the majority of time, however it is considered that femto-cells can host up to four FMSs [4]. Therefore, the probability tables may actually be determined through statistical analysis of femto-cell usage. In this thesis, equal probabilities are utilised to increase the number of MSs in the scenario, and consequently complicate scheduling procedures.

3.3.1.3 Heterogeneous Network

The HetNet deployment consists of a macro-cellular basis, pico-cells to enhance outdoor/macro-user coverage, and femto-cells to serve traffic from indoor MSs. The macro-cellular layout is described in Section 3.3.1.1.

Pico-cells In each macro-cell, N_{p} pico-BSs are placed at a distance $\hat{d}$ from the centre of the cell, and at a uniformly distributed angle $\left|\hat{\phi}\right| \leq \frac{2\pi}{3}$ from the central lobe of the serving macro-sector. The constraint is placed on $\hat{\phi}$ such that a PBS is not placed near the MBS, which would clearly be unrealistic. The PBSs are assumed to utilise omnidirectional antennas, and hence do not suffer from angular signal attenuation (*i.e.*, $L_{\theta}(\theta)$=0 dB). Finally, since BS-MS allocation is done based on path loss, MMSs can now be served by either a MBS or PBS dependent on the received reference signals.

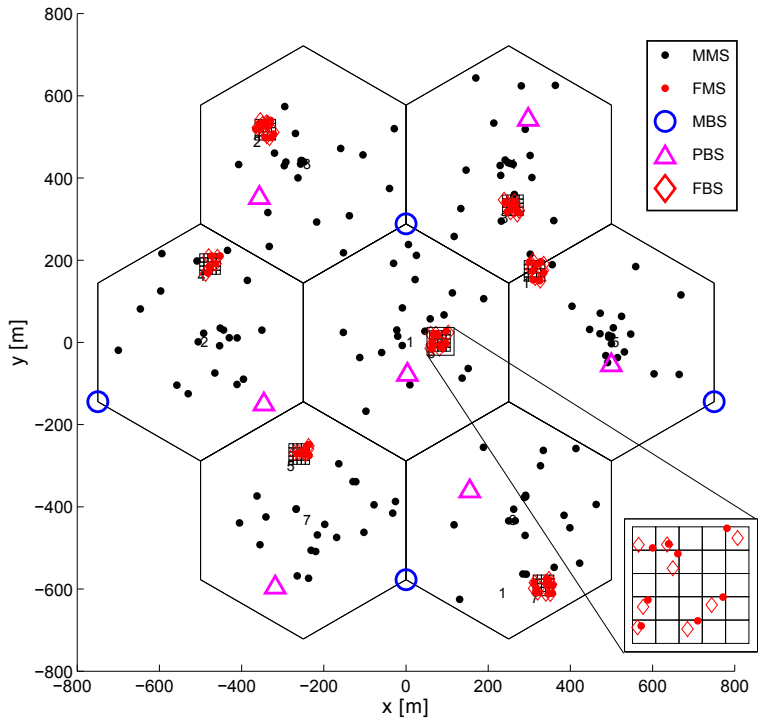

Figure 3.2: *Example of a HetNet construction for an ICD of* 500 *m, where each macro-cell contains* $\bar{N}$=20 *MSs,* N_{p}=1 *PBS to enhance the available resources, and* N_{app}=1 *apartment block with* p_{act}=0.25 *served by FBSs.*

Femto-cells Finally, in each macro-cell N_{app} 5×5 apartment blocks are uniformly distributed, the construction of which is described in Section 3.3.1.2. Furthermore, in the HetNet a single

FMS in each active femto-cell (*i.e.*, $\tilde{\mu}(u)=1$) is assumed.

An example construction of a HetNet scenario is portrayed in Fig. 3.2.

3.3.2 Time Evolution

Each run of the Monte Carlo simulation is iterated over z subframes, or time slots, such that long-term statistics can be gathered. Due to the random user distribution, plentiful runs with different network generations are considered in order to obtain statistically accurate results. At the start of each subframe, the scheduling and allocation of RBs is reperformed. The MSs are assumed to be quasi-static for the duration of a run.

The simulation is performed for a full-buffer model, which represents the worst-case scenario where all users in the network are active, and request the same data rate in each subframe. Furthermore, the users are assumed to be static for the duration of a subframe, such that effects due to Doppler spread can be neglected. Perfect synchronisation in time and frequency is assumed, such that intra-cell interference is avoided.

3.3.3 Benchmarks

To evaluate the performance of the proposed ICIC techniques, two well-known benchmark systems have been implemented for comparison purposes. These are

BM 1: *Maximum Power Transmission*: In the first benchmark, no power allocation is performed, and all MSs transmit at the maximum power on each RB. This is the standard downlink power allocation of today's networks.

BM 2: *LTE Power Control*: In the second benchmark, the transmit power is set utilising LTE FPC, which is given in (2.1). This power allocation is generally utilised in the uplink of cellular systems.

Furthermore, an additional benchmark is included specifically for application in the HetNet scenario

BM 3: *Random ABS Transmission*: In the third benchmark, again all links transmit at full power, however, in each subframe a user transmits an ABS ([92], see Fig. 2.15) with

probability p_{ABS}.

These benchmarks have been selected based on the power allocation procedures implemented in current wireless systems. Therefore, these represent practical, real-life system performance. Of course, the scheduling of resources is performed independent of these benchmarks, and the implemented schedulers are described in the Results section of each chapter.

3.4 Summary

This chapter provides a comprehensive description of the system and channel models utilised throughout this thesis. Furthermore, the simulation environment, along with the investigated scenarios and comparative benchmarks, is thoroughly introduced.

Chapter 4
Uplink Interference Management

4.1 Introduction

For future wireless networks, the demand for higher data rates coupled with full frequency reuse results in interference-limited systems, which cannot achieve full capacity without the implementation of one or more viable interference mitigation/cancellation/coordination techniques [45]. Furthermore, through the implementation of OFDMA in the downlink and single carrier frequency division multiple access (SC-FDMA) in the uplink as multiple access schemes, future systems will provide orthogonality between RBs in both directions, and hence also between all users within a cell [120]. Thus, system performance is mainly limited by CCI originating from users in neighbouring cells, which can be detrimental to the SINR and throughput performance of MSs using the same RBs [121]. A typical solution is to force interferers to leave those RBs idle. However, this severely harms the trunking efficiency of the network [122]. Hence, suppressing transmission is clearly suboptimal, and thus power control and ICIC are necessary to achieve desired sum and individual throughputs.

In [123], an optimisation-based heuristic inter-cell coordination scheme is proposed to regulate the uplink transmission in neighbouring cells such that inter-cell interference is mitigated. As the scheme operates iteratively on a two-cell basis, however, it is clearly unsuitable for multi-cellular resource allocation. In [124], a softer frequency reuse scheme is introduced, where cell-edge power masks are used to mitigate inter-cell interference. These fixed masks cannot, however, adapt to the service-dependent requirements of the neighbouring cells, potentially wasting bandwidth. Research in [125] presents a distributed uplink power allocation technique based on a maximum sum rate optimisation, yielding superior results in terms of average system throughput, however ignoring the tradeoff between cell-edge performance and overall spectral efficiency. Furthermore, in [126], an energy-aware cross-layer radio management framework is proposed, that partitions the global optimisation problem into subproblems, which can be solved locally. While achieving substantial gains, the focus of the work is on multimode communication (*i.e.*, cellular, WLANs, WMANs, etc.), and so an optimisation for pure cellular

communication is not offered. In general, it is evident that the challenge of resource and power allocation has been thoroughly investigated as an optimisation problem, however in most cases these problems are non-convex, very hard to solve, and hence suboptimal heuristics are developed. In this chapter, a resource and power allocation technique based on local interference requirements will be developed to manage this challenge.

Finally, much of the previous work on energy efficient systems concentrates on network optimisation and scheduling policies. Macro-cell size reduction for better energy efficiency is investigated in [127], with positive results. Of course, reducing the cell-sizes means increasing the number of BSs in an area, which is generally rejected due to the enhanced infrastructure expenses. In [128], game-theoretic approaches are utilised to minimise the cost per reliable bit sent in energy constrained networks. However, it is seen that there is a clear tradeoff between energy and spectral efficiency, and hence the energy-efficient resource allocations tend to be spectrally inefficient. This is further highlighted in [129], where an analytical model determines the optimal energy-spectral efficiency tradeoff for the downlink in OFDMA networks.

4.2 System Model

The uplink of an OFDMA network is considered, where the system and channel models are described in detail in Section 3.2. Furthermore, the scenario investigated here is a dense, small cell, and therefore high-interference **macro-cellular** environment. The construction of this scenario is described in Section 3.3.1.1.

4.3 Uplink Interference Protection (ULIP)

Traditional uplink power control methods use the estimated path gain on the intended link to perform MS transmit power adaptation [68, 130]. A better option is to utilise the interfering link, *i.e.*, to a neighbouring BS, to reduce the transmit power on the affected RBs, such that interference caused to neighbouring BSs is lessened. This way, vulnerable MSs in the cell of interest have a chance of maintaining sufficient SINR, while the offending links remain active.

4.3.1 Uplink Interference Scenario

Fig. 4.1 portrays the interference scenario of two MSs in the uplink. Here, the vulnerable MS_v

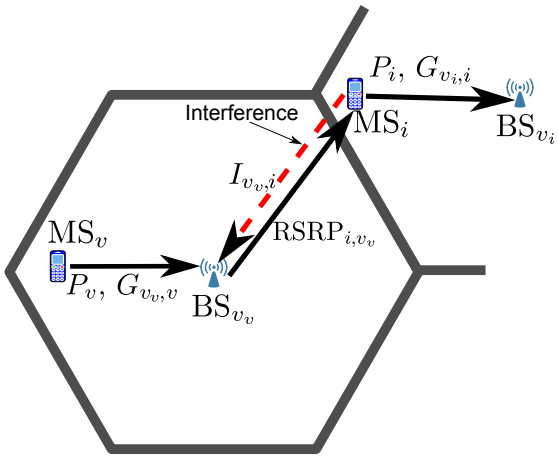

Figure 4.1: *Uplink interference scenario.*

served by BS_{v_v} and the interfering MS_i served by BS_{v_i} are transmitting on the same RB(s). Due to the uplink interference at BS_{v_v} caused by MS_i, the SINR of MS_v may fall below its SINR target, γ_v^*. To prevent such a situation, an interference protection technique is devised that reduces the transmit power P_i such that MS_v achieves a satisfactory SINR, $\gamma_v \geq \gamma_v^*$.

4.3.2 Interference Aware Power Reduction

The goal is to find an effective method to scale the transmit power on the interfering RBs. Here, the downlink reference signal of the neighbouring cells aid the MS in estimating the interference it causes to the neighbouring cells, assuming *channel reciprocity*. The channel can be considered reciprocal in terms of path loss and shadowing, however fast fading reciprocity is not assumed as this is not always the case, especially in FDD systems. For LTE, the RSRP in particular is utilised. The RSRP provides a cell-specific signal strength metric. It is used mainly to rank different cells according to signal strength and to perform handover and cell reselection decisions [9]. The reference signals facilitate the adaptation of the interfering RB transmit power, which is performed as follows:

1. Assume MS_v has been allocated the vulnerable RB_m. Let γ_v^* be the known, service-

dependent target SINR of MS_v, calculated as

$$\gamma_v^* = \frac{P_v^m G_{v_v,v}^m}{I_v^{m,\text{tol}} + \eta}, \tag{4.1}$$

where $I_v^{m,\text{tol}}$ is the tolerable interference such that γ_v^* can be met on RB_m.

2. Considering RSRPs of the neighbouring cells; as any reference signal is transmitted at a fixed power, an interfering MS_i can calculate the path gain on RB_m, G_{i,v_v}^m, from the affected BS_{v_v}, and assuming channel reciprocity, estimate the interference it is causing to the BS. It then uses the $I_v^{m,\text{tol}}$ from the vulnerable MS to calculate the maximum power, $\tilde{P}_{\text{max},\,i}^m$, for MS_i on RB_m

$$\tilde{P}_{\text{max},\,i}^m = \frac{I_v^{m,\text{tol}}}{G_{i,v_v}^m}. \tag{4.2}$$

It is clear that $\tilde{P}_{\text{max},\,i}^m$ is directly proportional to the tolerable interference, $I_v^{m,\text{tol}}$, at MS_v.

Given the power adaptation scheme and assuming channel reciprocity, MS_v should achieve the required SINR target on RB_m. However, in a FDD system where fast fading is not reciprocal, an interference margin must be applied. Lastly, since $I_v^{m,\text{tol}}$ is not directly available at MS_i, this needs to be signalled from BS_{v_v} to MS_i via existing backhaul infrastructures.

4.3.3 Priority Bands

In [51], SFR, where RBs are arranged into priority bands, is envisioned for LTE systems to facilitate interference protection. In this work, the available spectrum is split into different priority classes[1]. RBs assigned high-priority status are allocated to those MSs that require interference protection, and hence do not need to scale their transmit power. Looking from the other perspective, strongly interfering MSs are allocated RBs with a low-priority status, such that the transmit powers on these RBs may be reduced to provide interference protection. A *priority class reuse* scheme is established which, due to the power reduction, is an adaptive form of softer frequency reuse [124].

Three bands of communication, termed *high-priority*, *mid-priority*, and *low-priority*, are defined. These bands are allocated orthogonally, such that if a RB is assigned high-priority status

[1]These denote the priority status of the RBs within each class, and have no relation to user traffic priorities, which are not considered here.

in one cell, the same RB is assigned mid-priority and low-priority status in the neighbouring cells. In this sense, a priority class reuse factor of three results, which is shown in Fig. 4.3. When excessive interference is experienced, the owners of mid- and low-priority RBs in the

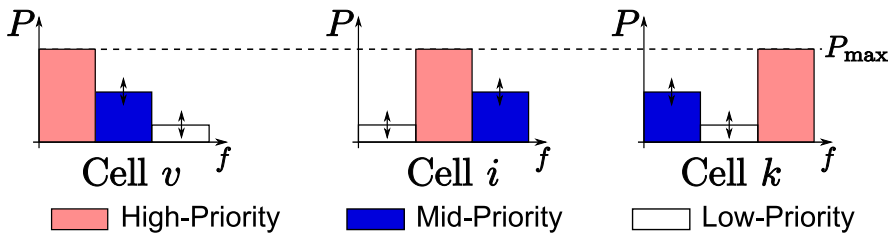

Figure 4.2: *Allocation of priority bands in neighbouring cells v, i, and k. The allocation of high-, mid- and low-priority RBs are complementary in the cells.*

neighbouring cells must reduce their transmit power. This boosts the SINR on both the high- and mid-priority RBs. The power reduction procedure for ULIP is performed as follows:

1. The $I_v^{m,\text{tol}}$ for the high-priority RBs are calculated from (4.1), and distributed to the neighbouring cells.

2. The transmit powers on mid-priority RBs are adjusted according to (4.2) based on the $\min\limits_{v \in \mathcal{I}_m} \left\{ I_v^{m,\text{tol}} \right\}$ received from high-priority RBs in neighbouring cells.

3. The $I_v^{m,\text{tol}}$ for the mid-priority RBs (after power scaling has been performed) are calculated from (4.1) and distributed.

4. The transmit powers on low-priority RBs are adjusted based on $\min\limits_{v \in \mathcal{I}_m} \left\{ I_v^{m,\text{tol}} \right\}$ received from both neighbouring high- and mid-priority RBs.

It is clear that $I_v^{m,\text{tol}}$ can be re-calculated in every time slot. However, to reduce the signalling burden on the network, these updates are only distributed when a sufficient difference, $\hat{\delta}$, to the last sent $I_v^{m,\text{tol}}$ has been observed.

Furthermore, all high-priority RBs receive interference protection, and consequently gains in achievable throughput. This is facilitated by the MSs assigned low- and mid-priority RBs, which have reduced their transmit power. MSs allocated mid-priority RBs may also receive a throughput boost, as the MSs assigned low-priority RBs also take the mid-priority $I_v^{m,\text{tol}}$ into account. MSs allocated low-priority RBs, however, exclusively sacrifice transmit power and, consequently, throughput. The allocation of users to these priority bands (*i.e.*, the assignment of x-priority RBs to MSs) is discussed in Sections 4.5.1 and 4.5.2.

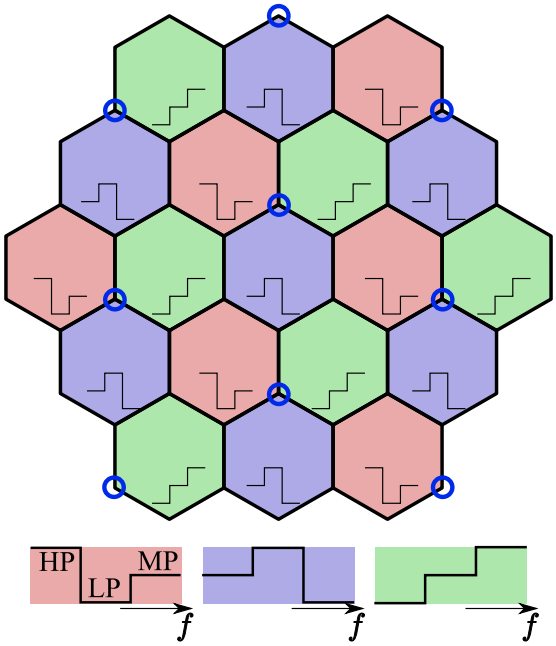

Figure 4.3: *Allocation of priority bands in a cellular network. The allocation of high-, mid- and low-priority RBs are complementary in the cells. A priority-class reuse scheme arises. The colour bar indicates which part of the spectrum is given high-priority in which cells.*

4.3.4 Practical Implementation in LTE Systems: An Example

In order to implement the ULIP procedure, the interfering (*i.e.*, low-priority) MS needs to be informed of the $I_v^{m,\mathrm{tol}}$ of its high-priority counterpart (in the neighbouring cell), to be able to then adjust its transmit power according to (4.2). This involves integrating the proposed ULIP technique within the network architecture. In abstract, the following procedure can be used to incorporate ULIP in the LTE network architecture[2]:

1. The vulnerable BS_{v_v} calculates the $I_v^{m,\mathrm{tol}}$ for all (allocated) high-priority RBs in the cell using the received uplink desired signal strength S_v^m.

2. The $I_v^{m,\mathrm{tol}}$ are sent to all neighbouring BSs over the X2 or (if no X2 connection is available) S1 interfaces (see Fig. 4.4 for LTE architecture).

3. The neighbouring BS identifies and stores the minimum $I_v^{m,\mathrm{tol}}$ received on each particular RB_m, including the cell-ID from which it came.

[2]In the interest of brevity, and without loss of generality, only the operation between high- and low-priority RBs is considered here. An equivalent procedure for the coordination of mid-priority RBs can be implemented.

4. The neighbouring BS prepares a Data Radio Bearer (DRB) containing the $\min_{v_v} \left\{ I_v^{m,\text{tol}} \right\}$ found and the cell-ID v_v for each of the low-priority RBs.

5. The DRBs are sent with the Radio Resource Control (RRC) protocol via the Physical Downlink Shared Channel (PDSCH) to each of the MSs allocated the low-priority RBs (see Fig. 4.5 for protocol).

6. MS_i (allocated low-priority RB) estimates G_{i,v_v}^m from BS v_v with $\min_{v_v} \left\{ I_v^{m,\text{tol}} \right\}$ indicated in DRB, using RSRP measurements.

7. MS_i calculates $\tilde{P}_{\text{max},\,i}^m$ according to (4.2) on RB_m, and adjusts the transmit power to provide interference protection in neighbouring cells.

The BS needs to inform the interfering MS_i of the interference margin $I_v^{m,\text{tol}}$ of MS_v on high-priority RB_m as calculated from (4.1). Thus, the transport of this information from BSs to the corresponding MSs must be defined using the LTE network architecture depicted in Fig. 4.4. The S1 interface connects the Serving Gateway (S-GW)/Mobility Management Entity (MME)

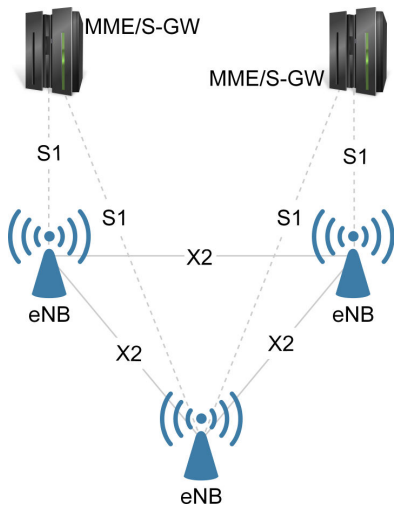

Figure 4.4: *Overall LTE architecture showing interconnection of BSs through S1 and X2 interfaces.*

with groups of neighbouring BSs. The MME processes the signalling between an MS and the CN. Neighbouring BSs (*i.e.*, within the groups connected by the S1 interface) are interconnected via the X2 interface, which carries control information regarding handover and interference coordination. The X2 interface is therefore highly suitable for ULIP related signalling.

In LTE, the RRC protocol is used to transfer *common* (*i.e.*, applicable to all MSs) and *dedicated* (*i.e.*, applicable to only a specific MS) non-access stratum (NAS) information [9]. The RRC protocol covers a number of functional areas, including the broadcasting of system information, RRC connection control, network controlled mobility procedures, and measurement configuration and reporting. The RRC connection control handles all procedures related to the establishment, modification and termination of an RRC connection, including, among others, the formation of DRBs, radio bearers carrying user data [9]. In Fig. 4.5, the construction, trans-

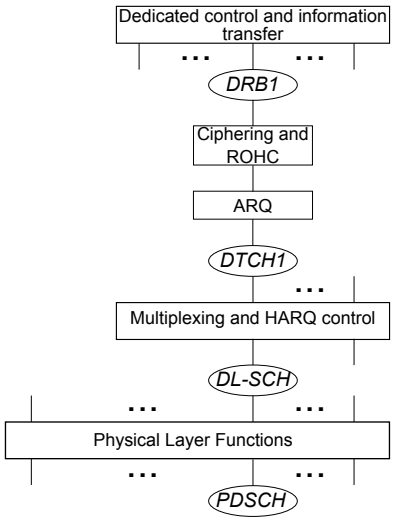

Figure 4.5: *Generation and transport of DRBs over the PDSCH in RRC protocol.*

lation, and transmission of such a DRB is shown. Here, the DRB is multiplexed with other Signalling Radio Bearers (SRBs) and DRBs to then be transmitted to MS$_i$. Furthermore, the Downlink Shared Channel (DL-SCH) and, consequently, the PDSCH are used for transmission of $\min_{v_v} \left\{ I_v^{m,\mathrm{tol}} \right\}$ and the cell-ID, meaning that no extra signalling on the control channels is required. Of course, the transmission of these DRBs in every subframe would be highly signalling-intensive, and hence is to be avoided. While the serving BS will continuously update the $I_v^{m,\mathrm{tol}}$ for all high-priority RBs, it only transmits these updates to the neighbouring BSs when a significant change, $\hat{\delta}$, in $I_v^{m,\mathrm{tol}}$ in comparison to the last transmission (*e.g.*, due to high mobility, call dropping, etc.) is achieved. This reduces the information transfer from the BSs to the MSs, and consequently lessens calculational intensity at the MSs.

Finally, knowledge of the cell-ID allows MS$_i$ to read the cell-specific reference signals of the neighbouring BS providing $\min_{v_v} \left\{ I_v^{m,\mathrm{tol}} \right\}$, which is necessary to carry out the RSRP measurements and estimate the channel gain between the MS and the vulnerable BS, G_{i,v_v}^m. This, of course, is needed by the MS$_i$ to perform its power adaptation according to (4.2). The RSRP for

a specific cell is defined as the linear average over the power contributions of the resource elements, within the considered measurement frequency bandwidth, which carry the cell-specific reference signals [131]. Using these measurements, the power reduction procedure can take place.

4.4 Performance Analysis

Given the detailed description of the ULIP technique, the expected performance of a system employing this mechanism can be explored. There are multiple analysis techniques that deal with such problems, more specifically with system capacity analysis. In [15, 132, 133], a reverse link capacity analysis assuming non-cooperative BSs (similar to the design of practical cellular systems) is unfortunately shown to be a long-standing open problem in information theory, but has been solved when treating the interference as Gaussian noise [134]. Clearly, since in ULIP the interference incident on each RB is dependent on the interference tolerances of other-cell high-priority MSs allocated that RB, the interference is most certainly not Gaussian. Hence, such an analysis is infeasible for a system employing ULIP. In [15, 135], the area spectral efficiency is introduced as a capacity measure that utilises stochastic geometry (statistical analysis of the positions and gains of MSs in the system) to estimate the expected capacity of a cellular network. Because in ULIP the users in a cell are split into three interdependent groups, such an analysis would be difficult as it is not always clear (by position) which MSs are assigned high-, mid-, or low-priority. Furthermore, in [135] the interference is estimated stochastically, and since in ULIP the interference is dependent on individual MS requirements, this analysis would be misguided.

On the other hand, optimisation techniques [13, 136] can be utilised to provide global solutions that optimise an overall performance goal (*e.g.*, energy/spectral efficiency). Furthermore, these offer an overall characterisation of the wireless system. In ULIP, however, the aim is not to maximise/minimise any objective, but rather to provide individual MSs with the necessary interference mitigation such that these can achieve their SINR/rate requirements. This is clearly not a system-wide goal, and hence such a description of a ULIP system is not applicable.

In general, the main difficulty that is not overcome (in the aforementioned methods) is the multitude of interdependencies on each RB over the network. The transmit powers on an RB are dependent on the signal qualities of the users allocated this RB in other cells in the network.

Furthermore, these interdependencies are constantly adapting depending on the SINRs of the individual MSs in each cell. Hence, the stochastic interference modelling used in capacity analysis techniques cannot be utilised to model cellular ULIP. Therefore, a theoretical comparison to the state-of-the-art is performed to highlight the potential benefits of ULIP for OFDMA networks. And while transmit power control is standard for the reverse link in future systems, it has been shown that maximum power transmission is capacity-achieving [15], and thus this is compared to ULIP here. Analytical derivations for the energy efficiency and system capacity performance of ULIP are presented.

4.4.1 Energy Efficiency in ULIP

In a system that employs ULIP, the transmit powers of low-priority MSs (MSs allocated low-priority RBs) are reduced so that interference to other cells is mitigated. Clearly, the throughput of the low-priority MSs is diminished relative to the reduction in transmit power. However, given a measure for energy efficiency, it can be shown that ULIP guarantees energy efficiency gains.

Given the metric for energy efficiency defined in (3.6), it will be shown that the energy efficiency of MS_u after ULIP is applied is always greater than in the benchmark, where all MSs transmit at maximum power. Here, the Shannon capacity is used for ease of derivability and without loss of generality;

$$\beta_u = \frac{C_u}{P_u} = \frac{B_u \log_2 (1 + \gamma_v)}{P_u} \quad \left[\frac{\text{bits}}{\text{J}}\right],$$

and the calculation is performed independent of RBs, also with no loss of generality. Essentially, it will be shown that

$$\beta_u^{\text{ULIP}} \geq \beta_u^{\text{BM}} \qquad \text{or} \qquad \frac{\beta_u^{\text{ULIP}}}{\beta_u^{\text{BM}}} \geq 1\,. \tag{4.3}$$

Proof The proof proceeds as follows

$$\frac{\beta_u^{\text{ULIP}}}{\beta_u^{\text{BM}}} = \frac{B_u \log_2 \left(1 + \frac{P_u^{\text{ULIP}} G}{I+N}\right) P_u^{\text{BM}}}{B_u \log_2 \left(1 + \frac{P_u^{\text{BM}} G}{I+N}\right) P_u^{\text{ULIP}}}\,, \tag{4.4}$$

where B_u is the bandwidth assigned to MS_u, G, I, and N are the nominal path gain, inter-

ference and noise, respectively, P_u^{BM} is the benchmark transmit power, and P_u^{ULIP} the power when ULIP is applied

$$P_u^{\mathrm{ULIP}} = \hat{\xi} P_u^{\mathrm{BM}}\,, \quad 0 \leq \hat{\xi} \leq 1\,,$$

where $\hat{\xi}$ is the scaling factor by which the ULIP MS reduces its transmit power. This is substituted into (4.4) to obtain (4.5)

$$\begin{aligned}\frac{\beta_u^{\mathrm{ULIP}}}{\beta_u^{\mathrm{BM}}} &= \frac{\log_2\left(1+\frac{\hat{\xi}P_u^{\mathrm{BM}}G}{I+N}\right)P_u^{\mathrm{BM}}}{\log_2\left(1+\frac{P_u^{\mathrm{BM}}G}{I+N}\right)\hat{\xi}P_u^{\mathrm{BM}}}\,,\\ &= \frac{\log_2\left(1+\hat{\xi}c\right)}{\hat{\xi}\log_2\left(1+c\right)}\,, \quad \text{where } c = \frac{P_u^{\mathrm{BM}}G}{I+N}\,. \end{aligned} \tag{4.5}$$

After rearranging (4.5) in the following manner

$$\frac{\log_2\left(1+\hat{\xi}c\right)}{\hat{\xi}\log_2\left(1+c\right)} \geq 1\,, \tag{4.6}$$

$$\log_2\left(1+\hat{\xi}c\right) \geq \hat{\xi}\log_2\left(1+c\right)\,,$$

$$1+\hat{\xi}c \geq (1+c)^{\hat{\xi}}\,, \tag{4.7}$$

the generalised Bernoulli's inequality can be applied to prove the inequality in (4.7), which states

$$(1+x)^r \leq 1+rx\,, \quad r\in\mathbb{R},\, 0\leq r\leq 1\,, \quad x\in\mathbb{R},\, x>-1\,. \tag{4.8}$$

To apply this to (4.7), r and x are set to

$$\begin{aligned} r &= \hat{\xi}\,, \quad 0\leq\hat{\xi}\leq 1 \quad &\rightarrow \quad 0\leq r\leq 1\\ x &= c\,, \quad c\geq 0 \quad &\rightarrow \quad x\geq 0>-1 \end{aligned}$$

and replaced in (4.8), such that

$$\begin{aligned}(1+x)^r &\leq 1+rx\,,\\ (1+c)^{\hat{\xi}} &\leq 1+\hat{\xi}c\,, \end{aligned} \tag{4.9}$$

exactly the inequality from (4.7). Hence, by proving (4.7), it has been shown that (4.3) is indeed true

$$\frac{\beta_u^{\mathrm{ULIP}}}{\beta_u^{\mathrm{BM}}} \geq 1\,, \quad \forall\, P_u^{\mathrm{BM}} \geq P_u^{\mathrm{ULIP}} \geq 0\,,$$

and hence it can be concluded that the energy efficiency of a low-priority MS employing ULIP is always greater than or equal to the energy efficiency of the same MS in the benchmark system (*i.e.*, transmitting at maximum power). Furthermore, since MSs on high-priority RBs receive a capacity boost through ULIP while maintaining transmit power, their energy efficiencies are also enhanced. □

Therefore, the energy efficiency of any/every MS in the system is augmented during ULIP operation, and consequently also the system energy efficiency

$$\beta_{\text{sys}}^{\text{ULIP}} \geq \beta_{\text{sys}}^{\text{BM}} . \tag{4.10}$$

It should be mentioned that future work could exploit the (ideally) logarithmic relationship between transmit power and throughput (*i.e.*, capacity) in order to optimise the energy efficiency of each MS, and by extension, the system.

For completeness, a similar proof can be constructed to show that in conjunction with a larger energy efficiency, the energy consumption $\hat{\beta}_u = {}^{P_u}/_{C_u}$ [137], measured in ${}^{\text{J}}/_{\text{bit}}$, for ULIP is lower (as expected) than for the benchmark. Essentially,

$$\frac{\hat{\beta}_u^{\text{ULIP}}}{\hat{\beta}_u^{\text{BM}}} \leq 1 , \quad \text{and} \quad \hat{\beta}_{\text{sys}}^{\text{ULIP}} \leq \hat{\beta}_{\text{sys}}^{\text{BM}} . \tag{4.11}$$

4.4.2 System Capacity in ULIP

It has been shown that through the application of ULIP the energy efficiency of not only the individual MSs but also of the system is always improved (at minimum no losses are incurred). However, due to the reduction in overall system power through ULIP, one would expect, in general, a similar decrease in system capacity. Here it will be shown that this is not always the case, and hence ULIP not only guarantees an energy efficiency boost, but can also provide a gain in system capacity

$$C_{\text{sys}}^{\text{ULIP}} \nleq C_{\text{sys}}^{\text{BM}} . \tag{4.12}$$

Proof To prove (4.12), a counter-argument to the assumption that

$$C_{\text{sys}}^{\text{ULIP}} \leq C_{\text{sys}}^{\text{BM}} , \tag{4.13}$$

must be found, where C_{sys} is defined in (3.5). Therefore, a scenario is designed where the above assumption (4.13) does not hold. A two-link scenario is chosen where MS_1 and MS_2 are allocated the same n_u^{RB} RBs in two neighbouring cells. Furthermore, the C_{sys} achieved in the benchmark system (BM 1), in which all transmitters (MS_1 and MS_2) transmit using maximum power, is compared to that achieved in the ULIP system. When ULIP is applied, MS_2 is given high-priority, and MS_1 low-priority status such that it may be required to scale it's power

$$\begin{aligned} \text{BM}: &\qquad P_1 = P_2\,, \\ \text{ULIP}: &\qquad \hat{\xi} P_1 \leq P_2, \qquad 0 \leq \hat{\xi} \leq 1\,. \end{aligned}$$

The proof is set up utilising the assumption that the system is interference-limited, and hence the thermal noise can be ignored. This assumption depends on the ISD in the network, as clearly in larger cells the CCI diminishes (given $P_{\text{max,MMS}}$ remains constant). The path gain and path loss equations are given by (3.8) and (3.9), respectively, and the thermal noise per RB is calculated to be $\eta{=}k_{\text{B}}TB_{\text{RB}}{=}{-}121\,\text{dBm}$, where k_{B} is the Boltzmann constant, the temperature $T{=}300\,\text{K}$, and the bandwidth $B_{\text{RB}}{=}180\,\text{kHz}$ per RB. Given that, on average, $|H_{k,l}|^2{=}1$ and $X_\sigma{=}0$, the minimum average interfering link gain can be calculated when the interfering MS is located at the maximum distance $d_{\text{max}}{=}\text{ISD}$ from the vulnerable BS (*i.e.*, next to a neighbouring BS):

$$L_d(d_{\text{max}}) = 15.3 + 37.6\log_{10}(350) = 110.9\,\text{dB}\,, \tag{4.14}$$

$$G_{\text{min},v_2} = -L_d(d_{\text{max}}) = -110.9\,\text{dB}\,. \tag{4.15}$$

And given $P_u{=}{P_{\text{max,MMS}}}/{n_u^{\text{RB}}}{>}{P_{\text{max,MMS}}}/{M}{\approx}6\,\text{dBm}$ per RB (since $n_u^{\text{RB}}{\leq}M$) the minimum received interference is $P_u G_{\text{min},v_2} \approx -104.9\,\text{dBm}$, which is significantly larger than η. In fact, even for $\text{ISD}{=}500\,\text{m}$, the minimum average interference comes to $-116.8\,\text{dBm}$, which is still more than double the noise power.

Hence, assuming the network is constructed with $\text{ISD}{<}500\,\text{m}$, it has been shown that the system is interference-limited, and therefore the noise can be neglected. This simplifies capacity calculations, as SIR can now be used rather than SINR. The individual user capacities are

$$C_1^{\text{BM}} = B_1 \log_2\left(1 + \frac{P_1 G_{v_1,1}}{P_2 G_{v_1,2}}\right) \qquad C_2^{\text{BM}} = B_2 \log_2\left(1 + \frac{P_2 G_{v_2,2}}{P_1 G_{v_2,1}}\right)\,, \tag{4.16}$$

in the benchmark system, where $B_1{=}B_2{=}n_u^{\mathrm{RB}}B_{\mathrm{RB}}$, and

$$C_1^{\mathrm{ULIP}} = B_1 \log_2\left(1 + \frac{\hat{\xi}P_1G_{v_1,1}}{P_2G_{v_1,2}}\right) \qquad C_2^{\mathrm{ULIP}} = B_2 \log_2\left(1 + \frac{P_2G_{v_2,2}}{\hat{\xi}P_1G_{v_2,1}}\right), \quad (4.17)$$

when ULIP is employed, where Shannon's equation is used for the calculations. Subsequently, the relationship between C_i^{BM} and C_i^{ULIP} is found:

$$C_1^{\mathrm{ULIP}} \geq B_1 \log_2\left(\left(1 + \frac{P_1G_{v_1,1}}{P_2G_{v_1,2}}\right)^{\hat{\xi}}\right) \qquad C_2^{\mathrm{ULIP}} \geq B_2 \log_2\left(\left(1 + \frac{P_2G_{v_2,2}}{P_1G_{v_2,1}}\right)^{\frac{1}{\hat{\xi}}}\right), \quad (4.18)$$

where Bernoulli's inequality (4.8) is used to arrive at (4.18) ($r{=}\hat{\xi}$ and $r{=}1/\hat{\xi}$ for $i{=}1$ and 2, respectively). Further,

$$C_1^{\mathrm{ULIP}} \geq \hat{\xi}B_1 \log_2\left(1 + \frac{P_1G_{v_1,1}}{P_2G_{v_1,2}}\right) \qquad C_2^{\mathrm{ULIP}} \geq \frac{1}{\hat{\xi}}B_2 \log_2\left(1 + \frac{P_2G_{v_2,2}}{P_1G_{v_2,1}}\right), \quad (4.19)$$

and finally, C_1^{BM} and C_2^{BM} are substituted into (4.19) to achieve (4.20)

$$C_1^{\mathrm{ULIP}} \geq \hat{\xi}C_1^{\mathrm{BM}} \qquad C_2^{\mathrm{ULIP}} \geq \frac{1}{\hat{\xi}}C_2^{\mathrm{BM}}. \quad (4.20)$$

For simplicity, it is assumed that $G_{v_1,1}{=}G_{v_2,2}$, and $G_{v_1,2}{=}G_{v_2,1}$ (*e.g.*, both MSs are at the cell-border). This creates the following set of equations:

$$C_1^{\mathrm{BM}} = C_2^{\mathrm{BM}} = C_i^{\mathrm{BM}}, \qquad C_1^{\mathrm{ULIP}} \geq \hat{\xi}C_i^{\mathrm{BM}}, \qquad C_2^{\mathrm{ULIP}} \geq \frac{1}{\hat{\xi}}C_i^{\mathrm{BM}} \quad (4.21)$$

Using (4.21), it can now be shown that the assumption in (4.13) does not hold for this system, and that hence (4.12) is true. In the benchmark,

$$C_{\mathrm{sys}}^{\mathrm{BM}} = C_1^{\mathrm{BM}} + C_2^{\mathrm{BM}} = 2C_i^{\mathrm{BM}}.$$

And when ULIP is applied,

$$C_{\mathrm{sys}}^{\mathrm{ULIP}} = C_1^{\mathrm{ULIP}} + C_2^{\mathrm{ULIP}}, \quad (4.22)$$

$$\geq \hat{\xi}C_1^{\mathrm{BM}} + \frac{1}{\hat{\xi}}C_2^{\mathrm{BM}} = \left(\hat{\xi} + \frac{1}{\hat{\xi}}\right)C_i^{\mathrm{BM}}, \quad (4.23)$$

$$\geq 2C_i^{\mathrm{BM}} = C_{\mathrm{sys}}^{\mathrm{BM}}\,, \tag{4.24}$$

where in (4.23), the equations from (4.21) are substituted into (4.22), and in (4.24), the inequality

$$\left(\hat{\xi} + \frac{1}{\hat{\xi}}\right) \geq 2$$

is used, which is proven by the inequality of arithmetic and geometric means

$$\frac{a+b}{2} \geq \sqrt{ab}\,, \tag{4.25}$$

$$a = \hat{\xi}\,, \quad b = \frac{1}{\hat{\xi}}\,, \qquad \left(\hat{\xi} + \frac{1}{\hat{\xi}}\right) \geq 2\sqrt{\hat{\xi}\frac{1}{\hat{\xi}}} \quad \geq 2\,.$$

In (4.22)-(4.24) it has been demonstrated that for the chosen scenario, the ULIP system capacity is greater than that of the benchmark system

$$C_{\mathrm{sys}}^{\mathrm{ULIP}} \geq C_{\mathrm{sys}}^{\mathrm{BM}}\,,$$

and that, hence, (4.13) is not true. Therefore, (4.12) is valid. □

In this section it was demonstrated that the energy efficiency of any MS in a network will be enhanced when ULIP is employed, and that this energy efficiency boost can also be accompanied by an increase in the system capacity

$$\beta_{\mathrm{sys}}^{\mathrm{ULIP}} \geq \beta_{\mathrm{sys}}^{\mathrm{BM}}\,, \qquad\qquad C_{\mathrm{sys}}^{\mathrm{ULIP}} \nleq C_{\mathrm{sys}}^{\mathrm{BM}}\,.$$

Although in certain scenarios a loss in system capacity is incurred by the system-wide power reduction (as (4.12) suggests), the guaranteed energy efficiency gain can compensate this deficit. Furthermore, the possibility of gains in both performance metrics, *i.e.*, when C_{sys} is improved, demonstrates the potential benefits of ULIP for future OFDMA-based wireless networks such as LTE and/or LTE-Advanced.

4.5 Scheduling

To facilitate the interference protection, a scheduling procedure is designed to assign MSs to specific priority bands, enhancing the effect of ULIP in the system. In general, a random

allocation of priority RBs can lead to undesired scenarios. For instance, the allocation of a high-priority RB to cell-centre MSs is wasteful, as such a MS-BS link is generally strong, and hence interference protection is unnecessary. At the cell-edge, allocating a low-priority RB to a MS is just as destructive. In this case, the MS$_u$ will most probably be unable to sustain its γ_u^*, and hence fall into outage. Therefore, an appropriate scheduling mechanism is necessary for ULIP to achieve its full potential.

4.5.1 Received-Signal Scheduling

In a fair allocation scheme, cell-edge MSs should be allocated high-priority RBs so as to be able to transmit at full power and achieve the maximum possible SINR. Cell-centre users, which are more likely to achieve their SINR target due to BS proximity, should be assigned low-priority RBs. In essence, the general rule is to allocate high-priority RBs to the MSs with the least favourable SINR conditions.

Therefore, an efficient scheduling procedure can increase the effectiveness of ULIP, and prevent throughput losses due to MS outages. In this section, a scheduling procedure relying on the reverse link signals of the active users is presented. By analysing the signals, an approximation of the relative positions of the MSs (and their interferers) can be obtained, which can then be used to schedule the users accordingly. This presents a low complexity scheduling solution, as the necessary information is readily available at the serving BS.

SINR Scheduling The scheduling procedure utilises the SINRs from transmissions in previous time slots. In (4.26), $\mathcal{R}_j$ denotes the N_j-tuple of average (*i.e.*, time average over the previous z_p time slots, where z_p is a system wide parameter) SINRs of the users in a cell

$$\mathcal{R}_j = \left(\bar{\gamma}_{j,1}, \bar{\gamma}_{j,2}, \ldots, \bar{\gamma}_{j,N_j}\right), \tag{4.26}$$

where $\bar{\gamma}_{j,i}$ is the average SINR (over all assigned RBs) of MS$_i$ in cell j, and N_j denotes the number of MSs in cell j. The MSs that are at the cell-edge experience, on average, weaker signals, and consequently low SINRs are received at their serving BS. Thus, the next step is to sort the $\bar{\gamma}_{j,i}$ in ascending order, so that the MSs that have the weakest SINRs can be identified

$$\mathcal{U}_j^* = f_{\bar{\gamma}}\left(\mathcal{R}_j\right) = \left(p_1, p_2, \ldots, p_{N_j}\right) \tag{4.27}$$

$$\text{s.t. if } p_k \leq p_l \text{ , then } \bar{\gamma}_{j,k} \leq \bar{\gamma}_{j,l} \text{ ,}$$

where $\mathcal{U}_j^*$ is the N_j-tuple of the positions p_k of $\bar{\gamma}_{j,k}$ in the tuple $\mathcal{R}_j^* = \text{order}\,(\mathcal{R}_j)$, which is sorted in ascending order. The function $f_{\bar{\gamma}}(\cdot)$ that defines this ordering can now be applied to the set of users in the cell of interest $\mathcal{S}_{\text{users},j}$, and the set of high-priority MSs, $\mathcal{S}_{\text{hp},j}$, can be found as

$$\mathcal{S}_{\text{hp},j} = \left\{ s \in \mathcal{S}_{\text{users},j} \;\middle|\; f_{\bar{\gamma}}(\bar{\gamma}_{j,s}) \leq \left\lceil \frac{N_j}{l_\text{p}} \right\rceil \right\} \tag{4.28}$$
$$\text{where } \mathcal{S}_{\text{hp},j} \subset \mathcal{S}_{\text{users},j} \text{ ,}$$

where l_p denotes the number of priority bands (here, l_p=3) such that the number of high-priority MSs yields $\lceil N_j/l_\text{p} \rceil$. In (4.28), the high-priority RBs are allocated to the $\lceil N_j/l_\text{p} \rceil$ MSs with the weakest average SINRs, and hence to the cell-edge. The low-priority RBs are allocated to the cell-centre, thus to the $\lceil N_j/l_\text{p} \rceil$ MSs with the strongest SINRs, and the mid-priority RBs to the remaining (middle set) MSs:

$$\mathcal{S}_{\text{mp},j} = \left\{ s \in \mathcal{S}_{\text{users},j} \;\middle|\; \left\lceil \frac{N_j}{l_\text{p}} \right\rceil \leq f_{\bar{\gamma}}(\bar{\gamma}_{j,s}) \leq \left\lceil \frac{2N_j}{l_\text{p}} \right\rceil \right\} \tag{4.29}$$
$$\mathcal{S}_{\text{lp},j} = \left\{ s \in \mathcal{S}_{\text{users},j} \;\middle|\; f_{\bar{\gamma}}(\bar{\gamma}_{j,s}) \geq \left\lceil \frac{2N_j}{l_\text{p}} \right\rceil \right\} \tag{4.30}$$
$$\text{where } \mathcal{S}_{\text{mp},j}, \mathcal{S}_{\text{lp},j} \subset \mathcal{S}_{\text{users},j} \text{ .}$$

One instance of the fair allocation for exactly N_j=M=50 users per cell is depicted in Fig. 4.6. It is clear to see that the farther MSs (from the serving BS) have been allocated high-priority RBs, and to the nearer MSs, which are shielded from neighbouring cell interference, the low-priority RBs are assigned. The mid-priority RBs have been assigned to the remaining MSs.

When a new MS enters the cell, the initial allocation is performed using the SNR (which can be approximated using the RSRP), as no SINR information is available *a priori*. In following time slots, however, the MS's SINR is used. Mean SINR statistics are employed to eliminate fast fading effects and prevent a MS from rapidly changing priority class, allowing the system to reach a stable operating point.

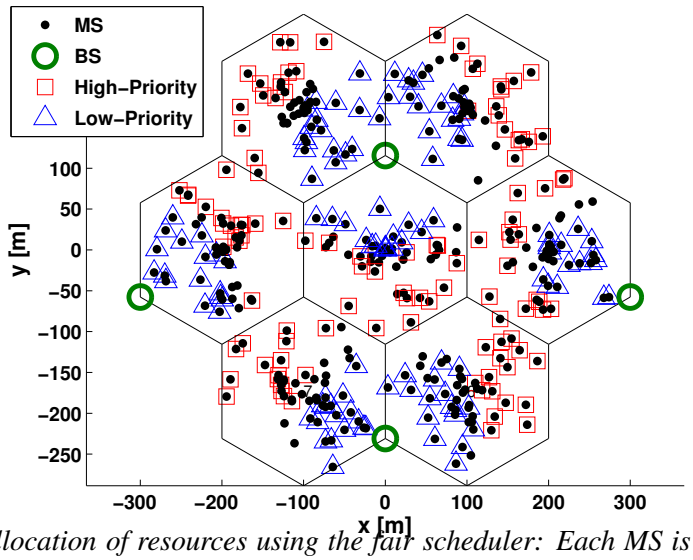

Figure 4.6: *Allocation of resources using the fair scheduler: Each MS is depicted with a dot. The MSs marked with squares have been assigned high-priority RBs, triangles represent low-priority RBs, and the (unmarked) rest are mid-priority. The system is dubbed fair as high-priority is assigned to the MSs with the least favourable SINR conditions.*

4.5.2 Frequency-Selective Scheduling

While the SINR scheduler takes prior rate statistics (rate is directly proportional to SINR, see (3.4)) into account, it fails to utilise knowledge of the instantaneous rate of MSs in the system. Frequency selective fading varies the channel conditions across the RBs such that each MS, as their positions are different, sees an independent channel fading profile (see Fig. 2.6). Hence, there is an optimal RB for each MS, which is identified by the RB on which the fading allows for the highest instantaneous rate, or SNR. The scheduler presented here utilises these channel characteristics to optimise the assignment of RBs to users in a cell, in order to improve the cell throughput.

Proportional Fair Scheduler (PFS) A PFS makes use of the channel characteristics of the individual MSs, and then attempts to assign the RBs such that each MS is allocated the RB(s) that are optimal, in terms of performance metric, for it. Of course, if the optimal RB(s) have already been assigned to another MS, then the next best RB(s) are allocated. Through this, the throughput performance is augmented, while maintaining a fair system.

Problem Formulation and Model: In the time domain, the proportional fair (PF) algorithm aims

to maximise the logarithmic utility function

$$\max \underbrace{\sum_i \log R_i}_{\text{log. utility fn.}}, \tag{4.31}$$

which is known as the *proportional fair criteria* [39], where R_i is the long term service rate of MS$_i$. It has been shown in [138] that in order to find a solution for (4.31), one should maximise $\sum_i {}^{d_i(t)}/_{R_i(t)}$, where $d_i(t)$ is the total transmitted data to MS$_i$ at time t. The PF algorithm delivers high throughput and maintains proportional fairness among the users by giving priority to users with a large instantaneous rate $r_i(t)$ and low average service rate $R_i(t)$.

In the frequency domain, a new (PF) metric is defined that takes the instantaneous rate on a particular RB into account, and normalises this again by the average service rate

$$\lambda_i^c = \frac{r_i^c(t)}{R_i(t)} \tag{4.32}$$

where $r_i^c(t)$ denotes the instantaneous[3] channel rate for MS$_i$ on RB$_c$ at time t. In the frequency domain, the equivalent optimisation problem is hence formulated as

$$\max \sum_i \sum_c x_i^c(t) \lambda_i^c(t), \tag{4.33}$$

where $x_i^c(t)$ is the indicator function of RB$_c$ assigned to user i at time slot t. It is clear that (4.33) maximises $\sum_i {}^{d_i(t)}/_{R_i(t)}$, and hence also the utility function in (4.31). In the downlink, each RB is assigned to an MS one-by-one, *i.e.*, the user with the largest $\lambda_i^c(t)$ is assigned RB$_c$ at time t. In the uplink however, where SC-FDMA is employed, the contiguous RB constraint must also be taken into account [39]. This requirement clearly constrains the optimisation of (4.33), and hence also reduces the optimality of the solution of (4.33) in (4.31). In general, however, the optimisation of (4.33) still generates a proportional fair system that benefits in terms of both individual MS and sum throughputs.

Algorithm: The ULIP PF algorithm consists of two parts: the arrangement of the MSs into their respective priority classes, and the PF scheduling within each priority class. The ULIP PFS is shown in Algorithm 1. In the first part of the algorithm, similar to the received signal

[3]This refers to the rate achievable at a given time depending on the frequency-selective fading characteristics of the channel. Hence, the rate on each RB will be different, making some more attractive to the respective MS than

Algorithm 1 ULIP PFS

1: Let R^* be the sorted list of all the metric values $R_i(t)$ in increasing order
2: Let S_L, S_M, S_H be the sets of not-yet-assigned low-, mid-, and high-priority RBs, respectively
3: Let U_L, U_M, U_H be the empty sets of low-, mid-, and high-priority MSs, respectively
4: **for** $k = 1$ to $|R^*|$ **do**
5: **if** $k \leq |S_H|$ **then**
6: $U_H = U_H + \{i_{R^*[k]}\}$
7: **else if** $k \leq |\{S_H, S_M\}|$ **then**
8: $U_M = U_M + \{i_{R^*[k]}\}$
9: **else**
10: $U_L = U_L + \{i_{R^*[k]}\}$
11: **end if**
12: **end for**
13: Let V_L be the sorted list of all the metric values λ_i^c, $i \in U_L$, $c \in S_L$ in decreasing order
14: Let V_M be the sorted list of all λ_i^c, $i \in U_M$, $c \in S_M$ in decreasing order
15: Let V_H be the sorted list of all λ_i^c, $i \in U_H$, $c \in S_H$ in decreasing order
16: **for** $P = \{H, M, L\}$ **do**
17: $k \leftarrow 1$
18: **while** $S_P \neq \emptyset$ **do**
19: pick RB c with k^{th} largest metric value $\lambda_i^c \in V_P$
20: Let I be RBs already assigned to user i
21: **if** (c is adjacent to I) or ($I = \emptyset$) **then**
22: assign RB c to user i
23: $S_P = S_P - \{c\}$; $V_P = V_P - \{\lambda_i^c\}$; $k \leftarrow 1$
24: **else**
25: $k \leftarrow k + 1$
26: **end if**
27: **end while**
28: **end for**

schedulers introduced in Section 4.5.1, the MSs are sorted in terms of a metric, and then divided into the three priority classes. Here, however, the service rates $R_i(t)$ of the users are used. This is similar to the SINR scheduling discussed above, but should provide a slightly fairer priority class allocation as the average rate is clearly a more direct performance measure (since performance is measured in terms of throughput) than average SINR.

The second part of the scheduler consists of the PF algorithm that assigns the RBs to the MSs in the respective priority classes based on the PF metric in (4.32). This metric provides a balance between the desire for throughput-optimal scheduling, which results from the numerator $r_i^c(t)$, and the goal of a fairer system, ensured by the denominator $R_i(t)$. This PF scheduling is

others. Without loss of generality, $r_i^c(t)$ is calculated via Shannon's equation, using the MS's SNR.

then performed separately in each of the priority classes such that, within the constraints of restricting the range of RBs of each MS (only RBs from within the priority class are available, not from the entire spectrum), the users and the system are proportionally fair scheduled.

It should be noted that some slight modifications can be made to alter the behaviour of the ULIP PFS, such as changing the MS ordering for the priority class assignment, or employing a more aggressive PF metric. For example, by setting $\lambda_i^c = r_i^c(t)$, the service rates are ignored in the PF scheduling, sacrificing fairness for MS and system capacity. This is called maximum rate (MR) scheduling.

4.6 Simulation and Results

The general simulation setup utilised is described in Section 3.3. As mentioned previously, the application scenario for ULIP is the dense macro-cellular environment described in Section 3.3.1.1. The relevant scenario and simulation parameters can be found in Table 4.1.

Parameter	Value
Simulation area	37 cells
Results area	inner 7 cells
ISD	$350\,\mathrm{m}$
ICD	$200\,\mathrm{m}$
Average MSs per cell, $\bar{N}$	20
Number of available RBs, M	50
RB bandwidth, B_{RB}	$180\,\mathrm{kHz}$
Subcarriers per RB, k_{sc}	12
Symbol rate per subcarrier, s_{sc}	$15\,\mathrm{ksps}$
Subframe duration, t_{sf}	$1\,\mathrm{ms}$
Time slots (subframes), z	10
Noise spectral density, η_0	$-174\,\mathrm{dBm/Hz}$
MS transmit power, $P_{\mathrm{max,MMS}}$	$23\,\mathrm{dBm}$
Sector $\theta_{3\mathrm{dB}}$	$70°$
MS SINR target, γ^*	$12\,\mathrm{dB}$
Outdoor channel parameters α_{o}, β_{o}	25.6, 36.7
Standard deviation, σ_{o}	$4\,\mathrm{dB}$
Auto-correlation distance	$50\,\mathrm{m}$

Table 4.1: *Chapter 4 Simulation Parameters*

4.6.1 Resource and Power Allocation

The performance of the ULIP procedure is investigated in conjunction with the two schedulers introduced in this chapter. In the first system, the allotment of users to priority classes is performed by the SINR scheduler introduced in Section 4.5.1. Within each class, the set of RBs is randomly (but still contiguously) allocated to the MMSs assigned to that class, with each user receiving at minimum one RB.

In the second, the PFS described in Section 4.5.2 is utilised. Here, MMSs are assigned to priority classes based on their average rate, and RBs are assigned contiguously to the MMSs with the largest PF metrics.

Benchmarks Finally, the benchmarks utilised for comparison to ULIP are max. power transmission (BM 1) and LTE $\text{FPC}_{\nu=1}$ (BM 2). For each of the benchmarks, the RB allocation from ULIP employing the SINR scheduler is adopted, resulting in a *soft frequency reuse* scheme [53].

4.6.2 Results and Discussion

From the simulation, the CDFs of the achieved system throughput and energy efficiency are generated for systems employing ULIP and compared against the two benchmark systems. General simulation parameters are taken from Table 4.1 and [139], and full power control (*i.e.*, ν=1) is implemented.

In Fig. 4.7(a), the CDFs of the achieved user throughput for the three systems is shown, and it is evident that ULIP achieves considerable gains for MMSs with low throughput in the benchmarks. At the 50th percentile, ULIP-SINR users achieve, on average, 2.8 times the user throughput of both benchmarks. Also, although at the 90th percentile a 31 % loss is incurred by the power reduction on low-priority (and therefore high-throughput) RBs, the crossing point of the CDFs signifies that 82 % of the users achieve a better SINR (and consequently throughput) in ULIP. Furthermore, the ≈20 % outage seen in both benchmarks is eliminated, and hence ULIP provides significant advantages for the users in a cellular network.

The PFS on the other hand provides 3.3 times the user throughput of both benchmarks at the median, and further it is evident that no losses at higher throughputs are incurred. However, due to the allocation of RBs according to instantaneous rate, it is evident that cell-edge MMSs

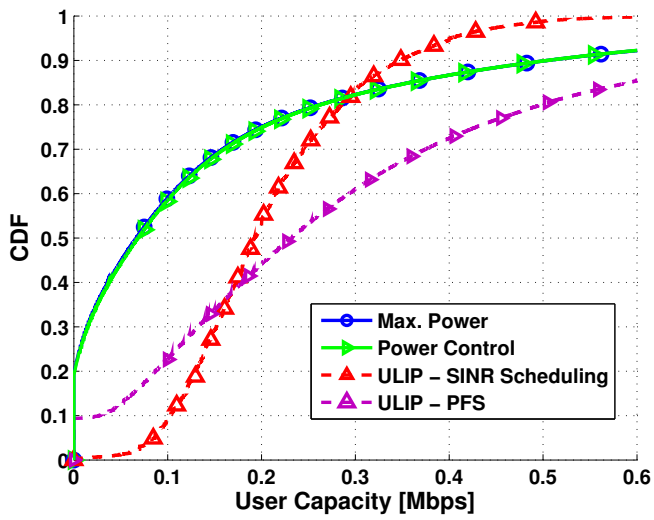

(a) Throughput

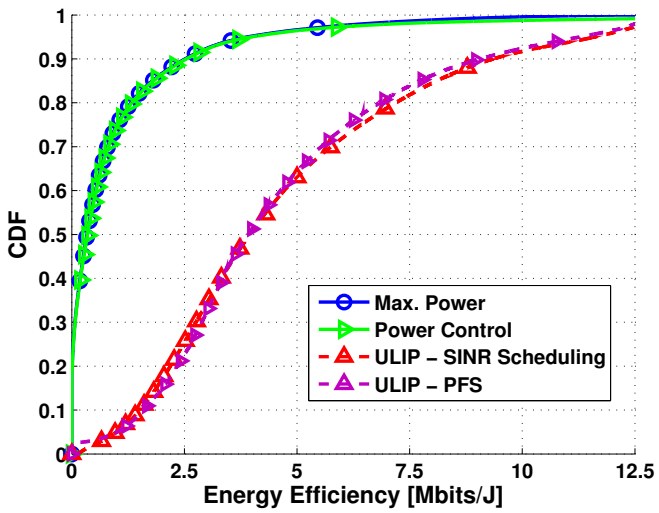

(b) Energy Efficiency

Figure 4.7: *User efficiency performance results for ULIP, LTE power control, and maximum power transmission.*

are slightly disregarded in the PFS, causing almost 9 % outage in the scenario. This comes mainly from the low transmit powers in the uplink, and the unfavourable resource assignment. On the other hand, ULIP-PFS provides throughput gains over almost all benchmark MMSs.

These throughput benefits are further seen in Fig. 4.7(b), where the user energy efficiencies of the four systems are displayed. Here it is clear that both ULIP systems provide vast energy efficiency improvements over the two benchmarks, which behave very similarly. At the 50th percentile, ULIP induces almost 11 times the user energy efficiency of both benchmarks.

Furthermore, ULIP achieves energy efficiency gains for all MMS over the maximum power benchmark, confirming the result of the performance analysis conducted in Section 4.4.1. Finally, it is interesting to note that the energy efficiency of ULIP is similar for both schedulers. This results directly from the ULIP procedure, which works on the priority classes, rather than the individual RB allocations.

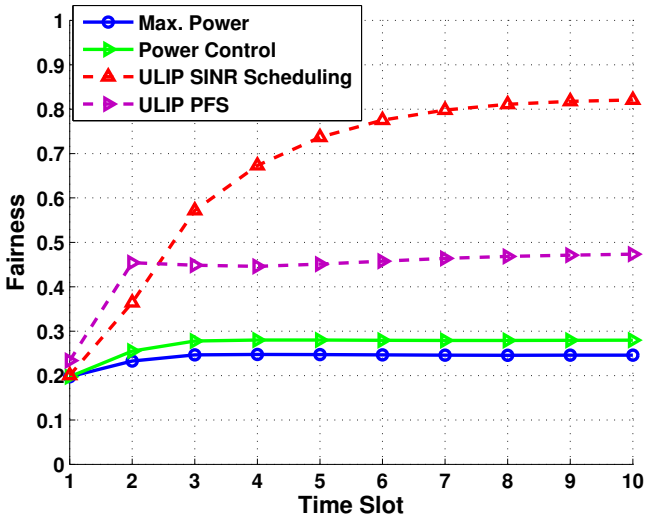

Figure 4.8: *System fairness performance results for ULIP, LTE power control, and maximum power transmission.*

Fig. 4.8 displays the system throughput fairness results of the four power allocation techniques. Here, it is clear to see that while power control provides some fairness gains (almost 14 %) over maximum power transmission, ULIP-SINR achieves by far the fairest system with over 0.8 fairness rating. The substantial gains achieved by ULIP over maximum power transmission (3.3 times) can be accounted for by the balancing of the system capacity from the cell-centre to the cell-edge, boosting high-priority throughput by sacrificing that of the low-priority MMSs, and hence achieving a more throughput fair system.

Surprisingly, the fairness of the PFS system is diminished with regards to the SINR scheduler, but this fact is already discernable from Fig. 4.7(a), where the slope of the PFS CDF is much more gradual. Essentially, the assignment of resources according to instantaneous rate gives an advantage to MMSs closer to the cell-centre, reducing the throughput fairness of the network.

This is clearly seen in Fig. 4.9, where the MMS throughput is plotted against the distance between the MMS and its serving MBS, a further indicator of the system fairness. While the max. power, power control and ULIP-PFS systems generate most of their capacity in the

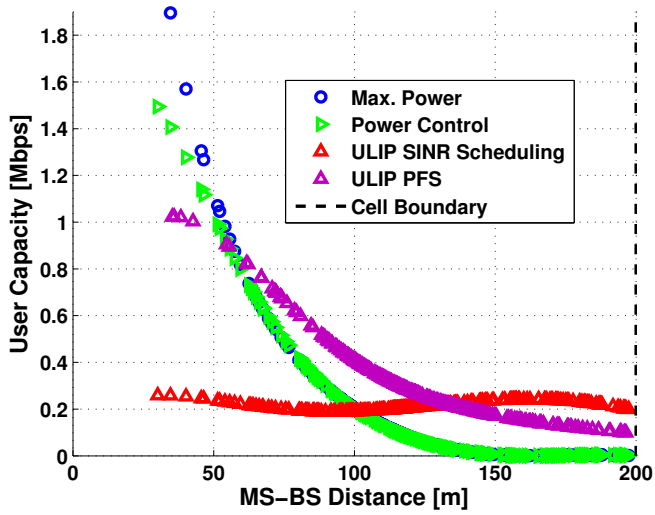

Figure 4.9: *System throughput vs. distance performance results for ULIP, LTE power control, and maximum power transmission.*

cell-centre (MMSs closer to the MBS), ULIP-SINR achieves an almost flat, much more even areal distribution of throughput in each cell. These findings confirm both the user throughput and fairness results shown in Fig. 4.7(a) and Fig. 4.8, respectively. Furthermore, due to the simulation environment, the gains for many MMSs are quite low, and hence power control very often needs max. transmit power to attempt to achieve the target SINR. Hence, there is little performance difference between the two systems, as is seen in Fig. 4.9. Finally, it is evident that ULIP-PFS provides throughput benefits over the benchmarks in almost the whole cell.

In Fig. 4.10, the system throughput CDF results for ULIP, power control and maximum power transmission are shown. At the 50th percentile, it can be clearly seen that while power control surrenders a slight portion ($\approx 4\,\%$) of the system capacity achieved by maximum power transmission, ULIP-SINR produces a gain of over $15\,\%$, and ULIP-PFS provides an $80\,\%$ augmentation, resulting from the large number of MMSs given throughput boosts (see Fig. 4.7(a)). This is a very encouraging result, as it shows that the throughput shift from low- to high-priority MMSs is beneficial for the system, achieving larger throughput gains for the high-priority users than losses by the low-priority MMSs. This is also a direct result of the link adaptation (LA), as any excess SINR (*i.e.*, $\gamma > 20\,\text{dB}$) at the cell-centre can be transferred to the cell-edge without incurring any throughput losses for the low-priority (cell-centre) users. Furthermore, Fig. 4.10 confirms the result achieved in Section 4.4.2, and shows further that system capacity gains are achievable. Finally, it is clear that the additional gains induced by the PFS ($56\,\%$ over the SINR

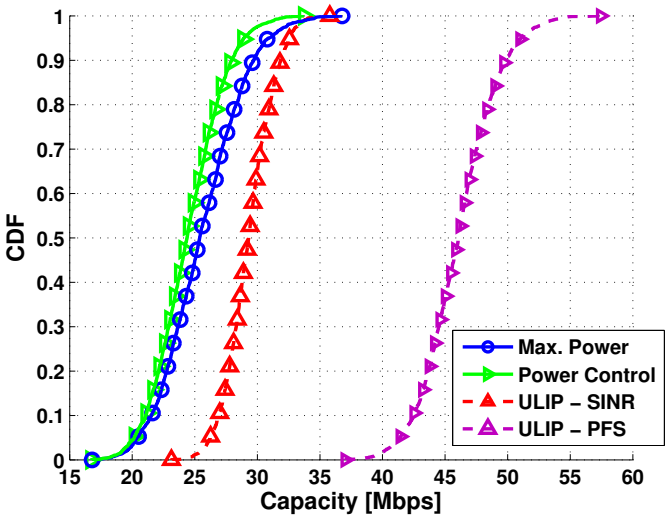

Figure 4.10: *System throughput performance results for ULIP, LTE power control, and maximum power transmission.*

scheduler) results from the tradeoff with the network fairness, as the cell capacity is shifted more towards the cell-centre.

In Fig. 4.11, it can be seen that, surprisingly, power control exhibits an even worse energy efficiency than maximum power transmission. This is mainly due to the system throughput losses incurred. As expected, however, ULIP provides substantial gains over both benchmark systems, achieving a stout 3.5 and 3.6 times the energy efficiency of max. power and power control at the 50th percentile, respectively. ULIP-PFS is able to improve these gains further, resulting in 5.2 and 5.4 times the system energy efficiency of the benchmarks, respectively. This may seem contradictory to the results shown in Fig. 4.7(b), however these simply show that the transmit power to throughput relation at each MMS is constant, which is expected as the ULIP procedure regulates this ratio, and not the scheduler. Essentially, the favourable allocation to higher-throughput MMSs allows the system capacity to be boosted with similar system transmit power. Therefore, the system energy efficiency is also augmented. Finally, the large gains seen by both ULIP systems are a combination of *a)* the system throughput boosts achieved via the effective shifting of SINR from the cell-centre to the cell-edge; and *b)* the substantial power reductions of the low- and mid-priority (cell-centre) users to protect the high-priority users from interference. Together, these two processes provide the significant energy efficiency gains seen in Fig. 4.11, and confirm (4.10).

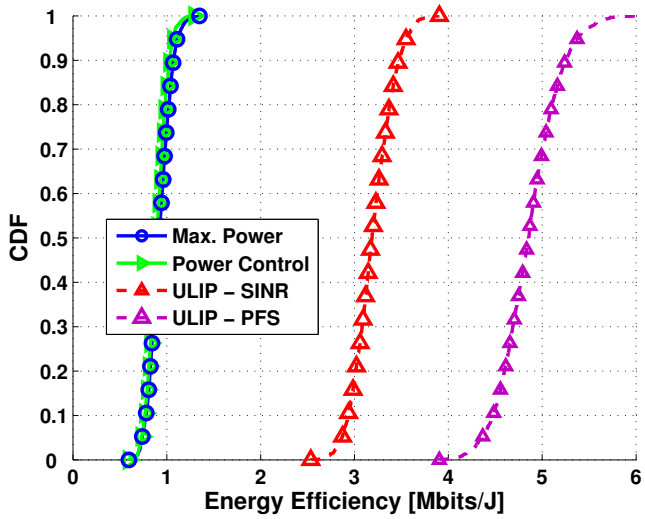

Figure 4.11: *System energy efficiency performance results for ULIP, LTE power control, and maximum power transmission.*

All in all, ULIP dominates each of the two benchmarks over the three performance criteria, especially providing a much more energy efficient and fair system. Furthermore, by achieving considerable gains in network capacity, it is clear that both performance analysis proofs have been confirmed.

4.7 Summary

Full frequency reuse and the resulting large CCI in OFDMA networks brings forth the necessity for ICIC in future wireless networks. A technique for ULIP has been presented in this chapter, which provides protection from CCI through the power reduction of a subset of the neighbouring cell RBs, based on the SINR targets of the MSs in the cell of interest. Aside from the fact that no extra signalling is necessary over the control channels, a further benefit of ULIP is a guaranteed increase in energy efficiency of all MSs in the system, and of the system as a whole. Furthermore, it was shown that while a loss in system capacity is possible, this is not certain, and hence gains in achievable system throughput are also possible. This is especially the case in networks where cell-edge capacity is limited, and most of the cell throughput is concentrated in the cell-centre.

It was shown that ULIP, combined with the SINR scheduler, achieves not only a 15% system capacity gain, but also substantially increases the system energy efficiency and fairness by 3.5

and 3.3 times, respectively. This is a direct result of the SINR displacement from the cell-centre to the cell-edge, and confirms the results in Section 4.4.1, highlighting the excellent energy efficiency of the ULIP protocol. Furthermore, when utilising the PFS, these gains are improved to an 80% in terms of system capacity, and 5.2 times for the system energy efficiency. However, this comes at the price of a reduction in system fairness, due to the larger throughputs in the cell-centre. Finally, ULIP-SINR eliminates the $\approx 20\,\%$ outage suffered in the benchmarks, and provides throughput gains for over $80\,\%$ of the MSs in the network. Consequently, ULIP diminishes the tradeoff between system capacity and fairness/energy efficiency, and is able to provide significant gains in all three performance areas.

Finally, ULIP presents an efficient technique for CCI mitigation in macro-cellular networks, benefitting from the multitude of MSs per cell and the time slotted balancing of the throughput over these users. However, it is clear that ULIP power control is ineffectual without an appropriate scheduler. Hence, a more centralised approach where MSs are grouped according to their interference environment (*e.g.*, similar to CoMP) may be able to provide higher coordination and protection between cells, and consequently further minimise the necessary system transmit power.

Chapter 5
Pareto Optimal Power Control Scheduling

5.1 Introduction

For OFDMA systems, some traditional centralised ICIC techniques, such as power control, interference cancellation, fractional frequency reuse, and SDMA [120], have been proposed. Most of these strategies, however, require knowledge about the position of a MS relative to it's own and neighbouring BSs, which clearly increases the signalling burden in the network. In [14], a dynamic channel acquisition algorithm based on convex optimisation for the wireless downlink is considered, which provides optimal power and throughput performance for i.i.d. channels. This optimality suffers however for general ergodic channels, and hence is not suitable for mobile environments. In [140], the authors propose a low-complexity algorithm to optimise the sum rate under individual rate and power constraints. Here though, because the water-filling solution is used for rate-optimal power allocation, a fairness of the solution is reduced. In [141], the uplink scheduling and power control problems are combined for optimal SIR distribution over large networks. While theoretically Pareto-optimal and practically sound algorithms are presented, the basis on maximisation of utilities heightens their implementation complexity. A simpler solution is sought after in this chapter.

In [142], a truncated closed-loop power control scheme is presented to cut off transmission of users when their short-term fading falls below a given threshold. While this leads to gains in both capacity and user availability, users are shown to suffer from large delays, a clearly undesirable result for mobile systems. Power control for OFDMA networks is presented in [104], where FPC offers a modification to conventional power control to control the tradeoff between system capacity and cell-edge rate. Due to this, however, many users will not achieve their SINR targets, and hence user throughput can suffer. Furthermore, an extension to FPC is developed where the power control mechanism takes interference caused to neighbouring cells into account. While this achieves a modest capacity increase, only the variance of interference to other cells, rather than the mean, is reduced. In [12] a computationally efficient power control

technique is introduced, where minimisation of transmit power is the main goal. However, by splitting the joint subcarrier and power allocation into two stages, the dependence between the two is disregarded, yielding suboptimal performance.

Finally, studies indicate that a substantial portion of wireless traffic originates indoors [4]. Poor signal reception through walls severely inhibits the operation of indoor data services, attracting considerable interest in the concept of femto-cells [4] (see Section 2.4.2). While abundant research on femto-to-macro interference has been carried out [106, 107], including the application of POPC [143, 144], few techniques have been considered to manage the interference between several densely deployed FBSs. Although, recent research into exactly this area has yielded capacity improvements for both centralised [145] and distributed techniques [146, 147].

As opposed to the ULIP technique introduced in Chapter 4, in which power control was performed via direct user inter-cell coordination, the methodology exploited here is based on the original power control work presented in [10, 11, 62]. This provides a more highly coordinated scheme among neighbouring BSs, where Pareto optimality in terms of transmit power usage for all MSs in the system is aspired.

5.2 System Model

A centralised technique is presented that can be implemented for both the downlink and uplink of an OFDMA network, where the system and channel models are described in detail in Section 3.2. For completeness, the technique introduced here is investigated in two scenarios:

- an equivalent dense, small cell, and high-interference **macro-cellular** environment as in Chapter 4, the construction of which is described in Section 3.3.1.1; and
- a dense, randomly deployed **femto-cell** scenario, as described in Section 3.3.1.2 with $\tilde{\mu}(u)=1$.

5.3 Pareto Optimal Power Control

In a wireless system, the quality of each link is determined by the SINR at the intended receiver, which is calculated in (3.3). Given each link is assigned a minimum SINR target, γ_u^*, $\gamma_u^m \geq \gamma_u^*$ for all RBs assigned to MS_u, this constraint can be represented in matrix form [10, 15, 62] with

component-wise inequalities for K interfering MSs

$$(\mathbf{I}-\mathbf{F})\mathbf{P} \geq \mathbf{u}\,, \quad \mathbf{P} > \mathbf{0}\,, \tag{5.1}$$

where $\mathbf{I}$ is the identity matrix and $\mathbf{P}=(P_1,\ldots,P_K)^\dagger$ is the vector of transmit powers,

$$\mathbf{u} = \left(\frac{(I_1+\eta)\gamma_1^*}{G_{1,v_1}},\cdots,\frac{(I_K+\eta)\gamma_K^*}{G_{K,v_K}}\right)^\dagger\,, \tag{5.2}$$

is the vector of interference (I_i) plus noise power scaled by the SINR targets and channel gains, $(\cdot)^\dagger$ is the transpose operator, and $\mathbf{F}$ is the interference matrix where

$$F_{i,j} = \begin{cases} 0, & \text{if } i=j \\ \frac{\gamma_i^* G_{j,v_i}}{G_{i,v_i}}, & \text{if } i \neq j \end{cases} \tag{5.3}$$

with $i,j=1,\ldots,K$. $\mathbf{F}$ is non-negative and irreducible [15].

Given $\rho_F = \max_i |\lambda_i|$ as the Perron-Frobenius eigenvalue of $\mathbf{F}$, if $\rho_F<1$, then there exists a vector $\mathbf{P}>\mathbf{0}$ such that the SINR requirements of all interfering users are satisfied, and

$$\mathbf{P}^* = (\mathbf{I}-\mathbf{F})^{-1}\mathbf{u} \tag{5.4}$$

is the Pareto optimal solution (*i.e.*, if there is any other solution $\mathbf{P}$ to (5.1), then $\mathbf{P}>\mathbf{P}^*$ component-wise) [10, 15]. Hence, if all the SINR requirements can be met simultaneously, the optimal power vector $\mathbf{P}^*$ minimises the transmit power of the users.

Foschini-Miljanic Algorithm Foschini and Miljanic developed in [62, 63] the following iterative power control algorithm that converges to $\mathbf{P}^*$ if $\rho_F<1$, and diverges to infinity (*i.e.*, $P_{\max}$) otherwise. This iterative Foschini-Miljanic algorithm is given by

$$\mathbf{P}(k+1) = \mathbf{F}\mathbf{P}(k) + \mathbf{u}\,, \tag{5.5}$$

for iteration $k=1,2,3,\ldots$. Furthermore, this can be simplified to a per-user basis

$$P_i(k+1) = \frac{\gamma_i^*}{\gamma_i(k)} P_i(k)\,, \tag{5.6}$$

for each link $i \in \{1, 2, \ldots, K\}$. Hence, each MS increases power when its SINR is below its target and decreases power when its SINR is greater than its target.

5.4 Power Control Scheduling (PCS)

In Pareto optimal power allocation, given a feasible link allocation, *i.e.*, $\rho_F < 1$, a vector $\mathbf{P}^* = (\mathbf{I} - \mathbf{F})^{-1}\mathbf{u}$ can be found such that all users achieve their SINR requirements with minimal power. This is of course a highly desirable result which, depending on the location and service requirements of the interfering MSs, is clearly not always possible. Hence, by scheduling users in such a manner to maximise the number of feasible $\mathbf{F}$ matrices (in principle, there can be as many $\mathbf{F}$ matrices as there are RBs, due to OFDMA resource orthogonality), the system spectral efficiency can be maximised. Such a scheduling algorithm, PCS, is developed here.

5.4.1 Analytical Basis

Since for a particular grouping of MSs (on the same RB(s) in different cells) to be feasible $\rho_F < 1$, it follows the modulus of all eigenvalues λ_i of $\mathbf{F}$ must also be less than unity, *i.e.*, $|\lambda_i| < 1$, $\forall i = 1, \ldots, K$. In other words, all eigenvalues must lie within the unit circle.

In [148], Jury provides a simplified analytic test of stability of linear discrete systems. The test also yields the necessary and sufficient conditions for any real polynomial to have all its roots inside the unit circle. Hence, this test can be directly applied to the characteristic function $f_{\mathbf{F}}(\lambda)$ of the matrix $\mathbf{F}$, whose roots are the eigenvalues of $\mathbf{F}$, and thus need to lie within the unit circle. The characteristic function of $\mathbf{F}$ for $K = 3$[1] interfering MSs can be expressed as follows:

$$\text{Given} \qquad \mathbf{F} = \begin{bmatrix} 0 & F_{1,2} & F_{1,3} \\ F_{2,1} & 0 & F_{2,3} \\ F_{3,1} & F_{3,2} & 0 \end{bmatrix}$$

$$\begin{aligned} f_{\mathbf{F}_3}(\lambda) &= \det(\mathbf{F} - \lambda\mathbf{I}) \\ &= -\lambda^3 + \lambda(F_{1,2}F_{2,1} + F_{1,3}F_{3,1} + F_{2,3}F_{3,2}) \\ &\quad + F_{1,2}F_{2,3}F_{3,1} + F_{1,3}F_{2,1}F_{3,2} \end{aligned} \tag{5.7}$$

[1] $K = 3$ cells are chosen for complexity reasons. For $K > 3$, the stability conditions in (5.9) and hence the derivation of PCS become highly complex, and is practically intractable.

$$= \lambda^3 + b\lambda + c \tag{5.8}$$

$$\text{Hence} \qquad b = -F_{1,2}F_{2,1} - F_{1,3}F_{3,1} - F_{2,3}F_{3,2}$$

$$c = -F_{1,2}F_{2,3}F_{3,1} - F_{1,3}F_{2,1}F_{3,2}$$

In [148], the stability constraints for a polynomial of order three are given as

$$\begin{aligned} & f(x) = a_3x^3 + a_2x^2 + a_1x + a_0, \quad a_3 > 0 \\ & 1) \;\; |a_0| < a_3 \\ & 2) \;\; a_0^2 - a_3^2 < a_0a_2 - a_1a_3 \\ & 3) \;\; a_0 + a_1 + a_2 + a_3 > 0, \; a_0 - a_1 + a_2 - a_3 < 0 \end{aligned} \quad . \tag{5.9}$$

These conditions can now be applied to the characteristic function $f_{\mathbf{F}_3}(\lambda)$

$$\begin{aligned} & f_{\mathbf{F}_3}(\lambda) = \lambda^3 + b\lambda + c \\ & \quad a_3 = 1, \; a_2 = 0, \; a_1 = b, \; a_0 = c, \\ & \quad 1) \;\; |c| < 1 \\ & \quad 2) \;\; c^2 - 1 < b \;\rightarrow\; b > 1 - d^2 \\ & \quad 3) \;\; c + b + 1 > 0 \;\rightarrow\; b > -c - 1, \\ & \qquad c - b - 1 < 0 \;\rightarrow\; b > c - 1 \end{aligned} \tag{5.10}$$

which describes the ranges of b and c for which $\mathbf{F}$ is feasible. These are shown in Fig. 5.1 by the dotted lines and the enclosed area. However, since from (5.3) $F_{i,j} \geq 0$, $\forall i, j$, it is clear that both $b, c \leq 0$, and hence the feasible area is reduced (from light to dark in Fig. 5.1), and the constraints are reduced to only a single one, such that the **feasibility condition** becomes:

$$\begin{aligned} & 3) \quad b > -c - 1 \\ & -F_{1,2}F_{2,1} - F_{1,3}F_{3,1} - F_{2,3}F_{3,2} > F_{1,2}F_{2,3}F_{3,1} + F_{1,3}F_{2,1}F_{3,2} - 1 \\ & \textbf{So, } \rho_F < 1 \textbf{ if:} \\ & F_{1,2}F_{2,1} + F_{1,3}F_{3,1} + F_{2,3}F_{3,2} + F_{1,2}F_{2,3}F_{3,1} + F_{1,3}F_{2,1}F_{3,2} < 1\,. \end{aligned} \tag{5.11}$$

Thus, a group of MSs, one in each cell (in the three-cell scenario), is feasible iff (if and only if) the condition in (5.11) is fulfilled. This is clearly dependent on the individual desired and interfering path gains, along with the SINR targets of the users. Therefore, a scheduler might

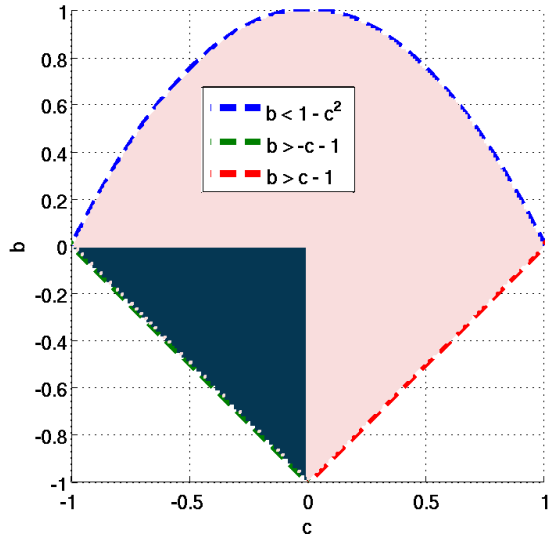

Figure 5.1: *Enclosed area depicting range of values for* b *and* c *in* (5.8) *for which all eigenvalues of* $\mathbf{F}$ *are within the unit circle. Due to the nature of* $b, c \leq 0$*, the blue area denotes specific feasibility area.*

make use of this condition to schedule users such that the number of feasible groups of MSs is maximised, hence also maximising the spectral efficiency of the system.

Feasibility for $K - 1 = 2$ In the case that the scheduler is unable to find feasible groups for particular MSs (due to *e.g.*, location at the cell-edge), the Stepwise Removal (SR) algorithm (described in Section 5.4.2) turns off one of the links in a group of MSs, resulting in a feasibility matrix $\mathbf{F}$ of size $K-1 \times K-1$, in the three-cell case 2×2:

$$\mathbf{F} = \begin{bmatrix} 0 & F_{1,2} \\ F_{2,1} & 0 \end{bmatrix} \tag{5.12}$$

And hence, the characteristic function is given by

$$\begin{aligned} f_{\mathbf{F}_2}(\lambda) &= \det(\mathbf{F} - \lambda \mathbf{I}) \\ &= \lambda^2 - F_{1,2}F_{2,1} \\ &= \lambda^2 + c \\ c &= -F_{1,2}F_{2,1} \end{aligned} \tag{5.13}$$

Again from [148], the stability constraints for a polynomial of order $K{-}1{=}2$ are

$$\begin{aligned} & f(z) = a_2 z^2 + a_1 z + a_0, \quad a_2 > 0 \\ & 1) \;\; |a_0| < a_2 \\ & 2) \;\; a_0 + a_1 + a_2 > 0, \quad a_0 - a_1 + a_2 > 0 \end{aligned} \quad . \tag{5.14}$$

Applying these conditions to the $f_{\mathbf{F}_2}(\lambda)$ yields

$$\begin{aligned} & f_{\mathbf{F}_2}(\lambda) = \lambda^2 + c \\ & \quad a_2 = 1, \; a_1 = 0, \; a_0 = c, \\ & \quad 1) \;\; |c| < 1 \\ & \quad 2) \;\; c + 1 > 0 \;\rightarrow\; 1 > -c, \end{aligned} \tag{5.15}$$

and hence the **feasibility condition** is given by

$$2) \quad \begin{array}{l} 1 > -c \\ 1 > F_{1,2}F_{2,1} \end{array} \qquad \textbf{So, } \rho_F < 1 \textbf{ if: } \quad F_{1,2}F_{2,1} < 1\,. \tag{5.16}$$

5.4.2 Stepwise Removal

In both POPC and the Foschini-Miljanic algorithm, if $\rho_F \not< 1$, no solution is available, and hence $\mathbf{P}{\rightarrow}\mathbf{0}$ or $\mathbf{P}{\rightarrow}(P_{\max}, \ldots, P_{\max})^{\dagger}$, respectively. In these cases, either none of the links will transmit, or with (most-likely) too much power, and hence these solutions are suboptimal.

A better way to address this problem is to successively remove single links [11] from the group of interfering MSs, until an $\mathbf{F}$ is achieved with $\rho_F{<}1$. It makes sense to, at each step, remove the link that is causing the largest interference to the other users. It is clear, however, that turning off one of the links will harm the system spectral efficiency, and hence for each link removal, the SINR target for the remaining links must be updated as follows

$$\gamma^*_{(1),\mathrm{up}} = \frac{\prod_j^K \left(1 + \gamma^*_j\right)}{1 + \gamma^*_{(2),\mathrm{up}}} - 1\,, \tag{5.17}$$

where $\gamma^*_{(i),\mathrm{up}}$ represents the updated SINR target of the ith *remaining* link. Since (5.17) has infinite solutions, $\gamma^*_{(1),\mathrm{up}}$ and $\gamma^*_{(2),\mathrm{up}}$ must be optimised with (5.17) as the constraint. This may

be a power minimisation

$$\text{Solve} \quad \min\left\{\gamma^*_{(1),\text{up}} + \gamma^*_{(2),\text{up}}\right\} \quad \text{s.t. (5.17) is satisfied.}, \tag{5.18}$$

or an equal absolute SINR increase[2].

$$\text{Solve} \quad \gamma^*_{(1),\text{up}} - \gamma^*_{(1)} = \gamma^*_{(2),\text{up}} - \gamma^*_{(2)} \quad \text{s.t. (5.17) is satisfied.}. \tag{5.19}$$

Finally, when two links have been removed and only a single link remains, $\gamma^*_{(1),\text{up}} = \prod_j^K \left(1+\gamma^*_j\right) - 1$, and $\mathbf{F}=0$, $\rho_F=0$, and $\mathbf{P}=\mathbf{u}=\frac{n\gamma^*_{(1),\text{up}}}{G_{1,v_1}}$.

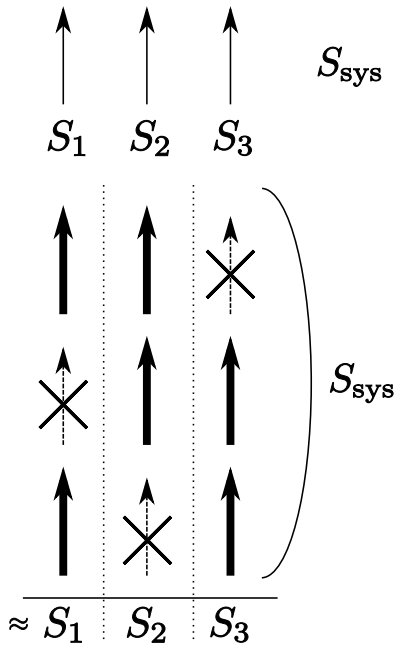

Figure 5.2: *Example of SR algorithm with SINR target updates. By rotationally scheduling the MSs with updated γ^*, the system and user spectral efficiencies can be maintained over multiple time slots.*

Through this form of link removal, the system spectral efficiency can be maintained while maximising the number of transmitting users according to the general feasibility constraint ρ_F. Furthermore, it prevents the convergence to maximum power that results from the Foschini-Miljanic algorithm, and the annihilation of links caused by POPC.

[2]Here, (5.18) is utilised in order to maintain the power minimisation of POPC.

5.4.3 Scheduling

The goal is to maximise the number of "MS-groups" for which (5.11) is satisfied and POPC can be applied. This is opposed to a random scheduler where the assignment of RBs, and hence also the MS-groups, is performed arbitrarily. The scheduler is split into three stages, corresponding to the number of cells considered and hence one more the number of link removals that are possible.

1. Find all feasible (5.11) combinations of MSs from each of K=3 cells. It is, of course, possible for an MS to be part of multiple feasible groups.
   (a) Schedule the MSs with the fewest feasible combinations (*i.e.*, "least feasible" MSs) first, to maximise the number of feasible groups.
   (b) Continue scheduling the least-feasible MSs until no feasible combinations of K=3 are remaining.
2. The unscheduled MSs are unable to form feasible groups of three, so must form groups with a link removed. Find all feasible (5.16) pairs or MSs, with updated γ_i^*'s, in the K=3 cells.
   (a) Schedule the least feasible MSs first. To complete the group, the least-feasible (or non-feasible) MS from the remaining cell is added.
   (b) Continue scheduling the least-feasible MSs until no feasible combinations remain.
3. Finally, the remaining unscheduled users cannot form any feasible group, so must transmit individually.
   (a) Form groups randomly among the remaining MSs, with updated γ_i^*'s.
   (b) The MS with the strongest path gain in each group is set as the active link.
4. Now that the groups have been formed, the corresponding transmit powers must be calculated and assigned.
   (a) POPC is applied to each group of users. $\mathbf{F}$ and $\mathbf{u}$ are sized appropriately given the number of active links.
5. The deactivated (removed) MSs need to be served, so these are permitted to transmit in later time slots.

(a) If two links are active, then over three time slots each MS should transmit twice, such that neither the system or link spectral efficiency are compromised.

(b) If only a single link is active, each MS transmits alone in one of three slots.

In essence, Step 5 enforces the "rotational" scheduling principle utilised in the SR algorithm (see Fig. 5.2), such that each MS has the opportunity to achieve its target over multiple time slots. Through this scheduler, all MSs in the system should attain the desired spectral efficiency, and if not, minimise the losses incurred.

5.4.4 Three-Cell Simulation Results

Fig. 5.3 shows the spectral efficiency results for varying SINR targets and ISDs in a three-cell scenario. The max. power spectral efficiency is independent of SINR targets and thus constant over all SINRs, while POPC suffers significantly from the random grouping (all comparative techniques are randomly scheduled), as the number of feasible groups disappears very rapidly with increasing SINR. The upper bound in Fig. 5.3 denotes the Shannon capacity of the given SINR target, *i.e.*, the attainable spectral efficiency if *all* MSs can be optimally scheduled.

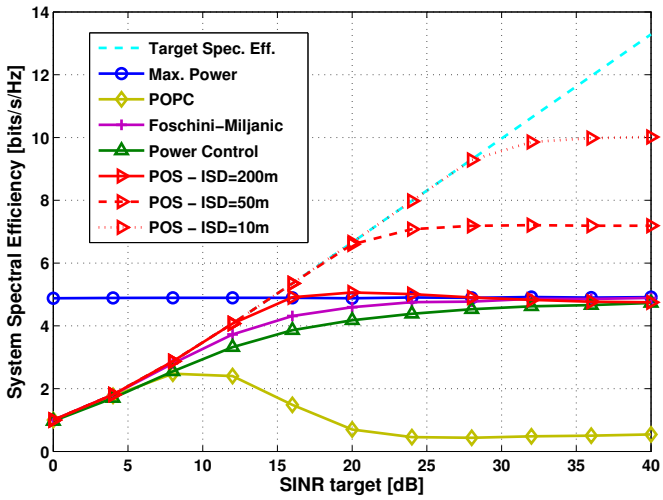

Figure 5.3: *System spectral efficiency (normalised Shannon capacity) results for the various power control techniques over a range of SINR targets. Three-cell scenario with a single omnidirectional antenna per cell.*

The ISD is a significant factor in the performance of PCS. Here, the smaller the ISDs, the better the performance; a key factor for shrinking cell sizes in future networks. When links are

deactivated, the larger transmit powers needed to meet γ^*_{up} are bounded by $P_{\max}$. Reducing the ISDs is equivalent to increasing $P_{\max}$ due to greater desired link gains. Lastly, it is evident that PCS outperforms all other techniques investigated, and has significant potential for future cellular networks.

5.4.5 Extension to Macro-cellular Network

Since PCS is developed for a three-cell system, on its own it is very ineffective for more realistic scenarios where there are clearly more than three cells. One option would be to derive the feasibility condition(s) for a larger number of cells, to henceforth be able to apply PCS to a larger network. From [148][3], however, it is evident that the feasibility conditions for even a four-cell scenario are excessively complex, and hence such extension to larger networks is highly impractical.

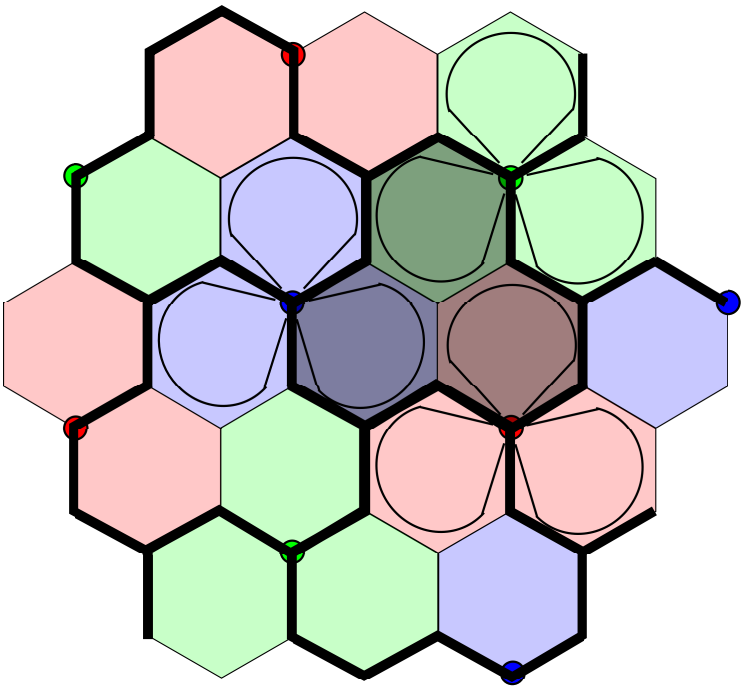

Figure 5.4: *Extension of three-cell PCS to larger multi-cellular networks. Universal frequency reuse is applied, and the differing colouration of the cells simply demarks which BS is serving them.*

A more pragmatic approach is to find a way to tessellate the three-cell PCS over a network of any dimensions. This is shown in Fig. 5.4, where the structure of a typical sectorised cellular

[3]In [148] the sufficient conditions for stability of nth order polynomials are presented, which were used to derive the feasibility condition in (5.11).

network can help the extension of PCS to multiple cells. By grouping three cells with coinciding beam patterns (see shaded cells in Fig. 5.4), PCS can be applied to mitigate interference between these cells. In addition, the cluster will be relatively shielded from neighbouring sectors' interference due to the nature of their beams. This clustering is then tessellated over the network, such that PCS can be applied separately in each cluster without overly excessive CCI from the surrounding cells, allowing the MSs to achieve their transmission requirements.

5.5 Power SINR Scheduling (PSS)

PCS is dependent on many users per cell to be able to iterate over multiple path gain combinations and, hence, find feasible MS-groups in these cells. In the femto-cell environment considered here, however, each cell contains only a single user, and hence in any grouping of three cells the users in these cells will directly form a MS-group. Now if this group is infeasible, then there is no possibility of a different (feasible) group being formed, and at least one link must be removed. Therefore, to avoid this, the SINR targets of the individual users (instead of the path gains) must be varied such that $\mathbf{F}$ becomes feasible.

5.5.1 SINR Variation

In PSS, the same feasibility conditions for $\mathbf{F}$ still apply, *i.e.*, (5.11) and (5.16). Hence, an intelligent mechanism for the variation of the individual SINRs must be formulated. This is done by reexamining these feasibility conditions.

The feasibility condition is given in (5.11) as

$$\begin{aligned} f(\mathbf{F}) =& F_{1,2}F_{2,1}+F_{1,3}F_{3,1}+F_{2,3}F_{3,2}+F_{1,2}F_{2,3}F_{3,1}+F_{1,3}F_{2,1}F_{3,2} \\ =& \gamma_1^*\gamma_2^*\left(\rho^2\frac{G_{1,v_2}G_{2,v_1}}{G_{1,v_1}G_{2,v_2}}\right)+\gamma_1^*\gamma_3^*\left(\rho^2\frac{G_{1,v_3}G_{3,v_1}}{G_{1,v_1}G_{3,v_3}}\right)+ \\ &+\gamma_2^*\gamma_3^*\left(\rho^2\frac{G_{2,v_3}G_{3,v_2}}{G_{2,v_2}G_{3,v_3}}\right)+ \\ &+\gamma_1^*\gamma_2^*\gamma_3^*\left(\rho^3\frac{G_{1,v_2}G_{2,v_3}G_{3,v_1}+G_{1,v_3}G_{2,v_1}G_{3,v_2}}{G_{1,v_1}G_{2,v_2}G_{3,v_3}}\right) \\ =& \gamma_1^*\gamma_2^*A_{1,2}+\gamma_1^*\gamma_3^*A_{1,3}+\gamma_2^*\gamma_3^*A_{2,3}+\gamma_1^*\gamma_2^*\gamma_3^*A_{1,2,3} \end{aligned} \tag{5.20}$$

where $\mathcal{A}=\{A_{1,2}, A_{1,3}, A_{2,3}, A_{1,2,3}\}$ is the set of coefficients of $f(\mathbf{F})$ that are constant through-

out the SINR variation. Therefore if $f(\mathbf{F})>1$, by finding $\max\{\mathcal{A}\}$ the largest coefficient can be found, and hence the SINR targets preceding the coefficient can be reduced to ultimately decrease $f(\mathbf{F})$.

Given $f(\mathbf{F})>1$ and $\max\{\mathcal{A}\}=A_{i,j}$, it is clear that γ_i^* and γ_j^* need to be reduced such that $f(\mathbf{F})<1$. The reduction is performed as follows:

$$\begin{aligned} r_{\mathrm{gr}} &= \frac{1}{r_{\mathrm{o}} n_{\mathrm{r}}} \left\lceil r_{\mathrm{o}} \left(1 - \frac{1}{f(\mathbf{F})}\right) \right\rceil \\ \gamma_i^{*,\mathrm{up}} &\leftarrow \gamma_i^*(1 - r_{\mathrm{gr}}) \\ \gamma_j^{*,\mathrm{up}} &\leftarrow \gamma_j^*(1 - r_{\mathrm{gr}}) \end{aligned} \tag{5.21}$$

where r_{gr} in (5.21) represents the SINR reduction factor rounded up to a factor[4] of $1/r_{\mathrm{o}}$ and n_{r} denotes the number of MSs whose SINR targets are being reduced (in the above case, $n_{\mathrm{r}}=2$). To maintain the desired system spectral efficiency, however, the remaining user's SINR target must be increased

$$\gamma_{k\neq\{i,j\}}^{*,\mathrm{up}} = \frac{(1+\gamma_1^*)(1+\gamma_2^*)(1+\gamma_3^*)}{(1+\gamma_i^*(1-r_{\mathrm{gr}}))(1+\gamma_j^*(1-r_{\mathrm{gr}}))} - 1\,. \tag{5.22}$$

Through this, the system spectral efficiency is maintained while the value of $f(\mathbf{F})$ is decreased. This procedure is repeated until either $\gamma_i^*, \gamma_j^* < \gamma_{\min}$, or $f(\mathbf{F})<1$, although it may achieve the desired SINR target constellation in the first step.

For the (rather unlikely) case that $\max\{\mathcal{A}\}=A_{1,2,3}$, the strongest interferer MS$_i$ is found, and the same reduction is performed, except $n_{\mathrm{r}}=1$ in (5.21). The SINR target increase of the remaining MSs is

$$\gamma_{\{j,k\}\neq i}^{*,\mathrm{up}} = \sqrt{\frac{(1+\gamma_1^*)(1+\gamma_2^*)(1+\gamma_3^*)}{(1+\gamma_i^*(1-r_{\mathrm{gr}}))}} - 1\,. \tag{5.23}$$

Feasibility for $K-1=2$ For the occasion that the scheduler is unable to find a set of $\{\gamma_1^{*,\mathrm{up}}, \gamma_2^{*,\mathrm{up}}, \gamma_3^{*,\mathrm{up}}\} \geq \gamma_{\min}$ such that $\mathbf{F}$ becomes feasible (*i.e.*, $f(\mathbf{F})<1$), the link causing the most interference is removed, and the SINR targets of the two remaining users are updated

[4]The reason for this rounding is two-fold; firstly, since $f(\mathbf{F})$ must be <1, without the rounding $f(\mathbf{F})$ would be steered towards 1 and not below, and secondly, because the consequent SINR rise of the third user will again slightly increase $f(\mathbf{F})$. Here, $r_{\mathrm{o}}=10$, corresponding to a rounding to 0.1, is utilised. However, this can be set differently (*e.g.*, $r_{\mathrm{o}}=5,\ 20,\ 100$) in order to manage the tradeoff between Pareto optimality (larger r_{o}) and convergence speed (smaller r_{o}).

according to the SR algorithm.

If, now, the feasibility condition (5.16) is not satisfied, the SINR target of the MS_i with the weaker desired channel gain must be reduced according to (5.21) with n_r=1, while MS_j with the stronger desired link receives a SINR target boost according to

$$\gamma_j^{*,\text{up}} = \frac{(1+\gamma_i^*)(1+\gamma_j^*)}{1+\gamma_i^*(1-r_{\text{gr}})} - 1\,, \tag{5.24}$$

to maintain the system spectral efficiency[5]. This is again repeated until either $\gamma_i^{*,\text{up}}<\gamma_{\min}$, or $f(\mathbf{F})<1$.

Finally, if the scheduler is unable to find $\{\gamma_i^{*,\text{up}}, \gamma_j^{*,\text{up}}\}\geq\gamma_{\min}$ such that $\mathbf{F}$ is feasible, the MS with the weaker desired link is removed, and the target of the remaining user is again updated.

5.5.2 Proof of Convergence

Here, a proof for the convergence of $f(\mathbf{F})$ by the SINR variations (5.21) and (5.22) is provided.

When implementing the scheduling algorithm, a check condition is built where the user grouping is *not* performed if $f(\mathbf{F})>1$ for $\{\gamma_i^*, \gamma_j^*, \gamma_k^*\}=\{\gamma_{\min}, \gamma_{\min}, \gamma_k^{*,\text{up}}\}=\mathbf{\Gamma}_{\min}$, as this signifies that SINR variation will be unable to satisfy (5.20). Thus, the convergence of the variation algorithm is based on this $\mathbf{\Gamma}_{\min}$, and is expressed as follows in Theorem 1.

Theorem 1 *Given $f(\mathbf{F}) \equiv f(\mathbf{\Gamma}) > 1$, where $\mathbf{\Gamma} = (\gamma_i, \gamma_j, \gamma_k)$, then iterative variations of $\mathbf{\Gamma}$ according to* (5.21) *and* (5.22) *will converge to $f(\mathbf{\Gamma}) < 1$ if*

$$f(\mathbf{\Gamma}_{\min}) < 1 \quad \textit{for} \quad \mathbf{\Gamma}_{\min} = (\gamma_{\min}, \gamma_{\min}, \gamma_k^{*,\text{up}})\,,$$

where γ_k^{up} is updated to maintain spectral efficiency.

[5]The MS with the stronger desired link is chosen for the SINR target boost as it will require less power than the weaker MS to achieve $\gamma^{*\text{up}}$ due to its enhanced desired channel gain, and hence cause less interference. This slightly reduces the fairness over a single slot, however through scheduling over multiple slots this is equalised.

Proof Given that $f(\mathbf{\Gamma})>1$, γ_i and γ_j are updated iteratively as follows

$$\gamma_i^{*,(m+1)} \leftarrow \gamma_i^{*,(m)}(1 - r_{\mathrm{gr}}^{(m)})$$
$$\gamma_j^{*,(m+1)} \leftarrow \gamma_j^{*,(m)}(1 - r_{\mathrm{gr}}^{(m)})$$

where r_{gr} is calculated by (5.21), $m = 0, 1, 2, \ldots$, and if $f(\mathbf{\Gamma})>1$ then $0<r_{\mathrm{gr}}^{(m)}<1$, and $(1 - r_{\mathrm{gr}}^{(m)})<1$. Hence, as long as $f(\mathbf{\Gamma})>1$, γ_i and γ_j will continue to be reduced, upper-bounded by the geometric sequence of $\gamma_i^*(1-\min_m\{r_{\mathrm{gr}}^{(m)}\})^m$, until

$$\gamma_i^{*,(n)} \leftarrow \gamma_{\min}$$
$$\gamma_j^{*,(n)} \leftarrow \gamma_{\min}$$

and hence $\mathbf{\Gamma} \leftarrow \mathbf{\Gamma}_{\min}=(\gamma_{\min}, \gamma_{\min}, \gamma_k^{*,\mathrm{up}})$, where $\gamma_k^{*,\mathrm{up}}$ is determined by (5.22).[6] Therefore, if $f(\mathbf{\Gamma}_{\min})<1$, then the algorithm will eventually enter the region where $f(\mathbf{F})\equiv f(\mathbf{\Gamma})<1$, and thus the algorithm converges. □

Corollary 1 *Theorem 1 and the corresponding proof also apply to* $\max\{\mathcal{A}\}=A_{1,2,3}$, *where* $n_{\mathrm{r}}=1$ *in* (5.21) *and* $\mathbf{\Gamma}_{\min}=(\gamma_{\min}, \gamma_j^{*,\mathrm{up}}, \gamma_k^{*,\mathrm{up}})$. *Furthermore, it can also be applied to* $K-1=2$, *where* $\mathbf{\Gamma}_{\min}=(\gamma_{\min}, \gamma_j^{*,\mathrm{up}})$, *and hence the algorithm converges in all of these cases.*

5.5.3 Scheduling

While it is clear from Section 5.5.1 how an infeasible grouping of MSs can be made feasible, these groups must still be found. In a randomly deployed femto-cell environment, this can be a challenging task as there is no pre-existing infrastructure to guide grouping mechanisms. Here, the cell-grouping part of PSS is described.

[6]Due to the calculation of r_{gr} in (5.21), $\gamma_i^{*,(n)}, \gamma_j^{*,(n)}$ may become smaller than $\gamma_{\min}$. However in this case, they are simply set to $\gamma_{\min}$ (as they should not go lower anyway), and $\gamma_k^{*,\mathrm{up}}$ is calculated accordingly.

5.5.3.1 Interference Graphs

To find groups of femto-cells suitable for POPC, an interference graph [149] for the network instance is constructed, through which the strongest interfering cells can be grouped together. Interference graphs are constructed by evaluating the interference users in the system cause to each other. For each FMS, the strongest interferers are removed (and consequently considered as interfering neighbours) until the minimum SIR, $\hat{\gamma}^*$, at the MS is achieved.

In the downlink, assuming each FBS will transmit at maximum power, $P{=}P_{\max}$, each user will achieve a certain SIR. If the SIR of FMS$_k$, $\hat{\gamma}_k{<}\hat{\gamma}_k^*$, the strongest interferers are removed until

$$\hat{\gamma}_k = \frac{S_k}{\sum_{l \in \mathcal{I}_k \setminus \mathcal{W}_k} I_{k,l}} \geq \hat{\gamma}_k^* \,, \tag{5.25}$$

where S_k is the desired received signal strength of FMS$_k$, $I_{k,l}$ the interference caused at FMS$_k$ from FMS$_l$'s BS, $\mathcal{I}_k$ all its interferers, and $\mathcal{W}_k$ the removed interferers, *i.e.*, neighbours. Hence, each user will have a list of strongly interfering neighbours based on its interference environment, and if cell l is a neighbour of cell k, the vice versa is also true.

Once this procedure has been done for all FMSs in the system, the interference graph can be constructed, an example of which is shown in Fig. 5.5. From this, groups of (up to) three femto-cells (and hence the three MSs in these cells) are formed by collecting the three strongest interfering and neighbouring cells together, and then the next, and so on. For cells with fewer than two neighbours, smaller groups are formed.

5.5.3.2 SINR and Power Allocation

As a result of the interference graph grouping, each MS will be able to remove two of its strongest interferers through POPC and SINR variation, if necessary. The SINR target and transmit power allocation for each group is performed as follows:

1. If (5.11) is satisfied, then (5.4) (POPC) can be performed and each MS should achieve its SINR target.

2. If (5.11) fails, then $\max\{\mathcal{A}\}$ is found, and the γ_k^* are modified by (5.21) and (5.22) (or (5.23) if $\max\{\mathcal{A}\} = A_{123}$) until (5.11) is satisfied and (5.4) can be used.

3. If this is not possible, the strongest interfering link is removed, and (5.16) must be satis-

fied (with updated γ_k^* due to SR) in order for (5.4) to be applied.

4. If (5.16) fails, then the γ_k^* are adjusted through (5.21) and (5.24) until (5.16) is satisfied and (5.4) can be utilised.

5. If this is again not possible, then a second link is removed, and (5.4) (which converges to conventional power control for a single user) is performed for updated γ_k^*.

6. Similar to PCS, the deactivated MSs must be served, and thus are scheduled in later time slots. Further, links that, in the previous steps, reduced their γ^* are given a chance to transmit at higher spectral efficiencies. Thus, the SINR adaptation procedure is rotated within the group, such that each MS may achieve its target.

Through this power allocation, over multiple time slots, the number of simultaneously serviced (*i.e.*, $\gamma_k \geq \gamma_k^*$) MSs in the system will be maximised, along with the achievable throughput.

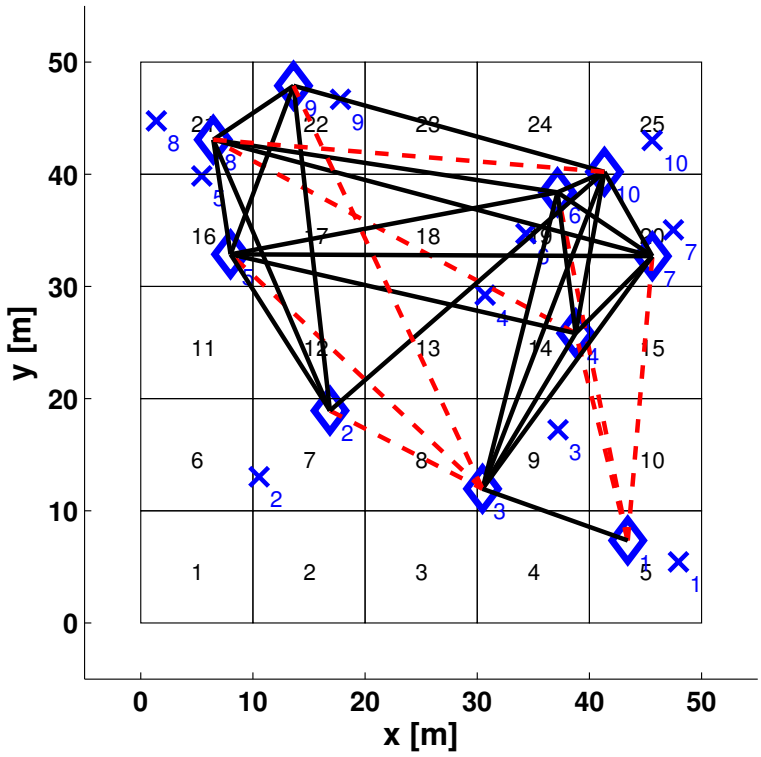

Figure 5.5: *Interference graphs for a given* 5×5 *grid femto-cell scenario for various SINR targets. The solid lines indicate neighbours for* $\gamma^*=0$ *dB, whereas the dashed lines indicate the additional neighbours when* $\gamma^*=8$ *dB.*

5.6 Simulation and Results

The general simulation setup utilised is described in Section 3.3. As mentioned previously, the application scenario for PCS is the dense macro-cellular environment described in Section 3.3.1.1, whereas PSS is implemented in the femto-cell deployment (see Section 3.3.1.2). The relevant simulation parameters for both scenarios can be found in Table 5.1.

Parameter	Value
Simulation area	37 cells
Results area	inner 7 cells
ISD	$350\,\mathrm{m}$
ICD	$200\,\mathrm{m}$
MMSs per cell, $\bar{N}$	10
Number of available RBs, M	50
RB bandwidth, B_{RB}	$180\,\mathrm{kHz}$
Noise spectral density, η_0	$-174\,\mathrm{dBm/Hz}$
Subcarriers per RB, k_{sc}	12
Symbol rate per subcarrier, s_{sc}	$15\,\mathrm{ksps}$
Time slots (subframes), z	12
Subframe duration, t_{sf}	$1\,\mathrm{ms}$
MBS transmit power, $P_{\mathrm{max,MBS}}$	$46\,\mathrm{dBm}$
MMS transmit power, $P_{\mathrm{max,MMS}}$	$23\,\mathrm{dBm}$
Sector $\theta_{3\mathrm{dB}}$	$70°$
Outdoor channel parameters α_{o}, β_{o}	25.6, 36.7
Apartment width, R_{a}	$10\,\mathrm{m}$
FBS probability, p_{act}	0.5
Max. MSs per femto-cell, $\tilde{\mu}$	1
FBS transmit power, $P_{\mathrm{max,FBS}}$	$10\,\mathrm{dBm}$
FMS transmit power, $P_{\mathrm{max,FMS}}$	$10\,\mathrm{dBm}$
Indoor channel parameters α_{i}, β_{i}	37, 30
Shadowing Std. Devs., σ_{i}, σ_{o}	10, $4\,\mathrm{dB}$
Auto-correlation distance	$50\,\mathrm{m}$

Table 5.1: *Chapter 5 Simulation Parameters*

5.6.1 Resource and Power Allocation

PCS For this study, MMSs in a cell are assigned a contiguous equal-sized block of RBs, where each block contains $\lfloor M/N_j \rfloor$ RBs. The scheduler assigns a block to each user in the cell. For PCS, the scheduling and allocation of power to the users is performed as described in Section 5.4.3. Furthermore, multiple time slots are utilised such that removed links can be scheduled in the next slot.

PSS Here, each FMS in a cell is assigned the full bandwidth (*i.e.*, all RBs), as only a single FMS per cell is considered. For PSS, the cell-grouping and allocation of power to the users is

performed as described in Section 5.5.3. Again, the simulation is run over multiple time slots, such that removed and γ^*-reduced links can be scheduled in later slots and achieve capacity.

Benchmarks Finally, the benchmarks utilised for comparison to PCS and PSS are max. power transmission (BM 1) and LTE FPC$_{\nu=1,\,0.5}$ (BM 2). For both, a random block assignment is employed.

5.6.2 PCS Results and Discussion

Fig. 5.6 shows the spectral efficiency results for PCS and the three benchmarks in a macro-cellular network. In general, PCS has a performance advantage over FPC$_{\nu=1}$ over all SINR targets (except γ^*=20 dB), whereas also substantial gains of $\approx$13 % are seen over max. power transmission in the mid-SINR (typically the operational) range. The PCS performance begins to suffer for higher SINRs as too many users are switched off each time slot by the SR protocol.

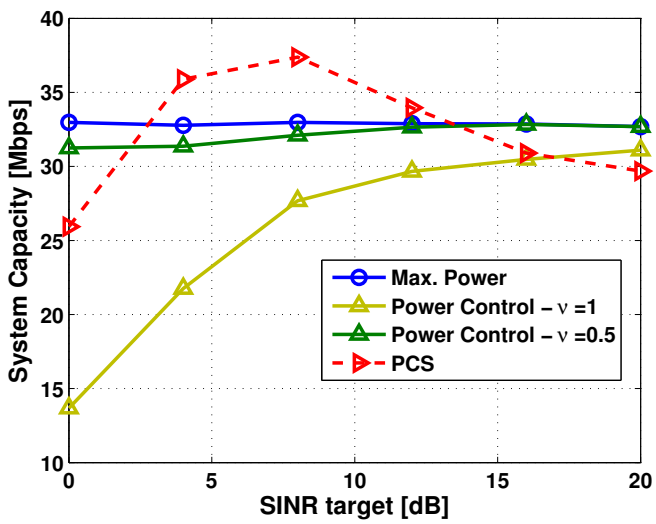

Figure 5.6: *System throughput performance results of PCS, LTE power control, and maximum power transmission.*

Furthermore, those users that are not able to achieve their targets are scarcely served, hence the decline in system throughput. On the other hand, the throughput reduction at lower SINRs results from the performance limitation of PCS to the required SINR targets. Therefore, the comparison to max. power and FPC$_{\nu=0.5}$ is rather unfair, since these are not bounded by targets. However, on average the PCS system throughput is equivalent to that of max. power transmission.

This becomes even more significant when considered together with the energy efficiency results shown in Fig. 5.7(a). As expected, maximum power transmission is the least energy efficient of the three considered techniques. PCS, on the other hand, provides massive energy efficiency benefits for the system, even when compared to $\text{FPC}_{\nu=1}$, with gains of almost 3 times for higher SINRs. This is due to the SR of links and Pareto optimality, reducing the system transmit power per time slot. Hence, it is quite clear that PCS drastically diminishes the transmit power consumption in a macro-cellular network.

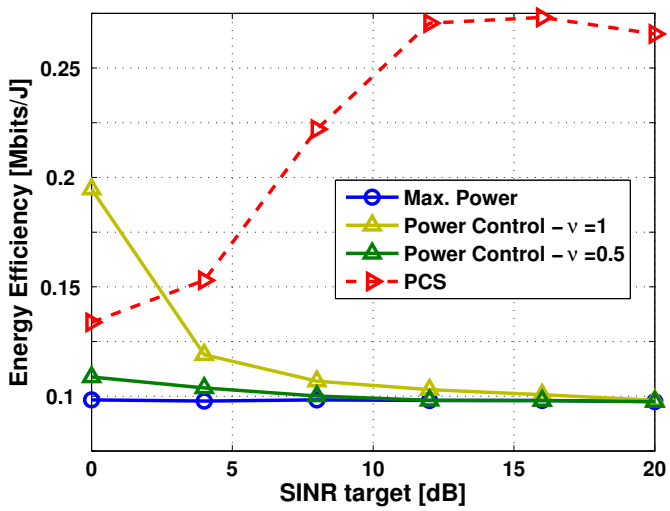

(a) Energy Efficiency

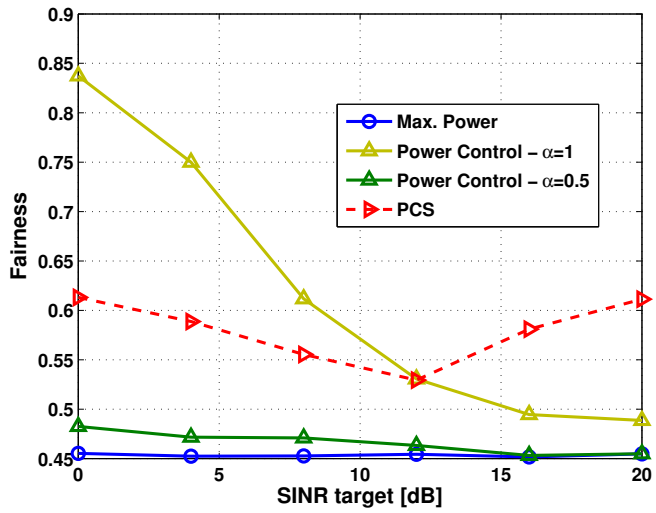

(b) Fairness

Figure 5.7: *System energy efficiency and fairness performance results of PCS, LTE power control, and maximum power transmission.*

The fairness of the compared techniques is displayed in Fig. 5.7(b), where unsurprisingly max. power and FPC$_{\nu=0.5}$ present the least fair systems. The PCS fairness offers the most consistent performance (of the power control schemes), resulting mainly from the rotational scheduling in the SR algorithm, allowing users to achieve similar throughputs over multiple time slots. As expected, the fairness of traditional power control falls with increasing SINR requirement, as clearly higher targets are more difficult to fulfil. Considering all of the results, it is evident that PCS provides overall superior system performance over the standard power allocation techniques. Furthermore, it is evident that an optimal SINR may be found that optimises the network according to one (or multiple) of the performance criteria. This leads into Chapter 6, where such an optimisation of network throughput is investigated.

5.6.3 PSS Results and Discussion

In Fig. 5.8, it is evident PSS produces large gains over conventional power control ($\nu = 1$), but does not achieve quite the system capacities of the other systems. It should be mentioned here that, again, the comparisons to both maximum power and FPC$_{\nu=0.5}$ are rather unfair (however are included as they represent the state-of-the-art power allocation in wireless networks), as

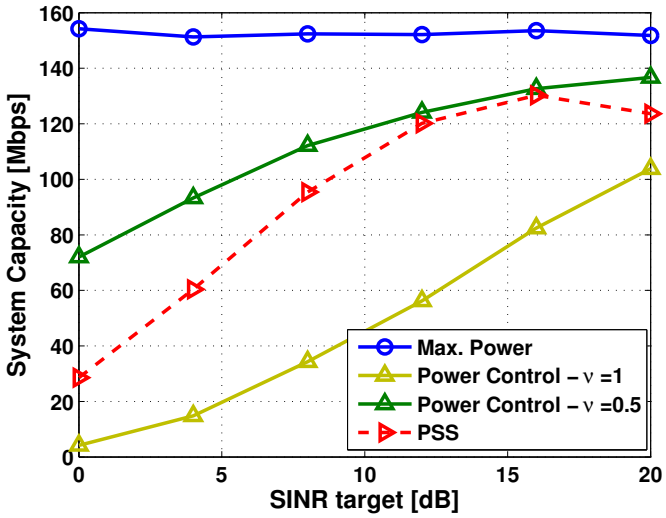

Figure 5.8: *System throughput performance results of PSS, LTE power control, and maximum power transmission.*

these are based much less on the actual SINR targets of the users (in the case of max. power not at all), and hence use significantly more power to achieve their larger system throughputs. Therefore, it is clear that the energy efficiency is a much more accurate performance comparison of the techniques.

This is shown in Fig. 5.9(a), where both maximum power and FPC$_{\nu=0.5}$ reveal diminished energy efficiency with regards to PSS. Furthermore, the energy efficiency of FPC$_{\nu=1}$ suffers due to the low throughput achieved in the high-interference scenario. Finally, in the high-SINR range it is evident that PSS can achieve more than twice the energy efficiency of the conventional schemes. All in all, PSS provides significant throughputs for almost all FMSs in the system while reducing the necessary transmit power.

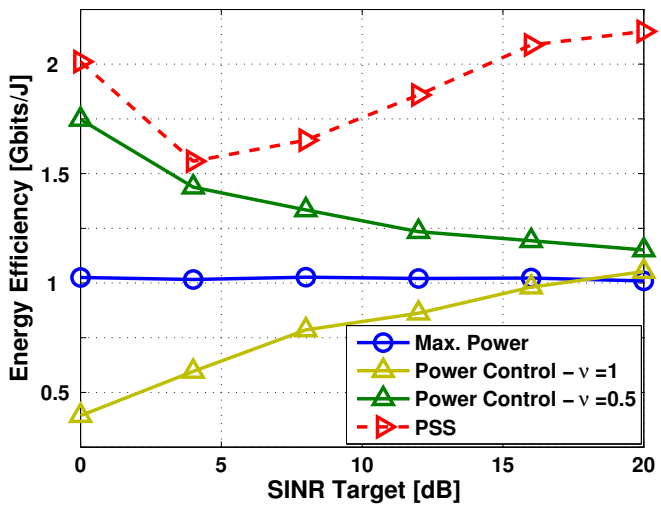

(a) Energy Efficiency

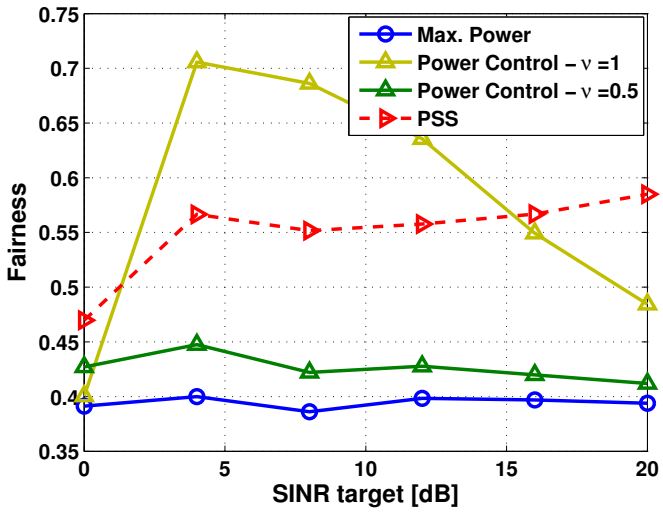

(b) Fairness

Figure 5.9: *System energy efficiency and fairness performance results of PSS, LTE power control, and maximum power transmission.*

Finally, Fig. 5.9(b) portrays the fairness results for the considered system, yielding the lowest fairness for maximum power (as expected) and the largest availability for $\text{FPC}_{\nu=1}$ in the mid-SINR range. PSS achieves an almost constant fairness over the SINR range (both PSS and $\text{FPC}_{\nu=1}$ suffer from outages at low SINRs due to the high interference in the scenario), indicating a balancing of user throughput over the FMSs due to the rotational scheduling of removed and SINR-diminished users, which are thus given equal opportunity to achieve their targets. Finally, as in the macro-cellular environment, the fairness of $\text{FPC}_{\nu=1}$ diminishes with increasing γ^*, indicating less satisfied FMSs. Overall, PSS manages to balance the benefits of max. power transmission and FPC, while boosting the energy efficiency of the network.

5.7 Summary

In this chapter, PCS, a scheduling technique designed to maximise the application of POPC, was introduced. By expressing the necessary conditions for power control in a simple feasibility condition of path gains and SINR targets, users are scheduled such that POPC can be applied. The addition of the SR algorithm in collaboration with SINR target updates allows the scheduler to achieve the target system spectral efficiency, while providing Pareto optimal power allocation for interfering users. Therefore, no significant losses in spectral efficiency are incurred while the total transmit power of the network is minimised, hence resulting in a more energy efficient system.

In addition, PSS, a derivative of PCS designed to maximise the application in femto-cells, is developed. Highly interfering femto-cells are grouped using interference graphs, such that the strong CCI can be mitigated via PSS. As only a single FMS per femto-cell is assumed, interfering MS groups (and thus path gains) cannot be modified, and hence a technique to adapt the SINR targets of the users was developed to render infeasible groupings feasible. Through this, MSs are allocated Pareto optimal transmit powers while limited losses in spectral efficiency are incurred.

It is quite clear from the three-cell results (in Fig. 5.3) that PCS provides close-to-optimal spectral efficiency over a wide range of SINR targets, and can significantly outperform standard power control techniques. Similar performance results are seen in the macro-cell environment, where PCS achieves throughput gains over the benchmark techniques for almost all γ^*. Furthermore, PCS provides large energy efficiency boosts over both power control and maximum

power transmission, significantly reducing the system transmit power.

In the femto-cell scenario, PSS provides substantial throughputs over a wide range of SINR targets, and significantly outperforms the purely target-based power control technique ($\text{FPC}_{\nu=1}$). However, both max. power transmission and $\text{FPC}_{\nu=0.5}$ are not strictly bound by SINR targets, and hence are able to transmit with higher power and achieve larger throughputs. On the other hand, it is evident that PSS provides again a low-power solution, significantly reducing the necessary FMS transmit powers, and hence creating "greener" femto-cellular systems.

Finally, while PCS and PSS provide successful combinations of resource and power allocation in cellular networks, it is clear that due to their centralised approach, a large amount of signalling is necessary to convey path gain (desired and especially interfering) and SINR target information among neighbouring BSs. Furthermore, deployment and backhauling issues in future networks (*e.g.*, HetNets) significantly enhance the complications of centralisation. Therefore, distributed and autonomous coordination that is scenario-adaptable should be envisioned for future systems in order to avoid such management difficulties.

Chapter 6
Fuzzy Logic Autonomous and Distributed Resource Allocation

6.1 Introduction

In Section 2.4, the upcoming challenges in future HetNets were presented, such as backhauling and interference management, among others. In general, these issues motivate the need for ***decentralised, autonomous*** interference coordination schemes that operate independently on each cell, utilising only local information, yet achieving efficient/near-optimal solutions for the network. By allowing BSs (all types) and MSs to individually optimise their resource allocations and transmission powers, a global optimum may be found without centralised algorithms governing the system. This would substantially reduce not only the amount of signalling but also the operation complexity of the network.

To this extent, recent research has seen the emergence of autonomous coordination techniques for SONs [108, 109], where transmit powers on subbands are adjusted independently in each cell via local and network utility optimisation. These utilities are based on the average rate in the cell, however do not examine user-specific resource allocation for additional interference coordination. Furthermore, the proposed strategies do not consider heterogeneous architectures that will inevitably describe future networks. Finally, the suggested algorithms assume still some signalling between neighbouring BSs, hence cannot be considered fully autonomous, and may also limit their applicability specifically for femto-cell networks.

On another note, there has been significant contribution to the modeling of HetNets [150–152], introducing important tools which may be used for network management, although solutions for scheduling and resource allocation utilising these models are not proposed. Such research is performed in [153], where the authors suggest a best-effort utility function based on QoS restricted priority users to provide cell association and power allocation. The splitting of these procedures however reduces the fairness among the different classes of users. In [18], a joint association and resource allocation problem is formulated, yielding very high complexity. Furthermore, in order to generate a heuristic to solve the problem, over-the-air signaling between

BSs is utilised, wasting wireless resources. Finally, it should be mentioned that recent research has seen the emergence of fuzzy logic for network interference management [84–86], and a similar technique is investigated here. A brief overview of such techniques is presented in Section 2.3.4.

In Chapters 4 and 5, coordinated techniques that required the signalling of interference tolerances (ULIP) and SINR/path gain (PCS) information augmented network operational complexity. Furthermore, a single-parameter optimisation (*i.e.*, power control) was performed in collaboration with centralised schedulers. This is a common approach in a multitude of work performed on interference management techniques [6, 84, 85, 104, 108, 122, 128], where in many cases a single system parameter is optimised at the link level according to a given system utility or goal. This is, of course, greatly suboptimal in a system with multiple constantly varying and mutually interdependent parameters. In general, works considering multiple parameters for system performance maximisation utilise convex optimisation techniques [12–14, 126], however because the problem is known to be $\mathcal{NP}$-hard [17] these necessarily result in suboptimal solutions with immense complexity. Therefore, in this chapter, fuzzy logic is employed directly to ICIC in a holistic approach, by considering many key parameters to perform resource allocation (*i.e.*, frequency reuse) and power control in all cells individually. In this manner, a completely distributed approach which avoids large signalling and considers the interdependencies within the wireless network is derived.

6.2 System Model

The downlink of an OFDMA network is considered, where the system and channel models are described in detail in Section 3.2. For completeness, the technique introduced here is investigated in two scenarios:

- purely the **femto-cell tier** for initial development, as described in Section 3.3.1.2 with $\tilde{\mu}(u)$=3; and

- a full **HetNet** as described in Section 3.3.1.3, in which the autonomocity of fuzzy logic is paramount.

6.3 Distributed and Autonomous Resource Allocation for Femto-Cellular Networks

Due to the customer-side random deployment of femto-cells, and the resulting lack of fixed connective infrastructure, FBSs must perform resource and power allocation utilising locally available information only. To maximise performance in its own cell, a FBS must attempt to allocate RBs such that the desired signal on these is maximised, while the interference incident from neighbouring cells is minimal. Furthermore, the BS must allocate enough resources such that the rate requirements of the user(s) in the cell are fulfilled. The necessary, and locally available, information is therefore clearly determined:

- the required rate of a user determines the number of RBs that need to be assigned;
- the quality (*i.e.*, strength) of the desired signal dictates the necessary transmit power;
- the frequency-selective fading profile also affects the preferable RBs to be allocated; and
- the level of interference incident on the RBs strongly influences their allocatability.

All of these variables are locally available at the FBS in the reverse link, and at the MS(s) in the forward link, necessitating no extra information to be exchanged between BSs.

6.3.1 Fuzzy Logic for Autonomous Interference Coordination

In general, the resource and power allocation problem for a multicellular wireless networks belongs to the class of MINLP problems; obtaining the solutions to these is known to be $\mathcal{NP}$-hard [16, 17]. Therefore, it is clear that a heuristic for local, autonomous resource management is required to solve this problem. A machine learning approach where FBSs acquire information about their transmission conditions over time would be such a viable solution, however can prove complex without the availability of training data. Therefore, fuzzy logic is introduced as the heuristic, through which "expert knowledge" is incorporated into the RB allocation decision process.

The decision system, in its most simplified form, is represented in Fig. 6.1. In broad terms, the system evaluates which RB(s) are most suitable to be allocated to an MS in a given time slot, and determines the transmit power on these RBs needed to generate the required SINR

such that the user's rate can be met. Obviously, a RB receiving little or no interference situated in a fading peak is most suitable for allocation to the user, whereas any RB(s) receiving high interference, or experiencing deep fades, are much less appropriate.

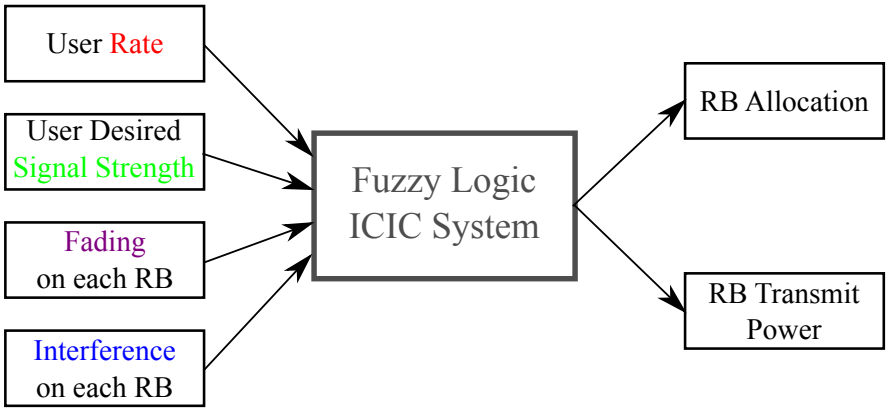

Figure 6.1: *Simplified graphical representation of the autonomous resource and power allocation technique.*

In fuzzy logic, an input range is divided into multiple "membership functions" which give a coarse evaluation of the variable. By combining the membership values of the inputs through various rules, the allocatability of each RB is determined. The output is also "fuzzy," indicating how suitable (or unsuitable) a RB is, avoiding a hard yes/no decision. An overview of fuzzy inference is offered in Section 2.3.4, and for more information on fuzzy logic, the reader is referred to [82] and related literature.

In each time slot, the FBS allocates the most applicable RBs to each FMS in its cell, and data transmission is performed. Based on the received signal levels from the desired user and interfering MSs, the FBS updates its information to more accurately represent the long-term interference and fading environments of its cell. This updated information is utilised in the next time slot to again carry out the, ideally improved, resource and power allocation. The same operation is performed in all femto-cells in the scenario, and the RB allocations are continuously individually optimised until the system converges to a stable solution, where the user(s) in each cell are satisfied.

6.3.1.1 Inputs

The input variables of the fuzzy logic system are:

- The **required rate** of the MS is defined by the service being demanded by the user. Here, the values "Low," "Low-medium," "Medium-high," and "High" are used to categorise the rate requested by the user. The ranges of these are dependent on the user scenario (*e.g.*, in femto-cells, a higher rate can be requested due to the superior channel conditions). This is a per-user requirement, and thus is equivalent for all RBs.

- The **desired signal level** describes the transmission conditions from transmitter to receiver, *i.e.*, the stronger the desired signal, the better the channel between the two. The signal power domain is divided into "Low," "Medium," and "High" values[1], to sort users depending on their useful channels. Since the fast fading component is considered as a separate input, the desired signal level is described per MS, and thus is equivalent over all RBs.

- The **fast fading component** for each RB may not always be readily available, however can become accessible by sounding, pilot/data transmission, or via cognitive radio. Users' frequency selective fading profiles extend over the whole available bandwidth, and hence certain RBs are more suitable to an MS than others; or than to other MSs. The fast fading domain is split into "Deep," "Average," and "Peak" values, centred around the mean fading level 1. In general, MSs should avoid RBs with "Deep" fades and try to acquire RBs with "Peak" fading values.

- The **level of interference** illustrates the immediate interference environment for each MS on each RB. RBs with strong interference may indicate a close neighbouring cell currently utilising them, or even multiple interfering cells. Low or zero interference RBs would obviously be very attractive to a MS. The interference power domain is divided into "Low," "Medium," and "High" values[1], to categorise RBs by the amount of interference they suffer.

6.3.1.2 Fuzzy System

The fuzzy logic system is responsible for determining the allocatability of each RB in the cell, and the corresponding transmit powers. This is performed in three stages, as can be seen in Fig. 6.7. First, the fuzzified values of the inputs (see. Fig. 6.7) are fed into the **rule evaluation**

[1]The cut off points and slopes of the values are determined from the CDFs in Figs. 6.3(b). "Low" is cut off at P[X$\leq$0.35], and "High" begins at P[X$\leq$0.65], with "Medium" in between.

stage, where these are combined to determine the "scores" of the membership functions of the outputs. These **rules** are defined in Table 6.1. Most of these rules are self-explanatory. In essence, they are intuitive guidelines as to why a specific RB should be assigned to the MS or not, *e.g.*, allocating an RB that is receiving high interference (3. and 6.) is generally never beneficial; or assigning medium-interference RBs should only be performed if the required rate is modest or the signal level is high enough (4. and 5.). Finally, almost any RB with low interference can be allocated and transmitted on with half power to achieve its rate (1.).

	Comb.	**Des. Rate**	**Signal**	**Interference**	**Fading**	**SINR**	**RB Alloc.**	**Power**	**Modulation**
1	AND	-	*not* Low	Low	-	-	Yes	Half	-
2	AND	Low	*not* Low	Med	Deep		Yes	Max.	-
3	AND	*not* Low	-	High	-	-	No	-	-
4	AND	Low-Med	*not* Low	Med	*not* Deep	-	Yes	Max.	-
5	AND	Med-High	*not* Low	Med	Peak	-	Yes	Max.	-
6	OR	-	-	High	Deep	-	No	-	-
7	AND	-	High	-	*not* Deep	-	Yes	Half	-
8	AND	-	Low	*not* Low	-	-	No	-	-
9	AND	Med-High	High	Med	Peak	-	Yes	Half	-
10	-	-	-	-	-	MuchWorse	-	-	Reduce3
11	-	-	-	-	-	Marg.Worse	-	-	Reduce2
12	-	-	-	-	-	Worse	-	-	Reduce1
13	-	-	-	-	-	Adequate	-	-	NoChange
14	-	-	-	-	-	Better	-	-	Increase1
15	-	-	-	-	-	Marg.Better	-	-	Increase2
16	-	-	-	-	-	MuchBetter	-	-	Increase3

Table 6.1: *Fuzzy Rules*

In the **rule output aggregation** stage, the results of all rules are combined for each RB to yield a fuzzy set representing *how much* an RB *should or should not* be allocated, and *how much* it *should or should not* transmit at half power (*i.e.*, if the majority of the rules yield "Yes" for RB allocation, then the RB *should* be allocated *more* than it *should not* be).

Finally, in the **defuzzification** stage, the *centre of gravity* (which is calculated using the integral-quotient in the Defuzzification box in Fig. 6.7) of the fuzzy set of each output is calculated to give a "score" for each RB. In essence, this stage determines finally the RB allocation (Yes/No) and the RB transmit power (Half/Max.), *e.g.*, an RB allocation score of 0.75 indicates a "Yes," and an RB transmit power score of 0.7 recommends maximum power transmission. Clearly, an RB with an allocation score of 0.9 is more allocatable than one with a score of 0.6.

6.3.1.3 Outputs

Finally, the outputs of fuzzy logic ICIC are:

- The **RB allocation** of the MS. The allocatability of each RB is calculated by fuzzy logic depending on the inputs. In the end, the BS assigns the required number of RBs to the MSs, choosing those that are most suitable for each. The higher the score, the better.
- The **transmit powers** of the RBs assigned to the MS. Each RB can transmit with either half or full (*i.e.*, maximum) power, depending on the inputs. For example, an RB with low interference may transmit at half power, whereas if the MS's desired signal is low or the fading on that RB is deep, full power should be utilised.

6.3.2 SINR-dependent Link Adaptation

In general, a wireless channel can change quite rapidly given alterations to its immediate environment, and hence there may be situations where a MS's desired link quality is much better/worse than necessary for its MCS. Alternatively, the scenario may arise when the MS receives high interference from a nearby transmitter, and hence the user's SINR may fall below its target. Therefore, it is imperative that a MS can modify its MCS depending on the channel conditions. In Fig. 6.2, such an ability is added to the fuzzy logic ICIC system.

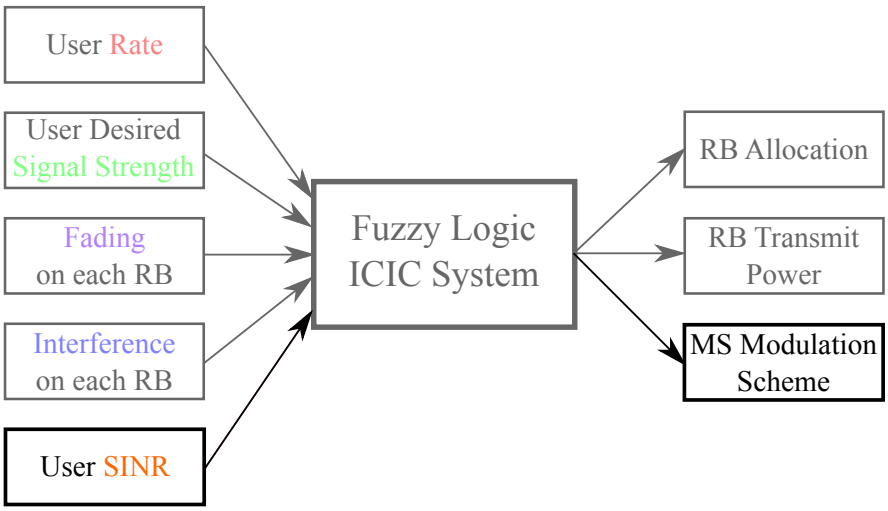

Figure 6.2: *Simplified graphical representation of the autonomous resource and power allocation technique with the opportunity for MCS adjustment.*

Since the success/failure of transmission on a given RB is mainly dependent on the SINR achieved on it, the MS SINR[2] is utilised to directly modify the MS's MCS: this is called *link adaptation (LA)*. More specifically, the difference between the user's achieved average SINR $\bar{\gamma_u}$ and its target γ_u^*

$$\Delta_\gamma = \bar{\gamma_u} - \gamma_u^* , \tag{6.1}$$

is utilised. The membership functions for the SINR input and MCS output are shown in Fig. 6.7. It should be mentioned that only Δ_γ is used in the LA procedure, such that

- if $\Delta_\gamma > 3$ dB the input is "Better", and the MS MCS order is "Increased by 1;"
- if $\Delta_\gamma > 5$ dB the input is "Marginally Better", and the MCS order is "Increased by 2;"
- if $\Delta_\gamma > 7$ dB the input is "Much Better", and the MCS order is "Increased by 3;"
- if $\Delta_\gamma < -3$ dB the input is "Worse", and the MCS order is "Reduced by 1;"
- if $\Delta_\gamma < -5$ dB the input is "Marginally Worse", and the MCS order is "Reduced by 2;"
- if $\Delta_\gamma < -7$ dB the input is "Much Worse", and the MCS order is "Reduced by 3;" or lastly
- if $-3 < \Delta_\gamma < 3$ dB the input is "Adequate", and the MCS order undergoes "No Change."

These rules are shown in Table 6.1. Through this procedure, a user may fit its MCS to its transmission environment, and hence more efficiently achieve its target rate. Moreover, the average SINR $\bar{\gamma_u}$ is considered to prevent a MS from "ping-pong"-ing between MCSs, which may severely complicate the scheduling procedure. Finally, it is possible to adjust the cut-off points for Δ_γ to tune the LA procedure, *e.g.*, values of "Better" for >5 dB and "Worse" for <-1 dB (and similar shift for all other membership functions) would be a much more conservative LA strategy.

6.3.3 Scheduling

Given the common assumption in femto-cell networks that only a single FMS is present per cell, this user can be allocated the RBs with the best scores (as determined by the fuzzy logic

[2]One might argue that given a user's signal strength and RB interference information, that a separate SINR input is unnecessary. However, because the MS can only receive interference information from other users transmitting on specific RBs, it is not guaranteed that it receives interfering signals on all RBs. Furthermore, the desired signal is also only measured on the allocated RBs, so a standard measure of the average SINR is the most precise description of an MS's overall transmission conditions.

system). In the reverse link, the contiguity constraint (specific to LTE) is fulfilled by allocating the required number of consecutive RBs with the least sum-score. With each FBS allocating the most suitable RBs in their cell, a natural frequency reuse will result. More specifically, it can be shown that neighbouring FBSs will allocate orthogonal sets of RBs, whereas femto-cells further from each other (*i.e.*, less interfering) may assign the same RBs without excessive interference.

Here, however, multiple users per cell are considered. For this case, there are many possibilities to perform resource allocation in the presence of multiple users. For instance, in the forward link an FBS may simply assign RBs in the descending order of scores calculated for all FMSs. This is clearly a greedy approach, and may not be optimal in cases where MSs have vastly different channel conditions (not usually the case in femto-cells, but possible). Another possibility, then, for resource allocation may be a PFS, where the RB scores for each user are scaled by the ratio of achieved and desired rates. Here, an MS that strongly underachieved its rate would be allocated RBs before an MS that was closer to its target. Lastly, a "priority" scheduler may give precedence to users with higher required rates/modulation orders, to more likely fulfil their QoS requirements.

6.3.4 Signal Statistics

In Fig. 6.7, the membership functions of the desired and interfering signal inputs are determined via analysis of the signal statistics in the deployment environment. While these statistics can be determined experimentally, they are analytically derived here such that they can be expanded to other scenarios. Thus, the power of any received signal P_r can be calculated as

$$\begin{aligned} P_r &= P_t G \\ P_{r,\mathrm{dB}} &= P_{t,\mathrm{dB}} + G_{\mathrm{dB}} = P_{t,\mathrm{dB}} - L_{\mathrm{dB}} \end{aligned} \tag{6.2}$$

where L_{dB}=$L_{s,\mathrm{dB}} + X_\sigma$ is the total signal attenuation, L_s=L_d is the signal path loss (which, due to the omnidirectional antenna used at a FBS is purely distance dependent), and L_d and X_σ are described in Section 3.2. Hence, the probability distribution function (PDF) of P_r (in dB) is given by

$$f_{P_r,\mathrm{dB}}(\varrho) = f_{P_t,\mathrm{dB}}(\theta) \circledast f_{L,\mathrm{dB}}(-l; D)\,. \tag{6.3}$$

where $\circledast$ denotes the convolution operator. And since

$$f_{L,\mathrm{dB}}(l;D) = f_{L_d,\mathrm{dB}}(l;D) \circledast f_{X_\sigma,\mathrm{dB}}(x)\,, \tag{6.4}$$

by finding $f_{L_d,\mathrm{dB}}(l;D)$ and $f_{P_t,\mathrm{dB}}(\theta)$, $f_{P_r,\mathrm{dB}}(\varrho)$ is derived for both desired and interfering signals, S and I, respectively.

Due to the random nature of the FBS and FMS positions, the first step in analysing the signal PDFs is estimating the distribution of the path losses between transmitter (whether it is desired or interfering) and receiver. From (3.9) it is clear that the path loss l is proportional to the Tx-Rx distance d, and the inverse relationship is given by

$$\rho_d(l) = d = 10^{(l-\alpha)/\beta}\,. \tag{6.5}$$

Thus, the distance dependent loss PDF $f_{L_d,\mathrm{dB}}(l;D)$ is derived

$$f_{L_d,\mathrm{dB}}(l;D) = \left|\frac{\mathrm{d}\rho_d(l)}{\mathrm{d}l}\right| f_d(\rho_d(l);D) \tag{6.6}$$

$$f_{L_d,\mathrm{dB}}(l;D) = \frac{\ln 10}{\beta}\rho_d(l) f_d(\rho_d(l);D)\,, \tag{6.7}$$

where $f_d(\rho(l);D)$ is the PDF of the Tx-Rx distance parametrised by the dimension D. This PDF is given in [154] by (6.8).

$$f_d(d;D) = \\ = \begin{cases} 2\frac{d}{D}\left(\left(\frac{d}{D}\right)^2 - 4\frac{d}{D} + \pi\right) & 0 \le d \le D \\ 2\frac{d}{D}\left[4\sqrt{\left(\frac{d}{D}\right)^2 - 1} - \left(\left(\frac{d}{D}\right)^2 + 2 - \pi\right) - 4\tan^{-1}\left(\sqrt{\left(\frac{d}{D}\right)^2 - 1}\right)\right] & D < d \le \sqrt{2}D \end{cases} \tag{6.8}$$

Hence, by evaluating (6.7), the distance-dependent path loss PDF $f_{L_d,\mathrm{dB}}(l;D)$ becomes (6.9),

$$f_{L_d,\mathrm{dB}}(l;D) = \frac{\ln 10}{\beta}\rho(l) \begin{cases} 2\delta(l)\left(\delta(l)^2 - 4\delta(l) + \pi\right) & \alpha \le l \le L_d(D) \\ 2\delta(l)\left[4\sqrt{\delta(l)^2 - 1} - \left(\delta(l)^2 + 2 - \pi\right) - \right. & \\ \qquad \left. -4\tan^{-1}\left(\sqrt{\delta(l)^2 - 1}\right)\right] & L_d(D) < l \le L_d\left(\sqrt{2}D\right) \end{cases} \tag{6.9}$$

where $\delta(l) = \rho(l)/D$. This PDF can be seen for both the desired signal ($D = R_\mathrm{a}$ m) and the inter-

fering signal (D=$5R_{\mathrm{a}}$ m, as interferer and receiver could be located in any two apartments in the scenario) in Fig. 6.3(a). Monte Carlo simulations that randomly place two nodes within the given dimensions $D \times D$, and calculate the resulting path loss, verify that the PDF given in (6.9) is indeed correct.

Referring back to (6.2), the path loss L_{dB} has been accurately described, and hence the distribution of the RB transmit powers P_t must now be found. In the downlink, each FBS transmits with a maximum *total* power $P_{\mathrm{max,FBS}}$ that is spread evenly over all RBs assigned to it. Further, the number of RBs n^{RB} allocated is directly dependent on the required rate C^* of the user(s) in the cell, thus P_t is defined by

$$\begin{aligned} P_t &= \frac{P_{\max}}{n^{\mathrm{RB}}} \qquad \text{where } n^{\mathrm{RB}} = \left\lceil \frac{C^*}{k_{\mathrm{sc}} s_{\mathrm{sc}}} \right\rceil \\ &= \frac{P_{\max} k_{\mathrm{sc}} s_{\mathrm{sc}}}{C^*} = \frac{A}{C^*} \,. \end{aligned} \tag{6.10}$$

Here, the ceiling operation is removed for ease of derivation, however without loss of generality. Therefore, it is clear from (6.10) that P_t is inversely proportional to the desired rate C^*, which here is modeled by a random variable with distribution $f_{C^*}(C^*)$. Hence, the CDF of the transmit power $F_{P_t}(p)$ is given by

$$\begin{aligned} F_{P_t}(p) &= \mathbf{P}\left[P_t \leq p\right] = \mathbf{P}\left[\frac{A}{C^*} \leq p\right] = \mathbf{P}\left[\frac{A}{p} \leq C^*\right] \\ &= 1 - \mathbf{P}\left[C^* \leq \frac{A}{p}\right] = 1 - F_{C^*}\left(\frac{A}{p}\right) \,, \end{aligned}$$

where $F_{C^*}(C^*)$ is the CDF of user desired rates, and therefore the PDF of the RB transmit power $f_{P_t}(p)$ is given by

$$f_{P_t}(p) = \frac{\mathrm{d}F_{P_t}(p)}{\mathrm{d}p} = \frac{A}{p^2} f_{C^*}\left(\frac{A}{p}\right) \tag{6.11}$$

The general expression is given in (6.11) for any rate PDF $f_{C^*}(C^*)$. Now, a random variable transformation (r.v.t) is performed to determine the PDF of the transmit power in dB (refer to (6.2)), ξ, for which the inverse relationship is given by

$$\rho_p(\xi) = p = 10^{\xi/10} \,. \tag{6.12}$$

Thus, the PDF of FMS transmit power $f_{P_t,\mathrm{dB}}(\xi)$ is calculated by

$$f_{P_t,\mathrm{dB}}(\xi) = \left|\frac{\mathrm{d}\rho_p(\xi)}{\mathrm{d}\xi}\right| f_{P,\mathrm{dB}}(\rho_p(\xi)) \tag{6.13}$$

$$= \frac{\ln 10}{10}\rho_p(\xi) f_{P_t}(\rho_p(\xi))$$

$$= \frac{\ln 10}{10}\frac{A}{\rho_p(\xi)} f_{C^*}\left(\frac{A}{\rho_p(\xi)}\right) \tag{6.14}$$

where (6.14) is the general expression for any rate distribution. Thus, the PDF of user transmit power has been derived, however under the assumption of transmission of a single bit per channel use. This is, of course, not a realistic assumption and, thus, here a user's ability to send with various MCSs (see Table 3.1) is considered. Clearly, the MCS affects the number of RBs required by an MS, and thus also the MS transmit power. This is shown in (6.15)

$$P_t = \frac{P_{\max}}{n_{\mathrm{RB}}} \qquad \text{where } n_{\mathrm{RB}} = \left\lceil \frac{C^*}{k_{\mathrm{sc}} s_{\mathrm{sc}} \varepsilon_{\mathrm{s}}} \right\rceil$$

$$= \frac{P_{\max} k_{\mathrm{sc}} s_{\mathrm{sc}} \varepsilon_{\mathrm{s}}}{C^*} = \frac{A\varepsilon_{\mathrm{s}}}{C^*}\,. \tag{6.15}$$

Further, assuming each user is uniformly distributed a MCS[3], by replacing (6.10) with (6.15) and performing the same CDF transformation, the transmit power PDFs (*i.e.*, $f_{P_t}(p)$ and $f_{P_t,\mathrm{dB}}(\theta)$) are modified correspondingly as

$$f_{P_t}(p) \to \frac{1}{16}\sum_{\tilde{m}=0}^{15} \frac{A\varepsilon_{\mathrm{s}}(\tilde{m})}{p^2} f_{C^*}\left(\frac{A\varepsilon_{\mathrm{s}}(\tilde{m})}{p}\right),$$

$$f_{P_t,\mathrm{dB}}(\theta) \to \frac{\ln 10}{160}\sum_{\tilde{m}=0}^{15} \frac{A\varepsilon_{\mathrm{s}}(\tilde{m})}{\varphi(\theta)} f_{C^*}\left(\frac{A\varepsilon_{\mathrm{s}}(\tilde{m})}{\varphi(\theta)}\right) \tag{6.16}$$

where $\tilde{m}$ is the CQI index in Table 3.1, and again, (6.16) is the general expression for any user rate distribution. Now, revisiting that $n_{\mathrm{RB}}=\left\lceil \frac{C^*}{k_{\mathrm{sc}} s_{\mathrm{sc}} \varepsilon_{\mathrm{s}}} \right\rceil$, it is clear that only integer number of RBs can be assigned to each FMS, and thus each user can only assume a transmit power from a discrete set of $P_t=\frac{P_{\max}}{n^{\mathrm{RB}}}$

$$P_t \in \left\{\frac{P_{\max}}{1}, \frac{P_{\max}}{2}, \cdots, \frac{P_{\max}}{M}\right\}, \tag{6.17}$$

[3]This would be independent of its signal quality. This is not the best assumption, admittedly, however the reason is to further randomise the user requirements, and hence the necessary RB allocations. Through this, the allocation problem becomes more challenging for ICIC techniques, including that presented here.

where M denotes the total number of RBs available in each cell. Thus, $f_{P_t}(p)$ is evaluated at the powers in (6.17), as are the histogram bins in the Monte Carlo simulation, the results of which are presented in Fig. 6.3(a) for $C^{*}\sim\mathrm{Rayl}\left(\hat{C}\right)$, where

$$\mathrm{Rayl}(\sigma_{\mathrm{R}}) \sim \frac{x}{\sigma_{\mathrm{R}}^{2}} e^{\frac{-x^{2}}{2\sigma_{\mathrm{R}}^{2}}}\,, \tag{6.18}$$

$\hat{C}{=}\bar{C}\sqrt{\frac{2}{\pi}}$, and $\bar{C}$ is the average desired rate. The close match of theoretical and empirical results confirms that the derivation for $f_{P_t,\mathrm{dB}}(\theta)$ is accurate.

Thus, accurate and precise analytical models have been found for the distributions of the path losses and transmit powers, which are directly dependent on the network topology of the investigated scenario. From (6.2) it is clear that

$$f_{P_r,\mathrm{dB}}(\varrho) = f_{P_t,\mathrm{dB}}(\xi) \circledast f_{L,\mathrm{dB}}(-l; D)\,. \tag{6.19}$$

Hence, the desired and interfering signal PDFs are given in (6.20) and (6.21), respectively,

$$f_{S,\mathrm{dB}}(s; D) = f_{P_t,\mathrm{dB}}(\xi) \circledast f_{L,\mathrm{dB}}(-l; D{=}R_{\mathrm{a}}) \tag{6.20}$$

$$f_{I,\mathrm{dB}}(i; D) = f_{P_t,\mathrm{dB}}(\xi) \circledast f_{L,\mathrm{dB}}(-l; D{=}5R_{\mathrm{a}})\,. \tag{6.21}$$

In Fig. 6.3(b) a comparison to simulation results is drawn, where it is evident that the theoretical CDFs are slightly shifted from their experimental counterparts. The general shape (*i.e.*, variance) of the CDFs is accurate, and while there is a minor shift (1-2 dB) between simulation and theory, this difference is within the numerical margin of error (especially considering the inherent heuristic nature of fuzzy logic), and thus acceptable here.

It is clear that the signal strength PDFs are mainly dependent on the distance between transmitter and receiver, and the transmit power. Therefore, extending fuzzy logic ICIC to other scenarios is straightforward, as simply the distance PDF $f_d(d; D)$ must be modified to fit the new environment, and the statistics can be found. Hence, not only have the received signals been derived for the femto-cell scenario, they can easily be modified to other environments, thus expanding the applicability of fuzzy logic ICIC to other wireless networks.

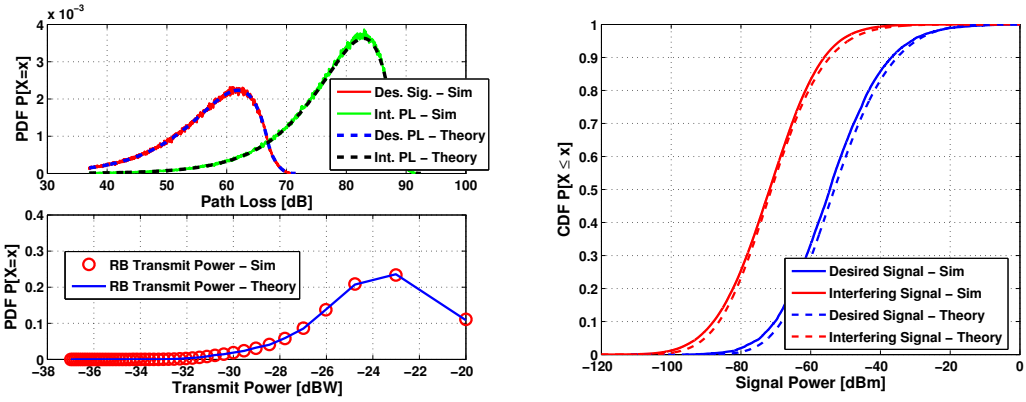

(a) Path Loss and Transmit Power PDFs

(b) Signal Energy CDFs

Figure 6.3: *Comparison of derived theoretical desired and interfering signal PDFs and CDFs to Monte Carlo simulation results, considering lognormal shadowing.*

6.4 Optimality of Fuzzy Logic ICIC

Due to the heuristic nature and non-linearity of fuzzy logic, it is very difficult to perform a comprehensive theoretical analysis of the system performance of fuzzy logic ICIC. Therefore, to analyse the optimality of this technique, fuzzy logic ICIC is experimentally compared to the system-optimal performance, and a greedy heuristic of similar complexity. It is demonstrated that fuzzy logic ICIC provides close-to-optimal throughput and coverage at significantly reduced complexity.

6.4.1 System Optimisation

The most obvious choice for performance comparison is that of posing the resource allocation as a system-wide optimisation problem. Since fuzzy logic is autonomous and, more importantly, distributed it *should*, on average, be suboptimal in terms of overall system performance. The optimal RB allocation of the system can be achieved by solving the problem posed in (6.22), and thus the aim of fuzzy logic is to as closely as possible approach the result of this problem. Given the definition for user throughput (3.4) and system sum throughput (3.5), the optimisation problem is constructed as follows

$$\max \quad C_{\text{sys}} = \sum_{u} C_u \qquad u{=}1,\, 2,\, \ldots\,,\, n_{\text{usr}}\,. \tag{6.22}$$

$$\text{s.t.} \quad \sum_{j=1}^{M} \mathbf{1}_{P_{u,j}>0} \leq n_u^{\text{RB}} \quad \forall u \tag{6.22a}$$

$$\sum_{j=1}^{M} P_{u,j} \leq P_{\max} \qquad \forall u \tag{6.22b}$$

$$P_{u,j} \geq 0 \qquad \forall u, j \tag{6.22c}$$

in order to determine the maximum rate achievable in a given scenario. In the constructed MINLP [17] problem, (6.22b) and (6.22c) describe the restrictions on transmit power allocation at each MS: the sum of the allocated powers on all RBs cannot exceed $P_{\max}$, and the individual powers must be non-negative, respectively. The constraint (6.22a) limits the number of transmitting RBs at a single MS to the n_u^{RB} the user needs to achieve its desired rate. This is necessary as since the objective is sum-rate-maximisation, the best solution is generally transmission on most, if not all RBs. However, since fuzzy logic ICIC only aims to satisfy user requirements[4], this would be an unfair comparison; hence the constraint (6.22a).

It is clear from the definition of C_u in (3.4) that (6.22) is non-linear, non-convex and, more significantly, *discrete*, which is further highlighted by the discrete set of constraints in (6.22a). In [155], the theory of Lagrange multipliers is extended to discrete space, utilising a *direction of maximum potential drop* to iterate through the solution space and optimise the objective function. This method is used here to find the system-optimal RB allocation. It should be mentioned that other techniques (*e.g.*, genetic algorithms) were tested, but could not overcome the discrete nature of the problem (Monte Carlo Markov chains may perform better in this regard).

6.4.2 Greedy Heuristic

While the comparison to the system-wide optimisation problem will demonstrate the optimality of fuzzy logic ICIC, it is important to note that a centralised and a distributed approach are being compared. Therefore, a commonly utilised distributed allocation technique is implemented, which "greedily" allocates the best RBs to the FMS(s) in the cell [48]. Here, the potential SINR achievable on each RB is calculated using prior interference, signal, and transmit power information; and then the RBs with the strongest SINRs will be allocated to the user.

[4]It should be mentioned that a minimum rate constraint was originally considered. However, if a single MS cannot achieve its target rate, then no solution can be found by the problem, and hence this constraint was removed.

$$\begin{aligned} \text{Given:} \quad & P_u = {}^{P_{\max}}/_{n_u^{\mathrm{RB}}},\ I_u^m,\ G_{u,v_u}^m \quad m{=}1,\,2,\,\ldots\,,\,M\,, \\ \text{Find:} \quad & \gamma_u^m = \frac{P_u G_{u,v_u}^m}{I_u^m + \eta} \qquad \forall m\,. \end{aligned} \tag{6.23}$$

In (6.23), the same information is available as for fuzzy logic, and a greedy approach is utilised to allocate the RBs. This technique should maximise the throughput in each cell, however it does not take a system view as in (6.22), and hence will be suboptimal in terms of network throughput.

Therefore, the comparison to this greedy heuristic will show the optimality of fuzzy logic on a cell-individual basis, whereas the comparison to the optimisation problem shows the optimality achieved at the network level.

6.4.3 Results Comparison

To compare the performance of these three methods, a Monte Carlo simulation is run utilising the apartment block described in Section 3.3.1.2, with $\tilde{\mu}(u){=}1$ (*i.e.*, a single user per cell), and $\bar{C}{=}1.25$ Mbps. Standard fuzzy logic ICIC without LA is utilised, as neither the optimisation technique nor the greedy heuristic employ LA. Further, as an additional performance measure, the *availability* χ is defined as the proportion of MSs that have acquired their desired rate, *i.e.*,

$$\chi{=}\frac{1}{n_{\mathrm{usr}}}\sum_{u=1}^{n_{\mathrm{usr}}} \mathbf{1}_{C_u \geq C_u^*}\,, \tag{6.24}$$

where n_{usr} is a random variable denoting the number of MSs in the scenario.

Fig. 6.4 shows the throughput and availability results for this scenario, where it is evident that the system-optimum solution cannot be reached by the distributed techniques. However, fuzzy logic is able to perform, on average, within 4% of the optimum throughput performance, and in fact the difference after 20 time slots (*i.e.*, two LTE frames) is less than 2%. Furthermore, it is clear that the average throughput of fuzzy logic is improved over the greedy heuristic (by 4%), even though after 15 time slots the performance is similar. This highlights that fuzzy logic ICIC is optimal on a cell-individual basis, however is able to (due to other inputs such as rate requirement and desired signal strength) converge to this optimum much quicker[5].

[5]The initial decline in performance by the greedy heuristic in the first time slots results from the lack of interference information. The unused RBs with "zero" interference are allocated in all cells simultaneously, thus causing large outages in these slots. After more accurate statistics are received, the performance improves as expected.

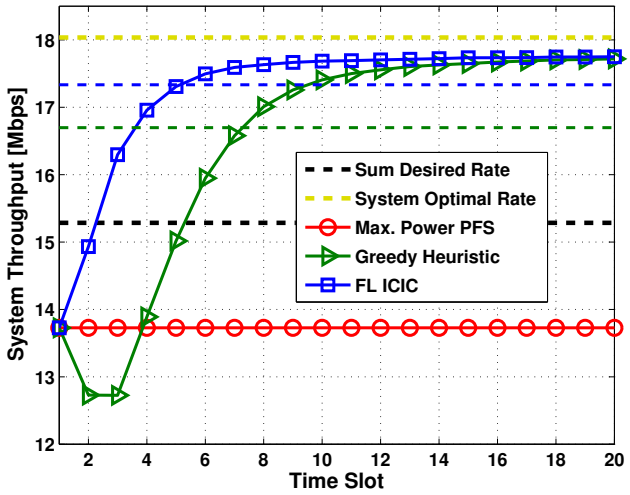

(a) Throughput

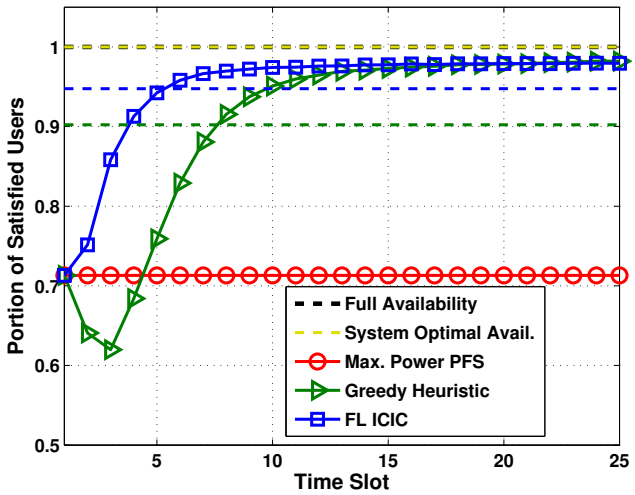

(b) Availability

Figure 6.4: *System performance comparison of fuzzy logic ICIC, the system-wide optimal solution, and the proposed greedy heuristic. The dashed lines represent the mean performance of each system.*

On the other hand, the performance difference to the optimum is minute, and therefore fuzzy logic ICIC provides a "near-optimal" solution for the network as a whole.

The same trends can be seen for the system availability, where while the optimum is clearly full availability (*i.e.*, χ=1), fuzzy logic ICIC achieves 98% coverage, and hence produces almost negligible outage. Furthermore, it is able to reach this availability much faster than the greedy heuristic, indicating that fuzzy logic ICIC employs a balance between system-wide optimisation

and cell-individual performance.

6.4.4 Complexity

To conclude the comparison, the complexities of the three schemes are analysed, to highlight the simplicity and efficiency of the fuzzy logic technique. In a cell where fuzzy logic ICIC is applied, $K{=}4$ inputs (see Fig. 6.1) are combined at each of M RBs available at the FBS, inducing a complexity of KM. Following this, the RBs are sorted according to their fuzzy score, in order to allocate the most appropriate to the MS. Since, in general, sorting algorithms demonstrate $O(N^2)$ complexity, the fuzzy logic complexity within a cell increases to $(KM)^2$. Furthermore, fuzzy logic ICIC requires multiple subframes $N_{\text{sf}}{\approx}10$ to converge to its operating performance. Finally, given a scenario with n_{usr} FMSs, the system complexity of fuzzy logic ICIC is given by

$$O\left(n_{\text{usr}} N_{\text{sf}} (KM)^2\right) .$$

The greedy heuristic utilises a similar methodology as fuzzy logic, in that it also computes a "score" (in this case the instantaneous SINR) for each RB and then orders them for allocation. Hence, the evaluation complexity at each RB is KM (where in this case $K{=}2$ inputs), the sorting complexity is $(KM)^2$ in each of $N_{\text{sf}}{\approx}20$ time slots, and the overall complexity is again given by

$$O\left(n_{\text{usr}} N_{\text{sf}} (KM)^2\right) .$$

For the optimisation problem (6.22), finding the solution complexity is more challenging than for the heuristics, as the problem is considered $\mathcal{NP}$-hard [17]. In general, $\mathcal{NP}$-hard problems are only solvable (if possible) in exponential time. Using [155], and defining a neighbour in the RB allocation space as having a Hamming distance of 2 (*i.e.*, a single RB re-allocation), there are $\sum_{u=1}^{n_{\text{usr}}} n_u^{\text{RB}} \left(M - n_u^{\text{RB}}\right)$ neighbours at each point in the search space. At each neighbour, the RB SINRs and consequent system throughput must be calculated, inducing a complexity of $O\left(M n_{\text{usr}} \left(1 + n_{\text{usr}}\right)\right)$. Finally, it was determined experimentally that the algorithm needs $N_{\text{step}}{\approx}10$ steps to converge, and hence the overall complexity of (6.22) is

$$O\left(N_{\text{step}} \sum_{u=1}^{n_{\text{usr}}} n_u^{\text{RB}} \left(M - n_u^{\text{RB}}\right) M n_{\text{usr}} \left(1 + n_{\text{usr}}\right)\right) .$$

This is clearly much greater than the complexity of the two heuristics, which is expected. A

comparison of the achieved throughputs and required complexities of the three techniques is shown in Fig. 6.5.

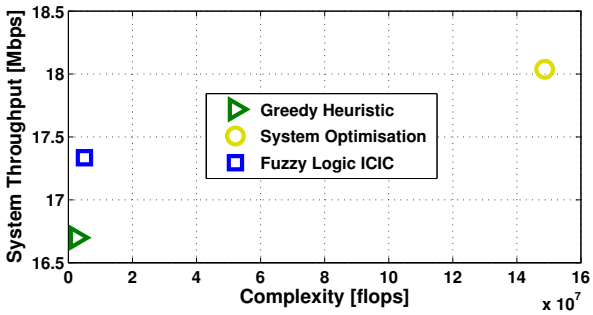

Figure 6.5: *System throughput versus required complexity for fuzzy logic ICIC, the system-wide optimal solution, and the proposed greedy heuristic.*

It is evident that, while (6.22) provides the greatest system throughput, it is substantially more complex than both fuzzy logic and the SINR heuristic, which only suffer slightly in terms of achieved throughput. On the other hand, it is clear that fuzzy logic ICIC provides enhanced throughput and coverage for the system compared to the greedy heuristic, even though the complexities are very similar. Hence, fuzzy logic provides low-complexity, near-optimal system performance in an autonomous and distributed manner.

6.5 Extension to HetNets

As alluded in Section 6.1, the key motivations behind the fuzzy logic ICIC technique were the inherent difficulties in managing not just femto-cell deployments, but HetNets as a whole. The challenges in self-optimisation, backhauling and especially interference in HetNets indicated the necessity for distributed and autonomous decision-making and network management. Hence, the next logical step in the development of fuzzy logic ICIC is its extension to HetNets, which is performed in the following.

6.5.1 Cell Association

The most important extension to the fuzzy logic system itself is the addition of the ability of autonomous BS/cell association. In the HetNet case when there are multiple APs within a macro-cell (here, MBSs and PBSs are considered), the MMS must be able to autonomously

connect to the most desirable one. This connection is based on two quantities received from the BS reference signals, namely the *RSRP* and the current *BS load factor*. The dominant term in this decision process is the RSRP, which governs the signal strength received from the BS, and clearly the greater, the more attractive this BS is to the MMS. However, connecting to a BS with

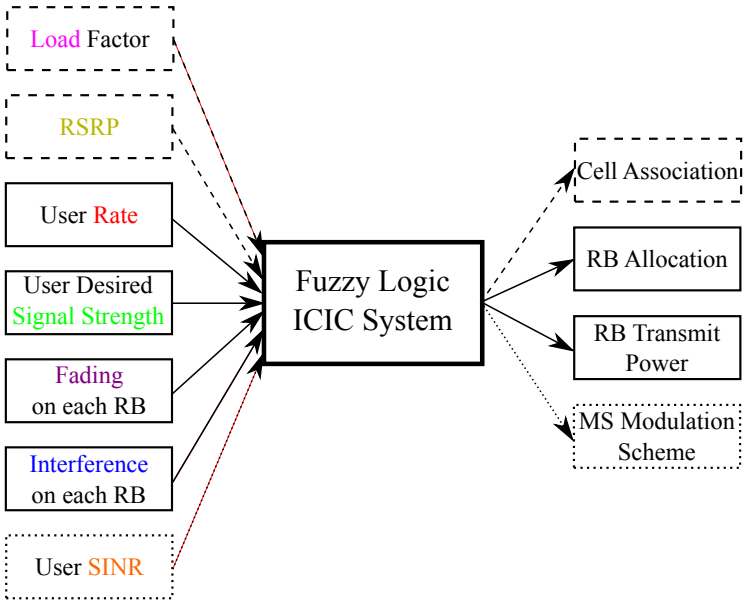

Figure 6.6: *Simplified graphical representation of the resource and power allocation technique with the inclusion of autonomous cell association.*

a strong signal that is highly or even fully loaded would be counter-productive, considering that the BS may not be able to serve the additional user. Therefore, in conjunction with the RSRP the load factor (from 0 to 1) of the BS is considered, in order to avoid such decisions. In general, an MS will perform best when connected to the BS with the highest RSRP, however it may be a better choice for the network to allocate, *e.g.*, the second strongest cell, if the load on the best cell is large. Thus, these two quantities must be balanced.

In the fuzzy logic system, each BS is given a score, Ω_{BS}, from 0 to 1, indicating its suitability to a particular MS. This is given by

$$\Omega_{\mathrm{BS}} = \Omega_{\mathrm{RSRP}} - w_{\mathrm{lf}}\Omega_{\mathrm{load}} \,, \tag{6.25}$$

where Ω_{RSRP} is the RSRP score (from 0 to 1) based on the received signal strength, Ω_{load} is the load factor and $0 \leq w_{\mathrm{lf}} \leq 1$ is the weighting of the load factor. Essentially, w_{lf} can be tuned towards the goals of the network, where $w_{\mathrm{lf}}=0$ serves a high capacity aim, and $w_{\mathrm{lf}}=1$ intends to maximise availability. A detailed graphic of the full fuzzy logic system is shown in Fig. 6.7.

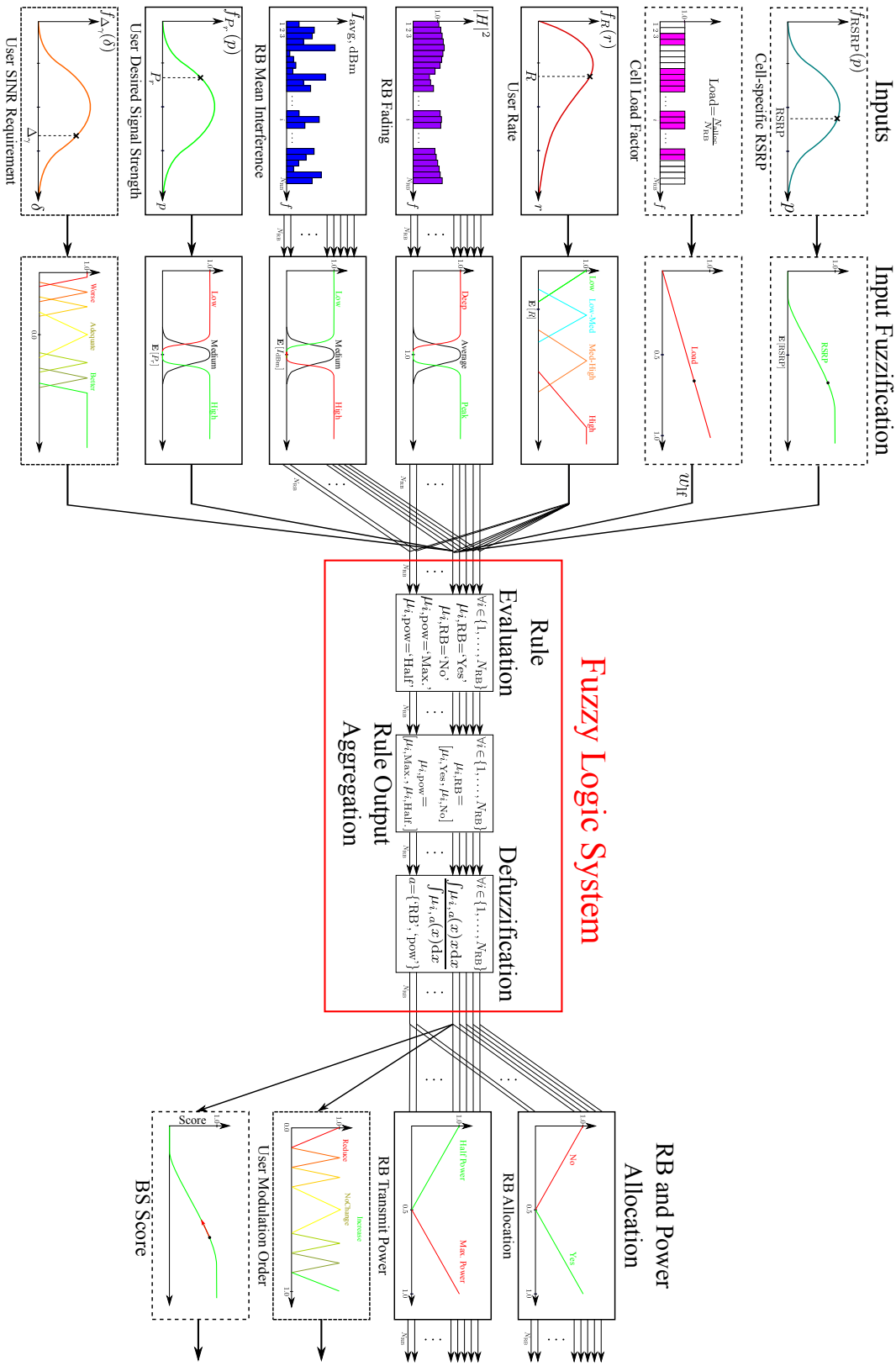

Figure 6.7: *Graphical representation of the fuzzy logic resource and power allocation system.*

6.5.2 HetNet Signal Statistics

Since in Section 6.3.4 the signal statistics for femto-cellular environments have been derived, the focus here lies on the macro- and pico-cellular layouts. Through this, fuzzy logic ICIC (*i.e.*, more specifically, the membership functions of the desired signal and interference inputs) can be tuned to the HetNet it is deployed in. For ease of overview, only the main statistics equations will be displayed in this section, while all derivations can be found in Appendix A.

6.5.2.1 Desired Signal

The received signal power P_r is given by (6.2) and since here a fully loaded HetNet is considered, the transmit powers of both the MBSs and PBSs are assumed to be constant over all RBs. Hence, the PDF of P_r (in dB) is given by

$$f_{P_r,\mathrm{dB}}(\varrho) = f_{L_s,\mathrm{dB}}(P_{\hat{b},\mathrm{dB}} - l; D)\,. \tag{6.26}$$

where, here, $\hat{b}$={MBS, PBS} depending on MBS or PBS transmission, respectively. Hence, by finding $f_{L_s,\mathrm{dB}}(l)$ for the macro- and pico-layers, $f_{P_r,\mathrm{dB}}(\varrho)$ is derived for both desired and interfering signals, S and $\sum I$, respectively.

Macro-BS To begin, the path loss distribution is analysed for uniformly distributed (in a macro-cell) users from the MBS serving the cell. From the MBS, the signal loss $L_{s,\mathrm{dB}} = L_{d,\mathrm{dB}}+L_{\theta,\mathrm{dB}}$ is dependent on both the distance from the BS (L_d given in (3.9)), and the angle from the central lobe (L_θ given in (3.10)). Clearly, the distance-dependent path loss is parametrised by the cell radius R, and hence

$$\begin{aligned} f_{L_{d,\mathrm{mac}},\mathrm{dB}}(l;R) &= \left|\frac{\mathrm{d}\rho_d(l)}{\mathrm{d}l}\right| f_{d,\mathrm{mac}}(\rho_d(l);R)\,, \\ &= \frac{2\ln 10}{\beta R^2\pi}\rho_d^2(l)\sin^{-1}\left(\sqrt{1-\left(\frac{\rho_d(l)}{2R}\right)^2}\right)\,, \\ &\qquad \alpha \le l \le \alpha + \beta\log_{10}(2R)\,, \end{aligned} \tag{6.27}$$

where $\rho_d(l)$ is defined in (6.5), and $f_{d,\mathrm{mac}}(d;R)$ is the PDF of distance from the MBS.

The signal loss associated with a MS located at an angle θ from the central lobe can be described

using the inverse relationship

$$\rho_\theta(l) = \theta = \sqrt{\frac{l}{12}}\theta_{3\mathrm{dB}}\,, \tag{6.28}$$

such that

$$\begin{aligned} f_{L_{\theta,\mathrm{mac}},\mathrm{dB}}(l) &= \left|\frac{\mathrm{d}\rho_\theta(l)}{\mathrm{d}l}\right| f_{\theta,\mathrm{mac}}(\rho_\theta(l)) \\ &= \frac{\theta_{3\mathrm{dB}}}{\pi\sqrt{48l}}\left(\cos\left(2\rho_\theta(l)\right)+1\right)\,, \qquad 0 \le l \le 20\,, \end{aligned} \tag{6.29}$$

where $f_{\theta,\mathrm{mac}}(\theta)$ is the angular distribution from the central lobe.

Finally, the signal path loss from the MBS to a uniformly distributed user in the macro-cell is calculated via

$$\begin{aligned} L_{s,\mathrm{mac},\mathrm{dB}} &= L_{d,\mathrm{mac},\mathrm{dB}} + L_{\theta,\mathrm{mac},\mathrm{dB}}\,, \\ f_{L_{s,\mathrm{mac}},\mathrm{dB}}(l;R) &= f_{L_{d,\mathrm{mac}},\mathrm{dB}}(l;R) \circledast f_{L_{\theta,\mathrm{mac}},\mathrm{dB}}(l)\,. \end{aligned} \tag{6.30}$$

Due to the complexity of both $f_{L_{d,\mathrm{mac}},\mathrm{dB}}(l;R)$ and $f_{L_{\theta,\mathrm{mac}},\mathrm{dB}}(l)$, (6.30) is numerically evaluated. It should be mentioned, however, that (6.30) is an approximation of $f_{L_{s,\mathrm{mac}},\mathrm{dB}}(l;R)$, as the dependence between d and θ is not taken into account. Clearly, θ is dependent on d (and vice versa), as only certain angles can be associated with a particular distance from the BS. Ideally,

$$f_{L_{s,\mathrm{mac}}}(l) = f_{L_d}(l) \circledast f_{L_{\theta|d}}(l) = f_{L_{d|\theta}}(l) \circledast f_{L_\theta}(l)\,,$$

however since the scope of this work is autonomous resource allocation and not system modelling, the approximation in (6.30) is accepted as within the margins of error.

Pico-BS In order to analyse the path loss from the PBS to a uniformly distributed user in the macro-cell, assumptions must be placed on the location of the PBS in the cell. Here, it is assumed that the PBS is placed uniformly at a specific distance D (*i.e.*, $D{=}\hat{d}$) from the centre of the macro-cell. Furthermore, omnidirectional antennas are used to serve the pico-cells, and hence there is no angular loss component as with MBSs. Thus, depending on the distance from the PBS, the path loss PDF is given by a piece-wise function parametrised by both R and D,

$$f_{L_{s,\mathrm{pic}},\mathrm{dB}}(l;R,D) = \left|\frac{\mathrm{d}\rho_d(l)}{\mathrm{d}l}\right| f_d(\rho_d(l);R)\,,$$
$$= \begin{cases} \frac{2\rho_d^2(l)\ln 10}{\beta R^2} & \alpha < l \leq L_d(R-D) \\ \frac{2\rho_d^2(l)\ln 10}{\beta R^2 \pi}\left(\pi - \sin^{-1}\left(\frac{1}{2\rho_d(l)D}\sqrt{4D^2\rho_d^2(l) - \left(R^2 - \rho_d^2(l) - D^2\right)^2}\right)\right) & L_d(R-D) < l \leq L_d(\sqrt{R^2-D^2}) \\ \frac{2\rho_d^2(l)\ln 10}{\beta R^2 \pi}\left(\sin^{-1}\left(\frac{1}{2\rho_d(l)D}\sqrt{4D^2\rho_d^2(l) - \left(R^2 - \rho_d^2(l) - D^2\right)^2}\right)\right) & L_d(\sqrt{R^2-D^2}) < l \leq L_d(R+D) \end{cases} \tag{6.31}$$

where $f_{d,\mathrm{pic}}(d;R,D)$ is the PDF of the distance from the PBS.

Now that the path loss distributions for both the macro- and pico-BSs have been derived, the desired signal can be found. In general, it is assumed that a MMS will connect to the BS with the strongest RSRP, and hence the desired signal for this MS will be

$$S_{\mathrm{dB}} = \max\left(P_{\mathrm{MBS,dB}} - L_{s,\mathrm{mac,dB}}, P_{\mathrm{PBS,dB}} - L_{s,\mathrm{pic,dB}}\right)\,. \tag{6.32}$$

Furthermore, given two independent random variables X and Y, the PDF of the maximum of these variables is given by

$$\begin{aligned} f_W(w) &= f_X(w)F_Y(w) + F_X(w)f_Y(w) \\ &= h(f_X, f_Y)\,. \end{aligned} \tag{6.33}$$

Therefore, utilising (6.26), the PDF of the desired signal, parametrised by R and D, of a uniformly distributed user in a HetNet macro-cell can be determined as

$$\begin{aligned} g_{\mathrm{MBS}} &= P_{\mathrm{MBS,dB}} - l\,, \\ g_{\mathrm{PBS}} &= P_{\mathrm{PBS,dB}} - l\,, \\ f_{S,\mathrm{dB}}(s;R,D) &= h\left(f_{L_{s,\mathrm{mac}},\mathrm{dB}}(g_{\mathrm{MBS}};R), f_{L_{s,\mathrm{pic}},\mathrm{dB}}(g_{\mathrm{PBS}};R,D)\right)\,. \end{aligned} \tag{6.34}$$

6.5.2.2 Interfering Signal

Given the HetNet construction described in Fig. 3.2, it is clear that the immediate interference scenario is rather more complicated than the desired signal. However, due to the rapid signal

attenuation as the distance from the transmitter increases, only interference from the first tier surrounding the cell of interest is considered. This is displayed in Fig. 6.8, where it is clear that

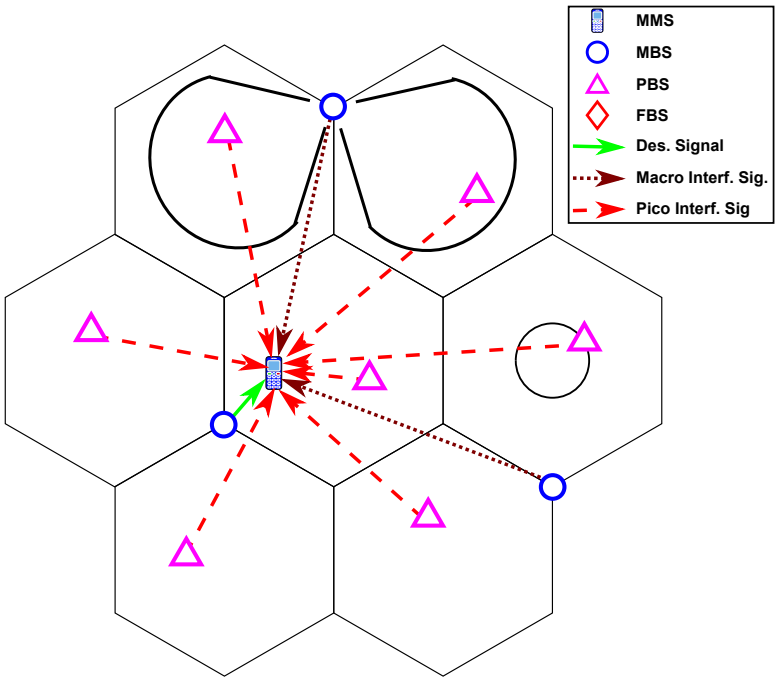

Figure 6.8: *First-tier interference scenario in the macro- and pico-cellular layout of a HetNet with* N_{p}=1. *The victim MS is connected to the MBS in its cell.*

a MMS must combat three different sources of interference:

- **MBS** interference from the two closest sites;
- **PBS** interference from each of the neighbouring cells; and, most importantly,
- **Own-cell** interference from the BS the MMS is *not* connected to.

Therefore, in a similar manner to the desired signal, these sources are characterised and hence determine the interfering signal PDF for a uniform user distribution in the cell.

Macro-Interference In the macro-layer, the distance-dependent path loss from a neighbouring macro-site is given by

$$f_{L_d,I_{\mathrm{mac}},\mathrm{dB}}(l;R) = \frac{2\ln 10}{\beta R^2 \pi}\rho_d^2(l)\sin^{-1}\left(\sqrt{1-\frac{1}{16R^2\rho_d^2(l)}\left(\rho^2(l)+3R^2\right)^2}\right),$$
$$\alpha+\beta\log_{10}(R) \leq l \leq \alpha+\beta\log_{10}(3R)\,, \tag{6.35}$$

and the angular loss is calculated as

$$f_{L_\theta,I_{\mathrm{mac}},\mathrm{dB}}(l) = \frac{\theta_{3\mathrm{dB}} \cos \rho_{\theta_I}(l)}{\pi\sqrt{3l}} \sqrt{4\cos^2 \rho_{\theta_I}(l) - 3}\,, \tag{6.36}$$

where the inverse relation is given by

$$\rho_{\theta_I}(l) = \theta_I = \sqrt{\frac{l}{12}}\theta_{3\mathrm{dB}} - \frac{\pi}{3}\,, \tag{6.37}$$

because θ_I is no longer the angle from the central lobe, but rather from the centre of two neighbouring lobes (*i.e.*, cells, as shown in Fig. 6.8). Therefore, the received macro-cell interference can be numerically calculated as

$$f_{L_s,I_{\mathrm{mac}},\mathrm{dB}}(l;R) = f_{L_d,I_{\mathrm{mac}},\mathrm{dB}}(l;R) \circledast f_{L_\theta,I_{\mathrm{mac}},\mathrm{dB}}(l)\,. \tag{6.38}$$

Again, it should be mentioned that (6.38) is an approximation, as the dependence of d and θ_I is not taken into account.

The total MBS interference is given by the sum of the interfering signals from the two closest macro-cell sites. Therefore, the PDF of the interfering signal in linear domain must be found

$$f_{L_s,I_{\mathrm{mac}}}(l;R) = \left|\frac{\mathrm{d}\rho_{\mathrm{dB}}(l)}{\mathrm{d}l}\right| f_{L_s,I_{\mathrm{mac}},\mathrm{dB}}(\rho_{\mathrm{dB}}(l);R)\,,$$

where

$$\rho_{\mathrm{dB}}(l) = L_{\mathrm{dB}} = 10\log_{10}(l)\,. \tag{6.39}$$

The summation of the two macro-interfering losses (this can be performed due to the equivalent transmit powers of the two MBSs) is given by the convolution of their PDFs

$$f_{L_s,\sum I_{\mathrm{mac}}}(l;R) = f_{L_s,I_{\mathrm{mac}}}(l;R) \circledast f_{L_s,I_{\mathrm{mac}}}(l;R)\,, \tag{6.40}$$

and, consequently, the transformation back into the decibel domain

$$f_{L_s,\sum I_{\mathrm{mac}},\mathrm{dB}}(l;R) = \left|\frac{\mathrm{d}\rho_p(l)}{\mathrm{d}l}\right| f_{L_s,\sum I_{\mathrm{mac}}}(\rho_p(l);R)\,. \tag{6.41}$$

It should be mentioned, however, that the straight convolution of the two interfering signals is an approximation of the sum-macro-interference. Due to the deterministic positions of the macro-cell sites, the interfering signals from the two MBSs are correlated, which is not expressed

in (6.40). However, it should be reiterated that the modelling of the system is a supplement to the actual scope of this work, and hence this approximation is accepted to be within the margins of error.

Pico-Interference Since a foreign PBS (*i.e.*, not within the cell of interest) is considered, the final part of (6.31) can be reused, and hence the path loss distribution to a uniformly distributed MS, dependent on the distance D of the interfering PBS from the centre of the cell of interest, and parametrised by R, is given by

$$f_{L_s,I_{\mathrm{pic}},\mathrm{dB}}(l|D;R) = \frac{2\ln 10}{\beta R^2 \pi}\rho_d^2(l)\sin^{-1}\left(\frac{1}{2D\rho_d(l)}\sqrt{4D^2\rho_d^2(l) - \left(R^2 - \rho_d^2(l) - D^2\right)^2}\right),$$
$$\alpha + \beta\log_{10}(D-R) \leq l \leq \alpha + \beta\log_{10}(D+R)\,. \tag{6.42}$$

Since a PBS is uniformly placed around the centre of its macro-cell (where $\hat{d}$ denotes the distance from the cell-centre), D becomes a random variable, and hence l becomes dependent on D, and not parametrised by.

Therefore, in order to calculate the path loss from the foreign PBS, the loss-marginal of the joint distribution of l and D must be found, which is shown in (6.43). Given the distribution $f_D(D;R)$ (derived along with $\rho_D(D)$ in Appendix A), the integral, which is to be numerically evaluated, that describes $f_{L_s,I_{\mathrm{pic}},\mathrm{dB}}(l;R)$ is given by

$$f_{L_s,I_{\mathrm{pic}},\mathrm{dB}}(l;R) = \int f_{L_s,I_{\mathrm{pic}},D,\mathrm{dB}}(l,D;R)\mathrm{d}D = \int f_{L_s,I_{\mathrm{pic}},\mathrm{dB}}(l|D;R)f_D(D;R)\mathrm{d}D\,, \tag{6.43}$$
$$= \int \frac{\ln 10\rho_d^2(l)D}{\sqrt{3}\pi\beta R^3\hat{d}\sqrt{1-\rho_D^2(D)}}\sin^{-1}\left(\frac{1}{2D\rho_l(l)}\sqrt{4D^2\rho_d^2(l) - \left(R^2 - \rho_d^2(l) - D^2\right)^2}\right)\mathrm{d}D\,,$$
$$\alpha + \beta\log_{10}\left(\left(\sqrt{3}-1\right)R - r\right) \leq l \leq \alpha + \beta\log_{10}\left(\left(\sqrt{3}+1\right)R + r\right)\,. \tag{6.44}$$

Finally, as can be seen from Fig. 6.8, a pico-cell present in each of the neighbouring macro-cells is assumed, and hence it is clear that these interfering signals will aggregate. Hence, (6.44) is converted into the linear domain, resulting in

$$
\begin{aligned}
f_{L_s,I_{\mathrm{pic}}}(l;R) &= \left|\frac{\mathrm{d}\rho_{\mathrm{dB}}(l)}{\mathrm{d}l}\right| f_{L_s,I_{\mathrm{pic}},\mathrm{dB}}(\rho_{\mathrm{dB}}(l)) \\
&= \frac{10\rho_d^2(\rho_{\mathrm{dB}}(l))}{\sqrt{3}\pi\beta R^3\hat{d}l}\int \frac{D}{\sqrt{1-\rho_D^2(D)}} \\
&\qquad \sin^{-1}\left(\frac{1}{2D\rho_d(\rho_{\mathrm{dB}}(l))}\sqrt{4D^2\rho_d^2(\rho_{\mathrm{dB}}(l)) - \left(R^2-\rho_d^2(\rho_{\mathrm{dB}}(l))-D^2\right)^2}\right)\mathrm{d}D\,.
\end{aligned}
\tag{6.45}
$$

When analysing (6.45), it is evident that it portrays a skewed Gaussian shape. Furthermore, since a PBS in all (*i.e.*, 6) neighbouring cells is considered, given the shape of $f_{L_s,I_{\mathrm{pic}}}(l;R)$ it is clear that the sum of interfering signals from these PBSs can be approximated using the central limit theorem (CLT) (again, this can be performed due to the equivalent transmit powers of the PBSs). Thus, the sum pico-interference for a uniformly distributed MMS in a HetNet macro-cell is approximated by

$$
f_{L_s,\sum I_{\mathrm{pic}}}(l;R) \sim \mathcal{N}\left(N_I\mu_{I_{\mathrm{pic}}}, N_I\sigma^2_{I_{\mathrm{pic}}}\right)\,, \tag{6.46}
$$

where $N_I{=}6N_{\mathrm{p}}$ denotes the number of neighbouring PBSs,

$$
\mu_{I_{\mathrm{pic}}} = \mathbf{E}\left[L_{s,I_{\mathrm{pic}}}\right]\,,
$$

and

$$
\sigma_{I_{\mathrm{pic}}} = \sqrt{\mathbf{E}\left[\left(L_{s,I_{\mathrm{pic}}}-\mu_{I_{\mathrm{pic}}}\right)^2\right]}\,,
$$

which are numerically evaluated.

Own-Cell Interference In Figs. 3.2 and 6.8, it is clear that each macro-user has the opportunity to connect to (at least) two BSs within its cell. Therefore, the most dominant source of interference for an MMS is the AP in its own cell that it has *not* connected to.

In Section 6.5.2.1, it was determined through (6.33) which BS (macro- or pico-) the MMS would connect to (*i.e.*, that with the greater received signal strength). Hence, the own-cell interferer is the AP with the weaker signal at the MMS, and this PDF can be found via

$$
\begin{aligned}
f_W(w) &= f_X(w) + f_Y(w) - f_X(w)F_Y(w) - F_X(w)f_Y(w) \\
&= m(f_X, f_Y)\,.
\end{aligned}
\tag{6.47}
$$

Utilising (6.26), the PDF of the own-cell interfering signal, parametrised by R and D, of a uniformly distributed user in a HetNet macro-cell is given as

$$f_{I_{s,\mathrm{oc}},\mathrm{dB}}(w;R,D) = m\left(f_{L_{s,\mathrm{mac}},\mathrm{dB}}(g_{\mathrm{MBS}};R), f_{L_{s,\mathrm{pic}},\mathrm{dB}}(g_{\mathrm{PBS}};R,D)\right) . \tag{6.48}$$

As this further adds to the total interference, this is converted to the linear domain

$$f_{I_{s,\mathrm{oc}}}(u;R,D) = \left|\frac{\mathrm{d}\rho_{\mathrm{dB}}(u)}{\mathrm{d}u}\right| f_{I_{s,\mathrm{oc}},\mathrm{dB}}(\rho_{\mathrm{dB}}(v);R,D)\,,$$

and then convolved with the interfering signals from the neighbouring MBSs and PBSs

$$f_{\sum I_s}(v;R) = f_{L_s,\sum I_{\mathrm{mac}}}(g_{\mathrm{MBS}};R) \circledast f_{L_s,\sum I_{\mathrm{pic}}}(g_{\mathrm{PBS}};R) \circledast f_{I_{s,\mathrm{oc}}}(v;R,D)\,. \tag{6.49}$$

Finally, this is converted back into the dB domain (as this domain is used in the fuzzy logic system)

$$f_{\sum I_s,\mathrm{dB}}(w;R) = \left|\frac{\mathrm{d}\rho_p(w)}{\mathrm{d}w}\right| f_{\sum I_s}(\rho_p(w);R)\,. \tag{6.50}$$

It should be noted that due to the dominance of the own-cell interference, $f_{\sum I_s}(v;R)$ greatly resembles $f_{I_{s,\mathrm{oc}}}(u;R,D)$, but is marginally shifted by the average aggregate interference from the neighbouring BSs (macro- and pico-). In the logarithmic domain, however, this shift is negligible.

In Fig. 6.9, a comparison to simulation results is drawn, where it is evident that the theoretical CDFs match quite closely to their experimental counterparts. Where the desired signal CDFs show almost negligible difference, a $\sim$4 dB discrepancy is apparent for the interfering signal, which is mainly due to *i)* the approximations that have been taken into account, and *ii)* the correlation due to network architecture between interfering MBSs and PBSs that has *not* been considered here due to complexity. However, as the goal of these derivations was not the modelling of the system, but rather the verification of the network statistics, these differences are within the acceptable margins of error. It is clear that the signal strength PDFs are mainly dependent on the path loss between transmitter and receiver, assuming a constant transmit power. Furthermore, these PDFs can be extended to consider any number of PBSs per cell, and also varying network parameters (*i.e.*, cell sizes, transmit powers, etc.). Therefore, extending fuzzy logic ICIC to other scenarios is straightforward, thus expanding the applicability of fuzzy logic ICIC to virtually any HetNet.

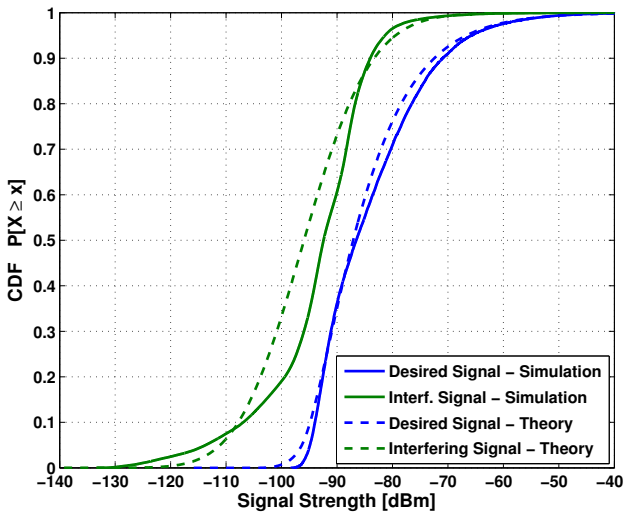

Figure 6.9: *Comparison of derived theoretical desired and interfering signal CDFs to Monte Carlo simulation results, considering lognormal shadowing.*

6.6 Simulation and Results

The general simulation setup utilised is described in Section 3.3. As mentioned previously, the initial application scenario for fuzzy logic ICIC is the femto-cell deployment (see Section 3.3.1.2), where solely the statistics derived in Section 6.3.4 are utilised to determine the desired and interfering signal membership functions, and no cell association is required.

Subsequently, fuzzy logic ICIC is utilised to operate a HetNet, the construction of which is given in Section 3.3.1.3. Here, cell association capability is provided to all MMSs. Furthermore, MBSs and PBSs are supplied the HetNet signal statistics derived in Section 6.5.2 to adjust the fuzzy logic system, whereas the FBSs clearly still utilise the femto-cell statistics. It should be mentioned that, due to the heterogeneous deployment and additional AP(s) in each macro-cell, the ICD of the network is larger than in the Chapters 4 and 5. The relevant simulation parameters for both scenarios can be found in Table 6.2.

6.6.1 Resource and Power Allocation

A MS is assigned two transmission requirements: a desired throughput and a MCS. The desired rate C_u^* of each user is generated by a random distribution[6] with mean $\bar{C}$. Thus, each MS_u will

[6]The distribution can be dependent on the scenario and traffic/applications (*i.e.*, internet, mobile TV, etc.) desired by the users.

Parameter	Value
Simulation area	37 cells
Results area	inner 7 cells
ISD	866 m
ICD	500 m
Apartment width, R_{a}	10 m
FBS probability, p_{act}	0.25
MMSs per cell, $\bar{N}$	20
PBSs per cell, N_{p}	1
PBS distance, $\hat{d}$	100 m
Blocks per cell, N_{app}	1
Number of available RBs, M	50
RB bandwidth, B_{RB}	180 kHz
Noise spectral density, η_0	$-174\,\mathrm{dBm/Hz}$
Average MMS rate, $\bar{C}_{\mathrm{m}}$	0.65 Mbps
Average FMS rate, $\bar{C}_{\mathrm{f}}$	1.25 Mbps
Subcarriers per RB, k_{sc}	12
Symbol rate per subcarrier, s_{sc}	15 ksps
Time slots (subframes), z	20
Subframe duration, t_{sf}	1 ms
MBS transmit power, $P_{\mathrm{max,MBS}}$	46 dBm
PBS transmit power, $P_{\mathrm{max,PBS}}$	30 dBm
FBS transmit power, $P_{\mathrm{max,FBS}}$	10 dBm
Load factor weight, w_{lf}	0.1
ABS prob., p_{ABS}	0.1
Outdoor channel parameters α_{o}, β_{o}	25.6, 36.7
Indoor channel parameters α_{i}, β_{i}	37, 30
Sector $\theta_{3\mathrm{dB}}$	70°
Shadowing Std. Devs., σ_{i}, σ_{o}	10, 4 dB
Auto-correlation distance	50 m

Table 6.2: *Chapter 6 Simulation Parameters*

require a different number of RBs n_u^{RB}, and hence the system will function best when strongly interfering users are assigned orthogonal resources. The MCS is also assigned randomly, with equal probabilities for all available spectral efficiencies. While this is not the most realistic assumption[7], it is applied here to further randomise the n_u^{RB} each MS$_u$ needs to meet its rate.

Finally, RBs are allocated independently at each BS. The benchmarks utilise a PFS, which improves frequency diversity relative to a random allocation. On the other hand, the autonomous fuzzy logic ICIC techniques assign RBs based on the available local information, optimising the MSs performance in the cell. It should be again noted that the fuzzy logic systems at the MBSs and PBSs utilise the HetNet signal statistics derived in Section 6.5.2, whereas the FBS fuzzy systems use the statistics derived in 6.3.4. Here, a greedy allocation of RBs to MSs is performed, as described in Section 6.3.3.

[7]When LA is applied, the user's MCS will more accurately reflect its SINR conditions. Furthermore, the number of RBs requested will clearly change dependent on the modulation order selected.

Benchmarks Finally, the benchmarks utilised for comparison to fuzzy logic ICIC are max. power transmission (BM 1) and ABS transmission (BM 3). For both, RBs are allocated to MSs via a PFS. Furthermore, specifically for the HetNet simulation, a fourth benchmark is included:

- *Femto-cell Fuzzy Logic*: Fuzzy logic ICIC utilising only the statistics for femto-cellular networks is applied. This highlights the importance of the HetNet signal statistics.

6.6.2 Femto-Cell Results and Discussion

It is clear from Fig. 6.10 that fuzzy logic ICIC provides substantially improved system performance over both benchmark techniques. Especially in terms of system throughput, where the fuzzy logic schemes are the only techniques which achieve the overall desired rate (*i.e.*, sum of individual desired rates). In fact, fuzzy logic substantially overachieves the sum desired rate, indicating almost maximum coverage and all but negligible outage. The additional rate results from the discrete allocation of bandwidth (*i.e.*, RBs), and hence the achieved user rate is generally slightly greater than what was desired. With LA this becomes more apparent, as with higher spectral efficiency the throughput "overshoot" becomes even greater.

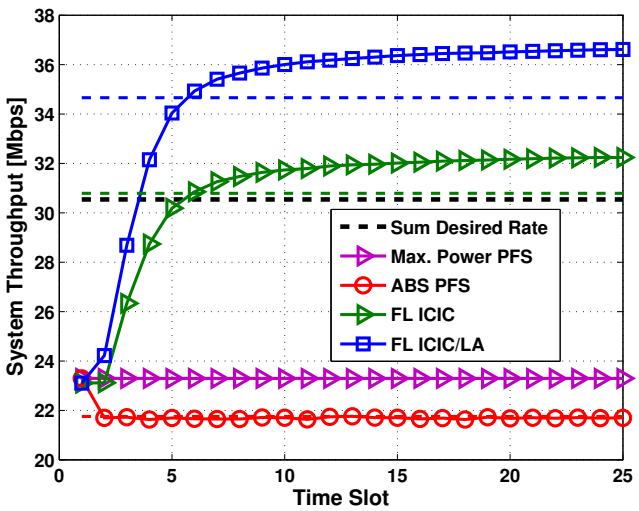

Figure 6.10: *System throughput performance results of femto fuzzy logic ICIC, random ABS transmission, and maximum power transmission. The dashed lines represent the mean performance of each system.*

The ABS performance is constant over all time slots (except the first), as the probability of ABS transmission(s) is identical in each slot. Hence, in each time slot 10%, on average, of the

FBSs transmit an ABS, providing some interference mitigation for the remaining cells. This abstinence of data transmission explains the throughput losses by the ABS system relative to full power transmission, as clearly the interference mitigation provided is less significant than the throughput sacrificed.

Fig. 6.11 displays the energy efficiency of the simulated scenario, yielding again very dominant results of the fuzzy logic systems. This is mainly due to the fact that fuzzy logic has the

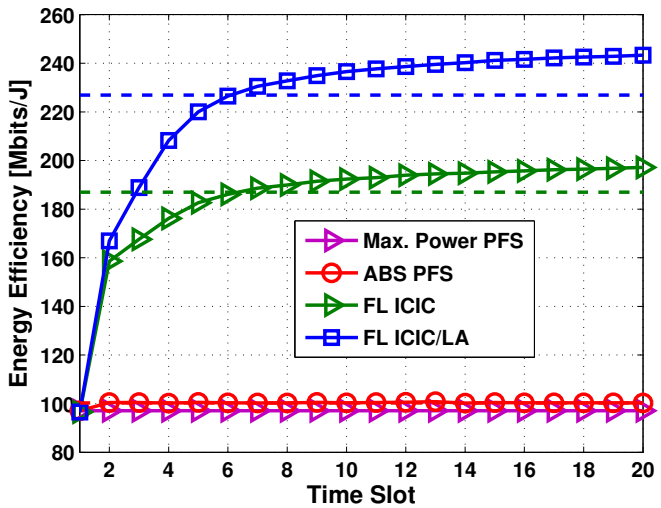

Figure 6.11: *System energy efficiency performance results of femto fuzzy logic ICIC, random ABS transmission, and maximum power transmission. The dashed lines represent the mean performance of each system.*

possibility of transmitting at half power, which is usually the case after multiple time slots and the achievement of a relatively orthogonal RB allocation. Furthermore, the high energy efficiency is achieved quite rapidly. The added energy efficiency due to LA is a direct result of the augmented throughputs (see (3.6)). It is shown that ABS transmission is slightly more energy efficient than maximum power, which is logical since on average 10% less power is used, but the loss in throughput is $<10\%$, thus enhancing the energy efficiency.

Lastly, the throughput fairness and availability in the system are displayed in Fig 6.12. It is clear that the fairness is greatly improved via fuzzy logic, especially when utilising LA. This is mainly due to the fact that users are (through LA) more adapted to their transmission environments, and hence better achieve their desired rates[8]. Furthermore, fuzzy logic ICIC/LA

[8]In fact, due to the reduced throughput granularity at higher modulation orders, more FMSs achieve the same throughput, and hence fuzzy logic ICIC/LA achieves a greater fairness than if all FMSs would exactly achieve their targets.

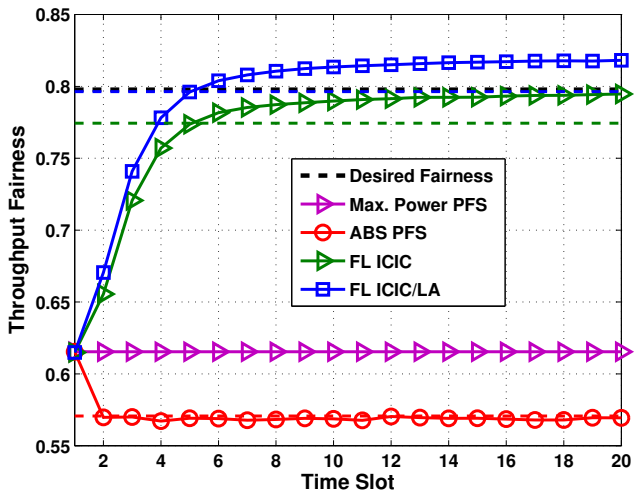

(a) Fairness

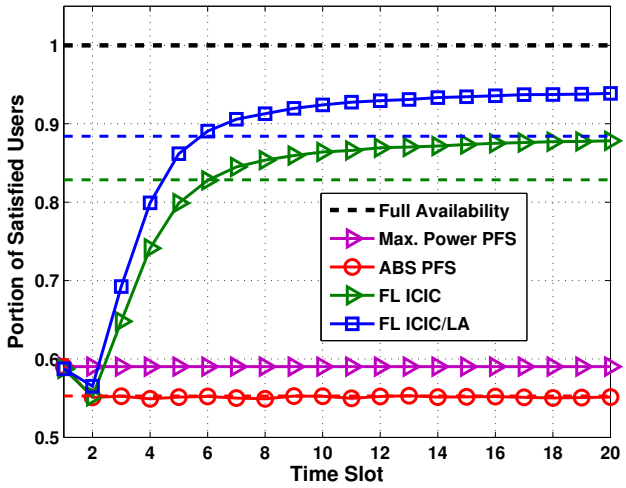

(b) Availability

Figure 6.12: *System coverage results of femto fuzzy logic ICIC, random ABS transmission, and maximum power transmission. The desired fairness is calculated via* (3.7) *utilising the user desired rates* $\mathbf{C}^*$. *The dashed lines represent the mean performance of each system.*

provides by far the best FMS availability, as can be seen from Fig. 6.12(b), achieving $\sim 94\%$ availability. This is expected as both the system throughputs are augmented, a direct result of the greater portion of satisfied FMSs. On another note, the max. power availability and fairness is boosted with regards to the ABS system, as all FMSs can transmit without restrictions or abstinence, and hence even unsatisfied (in terms of rate) users achieve decent throughputs. A summary of the quantitative results (at time slot 20) is shown in Table 6.3.

%-gain	vs.	C_{sys}	β_{sys}	χ_{sys}	$\Pi(\mathbf{C})$
FL ICIC/LA	Max. Pow.	57	151	59	33
FL ICIC	Max. Pow.	38	103	48	29
FL ICIC/LA	ABS	68	143	70	44
FL ICIC	ABS	48	97	59	40
FL ICIC/LA	FL. ICIC	14	24	7	3

Table 6.3: *Femto-Cell Performance Results: System Capacity, Energy Efficiency, Availability and Fairness*

6.6.3 HetNet Results and Discussion

Fig. 6.13 shows that the HetNet fuzzy logic technique provides substantially improved system performance over the three benchmarks. Especially in terms of system throughput, where the HetNet fuzzy logic schemes are the only techniques which achieve the overall desired rate (*i.e.*, sum of individual desired rates). In fact, after only four time slots, HetNet fuzzy logic greatly overachieves the sum desired rate, in a similar manner as in the femto-cellular scenario, resulting from the optimised allocation resources. The ABS and maximum power transmission

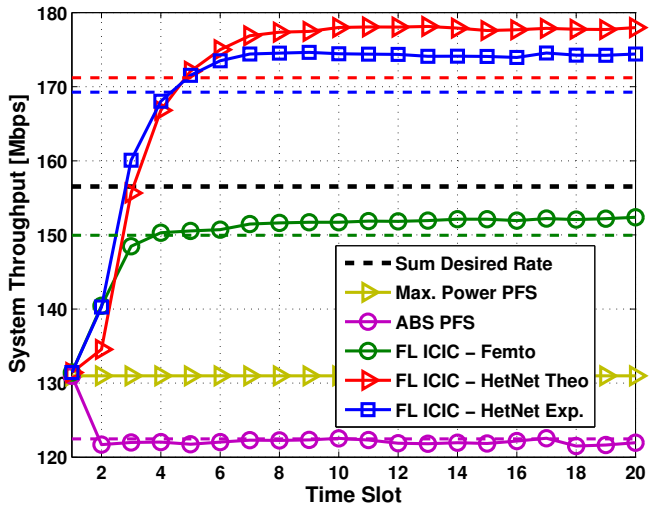

Figure 6.13: *System throughput performance results of femto fuzzy logic ICIC, random ABS transmission, and maximum power transmission. The dashed lines represent the mean performance of each system.*

systems also show equivalent trends to Fig. 6.10. Furthermore, femto fuzzy logic outperforms both these other benchmarks despite the usage of incorrect statistics in the macro/pico layer, indicating the robustness of the general fuzzy logic approach, and the rules in Table 6.1.

It should be noted that there is a minuscule discrepancy ($\sim$2%) between the HetNet fuzzy logic

schemes when employing the theoretical or experimental statistics. This is further verification of the results in Section 6.5.2 and Fig. 6.9. In fact, the theoretical system provides the improved throughput. This results from a more "aggressive" power allocation when using the experimental statistics, causing more RBs to be allocated half power (can be seen quite clearly in Fig. 6.14) as the threshold for "low interference" is higher than in the theoretical statistics. Because the system is fully loaded, some of these half power RBs do not achieve their SINR target, and hence cause the minor throughput losses evident in Fig. 6.13.

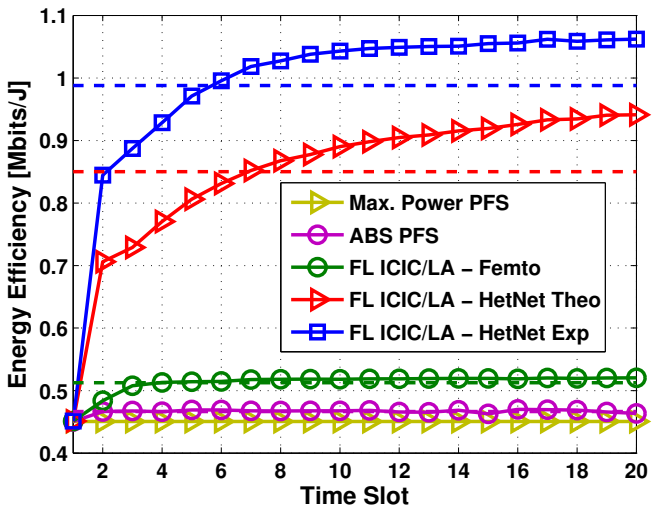

Figure 6.14: *System energy efficiency performance results of femto fuzzy logic ICIC, random ABS transmission, and maximum power transmission. The dashed lines represent the mean performance of each system.*

Fig. 6.14 displays the energy efficiency of the HetNet, yielding again very dominant results of the fuzzy logic systems. This is mainly due to the fact that fuzzy logic has the possibility of transmitting at half power, which is usually the case after multiple time slots and the achievement of orthogonal interfering-RB allocation. Furthermore, the high energy efficiency is achieved quite rapidly. Finally, as mentioned above, utilising the experimental statistics induces significant energy efficiency gains due to diminished transmit powers.

It is again clear that ABS transmission is slightly more energy efficient than maximum power transmission, as on average 10% less power is used and thus compensating the $<10\%$ throughput loss.

Lastly, the availability and throughput fairness in the system are investigated. As expected, HetNet fuzzy logic provides by far the best MMS availability ($>82\%$), as can be seen from Fig. 6.15. This is expected as the augmented system throughputs are a direct result of the great-

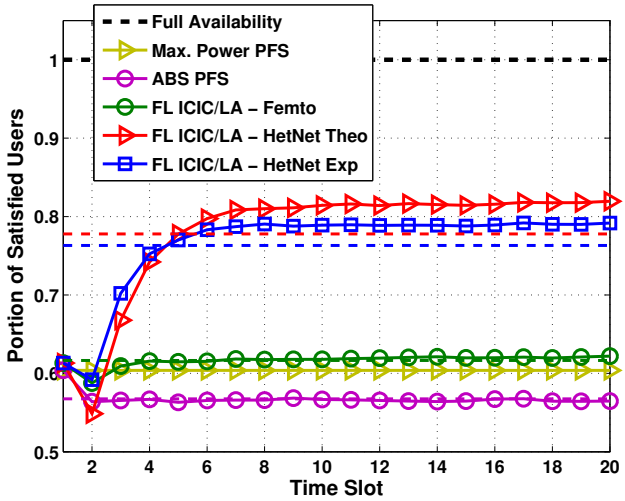

(a) Availability

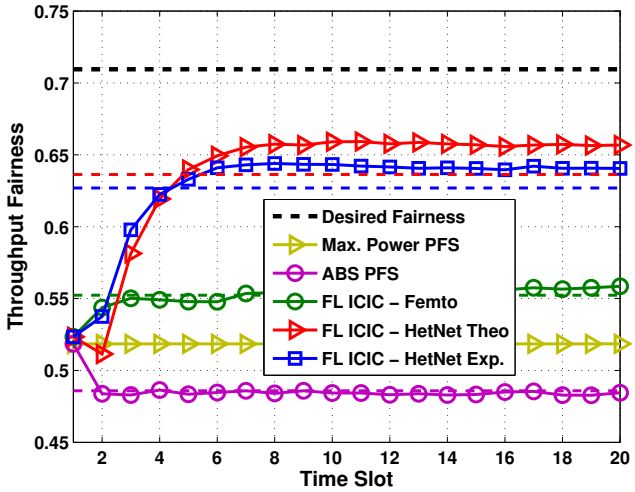

(b) Fairness

Figure 6.15: *System coverage results of fuzzy logic ICIC schemes, random ABS transmission, and maximum power transmission. The dashed lines represent the mean performance of each system.*

er portion of satisfied MSs. In addition, it is clear that the fairness is greatly enhanced as well, which is mainly due to the HetNet statistics utilised for macro/pico-users. In both measures, the performance is achieved after only 7 time slots, indicating a rapid convergence of the fuzzy logic technique. Furthermore, the dissimilarity between using theoretical or experimental statistics is again diminutive. It should be noted that, again, max. power achieves greater availability and fairness with regards to the ABS system, as all MSs can transmit without restrictions, and hence even unsatisfied (in terms of rate) MSs achieve decent throughputs. A summary of the

quantitative results is shown in Table 6.4.

%-gain over	$C_{\mathbf{sys}}$	$\beta_{\mathbf{sys}}$	$\chi_{\mathbf{sys}}$	$\Pi(\mathbf{C})$
Max. Pow.	35.9	110	22.0	26.9
ABS	45.9	100	25.0	34.7
FL ICIC Femto	16.8	81.0	20.0	18.6

Table 6.4: *HetNet Performance Results: System Capacity, Energy Efficiency, Availability and Fairness*

On another note, the difference between the fuzzy logic systems using theoretical and experimental CDFs, and further the unexpected superiority of the theoretical statistics, demonstrates the heuristic nature of fuzzy logic. The arbitrary selection of the signal membership functions as (approximately) thirds results in suboptimal allocations when the actual statistics are utilised, suggesting inappropriate membership regions. In this specific case, a "Low" membership should be assigned only to CDF values of 0.2 and lower, rather than 0.35. This indicates the need for a methodology to determine the optimal placement of the membership cut-off points, allowing the fuzzy logic ICIC system to further tune itself to its surrounding environment, potentially enhancing further the fuzzy logic ICIC operation.

6.7 Summary

A distributed and autonomous ICIC technique for HetNet interference management and resource allocation is presented. At every BS, the allocatability of the available RBs to each MS is evaluated utilising locally available information, such as the interference neighbourhood, MSs' requested rates, and the signal and fading environments. Fuzzy logic produces broad evaluations of the inputs, utilises a defined set of RB allocation rules to combine them, and informs the BS the most suitable resources and transmit powers for each MS to achieve successful and efficient communication. In addition, a LA procedure is appended to enable MSs to adjust their modulation order according to the channel environment. For HetNets, the fuzzy logic technique enables MMSs to autonomously choose connection among several nearby BSs in such a manner to benefit not only the user but the network as a whole. After multiple time slots and updated average signal statistics, the locally optimised resource allocations form a near-optimal global solution.

In order to facilitate the necessary signal statistics for this technique, the distributions of the desired and interfering signal strengths for the femto- and macro-tiers of a HetNet have been

analytically derived. For the macro-tier, a pico-cellular overlay is considered, and in both tiers a comparison to experimentally gathered statistics yielded a close match between simulation and theory. Furthermore, by comparing fuzzy logic ICIC to a system-wide optimisation problem, it was shown that fuzzy logic provides close-to-optimal system performance with drastically reduced complexity. A comparison to a greedy heuristic of similar complexity shows faster convergence to cell-individual optimum resource allocation. Hence, fuzzy logic provides a low-complexity near-system-optimal solution of ICIC in femto-cell networks.

This is confirmed in the simulation results, where in the femto-cell environment fuzzy logic ICIC satisfies the system throughput requirements and significantly outperforms the given benchmarks (57% over max. power and 68% over ABS transmission). The addition of LA to the fuzzy logic technique gives a further performance boost, achieving almost full availability along with enhanced throughput, energy efficiency, and fairness. In Section 6.6.3 it could be seen that, as expected, the HetNet fuzzy logic scheme substantially outperformed the comparative benchmarks in the deployment scenario. Especially in terms of system throughput (up to 46%) and energy efficiency (up to 110%), significant gains were seen when utilising the HetNet statistics in the fuzzy logic system. Furthermore, the system performance discrepancies between techniques utilising the theoretical and experimental sets of statistics was minute. Overall, fuzzy logic offers a highly effective, low-complexity solution to distributed and autonomous resource allocation in future wireless networks.

Chapter 7
Conclusions

7.1 Summary and Conclusions

In this thesis, Chapter 2 introduces the background for the undertaken research. To begin, a brief overview of the history of wireless communications is presented, discussing the evolution of cellular networks from the 1G mobile networks initially deployed in the 1980's, over 2G GSM, 3GPP networks and finally to LTE and 4G LTE-A. Furthermore, a description of the development of the multiple access techniques that supported this evolution was given, including in detail the OFDMA basis utilised for each part of this research. Next, an overview of the advancement of frequency reuse techniques was given, and the development of power control schemes was covered. Moreover, an overview of some of the most recent research areas in network interference management, along with their shortcomings is presented. Finally, the evolution of wireless networks to heterogeneous architectures was deliberated, and further the motivation for the current surge in femto-cell research and its concepts were discussed. Subsequently, Chapter 3 presented the common system model and simulation environment utilised throughout this thesis. Here, the investigated scenarios envisioned in future networks are described.

In Chapter 4, the well-known problem of uplink power control in macro-cellular networks is discussed. In particular, the envisioned dense macro-deployment in LTE and LTE-A networks is investigated. By reducing the transmit power on a subset of RBs in a given cell, ULIP is able to control CCI on these RBs in all neighbouring cells. Moreover, by signalling the interference tolerances dependent on the MSs that utilise these resources, ULIP provides direct user-based cooperative interference mitigation through power control. Analytical derivations determine that through ULIP the energy efficiency of all MSs in the system can be enhanced, hence inducing large system energy efficiency gains. Furthermore, it is shown that system capacity losses, which are expected when reducing the system power so drastically, are not necessarily incurred. Finally, an almost uniform areal distribution of throughput can be achieved by shifting capacity from the cell-centre to the cell-edge, enhancing system fairness and providing sought

after cell-edge performance maintenance. The exploitation of exisiting architectures such as the RSRP prevents additional signalling complexity, and further recommends the ULIP technique for future LTE/LTE-A networks.

Continued research in the area of dense, macro-cellular deployment is performed in Chapter 5, where a simplified criterion for joint power control and resource allocation is developed. By expressing this condition as a function of path gains and SINR targets, MSs in neighbouring cells can be allocated the same resources if the "feasibility" condition is fulfilled, and hence allocated Pareto optimum transmit powers such that each user can meet its SINR target. Furthermore, the extension of the link removal concept to OFDMA systems is performed, providing additional interference suppression in high-interference scenarios. The combination of these two algorithms yields substantial benefits in terms of network spectral and energy efficiency over traditional power control techniques.

In the second part of Chapter 5, the interference challenges in densely and randomly deployed femto-cell networks are addressed. Due to the assumption of a single user per femto-cell and full bandwidth utilisation, the joint resource and power allocation breaks down to a pure power control problem. PSS provides a low-complexity SINR variation algorithm which facilitates the projection of a group of interferers into the Pareto feasibility region. Hence, if a group of neighbouring MSs does not fulfil the feasibility condition, PSS adjusts their individual SINR targets until the group is feasible. The utilisation of interference graphs provides femto-cell clustering such that the centralised algorithms may be distributed among co-located clusters. Finally, the facilitation of POPC throughout the networks minimises their transmit power usage, and hence generates significant benefits in terms of system energy efficiency.

While the signalling burden incurred by the ULIP procedure is limited to the number of RBs in the system, the immense desired and interfering path gain information that must be signalled in PCS/PSS displays a certain unsuitability for future networks. Moreover, the evolution towards HetNets, and the associated backhauling, handover, and interference issues associated with these networks motivated the need for a distributed and autonomous approach to ICIC. Such research is demonstrated in Chapter 6. Fuzzy logic is utilised to combine locally available parameters to perform autonomous joint resource and power allocation in each cell of a dense and random femto-cell deployment, without the need for inter-BS signalling. It provides a holistic approach to resource and power allocation where many key parameters are combined to perform *close-to-optimal* network and interference management. Empirical comparisons to

the system optimal solution show that fuzzy logic ICIC is able to achieve 98% system throughput and availability performance after less than a single LTE frame, at a substantially (orders of magnitude) reduced operational complexity. A comparison to a low-complexity greedy heuristic shows much faster convergence and hence greater average throughput.

To finalise the work done throughout this project, the fuzzy logic ICIC system was extended to operation in HetNets. Here, intra- and inter-tier interference coordination is provided autonomously and distributedly, substantially reducing the operational complexity of such networks. Furthermore, a comprehensive analysis of received signal statistics in femto-cellular and HetNet scenarios is performed. Effectively, this yields a scenario-dependent modelling of the network environments, which ideally provides oppurtunities for future ICIC techniques to more efficiently control interference in such networks. Ultimately, in both the femto-cellular and HetNet scenarios, fuzzy logic ICIC achieves substantial gains over the benchmark techniques, in all areas of system throughput, energy efficiency, availability and fairness. Furthermore, fuzzy logic presents a basis for the evolution of ICIC to machine learning techniques designed to solve the multidimensional network optimisation problem. Nonetheless, the completely autonomous and distributed nature of fuzzy logic ICIC, and the complexities of centralised management in multi-tier HetNets, make this system a viable candidate for such future wireless communications networks.

7.2 Limitations and Scope for Further Research

Despite the significant work done in interference coordination for various types of wireless network deployments, there are a number of limitations that have been identified and need to be considered before the above techniques become implementable for real-life mobile networks.

In the context of the considered dense, macro-cell deployment and further the macro-cellular basis for HetNets, this work assumes a fully deterministic and perfectly hexagonal construction of the network. Furthermore, a uniform distribution of MSs throughout the (simulated) system area is implemented. It is clear, of course, that neither of these assumptions is fully realistic. In almost all macro-cellular deployments the placement of BSs is simply not possible to reflect a perfect tessellation of cells over a geographic area. While this may be overlooked, it is further clear that not all macro-cells will have the same size, as more sparesly populated suburban areas will require fewer resources, whereas dense urban environments suffering from

high shadowing will only be servable with smaller cells. Furthermore, the natural generation of user *hotspots* [156] in places such as shopping malls, amusement parks, train stations or airports is not considered in this work. Clearly, such hotspots generate concentrated interference to neighbouring cells, and further quickly expend the available wireless resources. Hence, a key area of further development for especially the ULIP and PCS techniques would be to handle such changing environments. Especially the variation in neighbouring cell densities may have adverse affects on the ability for PCS to schedule users appropriately, which may cause large outages and system spectral efficiency losses. On the other hand, the distributed and autonomous nature of fuzzy logic ICIC should be able to still perform precise resource and power allocations for such geographically varying networks.

On a similar note, it has been assumed throughout this work that MSs are quasi-static over multiple time frames, and further, static over the duration of a subframe. However, while this assumption may hold for femto-cells (as it is highly unlikely an indoor MS will be travelling at any great speed), it certainly ignores the everyday movement scenarios in urban environments. In the case of high mobility, due to the quick variations in channel quality, the ULIP technique may have difficulties to provide interference protection either to or from this MS. Especially, if the RSRPs are changing rapidly, which may lead to undesired interference at neighbouring high-priority MSs. Furthermore, while ULIP functions on a cell-by-cell basis (*i.e.*, priority band association and power reduction is performed in each cell individually), PCS relies on three-cell clusters to provide interference mitigation. Hence, the feasible groupings would be constantly changing with high mobility, and furthermore handovers would become a significant challenge. Finally, this leads again to fuzzy logic ICIC, where clearly an autonomous handover protocol would need to be developed such that cell re-assocation can be performed quickly and seamlessly. However, an additional parameter such as "RSRP change" included in the current cell assocation capability may be able to handle such rapid handovers through a system.

Coming more specifically to the techniques themselves, it is clear that the PCS system throughput performance degradation at higher SINRs results mainly from the inability to find suitable interfering MS-groupings. A similar problem is seen in the application of CoMP [80] for 4G cooperative networks, which has been solved through the implementation of *cover shifting* [157], where a larger number of cells is considered to find appropriate user groups than, in this case, three neighbours. This, in turn, results in additional signalling complexity, however has shown to provide throughput gains over pure CoMP transmission, and hence may incur similar benefits

for PCS.

In PSS, clearly the most limiting assumption is the single FMS per femto-cell. Through the relaxation of this assumption, however, the multi-user scheduling problem could be dealt with utilising a combination of PCS and PSS, where the resource allocation in the femto-cell cluster can be performed using PCS, and the further reduction (if necessary) of the feasibility condition is completed through PSS. On the other hand, the main drawback of PSS is the substantial throughput gap to maximum power transmission. While it is argued that this comparison is unfair, and the large gains over full power control are highlighted, PSS may benefit from a similar parametrisation as LTE power control, where a balance may be achieved between "full PSS" and max. power transmission. This should close the throughput performance gap, and further allow the central controller to tune the system according the network's needs.

A significant advantage of fuzzy logic ICIC is the low operational complexity, which results mainly from its heuristic nature. This, however, is also one of the main drawbacks of the system, as this clearly results in less than optimal decision-making. It is evident in the HetNet results in Section 6.6.3 that the fuzzy system based on the analytically derived signal CDFs provides superior performance to the system utilising actual, experimentally determined statistics. This should, of course, not be the case. However, this phenomenon indicates a suboptimal allotment of the membership functions for the RB interference input variable. Therefore, future work should provide a methodology for determining the optimal membership functions, which may rely on reinforcement learning techniques designed to optimise the membership functions based on previous decisions and resultant user performance. This should allow the fuzzy logic system to tune itself to the surrounding environment, further improving the system performance.

Finally, it is envisioned for future research to build on the fuzzy logic ICIC system through the implementation of machine learning techniques [88, 158]. While fuzzy logic allows an operator to input human expertise/knowledge about resource allocation decisions, the heuristic nature of the methodology imposes a limit on the functionality of the system. Therefore, a machine learning approach that is designed to gain this expertise itself, and function in a similar distributed and autonomous manner, would be able to extend the possibilities of such communications to any and all scenarios. Moreover, this would eliminate the need for statistics derivations or measurements, and furthermore allow the system to adapt itself to changing own and interference environments. Ideally, by using the knowledge gained and trends learnt from the fuzzy logic approach, this may be utilised as a stepping stone for a whole new branch of interference and

network management tools, which remove the necessity for any centralised control over the system, and hence improve not only the signalling efficiency but also the overall spectral and energy efficiencies of future mobile communications networks.

Appendix A
HetNet Signal Statistics Derivation

In Section 6.5.2, the desired and interfering signal statistics for the macro- and pico-cell layer of a HetNet were presented. As mentioned, the detailed derivations are given in this Appendix. It should be noted that all derived PDFs have been verified using Monte Carlo simulations.

A.1 Desired Signal

A.1.1 Macro-BS

The desired signal of a MBS to a uniformly distributed MMS in its macro-cell is derived. For ease of calculation, the hexagonal cell is approximated by a circle of equivalent area. Therefore, given a hexagonal radius R_H, the radius of the circular cell is calculated to be

$$R = \sqrt{\frac{3\sqrt{3}}{2\pi}} R_H \,, \qquad R_H = \frac{\mathrm{ICD}}{\sqrt{3}} \,. \tag{A.1}$$

This approximation will serve for all following derivations. Moreover, in the following D will denote the distance from the transmitter to the centre of the cell of interest.

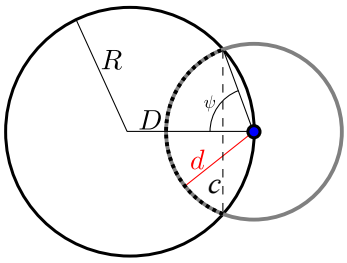

Figure A.1: *Calculation of the PDF of the distance from a MBS. The blue dot denotes a sectorised MBS placed on the outside of the cell. The concentric circle around the MBS represents the distance from it, of which the dashed part inside is the probability a MMS in the macro-cell is distance d from the MBS.*

Fig. A.1 displays the method for deriving the distance PDF from an MMS to its serving MBS. By calculating the chord (dashed vertical line in Fig. A.1) length c depending on the distance

from the BS d [159]

$$c(d) = \frac{1}{D}\sqrt{4D^2R^2 - (D^2 - d^2 + R^2)^2}\,, \tag{A.2}$$
$$\underset{D=R}{=} \frac{1}{R}\sqrt{4R^4 - (2R^2 - d^2)^2}\,,$$
$$= \frac{1}{R}\sqrt{4R^2d^2 - d^4}\,, \tag{A.3}$$

it is possible to calculate the arc length $\lambda_{\text{arc}}(d)$

$$\psi = \sin^{-1}\left(\frac{c(d)}{2d}\right)\,, \tag{A.4}$$
$$\lambda_{\text{arc}}(d) = 2d\psi\,, \tag{A.5}$$
$$= 2d\sin^{-1}\left(\frac{1}{2dR}\sqrt{4R^2d^2 - d^4}\right)\,,$$
$$= 2d\sin^{-1}\left(\sqrt{1 - \left(\frac{d}{2R}\right)^2}\right)\,, \tag{A.6}$$

which corresponds directly to an MS's *probability of location at distance* d from the macro-BS, $p_d(d)$. By evaluated this for all d from 0 to $2R$, and normalising by the total number of possibilities for d, it results that

$$f_{d,\text{mac}}(d;R) = \frac{\lambda_{\text{arc}}(d)}{\int_0^{2R}\lambda_{\text{arc}}(d)\mathrm{d}d}\,, \tag{A.7}$$
$$= \frac{2}{R^2\pi}d\sin^{-1}\left(\sqrt{1 - \left(\frac{d}{2R}\right)^2}\right)\,,\ 0 \le d \le 2R\,.$$

Utilising (3.9), $\rho_d(l)$ (defined in (6.5)) and $\left|\frac{\mathrm{d}\rho_d(l)}{\mathrm{d}l}\right| = \frac{\ln 10}{\beta}\rho_d(l)$, through r.v.t the MBS distance dependent path loss PDF is obtained, shown in (6.27).

Fig. A.2 shows the method for deriving the PDF of the angle θ of an MMS from the central lobe of the MBS. Here, the length of the chord dependent on θ, $c(\theta)$, and the resultant *probability of location at angle* θ, $p_\theta(\theta)$, is calculated

$$c(\theta) = 2R\cos(\theta)\,,$$
$$p_\theta(\theta) = \frac{c(\theta)^2\mathrm{d}\theta}{2}\,,$$
$$= 2R^2\cos^2(\theta)\,. \tag{A.8}$$

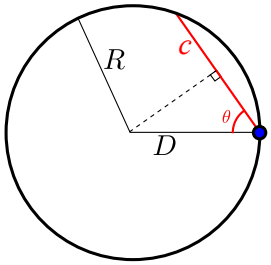

Figure A.2: *Calculation of the PDF of the angle from the central lobe of a MBS. The blue dot denotes a sectorised MBS placed on the outside of the cell. The red chord c represents the angle from the central lobe, and hence its length is the probability an MMS is located at this angle.*

From (A.8), the PDF is calculated by normalising over all possible angles

$$\begin{aligned} f_{\theta,\mathrm{mac}}(\theta; R) &= \frac{p_\theta(\theta)}{\int_{-\pi/2}^{\pi/2} p_\theta(\theta)\mathrm{d}\theta}\,, \\ &= \frac{2R^2\cos^2(\theta)}{R^2\pi}\,, \\ &= \frac{1}{\pi}\left(\cos(2\theta)+1\right)\,, \qquad -\frac{\pi}{2} \le \theta \le \frac{\pi}{2}\,. \end{aligned} \tag{A.9}$$

By utilising (3.10), $\rho_\theta(l)$ (defined in (6.28)) and $\left|\frac{\mathrm{d}\rho_\theta(l)}{\mathrm{d}l}\right| = \frac{\theta_{3\mathrm{dB}}}{\sqrt{48}l}$, through r.v.t the MBS angular loss PDF is derived, shown in (6.29).

These PDFs are then combined in (6.30) to form the MBS path loss PDF $f_{L_{s,\mathrm{mac}},\mathrm{dB}}(l; R)$.

A.1.2 Pico-BS

Fig. A.3 portrays the method for deriving the path loss PDF from a PBS placed uniformly at a distance D from the cell-centre. Since an omnidirectional antenna is assumed, the path loss is purely distance dependent, however is split into three cases depending on the distance d from the PBS. If $d \le R - D$, the entire circle around the PBS represents $p_d(d)$, and is given in [160] by

$$f_{d,\mathrm{pic}}(d; R, D) = \frac{2d}{R^2}\,, \qquad 0 < d \le R - D\,. \tag{A.10a}$$

For distances where the majority of the circle (middle circle, purple section) represents $p_d(d)$, the chord length (A.3) and angle (A.4) are used, however the arc length is now given by

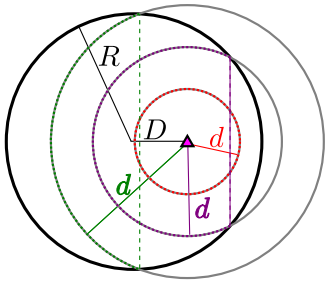

Figure A.3: *Calculation of the PDF of the distance from a uniformly placed PBS. The magenta triangle denotes a PBS at a distance D from the cell-centre. The three concentric circles represent the distance from the PBS, where the dashed part of each circle is the probability a MMS is that distance d from the PBS.*

$$\begin{aligned}\lambda_{\text{arc}}(d) &= 2d(\pi - \theta)\,,\\ &= 2d\left(\pi - \sin^{-1}\left(\frac{1}{2dD}\sqrt{4D^2d^2 - (R^2 - d^2 - D^2)^2}\right)\right)\,.\end{aligned}$$

Thus, the distance for this case is given by

$$\begin{aligned}f_{d,\text{pic}}(d; R, D) &= \frac{\lambda_{\text{arc}}(d)}{\int_0^{2R}\lambda_{\text{arc}}(d)\mathrm{d}d}\,,\\ &= \frac{2d}{R^2\pi}\left(\pi - \sin^{-1}\left(\frac{1}{2dD}\sqrt{4D^2d^2 - (R^2 - d^2 - D^2)^2}\right)\right)\,,\\ &\quad R - D < d \leq \sqrt{R^2 - D^2}\,.\end{aligned} \tag{A.10b}$$

Finally, when d grows so large that the minority of the circle (largest circle, green section) denotes $p_d(d)$, (A.6) can again be used for the arc length, and hence

$$\begin{aligned}&f_{d,\text{pic}}(d; R, D) =\\ &= \frac{2d}{R^2\pi}\left(\sin^{-1}\left(\frac{1}{2dD}\sqrt{4D^2d^2 - (R^2 - d^2 - D^2)^2}\right)\right)\,,\\ &\quad \sqrt{R^2 - D^2} < d \leq R + D\,.\end{aligned} \tag{A.10c}$$

Thus, the PDF of the distance d from a randomly located PBS to a uniformly distributed MMS can be fully described by

$$f_{d,\mathrm{pic}}(d;R,D) =$$
$$= \begin{cases} \frac{2d}{R^2} & 0 < d \leq R - D \\ \frac{2d}{R^2\pi}\left(\pi - \sin^{-1}\left(\frac{1}{2dD}\sqrt{4D^2d^2 - (R^2 - d^2 - D^2)^2}\right)\right) & R - D < d \leq \sqrt{R^2 - D^2} \\ \frac{2d}{R^2\pi}\left(\sin^{-1}\left(\frac{1}{2dD}\sqrt{4D^2d^2 - (R^2 - d^2 - D^2)^2}\right)\right) & \sqrt{R^2 - D^2} < d \leq R + D \end{cases} \tag{A.10}$$

And consequently, utilising (3.9) and $\rho_d(l)$, the corresponding path loss PDF in (6.31) can be derived.

Finally, to calculate the desired signal, it must be determined which AP the MMS will connect to based on the received signal strength, which is given by (6.33). In the following, the derivation of this function is presented.

$$\begin{aligned} W &= \max(X, Y)\ , \\ F_W(w) &= \mathbf{P}\left[W \leq w\right] = \mathbf{P}\left[\max(X,Y) \leq w\right]\ , \\ &= \mathbf{P}\left[X \leq w\right]\mathbf{P}\left[Y \leq w\right] = F_X(w)F_Y(w)\,. \\ f_W(z) &= \frac{\mathrm{d}}{\mathrm{d}w}F_W(w)\,, \end{aligned} \tag{A.11}$$

where $\mathbf{P}[\cdot]$ denotes the probability measure.

A.2 Interfering Signal

The derivation steps for the desired signal PDF are shown above; here, the steps for the interfering signal are described.

A.2.1 Macro-BS

Again, the MBS interference is derived first, where Fig. A.4 shows the macro-interference scenario. It is clear that the minority of the circle of radius d represents $p_d(d)$, and hence (A.10c) can be reused to calculate $f_d(d;R)$, and evaluate it at the deterministic interfering-MBS distance D=$2R$ (see Fig. 6.8)

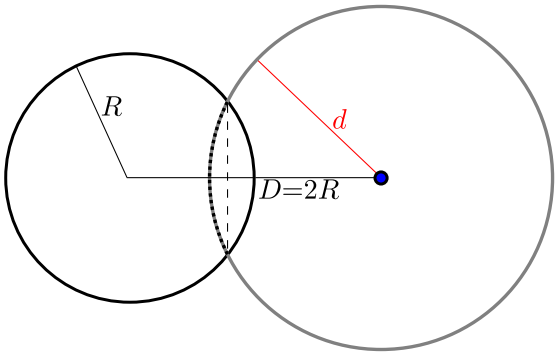

Figure A.4: *Calculation of the PDF of the distance from an interfering MBS. The blue dot denotes a sectorised interfering MBS located outside the cell. The concentric circle around the MBS represents the distance from it, of which the dashed part inside is the probability a MMS in the macro-cell is distance d from the interfering MBS.*

$$
\begin{aligned}
&f_{d,I_{\text{mac}}}(d;R,D)|_{D=2R} = \\
&= \frac{2d}{R^2\pi}\sin^{-1}\left(\frac{1}{4Rd}\sqrt{16R^2d^2-(-d^2-3R^2)^2}\right), \\
&= \frac{2d}{R^2\pi}\sin^{-1}\left(\sqrt{1-\frac{1}{16R^2d^2}\left(d^2+3R^2\right)^2}\right). \qquad \text{(A.12)}
\end{aligned}
$$

Utilising again (3.9) and $\rho_d(l)$, the PDF of the distance dependent path loss from an interfering MBS to a uniformly distributed MMS can be determined, shown in (6.35).

Fig. A.5 displays the calculation method of the angle from the central lobe (explained in further detail later) of the interfering macro-BS, where $p_{\theta_I}(\theta_I)$ is directly dependent on the chord

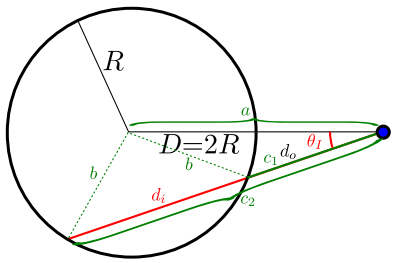

Figure A.5: *Calculation of the PDF of the angle from an interfering MBS. The blue dot denotes a sectorised interfering MBS located outside the cell. The red chord c_2 represents the angle from the interfering MBS, and hence its length inside the macro-cell (red chord d_i) is the probability an MMS is located at this angle.*

length d_i. In order to calculate d_i and d_o, the law of cosines (A.13) and the quadratic equa-

tion (A.14) are utilised.

$$b^2 = a^2 + c_i^2 - 2c_i a \cos B\,, \qquad B{=}\theta_I \tag{A.13}$$

$$\begin{aligned} 0 &= c_i^2 - 2a\cos\theta_I c_i - b^2 + a^2 \\ &= kc_i^2 + lc_i + m \\ c_i &= \frac{-l \pm \sqrt{l^2 - 4km}}{2k} \\ &= a\cos\theta \pm \sqrt{a^2\cos^2\theta_I - a^2 + b^2} \end{aligned} \tag{A.14}$$

$$\begin{aligned} c_2 &= 2R\cos\theta + \sqrt{4R^2\cos^2\theta_I - 3R^2} \\ d_o = c_1 &= 2R\cos\theta - \sqrt{4R^2\cos^2\theta_I - 3R^2} \\ d_i = c_2 - c_1 &= 2\sqrt{4R^2\cos^2\theta_I - 3R^2} \end{aligned} \tag{A.15}$$

From (A.15), $p_{\theta_I}(\theta_I)$ is determined by

$$\begin{aligned} p_{\theta_I}(\theta_I) &= d_i \frac{d_o \mathrm{d}\theta_I + (d_o{+}d_i)\mathrm{d}\theta_I}{2}\,, \\ &= d_i\left(d_o + \frac{1}{2}d_i\right)\mathrm{d}\theta_I\,, \\ &= 4R^2\cos\theta_I\sqrt{4\cos^2\theta_I - 3}\,, \end{aligned} \tag{A.16}$$

and, consequently, the angular PDF of a uniformly distributed MMS relative to the interfering MBS is derived as

$$\begin{aligned} f_{\theta_I}(\theta_I) &= \frac{p_{\theta_I}(\theta_I)}{\int_{-\pi/2}^{\pi/2} p_{\theta_I}(\theta_I)\mathrm{d}\theta_I}\,, \\ &= \frac{4R^2\cos\theta_I\sqrt{4\cos^2\theta_I - 3}}{R^2\pi}\,, \\ &= \frac{4}{\pi}\cos\theta_I\sqrt{4\cos^2\theta_I - 3}\,, \quad -\frac{\pi}{6} \le \theta_I \le \frac{\pi}{6}\,. \end{aligned} \tag{A.17}$$

The limits of θ_I in (A.17) are determined via simple trigonometry ($\theta_{I,\max}{=}\sin^{-1}\left({}^{R}\!/_{2R}\right){=}{}^{\pi}\!/_{6}$).

Now, in Fig. 6.8 it is clear that the interfering signal from a MBS does not actually have a central lobe, but rather this is given by two neighbouring lobes meeting at $\theta{=}{}^{\pi}\!/_{3}$. Hence, the signal attenuation is greatest at $\theta_I{=}0$ and decreases as θ_I grows. Thus, the angular loss $L_{\theta_I,\mathrm{dB}}$

is given by

$$L_{\theta_I,\mathrm{dB}} = \min\left(12\left(\frac{\frac{\pi}{3}-|\theta_I|}{\theta_{3\mathrm{dB}}}\right)^2, 20\right), \tag{A.18}$$

which is used in conjunction with $\rho_{\theta_I}(l)$ (defined in (6.37)) and $\left|\frac{\mathrm{d}\rho_{\theta_I}(l)}{\mathrm{d}l}\right| = \frac{\theta_{3\mathrm{dB}}}{\sqrt{48}l}$ to derive the angular loss PDF from and interfering MBS given in (6.38).

Finally, in order to add the two considered macro-interfering signals, $f_{L_s,I_{\mathrm{mac}},\mathrm{dB}}(l;R)$ is converted to the linear domain via $\rho_{\mathrm{dB}}(l)$ (defined in (6.39)) and $\left|\frac{\mathrm{d}\rho_{\mathrm{dB}}(l)}{\mathrm{d}l}\right| = \frac{1}{l\ln 10}$. The conversion back into the logarithmic domain is performed using $\rho_p(l)$ (defined in (6.12)) and $\left|\frac{\mathrm{d}\rho_p(l)}{\mathrm{d}l}\right| = \ln(10)10^{\frac{l}{10}-1}$.

A.2.2 Pico-BS

Fig. A.6 shows the interference scenario for a PBS located in a neighbouring cell. As the PBS is

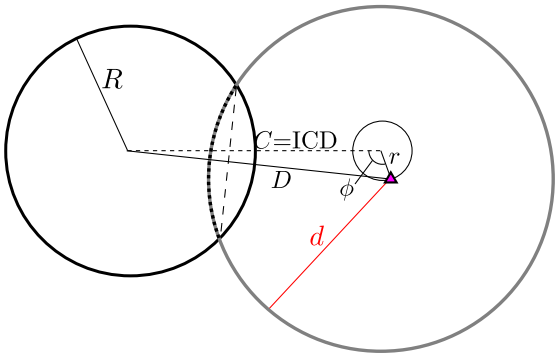

Figure A.6: *Calculation of the PDF of the distance from an interfering PBS. The magenta triangle denotes an interfering PBS at a distance r from the neighbouring cell-centre, and distance D from the centre of the cell of interest. The concentric circle represents the distance from the PBS, where the dashed part of the circle inside the macro-cell is the probability a MMS is that distance d from the interfering PBS.*

uniformly placed at a distance $r{=}\hat{d}$ from the centre of the neighbouring macro-cell, the distance D to the centre of the cell of interest becomes a random variable, upon which the interfering signal from this BS is clearly dependent. Therefore, this PDF must be derived first.

Using (A.13), the equation for D is found based on the network parameters.

$$D^2 = C^2 + r^2 - 2Cr\cos\phi\,,$$
$$D = \sqrt{A + B\varphi}\,, \qquad A{=}C^2 + r^2,\ B{=}-2Cr,\ \varphi{=}\cos\phi\,,$$

Now, given that ϕ is uniformly distributed,

$$\phi \sim \text{unif}(0, 2\pi]\,, \qquad f_\phi(\phi) = \frac{1}{2\pi}\,,$$

from which the distribution of φ is derived

$$\begin{aligned}
\rho(\varphi) = \phi = \cos^{-1}\varphi\,, \qquad & \left|\frac{\mathrm{d}\rho(\varphi)}{\mathrm{d}\varphi}\right| = \frac{1}{\sqrt{1-\varphi^2}}\,, \\
f_\varphi(\varphi) &= \left|\frac{\mathrm{d}\rho(\varphi)}{\mathrm{d}\varphi}\right| f_\phi(\rho(\varphi)) \\
&= \frac{1}{2\pi\sqrt{1-\varphi^2}}\,,
\end{aligned} \tag{A.19}$$

and then, ultimately, the PDF of the distance D of the interfering PBS to the macro-cell centre

$$\begin{aligned}
\rho_D(D) = \varphi = \frac{D^2 - A}{B}\,, \qquad & \left|\frac{\mathrm{d}\rho_D(D)}{\mathrm{d}D}\right| = \frac{2D}{B} = \frac{D}{Cr}\,, \\
f_D(D;R) &= \left|\frac{\mathrm{d}\rho_D(D)}{\mathrm{d}D}\right| f_\varphi(\rho_D(D))\,, \\
&= \frac{D}{2\sqrt{3}\pi Rr\sqrt{1-\rho_D^2(D)}}\,,
\end{aligned} \tag{A.20}$$

where C=ICD=$\sqrt{3}R$ is utilised to obtain (A.20). Consequently, (A.20) is substituted into (6.43) to obtain (6.44).

A.2.3 Own-Cell

The final contributor to the interfering signal is that from the AP in the macro-cell the MS has *not* connected to. This is determined by finding the minimum received signal strength of the macro- and pico-BSs. The derivation of this function is presented here.

$$\begin{aligned}
Z &= \min\left(X, Y\right)\,, \\
F_Z(z) &= \mathbf{P}\left[Z \le z\right] = \mathbf{P}\left[\min(X,Y) \le z\right] \\
&= 1 - \mathbf{P}\left[X > z\right]\mathbf{P}\left[Y > z\right] \\
&= 1 - \left(1 - F_X(z)\right)\left(1 - F_Y(z)\right) \\
&= F_X(z) + F_Y(z) - F_X(z)F_Y(z)\,,
\end{aligned}$$

Finally, (A.11) is utilised to achieve (6.47).

Appendix B
List of Publications

This section contains a list of papers either accepted for publication, pending publication or submitted for publication.

B.1 Accepted Publications

- **H. Burchardt**, Z. Bharucha, H. Haas and G. Auer, "Uplink Interference Protection and Fair Scheduling for Power Efficient OFDMA Networks," *8th International Workshop on Multi-Carrier Systems & Solutions (MC-SS)*, pp. 1–5, 3–4 May, 2011.

- **H. Burchardt**, Z. Bharucha, G. Auer and H. Haas, "Uplink Interference Protection and Scheduling for Energy Efficient OFDMA Networks," *EURASIP Journal on Wireless Communication and Networking Special Issue on Advanced Technologies for LTE Advanced*, May, 2012.

- **H. Burchardt**, S. Sinanović, G. Auer and H. Haas, "Pareto Optimal Power Control Scheduling for OFDMA Networks," *Proc. of IEEE Vehicular Technology Conference (VTC Fall)*, 2–9 Sept., 2012.

- **H. Burchardt**, S. Sinanović, G. Auer and H. Haas, "Pareto Optimal SINR Scheduling for Femto-cell Deployment in Wireless Networks," *Proc. of IEEE Vehicular Technology Conference (VTC Fall)*, 2–9 Sept., 2012.

- **H. Burchardt**, Z. Bharucha and H. Haas, "Distributed and Autonomous Resource Allocation for Femto-cellular Networks," *Forty-Sixth Asilomar Conference on Signals, Systems, and Computers*, 4–7 Nov., 2012.

- **H. Burchardt** and H. Haas, "Multi-Cell Cooperation: Evolution of Coordination and Cooperation in Large-Scale Cellular Networks," *IEEE Wireless Communications*, vol. 20, no. 1, pp. 19–26, Feb., 2013.

- **H. Burchardt**, S. Sinanović, Z. Bharucha and H. Haas, "Distributed and Autonomous Resource and Power Allocation for Wireless Networks," to be published in *IEEE Transactions on Communications*, 2013.

B.2 Submitted Papers

- **H. Burchardt**, S. Sinanović and H. Haas, "Distributed and Autonomous Resource and Power Allocation for Wireless Heterogeneous Networks," submitted to *IEEE Transactions on Mobile Computing*.

B.3 Patents

- **H. Burchardt**, S. Sinanović, H. Haas and G. Auer, "Pareto Optimal Power Control Scheduling in OFDMA Cellular System".
- **H. Burchardt**, S. Sinanović, H. Haas and G. Auer, "Pareto Optimal Power Control SINR Variation in Femto-Cell System".
- **H. Burchardt**, Z. Bharucha and H. Haas, "Distributed and Autonomous Resource and Power Allocation for Densely and Randomly Deployed Femto-Cells (*Fuzzy Logic ICIC*)".

Appendix C
Publications

This chapter contains all work either already published or awaiting publication.

Uplink Interference Protection and Fair Scheduling for Power Efficient OFDMA Networks

Invited Paper

Harald Burchardt*, Zubin Bharucha†, Harald Haas* and Gunther Auer†

*Institute for Digital Communications, Joint Research Institute for Signal and Image Processing,
The University of Edinburgh, EH9 3JL, Edinburgh, UK
Email: {h.burchardt, h.haas}@ed.ac.uk
†DOCOMO Euro-Labs, 80687 Munich, Germany, Email: {bharucha,auer}@docomolab-euro.com

***Abstract*—In this paper a new method for uplink inter-cell interference coordination (ICIC) in a full frequency reuse system is proposed. The technique is named uplink interference protection (ULIP). ULIP exploits existing reference signals transmitted by all base stations (BSs). The fact that path loss and lognormal shadowing can be considered reciprocal in such frequency-division duplex (FDD) systems is exploited. Therefore, no additional signalling is required for a new mobile station (MS) to estimate the level of inter-cell interference it would cause to ongoing uplink transmissions in neighbouring cells. Using the acquired knowledge, MSs can adjust their transmit power to ensure that existing links are not forced into outage. A scheduling scheme is suggested in which a fair allocation of priority resource blocks (RBs), based on user signal-to-interference-plus-noise ratios (SINRs), enhances both cell-edge throughput and user throughput fairness. Through this, also significant system throughput gains are generated. Finally, it is demonstrated that as a side effect of the interference reductions, considerable energy savings can be achieved.**

I. Introduction

In order to be able to significantly enhance the system spectral efficiency it must be possible in fourth generation (4G) wireless systems to use all available frequency channels in every cell. In such systems, interference originating from cell-edge users in the neighbouring cell can be detrimental to the SINR and throughput performance of MSs using the same set of RBs [1]. In addition, the necessity for more energy efficient, or "green," technologies is growing. Increasing traffic load is expected to double the network energy consumption within the next ten years [2]. In this paper, an interference mitigation technique that benefits both the spectral and energy efficiency of 4G networks is developed.

A typical ICIC solution is to reduce the frequency reuse among the cells, in order to reduce especially cell-edge interference [3]. However, this severely harms the trunking efficiency of the network. Further research suggests soft or softer frequency reuse [4, 5], where cell-edge frequency reuse is performed using power masks and frequency band alternation. An adaptive reuse scheme is proposed in [6] including a transmit power minimisation method. These solutions however, while maintaining full reuse in each cell, do not take into account local interference information, and hence cannot guarantee real-time interference protection. Furthermore, adaptive mechanisms such as in [6] are typically computationally complex and tend to generate large signalling overheads.

Cell-size reduction for better energy efficiency is investigated in [2], yielding an energy consumption decline as well as capacity boosts. Of course, reducing macro-cell sizes means increasing the number of BSs in a given area, which is generally undesirable due to increased expenses for the operator. In [7], the system power consumption is formulated as a minimisation problem, which however does not take cell-edge throughput or fairness into account. In this paper, power minimisation is used primarily for interference mitigation, rather than solely focusing on total system power.

This paper presents a novel interference-aware ICIC technique, which by exploiting existing network architecture provides protection for interference-prone users, whilst benefitting both the spectral and energy efficiency of the network. Furthermore, a scheduler is introduced to help achieve a fairer system. In the following, Section II presents the interference mitigation mechanism, and Section III the accompanying scheduler. Sections IV and V describe the simulation environment and results, respectively, and Section VI offers concluding remarks.

II. Uplink Interference Protection

Traditional Uplink (UL) power control methods use the estimated path gain on the intended link to perform MS transmit power adaptation [8]. A better option is to utilise the interfering link to reduce the transmit power on the affected RBs, such that interference caused at neighbouring BSs is diminished. This way, victim MSs in the cell of interest have a chance of maintaining a sufficient SINR, while the culprit links still remain active.

A. Uplink Interference Scenario

Fig. 1 portrays the interference scenario of two MSs in the UL. Here, the vulnerable MS_v served by BS_v and the interfering MS_i served by BS_i are transmitting on the same RB. Due to the uplink interference caused by MS_i at BS_v, the

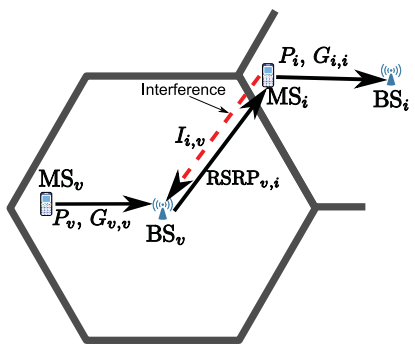

Fig. 1. UL interference scenario: Due to its cell-edge proximity, the culprit MS_i potentially causes excessive interference at the vulnerable BS_v, severely diminishing the victim MS_v's SINR.

978-1-61284-887-7/11/$26.00 ©2011 IEEE

SINR of MS_v may fall below the SINR target, γ_v^{tar}. To prevent such a situation, an interference protection technique is devised to reduce the transmit power P_i and mitigate the interference caused by MS_i such that MS_v achieves a satisfactory SINR.

B. Power Reduction Procedure

The goal is to find an effective method to scale the transmit power on an interfering RB. Here, the reference signals of the neighbouring cells received by a MS aid in estimating the interference it causes to the co-channel MSs in other cells (channel reciprocity is assumed). For notational simplicity, reference signal received power (RSRP), used in Long-Term Evolution (LTE) to rank different cells according to signal strength [9], will be used in this paper to describe the received reference signals. The RSRPs are used in the adaptation of interfering RB transmit power, which is performed as follows:

1) Assume MS_v has been allocated RB_m. Let γ_v^{tar} be the known, service-dependent target SINR of MS_v

$$\gamma_v^{\mathrm{tar}} = \frac{P_v G_{v,v}^m}{I_v^{m,\mathrm{tol}} + \eta}, \tag{1}$$

where P_v is the transmit power of MS_v, $G_{v,v}^m$ is the path gain between MS_v and BS_v on RB_m, η is the thermal noise, and $I_v^{m,\mathrm{tol}}$ is the tolerable interference such that γ_v^{tar} can be met on RB_m.

2) At MS_i, the RSRPs of the neighbouring cells are considered. As any reference signal is transmitted at a fixed power, the interfering MS_i can ascertain the average path gain on RB_m, $G_{i,v}^m$, to the affected BS_v, by assuming channel reciprocity for path loss and shadowing, and can hence estimate the interference it is causing. It then uses the $I_v^{m,\mathrm{tol}}$ from the vulnerable MS_v to calculate its maximum power

$$\tilde{P}_{\max,\,i} = \frac{I_v^{m,\mathrm{tol}}}{G_{i,v}^m}. \tag{2}$$

From (2), it is clear that $\tilde{P}_{\max,\,i}$ is directly proportional to the tolerable interference, $I_v^{m,\mathrm{tol}}$, at MS_v.

Given the above power adaptation scheme, the vulnerable RBs in each cell should achieve the required SINR target. However, it may happen that a number of the MSs reducing their power fall into outage. Lastly, it is clear that $I_v^{m,\mathrm{tol}}$ is not directly available at MS_i. For example, in LTE, this can be signalled from BS_v to BS_i over the X2 interface, and to MS_i via the Radio Resource Control protocol [9].

C. Priority Bands

In [10], soft frequency reuse, where RBs are arranged into priority bands, is employed to facilitate interference protection. In this work, three frequency bands, termed *high-priority*, *mid-priority*, and *low-priority*, are defined. These bands are allocated such that if a RB is assigned high-priority status in one cell, the same RB is assigned mid- and low-priority status in the neighbouring cells. In essence, no RB is assigned the same priority status in two neighbouring cells. When excessive interference is observed on an RB, it is the responsibility of the cell with low-priority on this RB to reduce the transmit power. This boosts the SINR of the high- and mid-priority RBs in the neighbouring cells. Fig. 2 shows this allocation, where it can be seen that the bands are assigned such that the priorities are mutually orthogonal to each other. This is the trademark feature borrowed from soft frequency reuse.

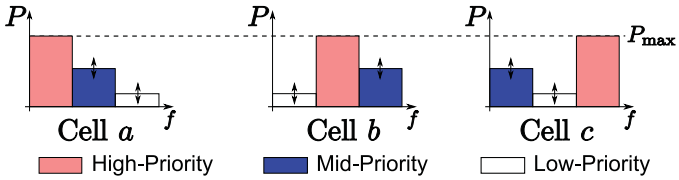

Fig. 2. Allocation of priority bands in neighbouring cells a, b, and c: The allocation of high-, mid-, and low-priority RBs is complementary in the cells.

III. Scheduling

In general, a random allocation of priority RBs can lead to undesired scenarios. For instance, the allocation of a high-priority RB to cell-centre MSs is wasteful, as such a MS-BS link is generally strong, and interference protection is unnecessary. The opposite holds true at the cell-edge if a MS is allocated a low-priority RB. In this case, the MS will most probably be unable to sustain its γ_v^{tar}, especially if ULIP is applied, and hence fall into outage. Therefore, an efficient scheduling procedure is essential for the effectiveness of ULIP.

A. SINR Scheduling

In a fair allocation scheme, cell-edge MSs should be allocated high-priority RBs to be able to transmit at full power and achieve maximum possible SINR. Cell-centre users, which are more likely to achieve their SINR target due to BS proximity, should be assigned low-priority RBs. In essence, the general rule is to allocate high-priority RBs to the MSs with the least favourable SINR conditions. Such an approach is less dependent on the actual MS position, allowing non-cell-edge users with strong interferers to also request high-priority RBs.

The scheduling procedure utilises the SINRs of the users from transmissions in previous time slots. As the UL is considered, this information is readily available at the BS. In (3), $\mathcal{R}_i$ denotes the set of average (*i.e.*, time average over the previous x time slots, where x is a system wide parameter) SINRs of the users in the cell

$$\mathcal{R}_i : \left\{\bar{\gamma}_{i,1}, \bar{\gamma}_{i,2}, \ldots, \bar{\gamma}_{i,N}\right\}, \tag{3}$$

where $\bar{\gamma}_{i,j}$ is the average SINR of MS_j in cell i, and N denotes the number of MSs in a cell. The MSs at the cell-edge are clearly those that, on average, achieve weaker signal strength, and consequently SINR, at the receiving BS. Thus, the next step is to sort the $\bar{\gamma}_{i,j}$ in ascending order, so that the MSs that have the weakest SINRs can be identified

$$\begin{aligned} \mathcal{R}_i^* = f\left(\mathcal{R}_i\right) &= \left\{\bar{\gamma}_{i,(1)}, \bar{\gamma}_{i,(2)}, \ldots, \bar{\gamma}_{i,(N)}\right\} \\ \text{s.t. } &\bar{\gamma}_{i,(1)} \leq \bar{\gamma}_{i,(2)} \leq \cdots \leq \bar{\gamma}_{i,(N)}, \end{aligned} \tag{4}$$

where $\mathcal{R}_i^*$ is the ordered set of SINR measurements, as denoted by the $(\cdot)$ in the indices. The function $f(\cdot)$ that defines this ordering can now be applied to the set of users in the cell of interest $\mathcal{S}_{\mathrm{users},v}$, $|\mathcal{S}_{\mathrm{users},v}| = N$, and the set of high-priority

MSs, $\mathcal{S}_{\mathrm{hp},v}$, can be found as

$$\mathcal{S}_{\mathrm{hp},v} = \left\{ s \in \mathcal{S}_{\mathrm{users},v} \mid f(s) \leq \left\lceil \frac{N}{l} \right\rceil \right\} \quad (5)$$
$$\text{where } \mathcal{S}_{\mathrm{hp},v} \subset \mathcal{S}_{\mathrm{users},v} \,,$$

where l denotes the number of priority bands (here, $l = 3$) such that $\lceil N/l \rceil$ denotes the number of high-priority MSs. In (5), the high-priority RBs are allocated to the $\lceil N/3 \rceil$ MSs with the weakest average SINRs, and hence to the cell-edge. The low-priority RBs are allocated to the cell-centre, thus to the $\lceil N/3 \rceil$ MSs with the strongest SINRs, and the mid-priority RBs to the remaining (middle set) MSs. One instance of the fair allocation for $N = 50$ users is depicted in Fig. 3. Here

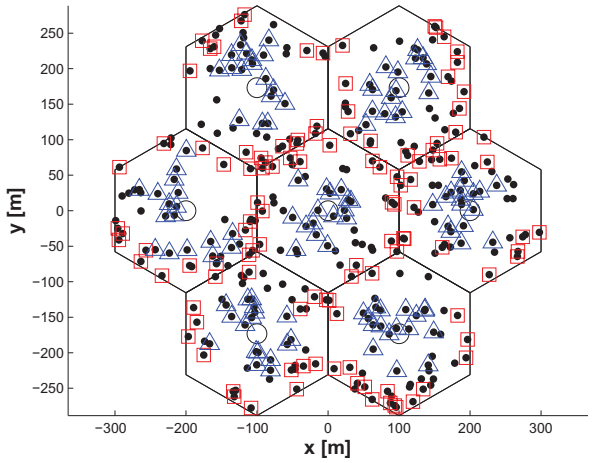

Fig. 3. Allocation of resources using the fair scheduler: Each MS is depicted with a dot. The MSs marked with squares have been assigned high-priority RBs, triangles represent low-priority RBs, and the (unmarked) rest are mid-priority. The system is dubbed "fair" as high-priority is assigned to the MSs with the least favourable SINR conditions.

it is clear to see that the cell-edge MSs have been allocated high-priority RBs, and in the cell-centre, where the MSs are shielded from neighbouring cell interference, the low-priority RBs are assigned.

When a new MS enters the cell, initial allocation is performed using the signal-to-noise ratio (SNR) (which can be approximated using the RSRP), as clearly no SINR information is available. In following time slots, however, the MS's SINR is used. Mean statistics are employed to eliminate fast fading effects and prevent MSs from rapidly changing priority class, so that the system can reach a stable operating point.

IV. Simulation

Monte Carlo simulations are used to provide cumulative distribution functions (CDFs) of the achieved capacities of the system with and without the use of ULIP.

A. System Setup

The simulation area is comprised of a single-tier, tessellated hexagonal cell distribution. Two additional tiers are simulated to eliminate border effects with regards to interference. Statistics are, however, only taken from the first tier (and centre cell). Each cell is served by a single omnidirectional BS.

In each cell the number of users per cell $N = 50$ are uniformly distributed. The assignment of MSs to each cell is exclusively based on path loss. In the centre cell, the l=3 priority bands are allocated randomly, with each band receiving $1/l$ of the available resources. In the neighbouring cells, the allocation of the priority classes is orthogonalised (see Fig. 2), such that a priority reuse scheme results. Furthermore, given that there are $M = 50$ RBs and $N = 50$ MSs for each BS, each MS in a cell is assigned a single RB.[1] The allocation of a RB to a MS is done using the scheduling technique introduced in Section III. Finally, each simulation is run over 20 time slots, to provide the scheduler with the necessary SINR information to perform the resource allocation.

B. Channel Model

In general, the channel gain, $G_{k,l}$, between a transmitter k and receiver l separated by d m is calculated as

$$G_{k,l} = |H_{k,l}|^2 \, 10^{\frac{-L(d)+X_\sigma}{10}} \,, \quad (6)$$

where $H_{k,l}$ describes the channel transfer function between transmitter k and receiver l, $L(d)$ is the distance-dependent path loss (in dB) and X_σ is the log-normal shadowing value (in dB) with standard deviation σ.

All MSs are assumed to lie outdoors, the associated distance dependent path loss of the link (desired or interfering) between a BS and an outdoor MS is calcuated as [11]

$$L(d) = 15.3 + 37.6 \log_{10}(d) \quad [\mathrm{dB}] \,. \quad (7)$$

where d is the distance between transmitter and receiver.

C. Power Allocation

Following the network and link setup, the UL transmit power of each MS is determined. According to ULIP, the power allocation varies between each priority class. On a high-priority RB, a MS always transmits with the maximum available power, as shown in Fig. 2. Using ULIP, MSs allocated RBs in the mid- and low-priority bands are generally required to scale their UL transmit power. MSs in the mid-priority band scale their power first, based on the $\min_v \left\{ I_v^{m,\mathrm{tol}} \right\}$ of the high-priority users (*i.e.*, for $v \in \mathcal{S}_{\mathrm{hp},v}$), and then calculate their own $I_v^{m,\mathrm{tol}}$s based on their new transmit powers. MSs in the low-priority band must then reduce their power, taking into account the $\min_v \left\{ I_v^{m,\mathrm{tol}} \right\}$ of both the high- and mid-priority users in the neighbouring cells. The power scaling is done using the procedure in (1)–(2), where the mid- and low-priority RB maximum transmit powers are set to $\tilde{P}_{\max}$ from (2):

$$\tilde{P}_{\max} = \frac{I_v^{\mathrm{tol}}}{G_{i,v}} \leq P_{\max} \,,$$

where $P_{\max}$ is the system-wide maximum UL transmit power.

[1] This is, of course, not a very practical scenario. However, this is chosen to isolate the effects of ULIP to a single power variation. With multiple RBs per MS, additional degrees of freedom are provided for ULIP to achieve γ^{tar} dependent on the channel characteristics.

D. Performance Statistics

After the transmit power adjustments in each cell, the performance statistics can be gathered. These are composed of mainly three values: the UL throughput, power efficiency, and fairness. First, the SINR, γ_u, of MS_u is calculated

$$\gamma_u = \frac{P_u G_{u,u}}{\sum_{k \neq u} P_k G_{k,u} + \eta}, \tag{8}$$

where P_u and P_k are the transmit powers of MS_u and interfering MSs, respectively, and η is the thermal noise.

Now, given the UL SINRs of all of the MSs in the scenario, the throughput, C_u, of MS_u using adaptive modulation and coding (AMC) is calculated

$$C_u(\gamma_u) = n_u^{\mathrm{RB}} k_{\mathrm{sc}} \varrho_{\mathrm{s}} \varepsilon_{\mathrm{s}}(\gamma_u) \ , \tag{9}$$

where n_u^{RB} is the number of RBs assigned to MS_u, k_{sc} the number of subcarriers per RB, ϱ_{s} the symbol rate per subcarrier, and $\varepsilon_{\mathrm{s}}(\gamma_u)$ the symbol efficiency given in Table I[2].

TABLE I
ADAPTIVE MODULATION AND CODING TABLE

CQI index	min. SINR [dB]	Modulation	Code rate	Efficiency ε_{s} [bits/sym]
0	-	None	-	0
1	-6	QPSK	0.076	0.1523
2	-5	QPSK	0.12	0.2344
3	-3	QPSK	0.19	0.3770
4	-1	QPSK	0.3	0.6016
5	1	QPSK	0.44	0.8770
6	3	QPSK	0.59	1.1758
7	5	16QAM	0.37	1.4766
8	8	16QAM	0.48	1.9141
9	9	16QAM	0.6	2.4063
10	11	64QAM	0.45	2.7305
11	12	64QAM	0.55	3.3223
12	14	64QAM	0.65	3.9023
13	16	64QAM	0.75	4.5234
14	18	64QAM	0.85	5.1152
15	20	64QAM	0.93	5.5547

The power efficiency β_u measures the data rate per unit of transmit power (or, alternatively, the data sent per unit of energy) of MS_u. This is defined as follows:

$$\beta_u = \frac{C_u}{P_u} = \frac{n_u^{\mathrm{RB}} k_{\mathrm{sc}} \varrho_{\mathrm{s}} \varepsilon_{\mathrm{s}}}{P_u} \quad \left[\frac{\mathrm{bits/s}}{\mathrm{W}}\right] \equiv \left[\frac{\mathrm{bits}}{\mathrm{J}}\right], \tag{10}$$

where P_u is the transmit power of MS_u, and C_u the throughput from (9).

Lastly, Jain's fairness index [13] is used to calculate the throughput fairness of the system in each time slot

$$\Gamma = \frac{\left[\sum_u C_u\right]^2}{\sum_u C_u^2} \ . \tag{11}$$

V. RESULTS

From the simulation, the CDFs of the achieved user throughputs are generated for systems employing ULIP and compared against a benchmark system in which all MSs transmit with power $P_{\max}$, keeping the RB allocation unchanged. General simulation parameters are shown in Table II.

TABLE II
SIMULATION PARAMETERS

Parameter	Value
MSs per macro-cell, N	50
Inter-site distance	200 m
Number of available RBs, M	50
RB bandwidth, B_{RB}	180 kHz
Subcarriers per RB, k_{sc}	12
Symbol rate per subcarrier, ϱ_{s}	15 ksps
Subframe duration, t_{sf}	1 ms
Thermal noise, η	-174 dBm/Hz
Total MS transmit power	23 dBm
SINR target, γ_v^{tar}	11 dB
Shadowing Std. Dev., σ	4 dB
Auto-correlation distance	50 m

In Fig. 4, the overall user performance in terms of throughput and fairness is displayed. As can be seen in Fig. 4(a), ULIP generates considerable gains for low-throughput (high- and mid- priority) users, while only sacrificing minimal high-end throughput. In fact, a substantial gain of over 105% is achieved at the 25th percentile, pointing towards a significant cell-edge capacity boost, whereas less than 10% is sacrificed at the 75th percentile by the low-priority cell-centre users.

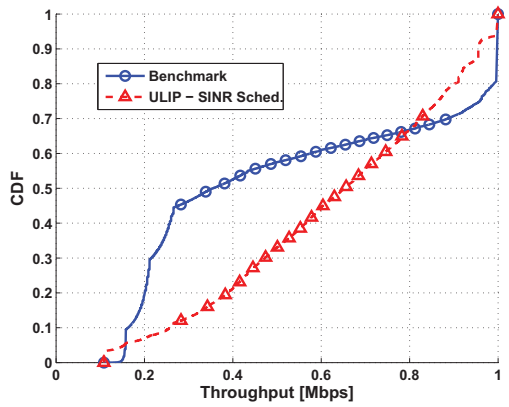

(a) Throughput

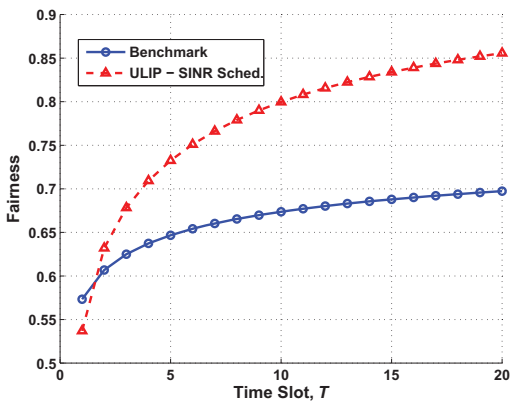

(b) Fairness

Fig. 4. Overall user performance in terms of throughput and fairness. The simulation is run over 20 time slots, where at time slot T the scheduler utilises MS SINR information from the previous $T-1$ slots. BM denotes benchmark.

[2]In Table I, the modulation and coding schemes are taken from LTE [9], and the SINR ranges from [12]. Here, the downlink values are used because no uplink implementation was found, as these values are operator specific.

In addition, the increased "steepness" (in the region of $0.3 - 0.9$ Mbps) of the ULIP user throughput CDF directly implies a higher fairness among the MSs in the system, which is highlighted in Fig. 4(b). Here, it is clear that ULIP boosts the fairness by almost 23% over the benchmark. This is a result of the displacement of SINR and, consequently, throughput from the cell-centre to the cell-edge enforced by the SINR scheduler, making the system fairer.

Due to the large throughput gains of high- and mid-priority users compared with the relatively small losses of the low-priority MSs (see Fig. 4(a)), a significant system throughput gain of over 21% at the 50th percentile can be observed in Fig 5(a). Furthermore, Fig 5(b) shows that the throughput

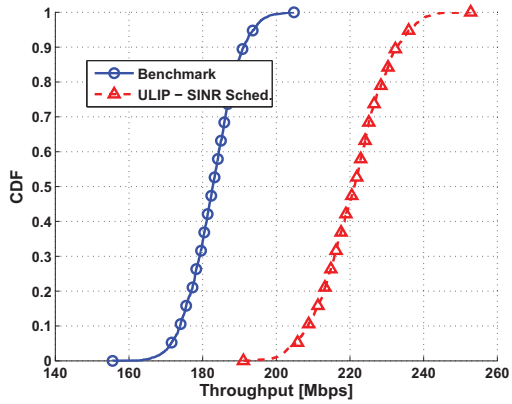

(a) Throughput

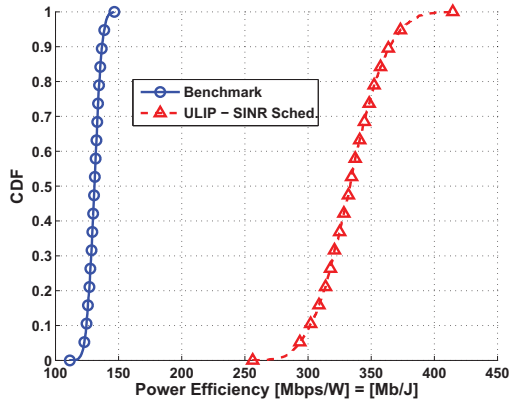

(b) Power Efficiency

Fig. 5. System performance in terms of throughput and power efficiency. System statistics are taken from the first tier (*i.e.*, inner 7 cells) of the network.

benefit combined with the reduced system power generates a remarkable system power efficiency gain of almost 155%. Therefore, not only does ULIP provide substantial throughput gains and a fairer system, it can also be considered as a green radio solution due to the large power efficiency improvement.

VI. Conclusion

ULIP presents a viable alternative to standard ICIC techniques in cellular networks. By dynamically scaling the transmit powers on a defined set of RBs, the throughputs of users suffering from poor SINRs can be greatly enhanced. Furthermore, by diminishing the transmit power, a more power efficient network results. And when combined with an appropriate scheduling scheme, ULIP not only provides throughput gains for high- and mid-priority users, but also a fairer system. Lastly, the use of RSRPs in the power reduction does not add signalling overhead in the system, although extra signalling of the interference margins $I_v^{m,\text{tol}}$ is necessary.

It was shown that ULIP, combined with the SINR scheduler, achieves not only a 23% fairness gain, but also a significant system throughput profit of 21%. Furthermore, a substantial low-percentile (*i.e.*, cell-edge) throughput improvement of over 100% is seen, at minimal cost to the high-percentile (*i.e.*, cell-centre) MSs. Finally, the large throughput gains, coupled with the power reduction, generate outstanding power efficiency boosts of over 150%, achieving a much greener system.

Given the promising results presented, future research should investigate the application of ULIP to more realistic scenarios, *i.e.*, with variable N and $n_u^{\text{RB}} \geq 1$. A further possibility is the exploitation of frequency-selective fading by the scheduler. This would provide an extra degree of freedom when allocating RBs to the MSs.

References

[1] P. Hosein, "On Uplink Interference Management for OFDMA Networks," in *Proc. of the 18th International Symposium on Personal, Indoor and Mobile Radio Communications (PIMRC)*, Athens, Greece, Sep. 2007.

[2] B. Badic, T. O'Farrrell, P. Loskot, and J. He, "Energy Efficient Radio Access Architectures for Green Radio: Large versus Small Cell Size Deployment," in *Proc. of the 70th Vehicular Technology Conference*, Anchorage, Sep. 2009.

[3] S.-E. Elayoubi, O. B. Haddada, and B. Fourestie, "Performance Evaluation of Frequency Planning Schemes in OFDMA-Based Networks," *IEEE Transactions on Wireless Communications*, vol. 7, pp. 1623–1633, May 2008.

[4] X. Mao, A. Maaref, and K. H. Teo, "Adaptive Soft Frequency Reuse for Inter-Cell Interference Coordination in SC-FDMA Based 3GPP LTE Uplinks," in *Proc. of the Global Telecommunications Conference*, New Orleans, Nov. 2008.

[5] X. Zhang, C. He, L. Jiang, and J. Xu, "Inter-Cell Interference Coordination Based on Softer Frequency Reuse in OFDMA Cellular Systems," in *Proc. of International Conference on Neural Networks and Signal Processing*, Zhenjiang, China, June 2008, pp. 270–275.

[6] T. Quek, Z. Lei, and S. Sun, "Adaptive interference coordination in multi-cell OFDMA systems," in *Proc. of Personal, Indoor and Mobile Radio Communications (PIMRC)*, Tokyo, Sep. 2009.

[7] A. He, S. Srikanteswara, K. K. Bae, T. R. Newman, J. H. Reed, W. H. Tranter, M. Sajadieh, and M. Verhelst, "System power consumption minimization for multichannel communications using cognitive radio," in *Proc. of Microwaves, Communications, Antennas and Electronics Systems COMCAS*, Tel Aviv, Nov. 2009.

[8] L. K. Tee, C. van Rensburg, and J.-A. Tsai, "Uplink Power Control for an OFDMA Mobile Cellular System," in *Proc. of the Vehicular Technology Conference*, Baltimore, MD, Sep./Oct. 2007.

[9] S. Sesia, I. Toufik, and M. Baker, *LTE - The UMTS Long Term Evolution: From Theory to Practice*, 1st ed., S. Sesia, I. Toufik, and M. Baker, Eds. Wiley, 2009.

[10] 3rd Generation Partnership Project (3GPP), Technical Specification Group Radio Access Network, *Soft Frequency Reuse Scheme for UTRAN LTE*, 3GPP TSG RAN WG1 R1-050507, 3GPP Std., May 9–13, 2005.

[11] 3GPP, "Simulation Assumptions and Parameters for FDD HeNB RF Requirements," 3GPP TSG RAN WG4 R4-092042, May 2008. Retrieved Sep. 1, 2009 from www.3gpp.org/ftp/Specs/.

[12] EDX Wireless, "Designing an LTE network using EDX SignalPro," Technical white paper, march 2010, retrieved Jan. 17 2011. [Online]. Available: http://www.edx.com/resources/documents/

[13] R. Jain, D. Chiu, and W. Hawe., "A Quantitative Measure of Fairness and Discrimination for Resource Allocation in Shared Computer Systems," DEC Technical Report, Tech. Rep. 301, 1984.

Burchardt et al. EURASIP Journal on Wireless Communications and Networking 2012, 2012:180
http://jwcn.eurasipjournals.com/content/2012/1/180

EURASIP Journal on Wireless Communications and Networking
a SpringerOpen Journal

RESEARCH Open Access

Uplink interference protection and scheduling for energy efficient OFDMA networks

Harald Burchardt[1*], Zubin Bharucha[2], Gunther Auer[2] and Harald Haas[1]

Abstract

One of the key challenges for future orthogonal frequency division multiple access-based networks is inter-cell interference coordination. With full frequency reuse and small inter-site distances, coping with co-channel interference (CCI) in such networks has become increasingly important. In this article, an uplink interference protection (ULIP) technique to combat CCI is introduced and investigated. The level of uplink interference originating from neighbouring cells (affecting co-channel mobile stations (MSs) in the cell of interest) can be effectively controlled by reducing the transmit power of the interfering MSs. This is done based on the target signal-to-noise-plus-interference ratio (SINR) and tolerable interference of the vulnerable link. Bands are prioritised in order to differentiate those (vulnerable/victim) MSs that are to be protected from interference and those (aggressor/interfering MSs) that are required to sacrifice transmission power to facilitate the protection. Furthermore, MSs are scheduled such that those users with poorer transmission conditions receive the highest interference protection, thus balancing the areal SINR distribution and creating a fairer allocation of the available resources. In addition to interference protection, the individual power reductions also serve to decrease the total system uplink power, resulting in a *greener* system. It is shown through analytic derivation that the introduction of ULIP guarantees an increase in energy efficiency for all MSs, with the added benefit that gains in overall system throughput are also achievable. Extensive system level simulations validate these findings.

Keywords: inter-cell interference coordination, uplink interference protection, OFDMA networks, fair scheduling

1. Introduction

In wireless networks, there is an increasing demand for higher user and system throughput, along with growing expectation for all mobile stations (MSs) in a cell to be capable of supporting data-heavy multimedia and Internet services. This is especially difficult to maintain at the cell-edge, where received signal and service clearly deteriorate. Furthermore, the necessity for more energy efficient, or "green," technologies is growing. With base stations (BSs) requiring up to 1.5 kW, a typical wide area network can consume tens of MW per annum [1]. In the uplink, while MSs do not consume nearly as much power, there are orders of magnitude more MSs then BSs in the network [2]. In addition with traffic loads increasing approximately ten times every 5 years, a doubling of the energy consumption results over the same time period. Clearly, such an increase raises serious environmental concerns. Consequently, smaller cell sizes, femto-cell deployment, relays [3,4] and especially inter-cell interference coordination (ICIC) techniques are envisioned for future wireless networks to improve user throughputs and network energy efficiency, while sacrificing minimal system capacity.

For future wireless networks, such a reduction in cell size is undertaken due to transmit power limitations and constraints on the link budget [5]. The demand for higher data rates coupled with full frequency reuse results in an interference-limited system, which cannot achieve full capacity without the implementation of one or more viable interference mitigation/cancellation/coordination techniques [5]. Furthermore, through the implementation of orthogonal frequency division multiple access (OFDMA) in the downlink and single carrier frequency division multiple access (SC-FDMA) in the uplink as multiple access schemes, future systems will provide orthogonality between resource blocks (RBs) in both directions, and hence also between all users within

* Correspondence: h.burchardt@ed.ac.uk
[1]Institute for Digital Communications, School of Engineering and Electronics, The University of Edinburgh, EH9 3JL, Edinburgh, UK
Full list of author information is available at the end of the article

a cell [2]. Thus, system performance is mainly limited by interference originating from users in neighbouring cells, which can be detrimental to the signal-to-noise-plus-interference ratio (SINR) and throughput performance of MSs using the same RBs [6]. A typical solution is to force interferers to leave those RBs idle. However, this severely harms the trunking efficiency of the network [7]. Hence, suppressing transmission is clearly suboptimal, and thus interference coordination techniques are necessary to achieve desired sum and individual throughputs.

For OFDMA systems, some traditional ICIC techniques, such as power control, interference cancellation, fractional frequency reuse, multiple-input multiple-output transmission and space division multiple access [2], have been proposed. Some of these strategies, however, require knowledge about the position of a MS relative to it's own and neighbouring BSs [2], which clearly increases the signalling burden in the network. In [8], other specific ICIC techniques are suggested, such as slow power control, frequency division multiplexing resource allocation, and coordination by MS alignment, though management of interference from other cells is not considered. Further research in [9] presents a distributed uplink power allocation technique based on a maximum sum rate optimisation, yielding superior results in terms of average system throughput, however ignoring the tradeoff between cell-edge performance and overall spectral efficiency. In [10], a softer frequency reuse scheme is introduced, where cell-edge power masks are used to mitigate inter-cell interference. These fixed masks cannot, however, adapt to the service-dependent requirements of the neighbouring cells, potentially wasting bandwidth. In [11], the downlink scheduling is formulated as an optimisation problem, and a decomposition of the problem is performed. Here, however, co-channel interference (CCI) (in future systems from neighbouring cells) is not taken into account, and hence the scheduling becomes suboptimal for multiple access channels and large networks.

In [12], a dynamic channel acquisition algorithm based on convex optimisation for the wireless downlink is considered, which provides optimal power and throughput performance for i.i.d. channels. This optimality suffers however for general ergodic channels, and hence is not suitable for mobile environments. In [13], the authors propose a low-complexity algorithm with fairness consideration to optimise the sum rate under individual rate and power constraints. Here though, because the water-filling solution is used for rate-optimal power allocation, a fair power distribution is neglected. In [14], an optimisation-based heuristic inter-cell coordination scheme is proposed to regulate the uplink transmission in neighbouring cells such that inter-cell interference is mitigated. As the scheme operates iteratively on a two-cell basis, however, it is clearly unsuitable for multi-cellular resource allocation. Finally, in [15], an energy-aware cross-layer radio management framework is proposed, that partitions the global optimisation problem into subproblems, which can be solved locally. While achieving substantial gains, the focus of the work is on multimode communication (i.e., cellular, WLANs, WMANs, etc.), and so an optimisation for pure cellular communication is not offered. In general, it is evident that the challenge of resource and power allocation has been thoroughly investigated as an optimisation problem, however in most cases these problems are non-convex, very hard to solve, and hence suboptimal heuristics are developed. In this work, a resource and power allocation technique based on local interference requirements will be developed to manage this challenge.

Much of the previous work on energy efficient systems concentrates on network optimisation and scheduling policies. Macro-cell size reduction for better energy efficiency is investigated in [16], with positive results. Of course, reducing the cell-sizes means increasing the number of BSs in an area, which is generally rejected due to the enhanced infrastructure expenses. In [17], game-theoretic approaches are utilised to, minimise the cost per reliable bit sent in energy constrained networks. However, it is seen that there is a clear tradeoff between energy and spectral efficiency, and hence the energy-efficient resource allocations tend to be spectrally inefficient. This is further highlighted in [18], where an analytical model determines the optimal energy-spectral efficiency tradeoff for the downlink in OFDMA networks. In this article, however, we present an ICIC technique which utilises interfering link gains to not only provide interference mitigation and spectral efficiency gains in the uplink, but also generate large energy savings.

An *energy efficient interference protection technique* for the uplink of OFDMA-based systems is introduced. By reducing the power on the interfering link, the SINRs of individual RBs can be enhanced. This power reduction also results in a more energy efficient system. By segregating the spectrum into priority bands, MSs allocated lower priority RBs provide interference protection for higher priority RBs in neighbouring cells by decreasing their transmit power. The priority bands (i.e., low to high) are allocated such that the same RBs in any neighbouring cells do not share the same priority class, and hence a priority reuse scheme [19] is established. Furthermore, the proposed power reduction is based on target SINRs, providing real-time service-dependent interference coordination and energy efficiency in the uplink.

The rest of the article is structured as follows: Section 2 describes the system and channel environment, Section 3 explains the uplink interference protection (ULIP) protocol and its performance in wireless networks is analysed

in Section 4. In Sections 5 and 6 the resource scheduler and simulation are described, respectively. Finally, Section 7 portrays and discusses the simulation results, and some concluding remarks are offered in Section 8.

2. System and channel model B/M

The reverse link of an OFDMA system is considered, where the system bandwidth B is divided into M RBs. A RB defines one basic time-frequency unit of bandwidth $B_{\mathrm{RB}} = B/M$. All MSs can transmit up to a maximum power $P_{\max}$, and hence up to $P_{\max}/M$ on each RB. Perfect time and frequency synchronisation is assumed.

Universal frequency reuse is considered, so that each macro-cell utilises the entire system bandwidth B. The set of RBs $\mathcal{M}$, where $|\mathcal{M}| = M$, is distributed by each BS to its associated MSs. Throughout this article, u is used to define any MS, and v_u the BS with which this MS is associated. The received signal observed by BS_{v_u} from MS_u on RB_m is given by

$$Y_u^m = \underbrace{P_u^m G_{u,u_u}^m}_{S_u^m} + I_u^m + \eta, \tag{1}$$

where G_{u,v_u}^m denotes the channel gain between the MS_u and its serving BS_{v_u}, observed on RB_m. Furthermore, P_u^m denotes the transmit power of MS_u on RB_m, S_u^m the desired received signal, η the thermal noise, and I_u^m the CCI received on RB_m from MSs in neighbouring cells. The interference I_u^m is defined by

$$I_u^m = \sum_{i \in \mathcal{I}_m} P_i^m G_{i,v_u}^m, \tag{2}$$

where $\mathcal{I}_m$ represents the set of interferers (i.e., the set of MSs in neighbouring cells that are also assigned RB_m). Hence, the SINR observed at the BS_{v_u} on RB_m is calculated by

$$\gamma_u^m = \frac{S_u^m}{I_u^m + \eta} = \frac{P_u^m G_{u,v_u}^m}{\sum_{i \in \mathcal{I}_m} P_i^m G_{i,v_u}^m + \eta}. \tag{3}$$

The achievable throughput on the link between MS_u and BS_{v_u} on RB_m using adaptive modulation and coding (AMC) is given by

$$C_u^m(\gamma_u^m) = k_{\mathrm{sc}} \varrho_{\mathrm{s}} \varepsilon_{\mathrm{s}}(\gamma_u^m) \quad \left[\frac{\mathrm{bits/s}}{\mathrm{RB}}\right], \tag{4}$$

where k_{sc} is the number of subcarriers per RB, ϱ_{s} the symbol rate per subcarrier, and $\varepsilon_{\mathrm{s}}(\gamma_u^m)$ the symbol efficiency given in Table 1.[a]

Table 1 Adaptive modulation and coding table

CQI index	min. SINR [dB]	Modulation	Code rate	Efficiency ε_s [bits/sym]
0	-	None	-	0
1	-6	QPSK	0.076	0.1523
2	-5	QPSK	0.12	0.2344
3	-3	QPSK	0.19	0.3770
4	-1	QPSK	0.3	0.6016
5	1	QPSK	0.44	0.8770
6	3	QPSK	0.59	1.1758
7	5	16QAM	0.37	1.4766
8	8	16QAM	0.48	1.9141
9	9	16QAM	0.6	2.4063
10	11	64QAM	0.45	2.7305
11	12	64QAM	0.55	3.3223
12	14	64QAM	0.65	3.9023
13	16	64QAM	0.75	4.5234
14	18	64QAM	0.85	5.1152
15	20	64QAM	0.93	5.5547

Further, C_u denotes the achievable throughput of MS_u, and is calculated by the aggregate throughput achieved on the RBs assigned to MS_u

$$C_u = \sum_{m \in \mathcal{M}_u} C_u^m = \sum_{m \in \mathcal{M}_u} k_{\mathrm{sc}} \varrho_{\mathrm{s}} \varepsilon_{\mathrm{s}}^m \quad \left[\frac{\mathrm{bits}}{\mathrm{s}}\right], \tag{5}$$

where $\mathcal{M}_u$ describes the set of RBs assigned to MS_u in the current transmission, and $\varepsilon_{\mathrm{s}}^m = \varepsilon_{\mathrm{s}}(\gamma_u^m)$. Finally, the system capacity is calculated as the sum of achievable throughput of all MSs

$$C_{\mathrm{sys}} = \sum_u C_u. \tag{6}$$

The energy efficiency β_u measures the data sent per unit of energy (or, alternatively, data rate per unit of transmit power) of MS_u. This is defined as follows:

$$\beta_u = \frac{C_u}{P_u} = \frac{\sum_{m \in \mathcal{M}_u} k_{\mathrm{sc}} \varrho_{\mathrm{s}} \varepsilon_{\mathrm{s}}^m}{\sum_{m \in \mathcal{M}_u} P_u^m} \left[\frac{\mathrm{bits/s}}{\mathrm{W}}\right] \equiv \left[\frac{\mathrm{bits}}{\mathrm{J}}\right], \tag{7}$$

where P_u is the total transmit power of MS_u, and C_u the throughput from (5).

Lastly, Jain's fairness index [20] is used to calculate the throughput fairness of the system in each time slot (i.e., Long-Term Evolution (LTE) subframe)

$$\Gamma(k) = \frac{\left[\sum_u C_u(k)\right]^2}{N_{\mathrm{sys}} \sum_u C_u(k)^2}. \tag{8}$$

where k indicates the time slot, N_{sys} the number of MS in the system, and $C_u(k)$ the achieved throughput of MS_u over all time slots 1: k.

2.1. Channel model

In general, the channel gain, $G_{k,l}^{m}$, between a transmitter k and receiver l, observed on RB_m and separated by d m is determined by the path loss, log-normal shadowing, and channel variations caused by frequency-selective fading:

$$G_{k,l}^{m} = |H_{k,l}^{m}|^2 10^{\frac{-L(d)+X\sigma}{10}}, \tag{9}$$

where $H_{k,l}^{m}$ describes the channel transfer function between transmitter k and receiver l on RB_m, $L(d)$ is the distance-dependent path loss (in dB) and X_σ is the log-normal shadowing value (in dB) with standard deviation σ, as described in [21]. The channel generally exhibits time and frequency dispersions, however channel fluctuations within a RB are not considered as the RB dimensions are significantly smaller than the coherence time and frequency of the channel [22]. Furthermore, the large-scale path loss $L(d)$ is identical on all RBs assigned to a MS. Finally, the delay profiles used to generate the frequency-selective fading channel transfer factor $H_{k,l}^{m}$ are taken from applicable propagation scenarios in [21,23].

The path loss model used to calculate $L(d)$ is for a purely outdoor link [24], i.e., the link (desired or interfering) between a BS and an outdoor MS, and calculates the path loss as

$$L(d) = 15.3 + 37.6 \log_{10}(d) \quad [\mathrm{dB}]. \tag{10}$$

where d is the distance between transmitter and receiver.

Log-normal shadowing is added to all links through the use of correlated shadowing maps. These are generated such that the correlation between two points is distance-dependent.

3. Uplink interference protection (ULIP)

Traditional uplink power control methods use the estimated path gain on the intended link to perform MS transmit power adaptation [25,26]. A better option is to utilise the interfering link, i.e., to a neighbouring BS, to reduce the transmit power on the affected RBs, such that interference caused to neighbouring BSs is lessened. This way, vulnerable MSs in the cell of interest have a chance of maintaining sufficient SINR, while the offending links remain active.

3.1. Uplink interference scenario

Figure 1 portrays the interference scenario of two MSs in the uplink.

Here, the vulnerable MS_v served by BS_{v_v} and the interfering MS_i served by BS_{v_i} are transmitting on the same RB. Due to the uplink interference at BS_{v_v} caused by MS_i, the SINR of MS_v may fall below the SINR target, γ_v^{tar}. To prevent such a situation, an interference protection technique is devised that reduces the transmit power P_i such that MS_v achieves a satisfactory SINR, $\gamma_v \geq \gamma_v^{\mathrm{tar}}$.

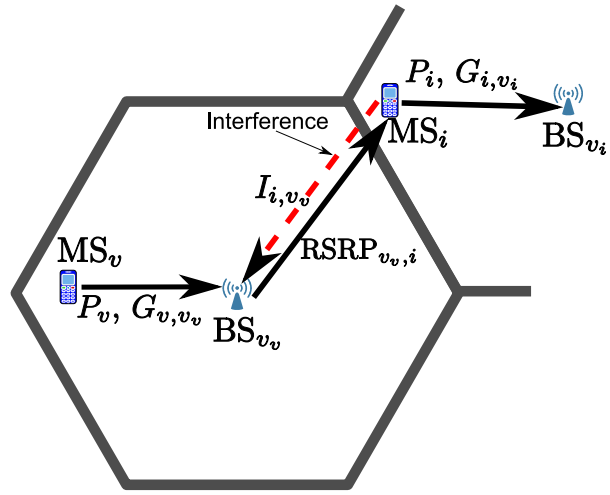

Figure 1 Uplink interference scenario.

3.2. Interference aware power reduction

The goal is to find an effective method to scale the transmit power on the interfering RBs. Here, the downlink reference signal of the neighbouring cells aid the MS in estimating the interference it causes to the neighbouring cells, assuming *channel reciprocity*. The channel can be considered reciprocal in terms of path loss and shadowing, however fast fading reciprocity is not assumed as this is not always the case, especially in frequency division duplex (FDD) systems. For LTE, the reference signal received power (RSRP) in particular is used. The RSRP provides a cell-specific signal strength metric. It is used mainly to rank different cells according to signal strength and to perform handover and cell reselection decisions [27]. The reference signals facilitate the adaptation of the interfering RB transmit power, which is performed as follows:

(1) Assume MS_v has been allocated the vulnerable RB_m. Let γ_v^{tar} be the known, service-dependent target SINR of MS_v, calculated as

$$\gamma_v^{\mathrm{tar}} = \frac{P_v^m G_{v,v_v}^m}{I_v^{m,\mathrm{tol}} + N}, \tag{11}$$

where P_v^m is the transmit power on RB_m, G_{v,v_v}^m is the path gain between MS_v and its BS_{v_v}, and $I_v^{m,\mathrm{tol}}$ is the tolerable interference such that γ_v^{tar} can be met on RB_m.

(2) Considering RSRPs of the neighbouring cells; as any reference signal is transmitted at a fixed power, an interfering MS_i can calculate the path gain on RB_m,

, to the affected BS_{v_v}, and assuming channel reciprocity, estimate the interference it is causing. It then uses the $I_v^{m,\mathrm{tol}}$ from the vulnerable MS to calculate the maximum power, $\tilde{P}_{\max,i}$, for MS_i as

$$\tilde{P}_{\max,i} = \frac{I_v^{m,\mathrm{tol}}}{G_{v_v,i}^m}. \tag{12}$$

It is clear that $\tilde{P}_{\max,i}$ is directly proportional to the tolerable interference, $I_v^{m,\mathrm{tol}}$ at MS_v.

Given the power adaptation scheme and assuming channel reciprocity, MS_v should achieve the required SINR target on RB_m. However, in a FDD system where fast fading is not reciprocal, an interference margin must be applied. Lastly, since $I_v^{m,\mathrm{tol}}$ is not directly available at MS_i, this needs to be signalled from BS_{v_v} to MS_i via existing backhaul infrastructures.

3.3. Priority bands

In [19], soft frequency reuse, where RBs are arranged into priority bands, is envisioned for LTE systems to facilitate interference protection. In this work, the available spectrum is split into different priority classes.[b] RBs assigned high-priority status are allocated to those MSs that require interference protection, and hence do not need to scale their transmit power. Looking from the other perspective, strongly interfering MSs are allocated RBs with a low-priority status, such that the transmit powers on these RBs may be reduced to provide interference protection. A *priority class reuse* scheme is established which, due to the power reduction, is an adaptive form of softer frequency reuse [10].

Three bands of communication, termed *high-priority*, *mid-priority*, and *low-priority*, are defined. These bands are allocated orthogonally, such that if a RB is assigned high-priority status in one cell, the same RB is assigned mid-priority and low-priority status in the neighbouring cells. In this sense, a priority class reuse factor of three results, which is shown in Figures 2 and 3.

When excessive interference is caused, the owners of mid- and low-priority RBs in the neighbouring cells must reduce their transmit power. This boosts the SINR on both the high-and mid-priority RBs. The power reduction procedure for ULIP is performed as follows:

(1) The $I_v^{m,\mathrm{tol}}$ for the high-priority RBs are calculated from (11), and distributed to the neighbouring cells.

(2) The transmit powers on mid-priority RBs are adjusted according to (12) based on the $\min_{v\in\mathcal{I}_m}\{I_v^{m,\mathrm{tol}}\}$ received from high-priority RBs in neighbouring cells.

(3) The $I_v^{m,\mathrm{tol}}$ for the mid-priority RBs (after power scaling has been performed) are calculated from (11) and distributed.

(4) The transmit powers on low-priority RBs are adjusted based on $\min_{v\in\mathcal{I}_m}\{I_v^{m,\mathrm{tol}}\}$ received from both neighbouring high- and mid-priority RBs.

It is clear that $I_v^{m,\mathrm{tol}}$ can be re-calculated in every time slot. However, to reduce the signaling burden on the network, these updates are only distributed when a sufficient difference, δ, to the last sent $I_v^{m,\mathrm{tol}}$ has been observed.

Furthermore, all high-priority RBs receive interference protection, and consequently gains in achievable throughput. This is facilitated by the MSs assigned low- and mid-priority RBs, which have reduced their transmit power. MSs allocated mid-priority RBs may also receive a throughput boost, as the MSs assigned low-priority RBs also take the mid-priority $I_v^{m,\mathrm{tol}}$ into account. MSs allocated low-priority RBs however, exclusively sacrifice transmit power and, consequently, throughput. The allocation of users to these priority bands (i.e., the assignment of x-priority RBs to MSs) is discussed in Section 5.

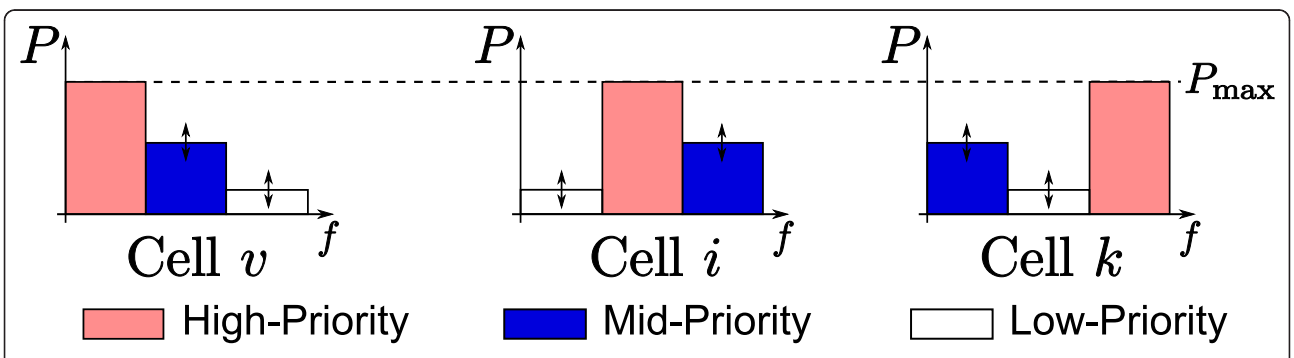

Figure 2 Allocation of priority bands in neighbouring cells *v*, *i*, and *j*. The allocation of high-, mid- and low-priority RBs are complementary in the cells.

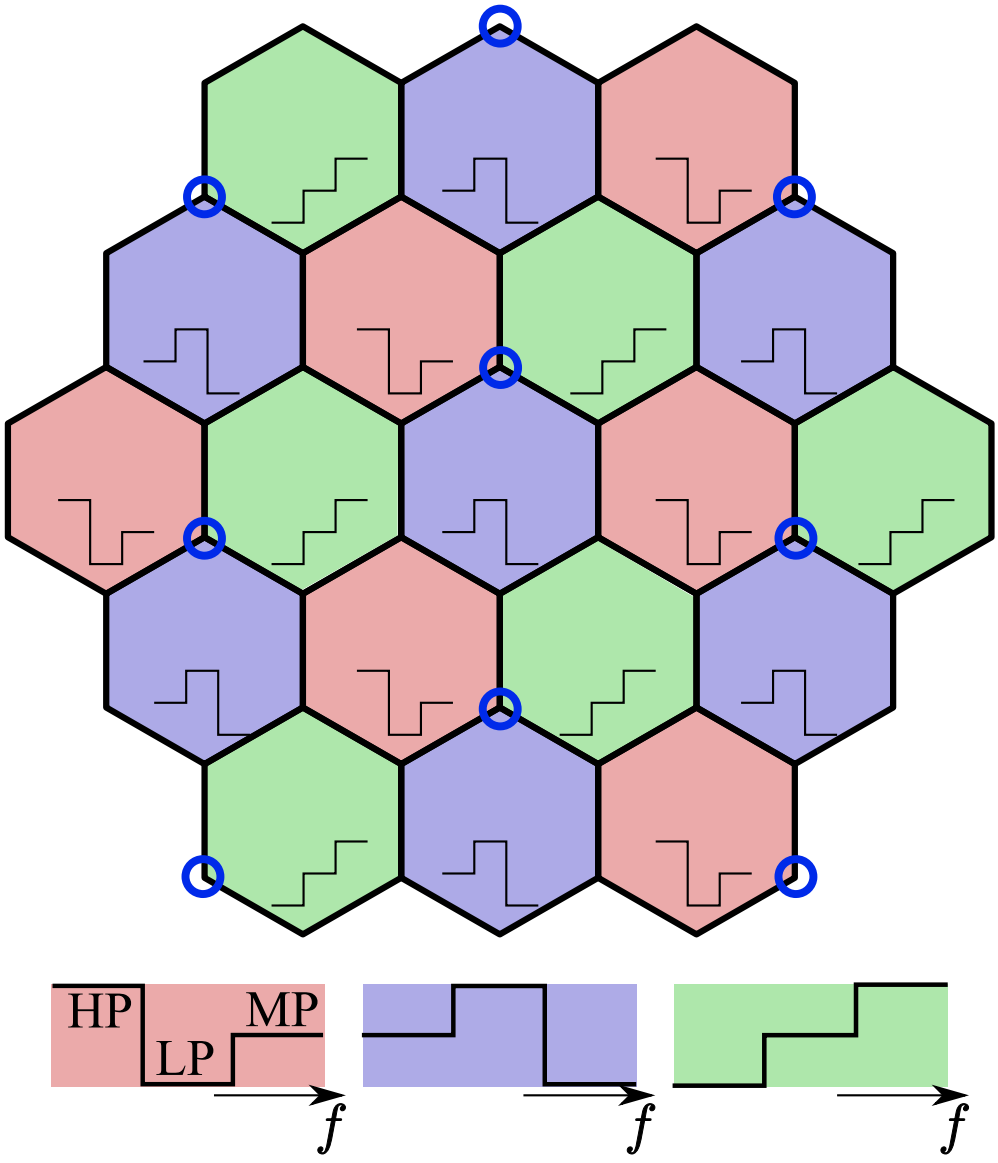

Figure 3 Allocation of priority bands in a multi-cellular network. The allocation of high-, mid- and low-priority RBs are complementary in the cells. A priority-class reuse scheme is arises. The colour bar indicates which part of the spectrum is given high-priority in which cells.

3.4. Practical implementation in LTE systems: an example

In order to implement the ULIP procedure, the interfering (i.e., low-priority) MS needs to be informed of the $I_v^{m,\mathrm{tol}}$ of its high-priority counterpart (in the neighbouring cell), to be able to then adjust its transmit power according to (12). This involves integrating the proposed ULIP technique within the network architecture. In abstract, the following procedure can be used to incorporate ULIP in the LTE network architecture:

(1) The vulnerable BS_{v_v} calculates the $I_v^{m,\mathrm{tol}}$ for all (allocated) high-priority RBs in the cell using the received uplink desired signal strength S_v^m.

(2) The $I_v^{m,\mathrm{tol}}$ are sent to all neighbouring BSs over the X2 or (if no X2 connection is available) S1 interfaces (see Figure 4 for LTE architecture).

(3) The neighbouring BS identifies and stores the minimum $I_v^{m,\mathrm{tol}}$ received on each particular RB_m, including the cell-ID from which it came.

(4) The neighbouring BS prepares a Data Radio Bearer (DRB) containing the $\min_{v_v}\left\{I_v^{m,\mathrm{tol}}\right\}$ found and the cell-ID v_v for each of the low-priority RBs.

(5) The DRBs are sent with the Radio Resource Control (RRC) protocol via the Physical Downlink Shared

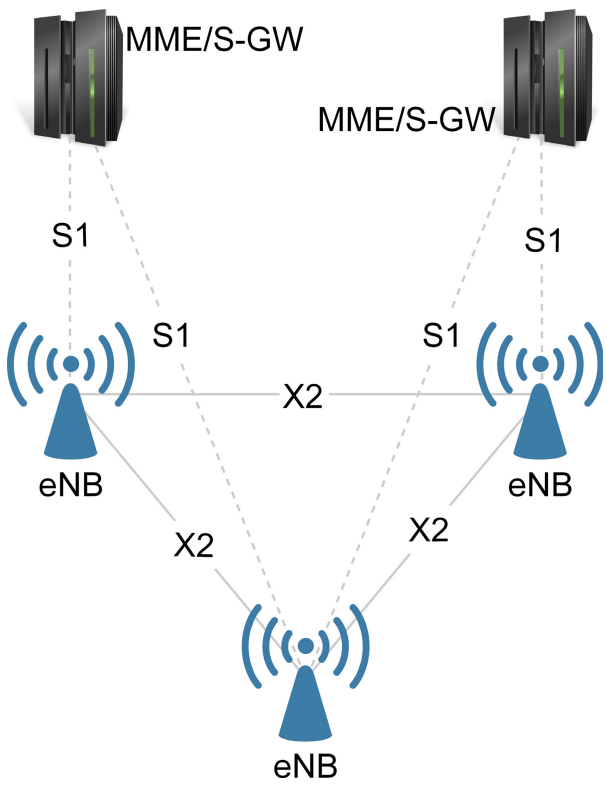

Figure 4 Overall LTE architecture showing interconnection of BSs through S1 and X2 interfaces.

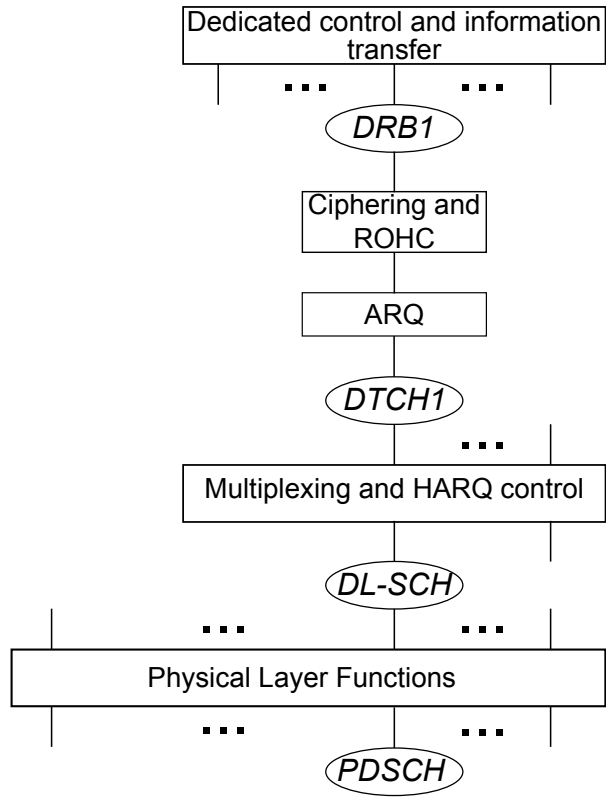

Figure 5 Generation and transport of DRB over PDSCH in RRC protocol.

Channel (PDSCH) to each of the MSs allocated the low-priority RBs (see Figure 5 for protocol).

(6) MS_i (allocated low-priority RB) estimates $G^m_{v_v,i}$ from BS v_v with $\min_{v_v}\{I^{m,\mathrm{tol}}_v\}$ indicated in DRB, using RSRP measurements.

(7) MS_i calculates $\tilde{P}_{\max,i}$ according to (12), and adjusts transmit power to provide interference protection in neighbouring cells.

The BS needs to inform the interfering MS_i of the interference margin $I^{m,\mathrm{tol}}_v$ of MS_v on high-priority RB_m as calculated from (11). Thus, the transport of this information from BSs to the corresponding MSs must be defined using the LTE network architecture depicted in Figure 4.

The S1 interface connects the Serving Gateway (S-GW)/Mobility Management Entity (MME) with groups of neighbouring BSs. The MME processes the signalling between an MS and the core network (CN). Neighbouring BSs (i.e., within the groups connected by the S1 interface) are interconnected via the X2 interface, which carries control information regarding handover and interference coordination. The X2 interface is therefore highly suitable for ULIP related signalling.

In LTE, the RRC protocol is used to transfer *common* (i.e., applicable to all MSs) and *dedicated* (i.e., applicable to only a specific MS) non-access stratum (NAS) information [27]. The RRC protocol covers a number of functional areas, including the broadcasting of system information, RRC connection control, network controlled mobility procedures, and measurement configuration and reporting. The RRC connection control handles all procedures related to the establishment, modification and termination of an RRC connection, including, among others, the formation of DRBs, radio bearers carrying user data [27].

In Figure 5, the construction, translation, and transmission of such a DRB is shown. Here, the DRB is multiplexed with other Signalling Radio Bearers (SRBs) and DRBs to then be transmitted to MS_i. Furthermore, the Downlink Shared Channel (DL-SCH) and, consequently, the PDSCH are used for transmission of $\min_{v_v}\{I^{m,\mathrm{tol}}_v\}$ and the cell-ID, meaning that no extra signalling on the control channels is required. Of course, the transmission of these DRBs in every subframe would be highly signalling-intensive, and hence is to be avoided. While the serving BS will continuously update the $I^{m,\mathrm{tol}}_v$ for all

high-priority RBs, it only transmits these updates to the neighbouring BSs when a significant change, δ, in $I_v^{m,\text{tol}}$ in comparison to the last transmission (e.g., due to high mobility, call dropping, etc.) is achieved. This reduces the information transfer from the BSs to the MSs, and consequently lessens calculational intensity at the MSs.

Finally, knowledge of the cell-ID allows MS_i to read the cell-specific reference signals of the neighbouring BS providing $\min_{v_v}\{I_v^{m,\text{tol}}\}$, which is necessary to carry out the RSRP measurements and estimate the channel gain between the MS and the vulnerable BS, $G_{v_v,i}^m$. This, of course, is needed by the MS_i to perform its power adaptation according to (12). The RSRP for a specific cell is defined as the linear average over the power contributions of the resource elements, within the considered measurement frequency bandwidth, which carry the cell-specific reference signals [28]. Using these measurements, the power reduction procedure can take place.

4. Performance analysis

Given the detailed description of the ULIP technique, the expected performance of a system employing this mechanism can be explored. There are multiple analysis techniques that deal with such problems, more specifically with system capacity analysis. In [29-31], a reverse link capacity analysis assuming non-cooperative BSs (similar to the design of practical cellular systems) is unfortunately shown to be a long-standing open problem in information theory, but has been solved when treating the interference as Gaussian noise [32]. Clearly, since in ULIP the interference incident on each RB is dependent on the interference tolerances of other-cell high-priority MSs allocated that RB, the interference is most certainly not Gaussian. Hence, such an analysis is infeasible for a system employing ULIP. In [29,33], the area spectral efficiency is introduced as a capacity measure that utilises stochastic geometry (statistical analysis of the positions and gains of MSs in the system) to estimate the expected capacity of a cellular network. Because in ULIP the users in a cell are split into three interdependent groups, such an analysis would be difficult as it is not always clear (by position) which MSs are assigned high-, mid-, or low-priority. Furthermore, in [33] the interference is estimated stochastically, and since in ULIP the interference is dependent on individual MS requirements, this analysis would be misguided.

On the other hand, optimisation techniques [11,34] can be utilised to provide global solutions that optimise an overall performance goal (e.g., energy/spectral efficiency). Furthermore, these offer an overall characterisation of the wireless system. In ULIP, however, the aim is not to maximise/minimise any objective, but rather to provide individual MSs with the necessary interference mitigation such that these can achieve their SINR/rate requirements. This is clearly not a system-wide goal, and hence such a description of a ULIP system is not applicable.

In general, the main difficulty that is not overcome (in the aforementioned methods) is the multitude of interdependencies on each RB over the network. The transmit powers on an RB are dependent on the signal qualities of the users allocated this RB in other cells in the network. Furthermore, these interdependencies are constantly adapting depending on the SINRs of the individual MSs in each cell. Hence, the stochastic interference modelling used in capacity analysis techniques cannot be utilised to model cellular ULIP. Therefore, a theoretical comparison to the state-of-the-art is performed to highlight the potential benefits of ULIP for OFDMA networks. And while transmit power control is standard for the reverse link in future systems, it has been shown that maximum power transmission is capacity-achieving [29], and thus this is compared to ULIP here. Analytical derivations for the energy efficiency and system capacity performance of ULIP are presented.

4.1. Energy efficiency in ULIP

In a system that employs ULIP, the transmit powers of low-priority MSs (MSs allocated low-priority RBs) are reduced so that interference to other cells is mitigated. Clearly, the throughput of the low-priority MSs is diminished relative to the reduction in transmit power. However, given a measure for energy efficiency, it can be shown that ULIP guarantees energy efficiency gains.

Given the metric for energy efficiency defined in (7):

$$\beta_u = \frac{C_u}{P_u} = \frac{B_u \log_2(1+\gamma_v)}{P_u} \quad \left[\frac{\text{bits}}{\text{J}}\right],$$

it will be shown that the energy efficiency of MS_u after ULIP is applied is always greater than in the benchmark, where all MSs transmit at maximum power. Here, the Shannon capacity is used for ease of derivability and without loss of generality; and the calculation is performed independent of RBs, also with no loss of generality. Essentially, it will be shown that

$$\beta_u^{\text{ULIP}} \geq \beta_u^{\text{BM}} \quad \text{or} \quad \frac{\beta_u^{\text{ULIP}}}{\beta_u^{\text{BM}}} \geq 1. \tag{13}$$

4.1.1. Derivation

The proof proceeds as follows

$$\frac{\beta_u^{\text{ULIP}}}{\beta_u^{\text{BM}}} = \frac{B_u \log_2\left(1+\frac{P_u^{\text{ULIP}} G}{I+N}\right) P_u^{\text{BM}}}{B_u \log_2\left(1+\frac{P_u^{\text{BM}} G}{I+N}\right) P_u^{\text{ULIP}}}, \tag{14}$$

where P_u^{BM} is the benchmark transmit power, and P_u^{ULIP} the power when ULIP is applied

$$P_u^{\mathrm{ULIP}} = \alpha P_u^{\mathrm{BM}}, \quad 0 \leq \alpha \leq 1.$$

This is substituted into (14) to obtain (15)

$$\begin{aligned} \frac{\beta_u^{\mathrm{ULIP}}}{\beta_u^{\mathrm{BM}}} &= \frac{\log_2\left(1 + \frac{\alpha P_u^{\mathrm{BM}} G}{I+N}\right) P_u^{\mathrm{BM}}}{\log_2\left(1 + \frac{P_u^{\mathrm{BM}} G}{I+N}\right) \alpha P_u^{\mathrm{BM}}}, \\ &= \frac{\log_2(1+\alpha c)}{\alpha \log_2(1+c)}, \quad \text{where } c = \frac{P_u^{\mathrm{BM}} G}{I+N}. \end{aligned} \tag{15}$$

After rearranging (15) in the following manner

$$\frac{\log_2(1+\alpha c)}{\alpha \log_2(1+c)} \geq 1, \tag{16}$$

$$\begin{aligned} \log_2(1+\alpha c) &\geq \alpha \log_2(1+c), \\ (1+\alpha c) &\geq (1+c)^{\alpha}. \end{aligned} \tag{17}$$

The generalised Bernoulli's inequality can be applied to prove the inequality in (17), which states

$$(1+x)^r \leq 1 + rx, \quad r \in \mathbb{R}, \ 0 \leq r \leq 1, \quad x \in \mathbb{R}, x > -1. \tag{18}$$

To apply this to (17), r and x are set to

$$\begin{aligned} r = \alpha, \quad 0 \leq \alpha \leq 1 \quad &\rightarrow \quad 0 \leq r \leq 1 \\ x = c, \quad c \geq 0 \quad &\rightarrow \quad x \geq 0 > -1 \end{aligned}$$

and replaced in (18), such that

$$\begin{aligned} (1+x)^r &\leq 1 + rx, \\ (1+c)^{\alpha} &\leq 1 + \alpha c, \end{aligned} \tag{19}$$

exactly the inequality from (17). Hence, by proving (17), it has been shown that (13) is indeed true

$$\frac{\beta_u^{\mathrm{ULIP}}}{\beta_u^{\mathrm{BM}}} \geq 1, \quad \forall P_u^{\mathrm{BM}} \geq P_u^{\mathrm{ULIP}} \geq 0,$$

and hence it can be concluded that the energy efficiency of a low-priority MS employing ULIP is always greater than or equal to the energy efficiency of the same MS in the benchmark system (i.e., transmitting at maximum power). Furthermore, since MSs on high-priority RBs receive a capacity boost while maintaining transmit power, their energy efficiencies are also enhanced. Therefore, the energy efficiency of any/every MS in the system is augmented during ULIP operation, and consequently also the system energy efficiency

$$\beta_{\mathrm{sys}}^{\mathrm{ULIP}} \geq \beta_{\mathrm{sys}}^{\mathrm{BM}}. \tag{20}$$

For completeness, a similar proof can be constructed to show that in conjunction with a larger energy efficiency, the energy consumption $\psi_u = P_u/C_u$ [35], measured in J/bit, for ULIP is lower (as expected) than for the benchmark. Essentially,

$$\frac{\psi_u^{\mathrm{ULIP}}}{\psi_u^{\mathrm{BM}}} \leq 1, \quad \text{and} \quad \psi_{\mathrm{sys}}^{\mathrm{ULIP}} \leq \psi_{\mathrm{sys}}^{\mathrm{BM}}. \tag{21}$$

4.2. System capacity in ULIP

It has been shown that through the application of ULIP the energy efficiency of not only the individual MSs but also of the system is always improved (at minimum no losses are incurred). However, due to the reduction in overall system power through ULIP, one would expect, in general, a similar decrease in system capacity. Here it will be shown that this is not always the case, and hence ULIP not only guarantees a energy efficiency boost, but can also provide a gain in system capacity.

$$C_{\mathrm{sys}}^{\mathrm{ULIP}} \nleq C_{\mathrm{sys}}^{\mathrm{BM}} \tag{22}$$

In essence, it is shown that (22) is true, which, combined with the energy efficiency results demonstrates the potential of ULIP for future OFDMA-based wireless networks such as LTE and/or LTE-Advanced. The proof is found in Appendix.

In the previous section it was demonstrated that the energy efficiency of any MS in a network will be enhanced when ULIP is employed, while here it has been shown that this energy efficiency boost can also be accompanied by an increase in the system capacity

$$C_{\mathrm{sys}}^{\mathrm{ULIP}} \nleq C_{\mathrm{sys}}^{\mathrm{BM}}, \qquad \beta_{\mathrm{sys}}^{\mathrm{ULIP}} \geq \beta_{\mathrm{sys}}^{\mathrm{BM}}.$$

Although in certain scenarios a loss in system capacity is incurred by the system-wide power reduction (as (22) suggests), the guaranteed energy efficiency gain can compensate this deficit. Furthermore, the possibility of gains in both performance metrics, i.e., when C_{sys} is improved, is a good indication of the benefits ULIP can bring to future wireless networks.

5. Scheduling

To facilitate the interference protection, a scheduling procedure is designed to assign MSs to specific priority bands, enhancing the effect of ULIP in the system. In general, a random allocation of priority RBs can lead to undesired scenarios. For instance, the allocation of a high-priority RB to cell-centre MSs is wasteful, as such a MS-BS link is generally strong, and hence interference protection is unnecessary. At the cell-edge, allocating a low-priority RB to a MS is just as destructive. In this case, the MS will most probably be unable to sustain its

γ^{tar}, and hence fall into outage. Therefore, an appropriate scheduling mechanism is necessary for ULIP to achieve its full potential.

In a fair allocation scheme, cell-edge MSs should be allocated high-priority RBs so as to be able to transmit at full power and achieve the maximum possible SINR. Cell-centre users, which are more likely to achieve their SINR target due to BS proximity, should be assigned low-priority RBs. In essence, the general rule is to allocate high-priority RBs to the MSs with the least favourable SINR conditions.

Therefore, an efficient scheduling procedure can increase the effectiveness of ULIP, and prevent throughput losses due to MS outages. In this section, a scheduling procedure relying on the reverse link signals of the active users is presented. By analysing the signals, an approximation of the relative positions of the MSs (and their interferers) can be obtained, which can then be used to schedule the users accordingly. This presents a low complexity scheduling solution, as the necessary information is readily available at the BS.

5.1. SINR scheduling

The scheduling procedure utilises the SINRs from transmissions in previous time slots. In (23), $\mathcal{R}_j$ denotes the N_j-tuple of average (i.e., time average over the previous z time slots, where z is a system wide parameter) SINRs of the users in a cell

$$\mathcal{R}_j = \left(\bar{\gamma}_{j,1}, \bar{\gamma}_{j,2}, \ldots, \bar{\gamma}_{j,N_j}\right), \tag{23}$$

where $\bar{\gamma}_{j,i}$ is the average SINR (over all assigned RBs) of MS_i in cell j, and N_j denotes the number of MSs in cell j. The MSs that are at the cell-edge experience, on average, weaker signals, and consequently low SINRs are received at their serving BS. Thus, the next step is to sort the $\bar{\gamma}_{j,i}$ in ascending order, so that the MSs that have the weakest SINRs can be identified

$$\begin{aligned} \mathcal{U}_j^* &= f_{\bar{\gamma}}\left(\mathcal{R}_j\right) = \left(p_1, p_2, \ldots, p_{N_j}\right) \\ &\text{s.t. if } p_k \le p_l, \text{ then } \bar{\gamma}_{j,k} \le \bar{\gamma}_{j,l}, \end{aligned} \tag{24}$$

where $\mathcal{U}_j^*$ is the N_j-tuple of the positions p_k of $\bar{\gamma}_{j,k}$ in the tuple $\mathcal{R}_j^* = \text{order}\left(\mathcal{R}_j\right)$, which is sorted in ascending order. The function $f_{\bar{\gamma}}(\cdot)$ that defines this ordering can now be applied to the set of users in the cell of interest $\mathcal{S}_{\text{users},j}$, and the set of high-priority MSs, $\mathcal{S}_{\text{hp},j}$, can be found

$$\begin{aligned} \mathcal{S}_{\text{hp},j} &= \left\{ s \in \mathcal{S}_{\text{users},j} \middle| f(\gamma_{j,s}) \le \left\lceil \frac{N_j}{l} \right\rceil \right\} \\ &\text{where } \mathcal{S}_{\text{hp},j} \subset \mathcal{S}_{\text{users},j}, \end{aligned} \tag{25}$$

where l denotes the number of priority bands such that the number of high-priority MSs yields $\lceil N_j/l \rceil$. In (25), the high-priority RBs are allocated to the $\lceil N_j/l \rceil$ MSs with the weakest average SINRs, and hence to the cell-edge. The low-priority RBs are allocated to the cell-centre, thus to the $\lceil N_j/l \rceil$ MSs with the strongest SINRs, and the mid-priority RBs to the remaining (middle set) MSs:

$$\mathcal{S}_{\text{mp},j} = \left\{ s \in \mathcal{S}_{\text{users},j} \middle| \left\lceil \frac{N_j}{3} \right\rceil \le f(\gamma_{j,s}) \le \left\lceil \frac{2N_j}{3} \right\rceil \right\} \tag{26}$$

$$\begin{aligned} \mathcal{S}_{\text{lp},j} &= \left\{ s \in \mathcal{S}_{\text{users},j} \middle| f(\gamma_{j,s}) \ge \left\lceil \frac{2N_j}{3} \right\rceil \right\} \\ &\text{where } \mathcal{S}_{\text{mp},j}, \mathcal{S}_{\text{lp},j} \subset \mathcal{S}_{\text{users},j}. \end{aligned} \tag{27}$$

One instance of the fair allocation for exactly $N_j = M = 50$ users per cell is depicted in Figure 6.

It is clear to see that the farther MSs (from the serving BS) have been allocated high-priority RBs, and to the nearer MSs, which are shielded from neighbouring cell interference, the low-priority RBs are assigned. The mid-priority RBs have been assigned to the remaining MSs.

When a new MS enters the cell, the initial allocation is performed using the SNR (which can be approximated using the RSRP), as no SINR information is available *a priori*. Mean SINR statistics are employed to eliminate fast fading effects and prevent a MS from rapidly changing priority class, so that the system can reach a stable operating point.

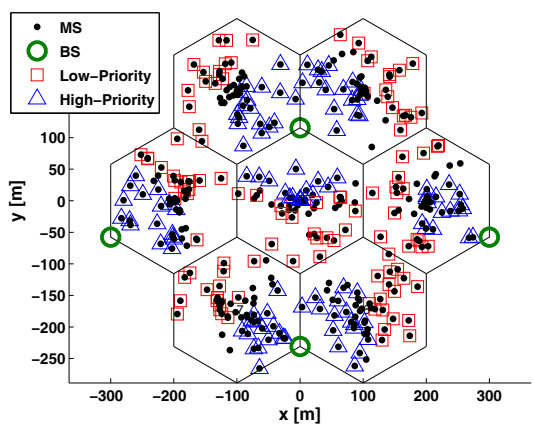

Figure 6 Allocation of resources using the fair scheduler: Each MS is depicted with a dot. The MSs marked with squares have been assigned high-priority RBs, triangles represent low-priority RBs, and the (unmarked) rest are mid-priority. The system is dubbed "fair" as high-priority is assigned to the MSs with the least favourable SINR conditions.

6. Simulation

Monte Carlo simulations are used to provide performance statistics of the users and the system with and without ULIP. The simulator is built following LTE specifications.

6.1. Network construction and user distribution

The simulation area is comprised of a single-tier, *tessellated hexagonal cell* distribution. To eliminate border effects with regards to interference, an additional two tiers are simulated. However, statistics are only taken from the first tier (and centre cell). Users are distributed uniformly over the simulation area such that each cell hosts, on average, $\bar{N}_j$ MSs. Further, BS-MS allocation is done based on path loss, such that each MS is assigned to the BS with the most favourable channel conditions.

Each cell is served by a sector of a macro-BS, where a BS has three 120° sectors. Each BS is placed at the junction of the three hexagonal cells it serves. Figure 3 shows an example of the network construction and priority band allocation, and Figure 6 shows an example of the inner tier simulation area.

The (horizontal) azimuth antenna pattern, $A(\theta)$, is described by

$$A(\theta) = -\min\left\{12\left(\frac{\theta}{\theta_{3\mathrm{dB}}}\right)^2, A_m\right\} \tag{28}$$

where θ is the angle the MS-BS link deviates from the central lobe, $\theta_{3\ \mathrm{dB}}$ is the angle at which the gain is half that of at the centre of the lobe, and A_m is the maximum possible attenuation [24]. Through (28), the horizontal signal attenuation due to MS position is determined.

6.2. Resource allocation

The priority classes in each cell are organised in the manner portrayed in Figure 3, such that when a MS is allocated to a particular priority class, its RBs (if it is assigned more than one) can be allocated contiguously, a feature particular to an LTE uplink. The allotment of users to priority classes is performed by the SINR scheduler introduced in Section 5. Within each class, the set of RBs is randomly (but still contiguously) allocated to the MSs assigned to that class, with each user receiving at minimum one RB.

6.3. Time evolution

Each run of the Monte Carlo simulation is iterated over $z = 10$ subframes, or, equivalently, one LTE frame, such that long-term SINR statistics can be gathered. Due to the random user distribution, plentiful runs with different network generations are considered in order to obtain statistically accurate results. In each run, i.e., at the start of each subframe, the scheduling and allocation of RBs is reperformed. The MSs are assumed to be quasi-static for the duration of a run.

The simulation is performed for a full-buffer model, which represents the worst-case scenario where all users in the network are active, and no RB is left idle. Furthermore, the users are assumed to be static for the duration of a subframe, such that effects due to Doppler spread can be neglected. Perfect synchronisation in time and frequency is assumed, such that intra-cell interference is avoided. The relevant simulation parameters can be found in Table 2.

6.4. Benchmark

To evaluate the performance of ULIP, two well-known benchmark systems have been implemented for comparison purposes. These are:

- *Maximum power transmission*: In the first benchmark, no power allocation is performed, and all MSs transmit at the maximum power on each RB.
- *LTE power control*: In the second benchmark, the transmit power is set dependent on the nominal SINR target Γ, the desired link path loss L_{des}, the strongest interfering link loss L_{int}, and the average interference received on that RB I^m_{avg}. Here, LTE fractional power control (FPC) [26] is used, where

$$P^m_{\mathrm{dBm}} = \min\left\{\Gamma_{\mathrm{dB}} + I^m_{\mathrm{avg,dBm}} + \alpha L_{\mathrm{des,dB}} + (1-\alpha)L_{\mathrm{int,dB}},\ P_{\mathrm{max,dBm}}\right\}, \tag{29}$$

Table 2 Simulation parameters

Parameter	Value
Simulation area	37 cells
Results area	inner 7 cells
Inter-site distance, d_{IS}	350 m
Average MSs per cell, $\bar{N}_j$	20
Uplink FDD band	[2.50, 2.51] GHz
Number of available RBs, M	50
RB bandwidth, B_{RB}	180 kHz
Subcarriers per RB, k_{sc}	12
Symbol rate per subcarrier, ϱ_s	15 ksps
Subframe duration, t_{sf}	1 ms
Subframes (time slots), z	10
Thermal noise, η	-174 dBm/Hz
Total MS transmit power	23 dBm
Sector width	120°
Sector $\theta_{3\ \mathrm{dB}}$	70°
MS SINR target, γ^{tar}	12 dB
Standard deviation, σ	4 dB
Auto-correlation distance	50 m

which, depending on α, achieves a balance between conventional power control (α = 1) and maximum power transmission (α = 0).

For each of the benchmarks, the RB allocation from the ULIP system is adopted, resulting in a *soft frequency reuse* scheme [36]. By comparing the performance of ULIP to these two benchmarks, the effect ULIP has on the performance of the system can be quantified.

6.5. Results

The performance of the system is measured by three criteria: achievable throughput, energy efficiency and fairness (as defined in (5), (7), and (8), respectively). Multiple iterations are run for a system employing ULIP and the benchmark systems. The cumulative distribution functions (CDFs) of achievable throughput and energy efficiency of individual MSs and of the network are compared. From this, quantitative average gain/loss statistics are generated.

7. Results and discussion

From the simulation, the CDFs of the achieved system throughput and energy efficiency are generated for systems employing ULIP and compared against the two benchmark systems, keeping the RB allocation unchanged. General simulation parameters are taken from Table 2 and [37], and full power control (i.e., α = 1) is implemented.

In Figure 7, the CDFs of the achieved user throughput for the three systems is shown, and it is evident that ULIP achieves considerable gains for MSs with low throughput in the benchmarks. At the 50th percentile, ULIP users achieve, on average, 2.8× the user throughput of both benchmarks.

Also, although at the 90th percentile a 31% loss is incurred by the power reduction on low-priority (and therefore high-throughput) RBs, the crossing point of the CDFs signifies that 82% of the users achieve a better SINR (and consequently throughput) in ULIP. Furthermore, the ≈20% outage seen in both benchmarks is eliminated, and hence ULIP provides significant advantages for the users in a cellular network.

These benefits are further seen in Figure 8, where the user energy efficiencies of the three systems are displayed. Here it is clear that ULIP provides a vast energy

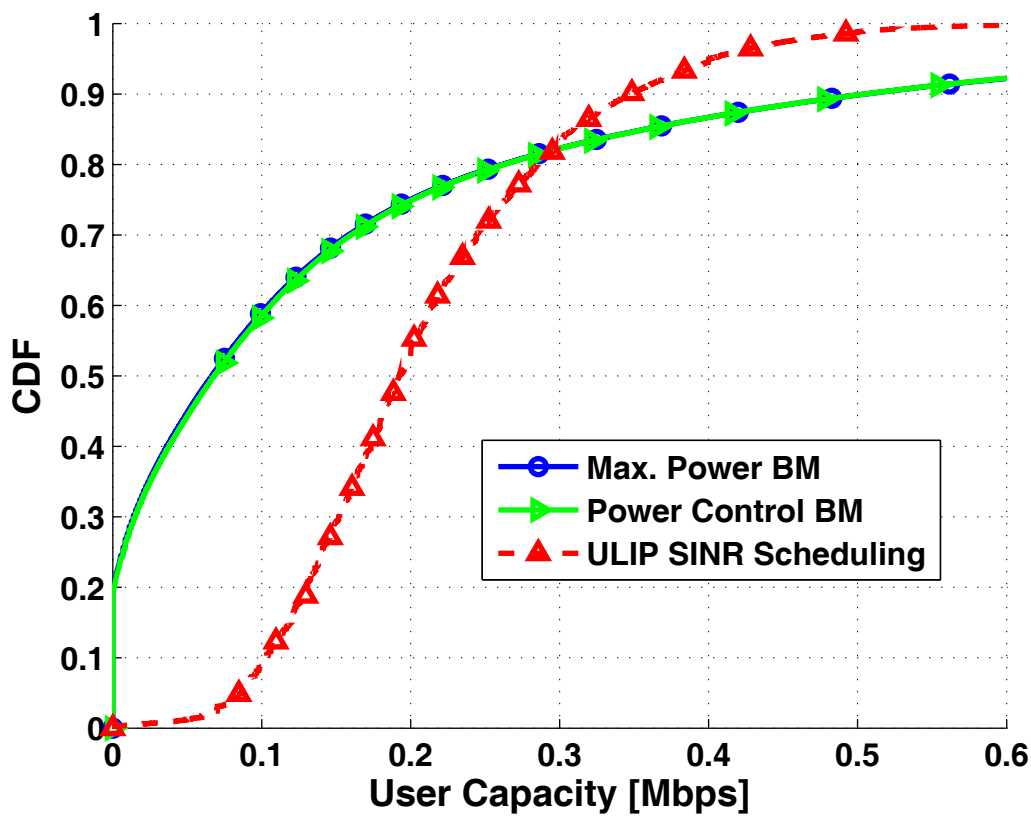

Figure 7 User throughput performance for ULIP and two benchmarks. System statistics are taken from the first tier (i.e., inner 7 cells) of the network over z = 10 time slots, ULIP and power control γ^{tar} = 12 dB.

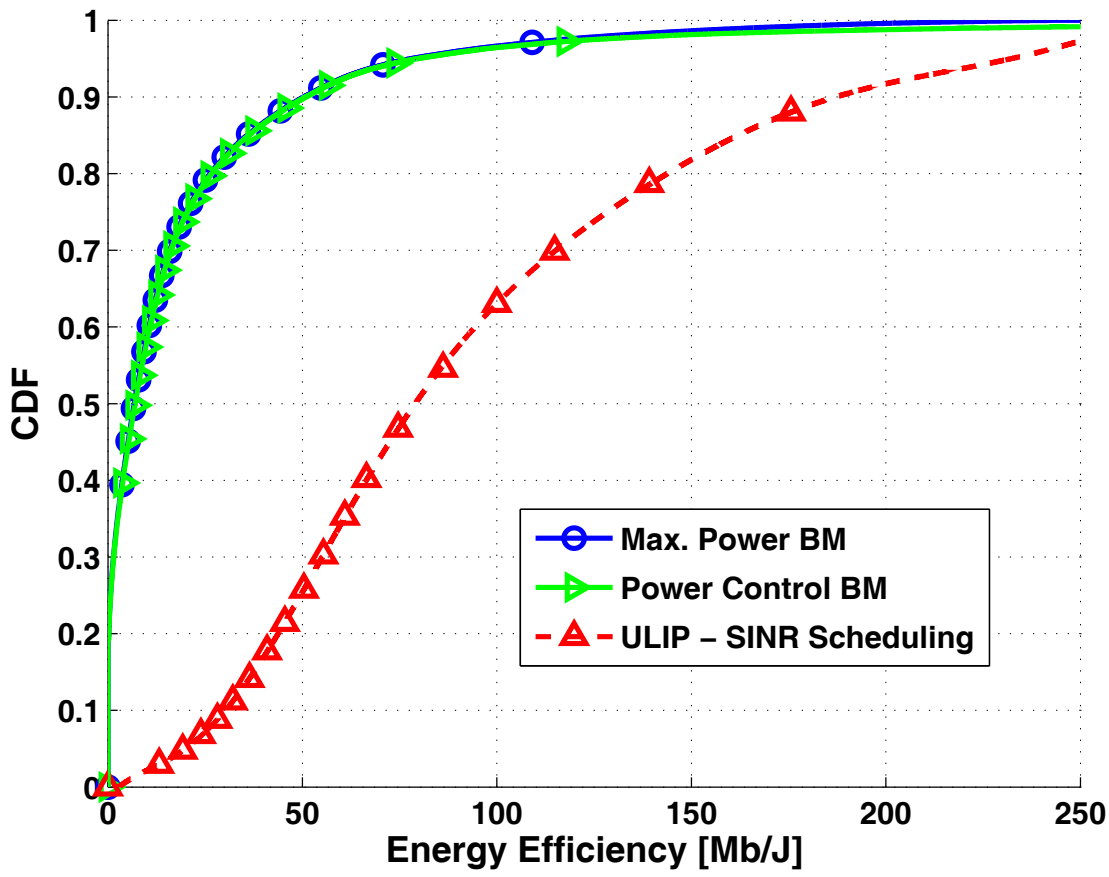

Figure 8 User energy efficiency performance.

efficiency improvement over the two benchmarks, which behave very similarly. At the 50th percentile, ULIP induces almost 11× the user energy efficiency of both benchmarks.

Furthermore, ULIP achieves energy efficiency gains for all MS over the maximum power benchmark, confirming the result of the performance analysis conducted in Section 4.1.

Figure 9 displays the system throughput fairness results of the three power allocation techniques. Here, it is clear to see that while power control provides some fairness gains (almost 14%) over maximum power transmission, ULIP achieves by far the fairest system with over 0.8 fairness rating.

The substantial gains achieved by ULIP over maximum power transmission (3.3×) can be accounted for by the balancing of the system capacity from the cell-centre to the cell-edge, boosting high-priority throughput by sacrificing that of the low-priority MSs, and hence achieving a more throughput fair system.

A further indicator of the enhanced fairness of the network is shown in Figure 10, where the MS throughput is plotted against the distance between the MS and its serving BS. And while both the maximum power and power control generate most of their capacity in the cell-centre (MSs closer to the BS), ULIP achieves an almost flat, much more even areal distribution of throughput in each cell. These findings confirm both the user throughput and fairness results shown in Figures 7 and 9, respectively. Furthermore, due to the simulation environment, the gains for many MSs are quite low, and hence power control very often utilises maximum transmit power to attempt to achieve the target SINR. Hence, there is little performance difference between the two systems, as is evident in Figure 10.

In Figure 11, the system throughput CDF results for ULIP, power control and maximum power transmission are shown. At the 50th percentile, it can be clearly seen that while power control surrenders a slight portion (≈ 4%) of the system capacity achieved by maximum power

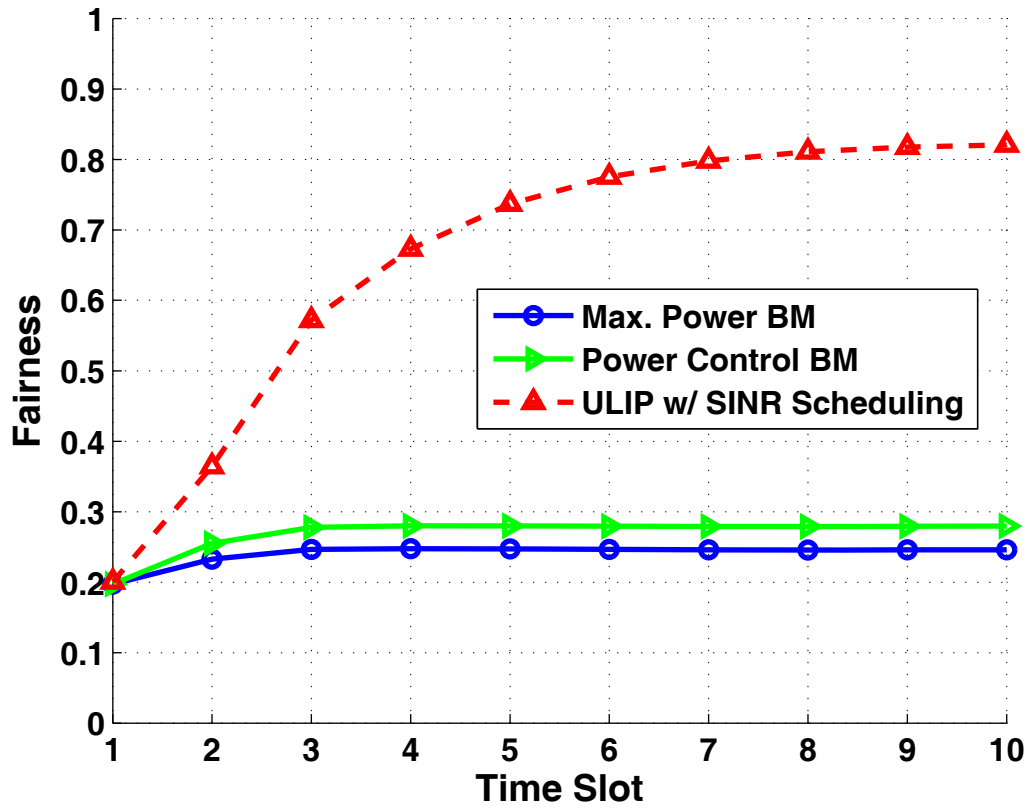

Figure 9 System throughput fairness performance.

transmission, ULIP produces a gain of over 15%, resulting from the large number of MSs given throughput boosts (see Figure 7).

This is a very encouraging result, as it shows that the throughput shift from low- to high-priority MSs is beneficial for the system, achieving larger throughput gains for the high-priority users than losses by the low-priority MSs. This is also a direct result of the link adaptation, as any excess SINR (i.e., γ >20 dB) at the cell-centre can be transferred to the cell-edge without incurring any throughput losses for the low-priority (cell-centre) users. Furthermore, Figure 11 confirms the result achieved in Section 4.2, and shows further that system capacity gains are achievable.

In Figure 12, it can be seen that, surprisingly, power control exhibits an even worse energy efficiency than maximum power transmission. This is mainly due to the system throughput losses incurred. As expected, however, ULIP provides substantial gains over both benchmark systems, achieving a stout 3.5× and 3.6× the energy efficiency of max. power and power control at the 50th percentile, respectively. The large gains seen by ULIP are a combination of (a) the system throughput boosts achieved via the effective shifting of SINR from the cell-centre to the cell-edge; and (b) the substantial power reductions of the low- and mid-priority (cell-centre) users to protect the high-priority users from interference. Together, these two processes provide the significant energy efficiency gains seen in Figure 12, and confirm (20).

All in all, ULIP dominates each of the two benchmarks over the three performance criteria, especially providing a much more energy efficient and fair system. Furthermore, by achieving considerable gains in network capacity, it is clear that both performance analysis proofs have been confirmed.

8. Summary and conclusions

Full frequency reuse and the resulting large CCI in OFDMA networks brings forth the necessity for ICIC in future wireless networks. A technique for ULIP has been presented in this article, which provides protection from CCI through the power reduction of a subset of the neighbouring cell RBs, based on the SINR targets of the MSs in the cell of interest. Aside from the fact that no extra signalling is necessary over the control

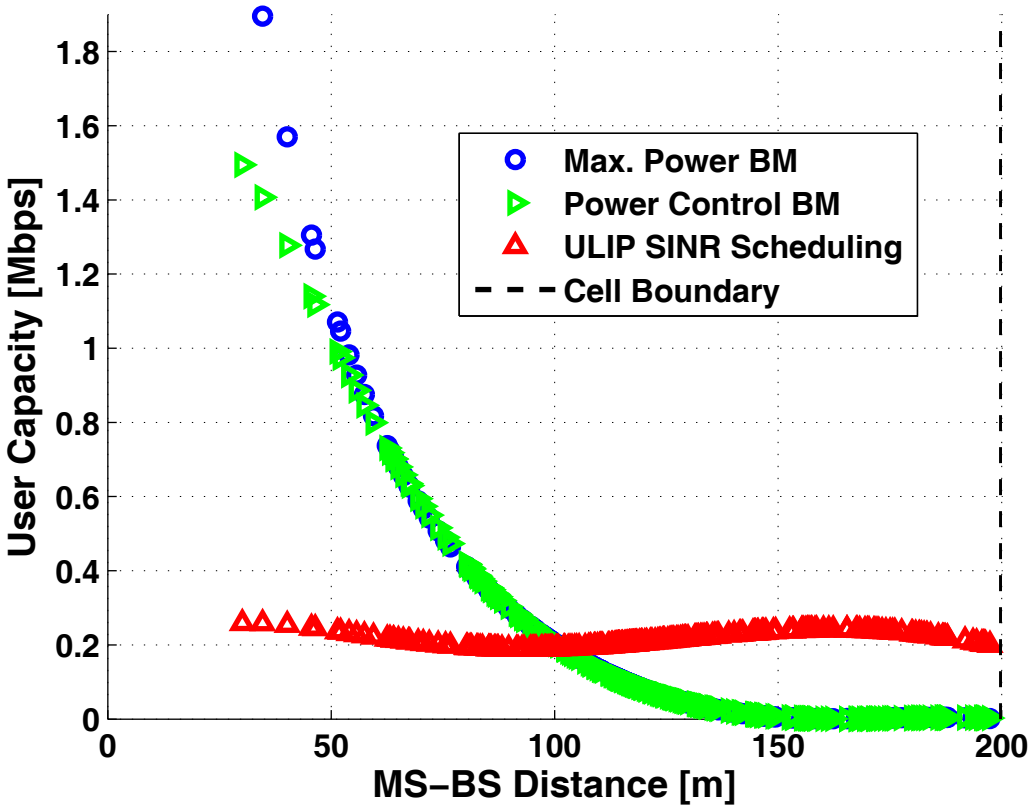

Figure 10 System throughput versus distance from serving BS.

channels, a further benefit of ULIP is a guaranteed increase in energy efficiency of all MSs in the system, and of the system as a whole. Furthermore, it was shown that while a loss in system capacity is possible, this is not certain, and hence gains in achievable system throughput are also possible. This is especially the case in networks where cell-edge capacity is limited, and most of the cell throughput is concentrated in the cell-centre.

It was shown that ULIP, combined with the SINR scheduler, achieves not only a 15% system capacity gain, but also substantially increases the system energy efficiency and fairness by 3.5× and 3.3×, respectively. This is a direct result of the SINR displacement from the cell-centre to the cell-edge, and confirms the results in Section 4, highlighting the excellent energy efficiency of the ULIP protocol. A throughput drop is seen when power control is applied, mainly due to the SINR targeting of the system in comparison to maximum power, which does not restrict transmit power according to service requirements. Furthermore, ULIP eliminates the ≈20% outage suffered in the benchmarks, and provides throughput gains for over 80% of the MSs in the network. Consequently, ULIP diminishes the tradeoff between system capacity and fairness/energy efficiency, and provides significant gains in all three performance areas.

Endnotes

[a]In Table 1, the modulation and coding schemes are taken from LTE [27], and the SINR ranges from [38]. Here, the downlink values are used because no uplink implementation was found, as these values are operator specific. [b]These denote the priority status of the RBs within each class, and have no relation to user traffic priorities, which are not considered here.

Appendix

System capacity proof derivation

To prove (22), a counter-argument to the assumption that

$$C_{\text{sys}}^{\text{ULIP}} \leq C_{\text{sys}}^{\text{BM}}, \tag{30}$$

must be found, where C_{sys} is defined in (6). Therefore, a scenario is designed where the above assumption (30)

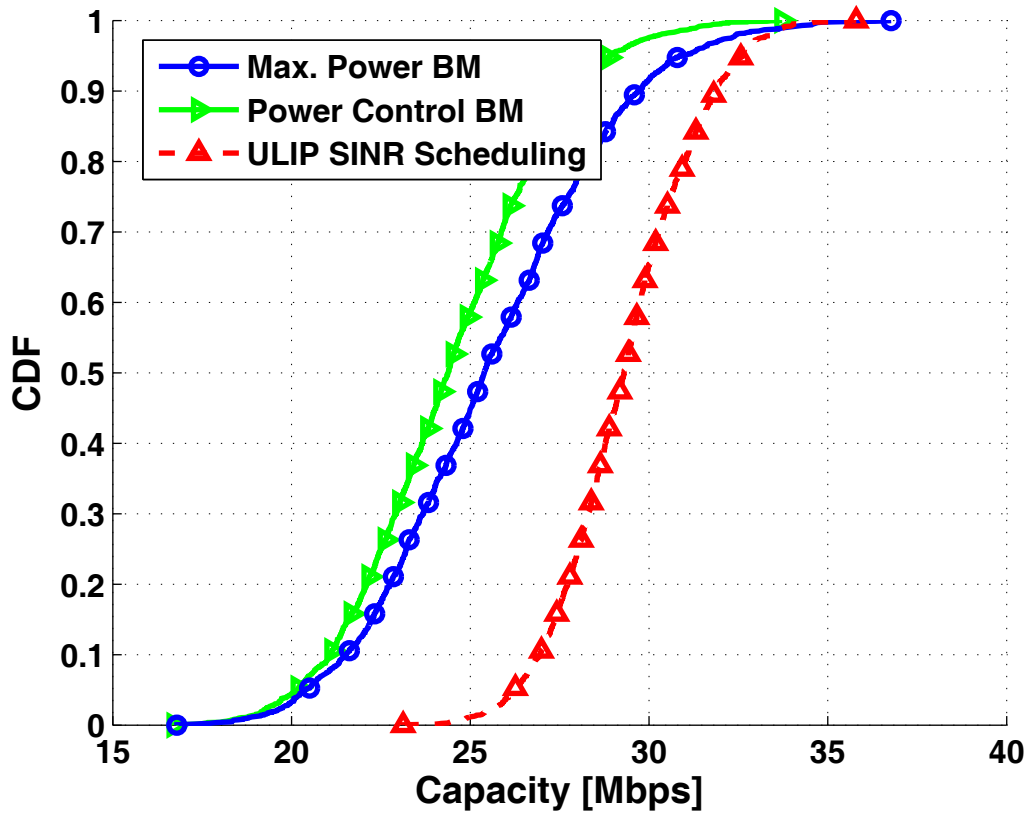

Figure 11 System sum throughput performance.

does not hold. A two-link scenario is chosen where MS_1 and MS_2 are allocated the same RBs in two neighbouring cells. Furthermore, we compare the C_{sys} achieved in the benchmark (BM) system, in which all transmitting stations (MS_1 and MS_2) transmit using maximum transmit power, to that achieved in the ULIP system. When ULIP is applied, MS_2 is given high-priority, and MS_1 low-priority status such that it may be required to scale it's power

$$\begin{aligned} \text{BM}: &\quad P_1 = P_2 \\ \text{ULIP}: &\quad \alpha P_1 \leq P_2, \quad 0 \leq \alpha \leq 1 \end{aligned}$$

where α is the scaling factor by which MS_1 reduces its transmit power.

The proof is set up by making the assumption that the system is interference-limited, and hence the thermal noise can be ignored. This assumption depends on the inter-site distance d_{IS} in the network, as clearly in larger cells the CCI diminishes (given P_{max} remains constant). The path gain and path loss equations are given by (9) and (10), respectively, and the thermal noise is calculated to be $\eta = kTB_{RB}$ = -121 dBm, where k is Boltzmann's constant, the temperature T = 300 K, and the bandwidth B_{RB} = 180 kHz per RB. Given that, on average, $|H_{k,\ l}|^2 = 1$ and $X_\sigma = 0$, the minimum average interfering link gain can be calculated when the interfering MS is located at the maximum distance $d_{max} = d_{IS}$ from the vulnerable BS (i.e., next to a neighbouring BS):

$$L(d_{max}) = 15.3 + 37.6\log_{10}(350) = 110.9 \text{ dB}, \tag{31}$$

$$G_{\min,\nu_2} = 10^{\frac{-L(d)}{10}} = -110.9 \text{ dB}. \tag{32}$$

And given $P_u = P_{max}/M \approx 6$ dBm, the minimum received interference is $P_u G_{\min,\nu_2} \approx -104.9$ dBm, which is significantly larger than η. In fact, even for d_{IS} = 500 m, the minimum average interference comes to -116.8 dBm, which is still more than double the noise power.

Hence, assuming the network is constructed with d_{IS} <500 m, it has been shown that the system is interference-limited, and therefore the noise can be neglected.

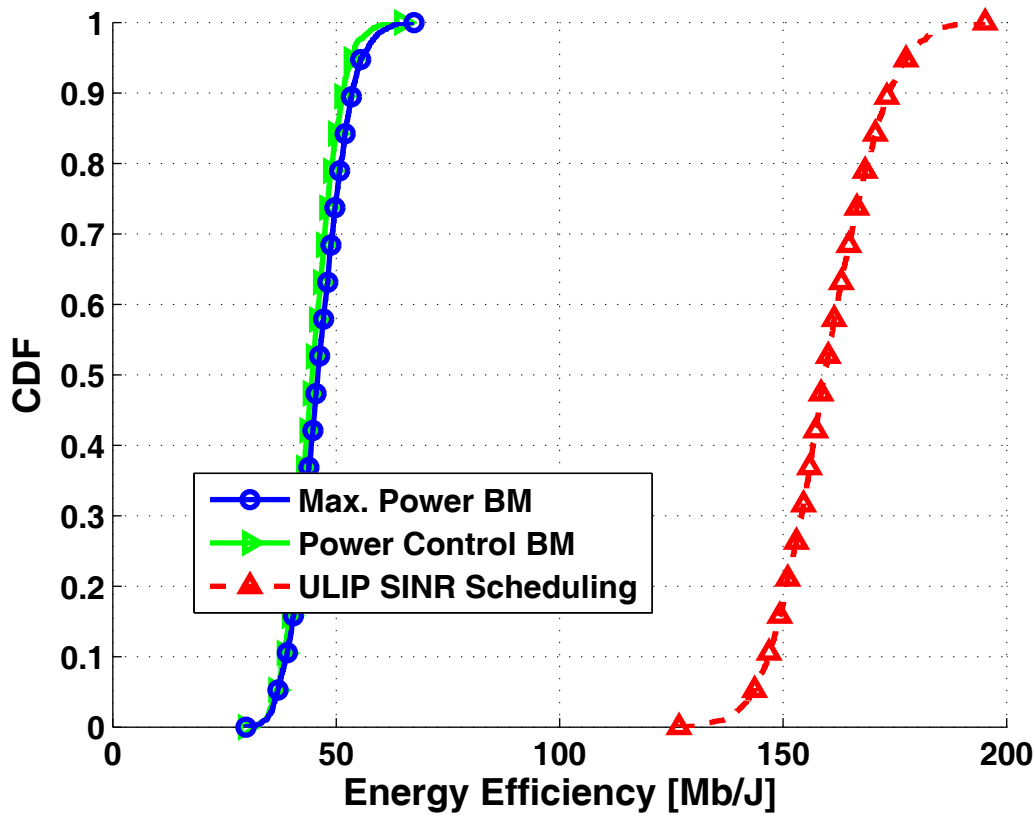

Figure 12 System energy efficiency performance.

This simplifies capacity calculations, as SIR can now be used rather than SINR. The individual user capacities are

$$C_1^{\mathrm{BM}} = W\log_2\left(1+\frac{P_1G_{11}}{P_2G_{21}}\right) \quad C_2^{\mathrm{BM}} = W\log_2\left(1+\frac{P_2G_{22}}{P_1G_{12}}\right), \tag{33}$$

in the benchmark system, and

$$C_1^{\mathrm{ULIP}} = W\log_2\left(1+\frac{\alpha P_1G_{11}}{P_2G_{21}}\right) \quad C_2^{\mathrm{ULIP}} = W\log_2\left(1+\frac{P_2G_{22}}{\alpha P_1G_{12}}\right), \tag{34}$$

when ULIP is employed, where Shannon's equation is used for the calculations. Subsequently, the relationship between C_i^{BM} and C_i^{ULIP} is found:

$$C_1^{\mathrm{ULIP}} \geq W\log_2\left(\left(1+\frac{P_1G_{11}}{P_2G_{21}}\right)^{\alpha}\right) \quad C_2^{\mathrm{ULIP}} \geq W\log_2\left(\left(1+\frac{P_2G_{22}}{P_1G_{12}}\right)^{\frac{1}{\alpha}}\right), \tag{35}$$

where Bernoulli's Inequality (18) is used to arrive at (35) (where $r = \alpha$ and $r = 1/\alpha$ for $i = 1$ and 2, respectively). Further,

$$C_1^{\mathrm{ULIP}} \geq \alpha W\log_2\left(1+\frac{P_1G_{11}}{P_2G_{21}}\right) \quad C_2^{\mathrm{ULIP}} \geq \frac{1}{\alpha}W\log_2\left(1+\frac{P_2G_{22}}{P_1G_{12}}\right), \tag{36}$$

and finally, C_1^{BM} and C_2^{BM} are substituted into (36) to achieve (37)

$$C_1^{\mathrm{ULIP}} \geq \alpha C_1^{\mathrm{BM}} \quad C_2^{\mathrm{ULIP}} \geq \frac{1}{\alpha}C_2^{\mathrm{BM}}. \tag{37}$$

For further simplicity, let us assume that $G_{11} = G_{22}$, and $G_{12} = G_{21}$ (e.g., both MSs are at the cell-border). This creates the following set of equations:

$$C_1^{\mathrm{BM}} = C_2^{\mathrm{BM}} = C_i^{\mathrm{BM}}, \quad C_1^{\mathrm{ULIP}} \geq \alpha C_i^{\mathrm{BM}}, \quad C_2^{\mathrm{ULIP}} \geq \frac{1}{\alpha}C_i^{\mathrm{BM}}. \tag{38}$$

Using (38), it can now be shown that the assumption in (30) does not hold for this system, and that hence (22) is true. In the benchmark,

$$C_{\mathrm{sys}}^{\mathrm{BM}} = C_1^{\mathrm{BM}} + C_2^{\mathrm{BM}} = 2C_i^{\mathrm{BM}}.$$

And when ULIP is applied,

$$C_{\mathrm{sys}}^{\mathrm{ULIP}} = C_1^{\mathrm{ULIP}} + C_2^{\mathrm{ULIP}}, \tag{39}$$

$$\geq \alpha C_1^{\mathrm{BM}} + \frac{1}{\alpha} C_2^{\mathrm{BM}} = \left(\alpha + \frac{1}{\alpha}\right) C_i^{\mathrm{BM}}, \tag{40}$$

$$\geq 2C_i^{\mathrm{BM}} = C_{\mathrm{sys}}^{\mathrm{BM}}, \tag{41}$$

where in (40), the equations from (38) are substituted into (39), and in (41), the inequality

$$\left(\alpha + \frac{1}{\alpha}\right) \geq 2$$

is used, which is proven by the inequality of arithmetic and geometric means

$$\frac{a+b}{2} \geq \sqrt{ab}, \tag{42}$$

$$a = \alpha, \quad b = \frac{1}{\alpha}, \quad \left(\alpha + \frac{1}{\alpha}\right) \geq 2\sqrt{\alpha \frac{1}{\alpha}} \quad \geq 2.$$

In (39)-(41) it has been demonstrated that for the chosen scenario, the ULIP system capacity is greater than that of the benchmark system

$$C_{\mathrm{sys}}^{\mathrm{ULIP}} \geq C_{\mathrm{sys}}^{\mathrm{BM}},$$

and that, hence, (30) is not true. Therefore, (22) is valid.

Author details
[1]Institute for Digital Communications, School of Engineering and Electronics, The University of Edinburgh, EH9 3JL, Edinburgh, UK [2]DOCOMO Euro-Labs, Landsbergerstr. 312, 80687 Munich, Germany

Competing interests
The authors declare that they have no competing interests.

Received: 14 September 2011 Accepted: 28 May 2012
Published: 28 May 2012

References

1. G Auer, V Giannini, C Desset, I Godor, P Skillermark, M Olsson, M Imran, D Sabella, M Gonzalez, O Blume, A Fehske, How much energy is needed to run a wireless network? IEEE Wirel Commun. **18**(5), 40–49 (2011)
2. D Astely, E Dahlman, A Furuskar, Y Jading, M Lindstrom, S Parkvall, LTE: the evolution of mobile broadband. IEEE Commun Mag. **47**(4), 44–51 (2009)
3. M Alouini, A Goldsmith, Area spectral efficiency of cellular mobile radio systems. IEEE Trans Veh Technol. **48**(4), 1047–1066 (1999). doi:10.1109/25.775355
4. S McLaughlin, PM Grant, JS Thompson, H Haas, DI Laurenson, C Khirallah, Y Hou, R Wang, Techniques for improving cellular radio base station energy efficiency. IEEE Wirel Commun Green Radio Special Issue. **18**(5), 10–17 (2011)
5. G Boudreau, J Panicker, N Guo, R Chang, N Wang, S Vrzic, Interference coordination and cancellation for 4G networks. IEEE Commun Mag. **47**(4), 74–81 (2009)
6. P Hosein, On uplink interference management for OFDMA networks, in *Proc of the 18th International Symposium on Personal, Indoor and Mobile Radio Communications (PIMRC)*, Athens, Greece, 1–5 (Sept 2007)
7. M Al-Shalash, F Khafizov, Z Chao, Interference constrained soft frequency reuse for uplink icic in lte networks, in *Personal Indoor and Mobile Radio Communications (PIMRC), 2010 IEEE 21st International Symposium*, Istanbul, Turkey, 1882–1887 (Sept 2010)
8. W Xiao, R Ratasuk, A Ghosh, R Love, Y Sun, R Nory, Uplink power control, interference coordination and resource allocation for 3GPP E-UTRA, in *Proc of the Vehicular Technology Conference (VTC)*, Montreal, Canada, 1–5 (Sept 2006)
9. T Zhang, Z Zeng, C Feng, J Cheng, L Song, Uplink power allocation for interference coordination in multi-cell OFDM systems, in *Proc of the Third International Conference on Communications and Networking*, Hangzhou, China, 716–720 (Aug 2008)
10. X Zhang, C He, L Jiang, J Xu, Inter-cell interference coordination based on softer frequency reuse in OFDMA cellular systems, in *Proc of International Conference on Neural Networks and Signal Processing*, Zhenjiang, China, 270–275 (June 2008)
11. L Miao, CG Cassandras, Optimal transmission scheduling for energy-efficient wireless networks, in *Proc of 25th IEEE International Conference on Computer Communications*, Barcelona, Spain, 1–11 (Apr 2006)
12. C Li, MJ Neely, Energy-optimal scheduling with dynamic channel acquisition in wireless downlinks. IEEE Trans Mobile Comput. **9**(4), 527–539 (2010)
13. L Gao, S Cui, Efficient subcarrier, power, and rate allocation with fairness consideration for OFDMA uplink. IEEE Trans Wirel Commun. **7**(5), 1507–1511 (2008)
14. M Al-Rawi, R Jantti, J Torsner, M Sagfors, Channel-aware inter-cell interference coordination for the uplink of 3G LTE networks, in *Proc of the Wireless Telecommunications Symposium (WTS)*, (Prague, Czech Republic, Apr 2009), pp. 1–5
15. A Dejonghe, B Bougard, S Pollin, J Craninckx, A Bourdoux, LV der Perre, F Catthoor, Green reconfigurable radio systems. IEEE Signal Process Mag. **24**(3), 90–101 (2007)
16. B Badic, T O'Farrrell, P Loskot, J He, Energy efficient radio access architectures for green radio: large versus small cell size deployment, in *Proc of the 70th Vehicular Technology Conference*, Anchorage, 1–5 (Sept 2009)
17. F Meshkati, V Poor, S Schwartz, Energy-efficient resource allocation in wireless networks: an overview of game theoretic approaches. IEEE Signal Proces Resource-Constrained Signal Processing, Communications and Networking Special Issue. **24**(3), 58–68. (207)
18. C Xiong, G Li, S Zhang, Y Chen, S Xu, Energy- and spectral-efficiency tradeoff in downlink ofdma networks, in *Communications (ICC), 2011 IEEE International Conference on*, Kyoto, Japan, 1–5 (June 2011)
19. 3rd Generation Partnership Project (3GPP), Technical Specification Group Radio Access Network, Soft Frequency Reuse Scheme for UTRAN LTE, 3GPP TSG RAN WG1 R1-050507, 3GPP Std., 9–13 (May 2005)
20. R Jain, D Chiu, W Hawe, A Quantitative Measure of Fairness and Discrimination for Resource Allocation in Shared Computer Systems. DEC Technical Report, Tech Rep 301 (1984)
21. ITU-R Working Party 5D (WP5D) - IMT Systems, Report 124, Report of correspondence group for IMT.EVAL (United Arab Emirates, May 2008)
22. W Wang, T Ottosson, M Sternad, A Ahlen, A Svensson, Impact of multiuser diversity and channel variability on adaptive OFDM, in *Proc of the 58th IEEE Vehicular Technology Conference (VTC)*, Orlando, USA, 547–551 (6–9 Oct 2003)
23. NTT DOCOMO, New Evaluation Models (Micro Cell, Indoor, Rural/High-Speed), 3GPP TSG RAN WG1 R1-082713 (July 2008), http://www.3gpp.org/ftp/tsg_ran/WG1_RL1/TSGR1_53b/Docs/. Accessed 27 Nov 2009
24. 3GPP, Simulation Assumptions and Parameters for FDD HeNB RF Requirements, 3GPP TSG RAN WG4 R4-092042 (July 2008), http://www.3gpp.org/ftp/Specs/. Accessed 1 Sept 2009
25. LK Tee, C van Rensburg, J-A Tsai, Uplink power control for an OFDMA mobile cellular system, in *Proc of the Vehicular Technology Conference*, Baltimore, MD, 357–361 (Sept/Oct 2007)
26. A Rao, Reverse link power control for managing inter-cell interference in orthogonal multiple access systems, in *Proc of Vehicular Technology Conference (VTC)*, Baltimore, MD, 1837–1841 (Sept/Oct 2007)
27. S Sesia, I Toufik, M Baker, in *LTE–The UMTS Long Term Evolution: From Theory to Practice*, ed. by S Sesia, I Toufik, M Baker 1st ed. (Wiley, Chichester, 2009)
28. 3GPP, Physical Channels and Modulation (Release 8), 3GPP TS 36.211 V 8.2.0 (2008-03) (Mar 2008), http://www.3gpp.org/ftp/Specs/. Accessed 1 Sept 2009

29. A Goldsmith, *Wireless Communications* (Cambridge University Press, Cambridge, 2005)
30. TM Cover, JA Thomas, in *Elements of Information Theory*, ed. by DL Schilling 1st ed. (Wiley Series in Telecommunications Wiley, New York, 1991)
31. EC van der Meulen, Some reflections on the interference channel, in *Communications and Cryptography: Two Sides of One Tapestry*, ed. by RE Blahut, DJ Costello Jr., T Mittelholzer (Kluwer Academic Publishers, Boston, 1994), pp. 409–421
32. S Shamai, A Wyner, Information-theoretic considerations for symmetric, cellular, multiple-access fading channels. IEEE Trans Inf Theory. **43**(6), 1877–1894 (1997). doi:10.1109/18.641553
33. Y Kim, T Kwon, D Hong, Area spectral efficiency of shared spectrum hierarchical cell structure networks. IEEE Trans Veh Technol. **59**(8), 4145–4151 (2010)
34. Y Ma, D Kim, Rate-maximization scheduling schemes for uplink OFDMA. IEEE Trans Wirel Commun. **8**(6), 3193–3205 (2009)
35. C Han, T Harrold, S Armour, I Krikidis, S Videv, P Grant, H Haas, J Thompson, I Ku, C-X Wang, TA Le, M Nakhai, J Zhang, L Hanzo, Green radio: radio techniques to enable energy-efficient wireless networks. IEEE Commun Mag. **49**(6), 46–54 (2011)
36. X Mao, A Maaref, KH Teo, Adaptive soft frequency reuse for inter-cell interference coordination in SC-FDMA based 3GPP LTE uplinks, in *Proc of the Global Telecommunications Conference*, New Orleans, 1–6 (Nov 2008)
37. 3GPP, X2 General Aspects and Principles (Release 8), 3GPP TS 36.420 V8.0.0 (2007-12) (Dec 2007), http://www.3gpp.org/ftp/Specs/. Accessed 1 Sept 2009
38. EDX Wireless, Designing an LTE network using EDX SignalPro, Technical white paper (2010) retrieved 17 Jan 2011 http://www.edx.com/resources/documents/

doi:10.1186/1687-1499-2012-180
Cite this article as: Burchardt *et al.*: Uplink interference protection and scheduling for energy efficient OFDMA networks. *EURASIP Journal on Wireless Communications and Networking* 2012 **2012**:180.

Pareto Optimal Power Control Scheduling for OFDMA Networks

Harald Burchardt*, Sinan Sinanovic*, Gunther Auer† and Harald Haas*

*Institute for Digital Communications, Joint Research Institute for Signal and Image Processing,
The University of Edinburgh, EH9 3JL, Edinburgh, UK
Email: {h.burchardt, s.sinanovic, h.haas}@ed.ac.uk

†DOCOMO Euro-Labs, 80687 Munich, Germany,
Email: {auer}@docomolab-euro.com

***Abstract*—In this paper, a novel scheduling mechanism that enhances both network spectral and energy efficiency is presented. In Pareto Optimal Scheduling (POS), mobile stations (MSs) are scheduled based on path gains such that the sufficient conditions for Pareto optimal power control (POPC) are fulfilled. This is performed in such a manner to maximise the number of concurrently transmitting MSs. Furthermore, a Stepwise Removal (SR) algorithm is introduced for the situation where links do not meet the sufficient conditions for power control. In this case, links are removed in order for other MSs to achieve their signal-to-interference-plus-noise ratio (SINR) targets. The targets of these remaining MSs are updated to prevent losses in system spectral efficiency caused by the link removals. Large network simulation results show that significant gains in spectral efficiency can be achieved over standard power control techniques, while additionally providing substantially improved energy efficiency.**

I. Introduction

With higher-speed wireless services becoming increasingly in-demand, there is a great need for increased throughput per bandwidth to accommodate higher data rates whilst guaranteeing quality of service. In addition, the necessity for more energy efficient, or "green," technologies is growing. Increasing traffic load is expected to double the network energy consumption within the next ten years [1]. Power control mechanisms attempt to minimise transmit power while maintaining sufficient spectral efficiency for the users in the network. In this paper, a scheduling and power control technique that benefits both the spectral and energy efficiency of future networks is developed.

In [2], a truncated closed-loop power control scheme is presented to cut off transmission of users when their short-term fading falls below a given threshold. While this leads to gains in both capacity and user availability, users are shown to suffer from large delays, a clearly undesirable result for wireless systems. Fractional power control (FPC) for orthogonal frequency division multiple access (OFDMA) networks is introduced in [3], which offers a slight adaptation to conventional power control to trade off spectral efficiency and cell-edge bit rate. Due to this, however, many users will not achieve their SINR targets, and hence user throughput suffers.

An extension to FPC is developed in [4], where the power control expression takes interference caused to neighbouring cells into account. While this achieves a modest capacity increase, the mean level of interference to other cells is not reduced, but rather only the variance. In [5] on the other hand, closed-loop power control offers significant gains in user throughput and transmit power. These are achieved, however, for very low SINRs, whereas almost no benefits are seen in the high SINR range. Finally, a computationally efficient power control mechanism is introduced in [6], where the problem of minimising transmit power is formulated. However, the joint subcarrier and power allocation is split into two stages, thus disregarding the dependence between the two.

This paper presents a novel technique to combine scheduling and power control, to not only minimise power consumption but also maximise system spectral efficiency through fair allocation of users. The rest of the paper is structured as follows, Section II presents POPC, and Section III describes the analytic basis and implementation of POS and the SR algorithm. Sections IV and V describe the simulation environment and results, respectively, and Section VI offers a conclusion.

II. Pareto Optimal Power Control

In a wireless system, the quality of each link is determined by the SINR at the intended receiver. In an uplink with K interferers, the SINR of the ith user is denoted by:

$$\gamma_i = \frac{P_i G_{i,v_i}}{\phi \sum_{j \neq i}^{K-1} P_j G_{j,v_i} + \eta}\,, \quad i = 1, \ldots, K\,, \tag{1}$$

where P_i is the transmit power of MS_i, G_{j,v_i} the channel gain from MS_j to base station $(\text{BS})_{v_i}$ that serves MS_i, the thermal noise power is denoted by η, and ϕ is the interference reduction due to signal processing ($\phi = 1$ for OFDMA). Furthermore, since in OFDMA systems the interference between MSs can be broken down to interference between the resource blocks (RBs)[1] assigned to those MSs, K can be equated to the number of cells being considered. As a basis for this work, K=3.

Given each link is assigned a minimum SINR target, γ_i^*, this constraint can be represented in matrix form [7] with component-wise inequalities

$$(\mathbf{I} - \mathbf{F})\mathbf{P} \geq \mathbf{u}\,, \quad \mathbf{P} > \mathbf{0}\,, \tag{2}$$

where $\mathbf{I}$ is the identity matrix and $\mathbf{P} = (P_1, \ldots, P_K)^T$ is the vector of transmit powers,

$$\mathbf{u} = \left(\frac{(I_1 + \eta)\gamma_1^*}{G_{1,v_1}}, \cdots, \frac{(I_K + \eta)\gamma_K^*}{G_{K,v_K}} \right)^T\,, \tag{3}$$

is the vector of interference (I_i) plus noise power scaled by the SINR targets and channel gains, and $\mathbf{F}$ is the interference matrix where

$$F_{ij} = \begin{cases} 0, & \text{if } i = j \\ \frac{\gamma_i^* G_{j,v_i} \phi}{G_{i,v_i}}, & \text{if } i \neq j \end{cases} \tag{4}$$

[1]Due to the orthogonality of subcarriers and, hence, also RBs.

978-1-4673-1881-5/12/$31.00 ©2012 IEEE

with $i, j = 1, \ldots, K$. $\mathbf{F}$ is non-negative and irreducible [7].

Given $\rho_F = \max_i |\lambda_i|$ as the Perron-Frobenius eigenvalue of $\mathbf{F}$, if $\rho_F < 1$, then there exists a vector $\mathbf{P} > \mathbf{0}$ such that the SINR requirements of all interfering users are satisfied, and $\mathbf{P}^* = (\mathbf{I} - \mathbf{F})^{-1}\mathbf{u}$ is the Pareto optimal solution (*i.e.*, if there is any other solution $\mathbf{P}$ to (2), then $\mathbf{P} > \mathbf{P}^*$ component-wise) [7]. Hence, if all the SINR requirements can be met simultaneously, the optimal power vector $\mathbf{P}^*$ minimises the transmit power of the users.

III. Pareto Optimal Scheduling (POS)

In Pareto optimal power allocation, given a feasible link allocation, *i.e.*, $\rho_F < 1$, a vector $\mathbf{P}^* = (\mathbf{I} - \mathbf{F})^{-1}\mathbf{u}$ can be found such that all users achieve their SINR requirements with minimal power. This is of course a highly desirable result which, depending on the location and service requirements of the interfering MSs, is clearly not always possible. Hence, by scheduling users in such a manner to maximise the number of feasible $\mathbf{F}$ matrices (in principle, there can be as many $\mathbf{F}$ matrices as there are RBs in the system), the system spectral efficiency can be maximised. Such a scheduling algorithm is developed here.

A. Analytical Basis

Since for a particular grouping of MSs (on the same RB(s) in different cells) to be feasible $\rho_F < 1$, it follows the modulus of all eigenvalues λ_i of $\mathbf{F}$ must also be less than unity, *i.e.*, $|\lambda_i| < 1, \forall i = 1, \ldots, K$. In other words, all eigenvalues must lie within the unit circle.

In [8], Jury provides a simplified analytic test of stability of linear discrete systems, *i.e.*, the necessary and sufficient conditions for any real polynomial to have all its roots inside the unit circle. Hence, this test can be directly applied to the characteristic function $f_{\mathbf{F}}(\lambda)$ of the matrix $\mathbf{F}$, whose roots are the eigenvalues of $\mathbf{F}$, and thus need to lie within the unit circle. The characteristic function $f_{\mathbf{F}_3}(\lambda)$ is expressed as follows:

$$\text{Given} \quad \mathbf{F} = \begin{bmatrix} 0 & F_{12} & F_{13} \\ F_{21} & 0 & F_{23} \\ F_{31} & F_{32} & 0 \end{bmatrix}$$

$$\begin{aligned} f_{\mathbf{F}_3}(\lambda) &= \det(\mathbf{F} - \lambda\mathbf{I}) \\ &= -\lambda^3 + \lambda(F_{12}F_{21} + F_{13}F_{31} + F_{23}F_{32}) \\ &\quad + F_{12}F_{23}F_{31} + F_{13}F_{21}F_{32} \qquad (5) \\ &= \lambda^3 + c\lambda + d \qquad (6) \end{aligned}$$

$$\text{Hence} \quad \begin{aligned} c &= -F_{12}F_{21} - F_{13}F_{31} - F_{23}F_{32} \\ d &= -F_{12}F_{23}F_{31} - F_{13}F_{21}F_{32} \end{aligned}$$

In [8], the stability constraints for a polynomial of order K=3 are given as[2]

$$\begin{aligned} & f(z) = a_3z^3 + a_2z^2 + a_1z + a_0, \quad a_3 > 0 \\ & 1) \;\; |a_0| < a_3 \\ & 2) \;\; a_0^2 - a_3^2 < a_0a_2 - a_1a_3 \\ & 3) \;\; a_0 + a_1 + a_2 + a_3 > 0, \; a_0 - a_1 + a_2 - a_3 < 0 \end{aligned} \quad . \qquad (7)$$

[2] K=3 cells are chosen for complexity reasons. For K >3, the stability conditions in (7) and hence the derivation of POS becomes highly complex, and is practically intractable.

These conditions can now be applied to $f_{\mathbf{F}_3}(\lambda)$

$$\begin{aligned} & f_{\mathbf{F}_3}(\lambda) = \lambda^3 + c\lambda + d \\ & \quad a_3 = 1, \; a_2 = 0, \; a_1 = c, \; a_0 = d, \\ & 1) \;\; |d| < 1 \\ & 2) \;\; d^2 - 1 < c \;\rightarrow\; c > 1 - d^2 \\ & 3) \;\; d + c + 1 > 0 \;\rightarrow\; c > -d - 1, \\ & \quad d - c - 1 < 0 \;\rightarrow\; c > d - 1 \end{aligned} \qquad (8)$$

which describes the ranges of c and d for which $\mathbf{F}$ is feasible. However, since from (4) $F_{ij} \geq 0, \forall i, j$, it is clear that both $c, d \leq 0$, and the constraints are reduced to only a single one, such that the **feasibility condition** becomes:

$$\begin{aligned} & 3) \quad c > -d - 1 \\ & -F_{12}F_{21} - F_{13}F_{31} - F_{23}F_{32} > F_{12}F_{23}F_{31} + F_{13}F_{21}F_{32} - 1 \end{aligned}$$

So, $\rho_F < 1$ **if**: (9)

$$F_{12}F_{21} + F_{13}F_{31} + F_{23}F_{32} + F_{12}F_{23}F_{31} + F_{13}F_{21}F_{32} < 1\,.$$

So, a group of MSs, one in each cell (in the three-cell scenario), is feasible if and only if the condition in (9) is fulfilled. This is clearly dependent on the individual desired and interfering path gains, along with the SINR targets of the users. Therefore, a scheduler might make use of this condition to schedule users such that the number of feasible groups of MSs is maximised, hence also maximising the spectral efficiency of the system.

1) Feasibility for $K - 1 = 2$: In the case that the scheduler is unable to find feasible groups for particular MSs (due to *e.g.*, location at cell-edge), the SR algorithm turns off one of the links in a group of MSs, resulting in a feasibility matrix $\mathbf{F}$ of size $K - 1 \times K - 1$, in the three-cell case 2×2:

$$\mathbf{F} = \begin{bmatrix} 0 & F_{12} \\ F_{21} & 0 \end{bmatrix} \qquad (10)$$

And hence, the characteristic function is given by

$$\begin{aligned} f_{\mathbf{F}_2}(\lambda) &= \det(\mathbf{F} - \lambda\mathbf{I}) \\ &= \lambda^2 - F_{12}F_{21} \\ &= \lambda^2 + c \\ c &= -F_{12}F_{21} \end{aligned} \qquad (11)$$

Stability constraints [8] for polynomials of order K−1=2 are applied to $f_{\mathbf{F}_2}(\lambda)$, yielding the **feasibility condition** given by

$$2) \quad \begin{aligned} 1 &> -c \\ 1 &> F_{12}F_{21} \end{aligned} \qquad \textbf{So, } \rho_F < 1 \textbf{ if}: \quad F_{12}F_{21} < 1\,. \qquad (12)$$

B. Stepwise Removal

In POPC, if $\rho_F \not< 1$, no solution is available, and hence $\mathbf{P} \rightarrow \mathbf{0}$. In this case, none of the links will transmit, hence this solution is highly suboptimal. A better way to address this problem is to successively remove single links from the group of interfering MSs, until an $\mathbf{F}$ is achieved with $\rho_F < 1$. It makes sense to, at each step, remove the link that is causing the largest interference to the other users. It is clear, however, that turning off one of the links will harm the system spectral efficiency, and hence for each link removal, the SINR target for the remaining links (assuming link 3 has been switched

off) must be updated as follows

$$\gamma^*_{(1),\mathrm{up}} = \frac{\prod_j^K \left(1+\gamma^*_j\right)}{1+\gamma^*_{(2),\mathrm{up}}} - 1\,, \tag{13}$$

where $\gamma^*_{(i),\mathrm{up}}$ represents the updated SINR target of the ith *remaining* link. Since (13) has infinite solutions, an additional condition on $\gamma^*_{(1),\mathrm{up}}$ and $\gamma^*_{(2),\mathrm{up}}$ such as a power minimisation

$$\text{Solve (13) s.t.} \qquad \min\left\{\gamma^*_{(1),\mathrm{up}} + \gamma^*_{(2),\mathrm{up}}\right\}\,, \tag{14}$$

or an equal absolute SINR increase

$$\text{Solve (13) s.t.} \qquad \gamma^*_{(1),\mathrm{up}} - \gamma^*_{(1)} = \gamma^*_{(2),\mathrm{up}} - \gamma^*_{(2)}\,, \tag{15}$$

is necessary[3]. Finally, when two links have been removed and only a single link remains, $\gamma^*_{(1),\mathrm{up}} = \prod_j^K \left(1+\gamma^*_j\right) - 1$, and $\mathbf{F} = 0$, $\rho_F = 0$, and $\mathbf{P} = \mathbf{u} = \frac{n\gamma^*_{(1),\mathrm{up}}}{G_{1,v_1}}$.

Through this form of link removal, system spectral efficiency is maintained while maximising the number of transmitting users according to the feasibility constraint ρ_F. Furthermore, it prevents the annihilation of links caused in POPC.

C. Scheduling

The goal is to maximise the number of "MS-groups" for which (9) is satisfied and POPC can be applied. This is opposed to a random scheduler where the assignment of RBs, and hence also MS-groups, is performed arbitrarily.

The scheduler is split into three stages, corresponding to the number of cells considered and hence one more than the number of stepwise removals possible. In the first round of grouping, the scheduler searches through all combinations of MSs (*i.e.*, one in each cell) that fulfil the feasibility condition (9). Clearly, it is possible for an MS to be part of multiple feasible groups, but also part of none. Hence, to maximise the number of feasible combinations, those MSs with the fewest feasible combinations (*i.e.*, "least feasible" MSs) should be scheduled first along with the two least feasible partners. This is done until all MSs have been scheduled/grouped.

In the second round, the MSs that have not been scheduled cannot form groups of three, and hence groups will be allocated with one link deactivated. Furthermore, through the SR algorithm the SINR targets are raised according to (13) to maintain system spectral efficiency. Thus, all "MS-pairs" that satisfy (12) can be allocated. Again, the least feasible MSs are scheduled first, and to complete each group, the least feasible MS is selected from the unscheduled cell.

Finally, in the third round, MS-groups with two deactivated links are scheduled. Here, the activated link in each group should have the best path gain to minimise the necessary transmit power. Therefore, each of the remaining groups is constructed by the MS with the best path gain and the MSs in the two other cells with the worst path gains. This is done until all MSs have been scheduled. The SINR target is again updated to maintain system spectral efficiency.

In the power allocation stage, $\mathbf{F}$ and $\mathbf{u}$ (sized appropriately for groups with three or two links) are constructed for each MS-group, and POPC is performed. The MS transmit power is limited by the maximum power $P_{\max}$, which may reduce the optimality of some solutions. This is, however, unavoidable.

Lastly, over multiple time slots the deactivated MSs are scheduled in later slots, such that they too can achieve their target spectral efficiency. Here, this is done over three slots, such that when only a single link in a group can be active, each mobile has its own slot to transmit. Through this scheduler, all MSs in the system should attain the desired spectral efficiency, and if not, reduce the losses incurred.

D. Three-Cell Simulation Results

Fig. 1 shows the spectral efficiency results for varying SINR targets and inter-site distances (ISDs) in a three-cell scenario. The max. power spectral efficiency is independent of MS SINR targets and thus constant over all SINRs, while POPC suffers significantly from the random grouping (all benchmarks are randomly scheduled), as the number of feasible groups disappears very rapidly with increasing SINR. The upper bound in Fig. 1 denotes the Shannon capacity of the given SINR target, *i.e.*, the attainable spectral efficiency if *all* MSs can be optimally scheduled.

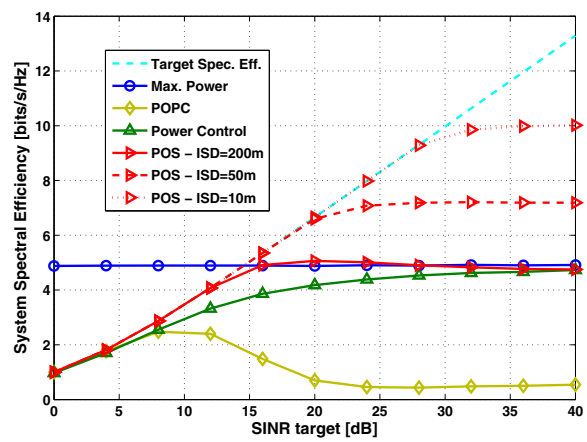

Fig. 1. System spectral efficiency (calculated using Shannon's equation) results for the various power control techniques over a range of SINR targets. Three-cell scenario with a single omni-directional antenna per cell.

The ISD is a significant factor in the performance of POS. Here, the smaller the ISDs, the better the performance; a key factor for shrinking cell sizes in future networks. When links are deactivated, the larger transmit powers needed to meet γ^*_{up} are bounded by $P_{\max}$. Reducing the ISDs is equivalent to increasing $P_{\max}$ due to greater desired link gains. Lastly, it is evident that POS outperforms all other techniques investigated, and has significant potential for future wireless networks.

E. Extension to Macro-cellular Network

Since POS is developed for a three-cell system, on its own it is very ineffective for more realistic scenarios where there are clearly more than three cells. One option would be to derive the feasibility condition(s) for a larger number of cells, to henceforth be able to apply POS to a larger network. From [8][4],

[3]In this paper, a system wide SINR target γ^* is used, in which case (14) and (15) yield equivalent results for (13).

[4]In [8] the sufficient conditions for stability of nth order polynomials are presented, which were used to derive the feasibility condition in (9).

however, we can infer that the feasibility conditions for even a four-cell scenario are excessively complex, and hence such extension to larger networks is highly impractical.

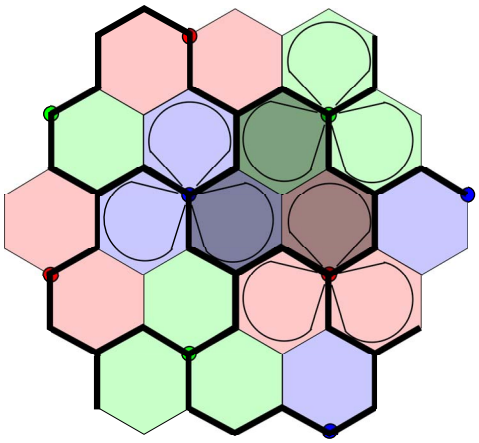

Fig. 2. Extension of three-cell POS to larger multi-cellular networks. Universal frequency reuse is applied, and the differing colouration of the cells simply demarks which BS is serving them.

A more pragmatic approach is to find a way to tessellate the three-cell POS over a network of any dimensions. This is shown in Fig. 2, where the structure of a typical sectorised cellular network can help the extension of POS to multiple cells. By grouping three cells with coinciding beam patterns (see shaded cells in Fig. 2), POS can be applied to these three cells, and the cluster will be relatively shielded from neighbouring sectors' interference due to the nature of the beam patterns. This clustering is then tessellated over the network, such that POS can be applied separately in each of these clusters without overly excessive co-channel interference (CCI) from the surrounding cells, allowing the MSs to achieve their transmission requirements.

IV. Simulation

Monte Carlo simulations are used to provide mean performance statistics for a system using various power allocation techniques, including POS.

A. System Setup

The simulation area comprises 19 cells, where each cell is served by a sector of its BS (see Fig. 2 for an example). Furthermore, an antenna downtilt is considered to mitigate interference between cells. In each cell the N users per cell are uniformly distributed. The assignment of MSs to each cell is done on path loss alone. The general simulation parameters utilised for the simulation are shown in Table I.

B. Channel Model

In general, the channel gain, $G_{k,l}$, between a transmitter k and receiver l separated by d m is calculated as

$$G_{k,l} = |H_{k,l}|^2 \, 10^{\frac{-L(d)+X_\sigma}{10}}, \tag{16}$$

where $H_{k,l}$ describes the channel transfer function between transmitter k and receiver l, $L(d)$ is the distance-dependent path loss (in dB) and X_σ is the log-normal shadowing value (in dB) with standard deviation σ.

TABLE I
Simulation Parameters

Parameter	Value
ISD	200 m
Number of cells	19
Antenna tilt	5°
Users per cell, N	10
Number of available RBs, M	50
RB bandwidth, B_{RB}	180 kHz
Subcarriers per RB, k_{sc}	12
Symbol rate per subcarrier, ϱ_{s}	15 ksps
Time slots	6
Noise spectral density, η_0	-174 dBm/Hz
Total MS transmit power	10 dBm
Shadowing Std. Dev., σ	4 dB
Auto-correlation distance	50 m

The path loss model used to calculate $L(d)$ is for a purely outdoor link [9], *i.e.*, the link (desired or interfering) between a BS and an outdoor MS, and calculates the path loss as

$$L(d) = 15.3 + 37.6 \log_{10}(d) \quad [\mathrm{dB}]\,. \tag{17}$$

C. Scheduling and Power Allocation

For this study, MSs in a cell are assigned a contiguous equal-sized block of RBs, where each block contains $M/N = 50/10 = 5$ RBs. The scheduler assigns a block to each user in the cell. For POS, the scheduling and allocation of power to the users is performed as described in Section III-C. Furthermore, multiple time slots are utilised such that removed links can be scheduled in the next slot. For the benchmarks, a random resource allocation is utilised.

D. Performance Statistics

After the transmit powers adjustment in each cell, the performance statistics can be gathered. These are composed of two values: the uplink system spectral efficiency and energy efficiency. Given the SINR as calculated in (1), the throughput C_u of MS$_u$ using adaptive modulation and coding (AMC) is calculated

$$C_u(\gamma_u) = n_u^{\mathrm{RB}} k_{\mathrm{sc}} \varrho_{\mathrm{s}} \varepsilon_{\mathrm{s}}(\gamma_u)\ , \tag{18}$$

where n_u^{RB} is the number of RBs assigned to MS$_u$, k_{sc} the number of subcarriers per RB, ϱ_{s} the symbol rate per subcarrier, and $\varepsilon_{\mathrm{s}}(\gamma_u)$ the symbol efficiency[5].

The energy efficiency β_u measures the the data sent per unit of energy (or, alternatively, data rate per unit of transmit power) of MS$_u$. This is defined as follows:

$$\beta_u = \frac{C_u}{P_u} = \frac{n_u^{\mathrm{RB}} k_{\mathrm{sc}} \varrho_{\mathrm{s}} \varepsilon_{\mathrm{s}}}{P_u} \quad \left[\frac{\mathrm{bits/s}}{\mathrm{W}}\right] \equiv \left[\frac{\mathrm{bits}}{\mathrm{J}}\right], \tag{19}$$

where P_u is the total transmit power of MS$_u$, and C_u the throughput from (18).

V. Results

Fig. 3 shows the spectral efficiency results for POS and the two benchmarks in a macro-cellular network. As expected, the antenna downtilt and sectorisation decrease the spectral efficiency of all three systems (in comparison to Fig. 1) due

[5]The modulation and coding is taken from Long-Term Evolution (LTE) [10], and the SINR ranges from [11]. The downlink is used because no uplink implementation was found, as these values are operator specific.

to the increased interference among the cells and diminished desired path gains, respectively (the use of AMC is also significant). However, it is evident that POS benefits from this additional interference, as it is more able to mitigate it than the benchmark systems. In general, POS has a performance

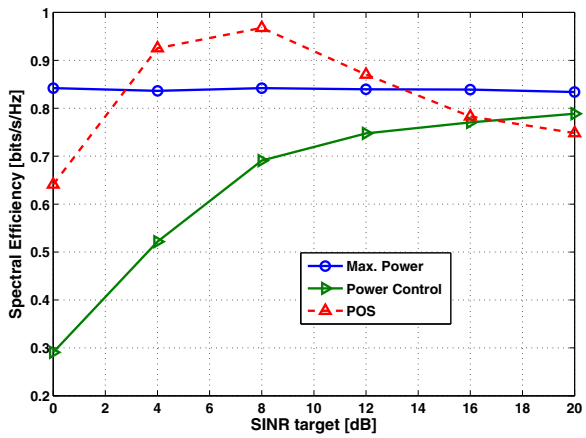

Fig. 3. System spectral efficiency results for the various power control techniques.

advantage over power control over all SINR targets (except γ^{*}=20 dB), whereas also substantial gains over 13 % are seen over max. power transmission in the mid-SINR (typically the operational) range. The POS performance begins to suffer for higher SINRs as too many users are switched off each time slot by the SR protocol. However, on average the POS spectral efficiency is equivalent to that of max. power transmission.

This becomes even more significant when considered together with the energy efficiency results shown in Fig. 4. As expected, maximum power transmission is the least energy efficient of the three considered techniques. POS, on the other hand, provides massive energy efficiency benefits for the system, even when compared to power control, with gains

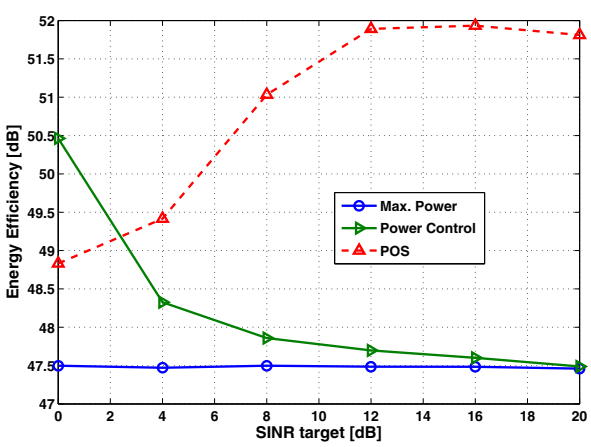

Fig. 4. System energy efficiency results for the various power control techniques. Decibel (dB), *i.e.*, $10\log_{10}(\text{bits}/\text{J})$, are utilised as the energy efficiency unit for ease of comparison.

of up to 5 dB for higher SINRs. Hence, it is quite clear that POS drastically reduces the transmit power consumption in a macro-cellular network. Considering this together with the spectral efficiency results, it is evident that POS provides overall superior system performance over the standard power allocation techniques.

VI. Conclusion

In this paper, POS, a scheduling technique designed to maximise the application of POPC, was introduced. By expressing the necessary conditions for power control in a simple feasibility condition of path gains and SINR targets, users are scheduled such that the Pareto optimal power control can be applied. The addition of the SR algorithm in collaboration with SINR target updates allow the scheduler to achieve the target system spectral efficiency, while providing a Pareto optimal power allocation. Therefore, no significant losses in spectral efficiency are incurred while the total transmit power of the network is minimised, hence resulting in a more energy efficient system.

It is quite clear from the simulation results that POS provides close to optimal spectral efficiency over a wide range of SINR targets, and can significantly outperform standard power control techniques. Furthermore, since the necessary calculations are performed at the BS-side, only minimal additional signalling between neighbouring BSs is required, while no extra information other than the resource and power allocation is sent to the MSs. Finally, POS provides large energy efficiency boosts over both power control and maximum power transmission, providing a low-power solution, and hence "greener" wireless systems.

References

[1] B. Badic, T. O'Farrell, P. Loskot, and J. He, "Energy Efficient Radio Access Architectures for Green Radio: Large versus Small Cell Size Deployment," in *Proc. of the 70th Vehicular Technology Conference*, Anchorage, Sep. 2009.

[2] C.-H. Lee and C.-J. Chang, "Performance Analysis of a Truncated Closed-loop Power-control Scheme for DS/CDMA Cellular Systems," *IEEE Transactions on Vehicular Technology*, vol. 53, no. 4, pp. 1149 – 1159, 2004.

[3] A. Rao, "Reverse Link Power Control for Managing Inter-Cell Interference in Orthogonal Multiple Access Systems," in *Proc of. Vehicular Technology Conference (VTC)*, Oct. 2007, pp. 1837 –1841.

[4] Z. Li, Y. Wang, and D. Yang, "A Novel Power Control Scheme in OFDMA Uplink," in *Proc. of International Conference on Signal Processing (ICSP)*, 2008, pp. 2880 –2883.

[5] L. K. Tee, C. van Rensburg, and J.-A. Tsai, "Uplink Power Control for an OFDMA Mobile Cellular System," in *Proc. of the Vehicular Technology Conference*, Baltimore, MD, Sep./Oct. 2007.

[6] D. Kivanc, G. Li, and H. Liu, "Computationally Efficient Bandwidth Allocation and Power Control for OFDMA," *IEEE Transactions on Wireless Communications*, vol. 2, no. 6, pp. 1150 – 1158, 2003.

[7] A. Goldsmith, *Wireless Communications*. Cambridge University Press, 2005.

[8] E. Jury, "A simplified stability criterion for linear discrete systems," *Proceedings of the IRE*, vol. 50, no. 6, pp. 1493 –1500, 1962.

[9] 3GPP, "Simulation Assumptions and Parameters for FDD HeNB RF Requirements," 3GPP TSG RAN WG4 R4-092042, May 2008. Retrieved Sep. 1, 2009 from www.3gpp.org/ftp/Specs/.

[10] S. Sesia, I. Toufik, and M. Baker, *LTE - The UMTS Long Term Evolution: From Theory to Practice*, 1st ed., S. Sesia, I. Toufik, and M. Baker, Eds. Wiley, 2009.

[11] EDX Wireless, "Designing an LTE network using EDX SignalPro," Technical white paper, march 2010, retrieved Jan. 17 2011. [Online]. Available: http://www.edx.com/resources/documents/

Pareto Optimal SINR Scheduling for Femto-cell Deployment in Wireless Networks

Harald Burchardt*, Sinan Sinanovic*, Gunther Auer† and Harald Haas*

*Institute for Digital Communications, Joint Research Institute for Signal and Image Processing,
The University of Edinburgh, EH9 3JL, Edinburgh, UK
Email: {h.burchardt, s.sinanovic, h.haas}@ed.ac.uk

†DOCOMO Euro-Labs, 80687 Munich, Germany,
Email: auer@docomolab-euro.com

***Abstract*—In this paper, Pareto Femto-Cell Scheduling (PFCS), a novel scheduling mechanism for randomly deployed femto-cells, is presented. Here, the signal-to-interference-plus-noise ratio (SINR) targets of femto-users are adapted such that the sufficient conditions for Pareto optimal power control (POPC) are fulfilled. Furthermore, interference from full bandwidth users is managed such that as many mobile stations (MSs) as possible can transmit. Due to the random nature of femto-base station (FBS) deployment, interference graphs are used to group femto-cells (and hence, users) such that target spectral efficiencies can be achieved at Pareto optimum power. Simulation results show that PFCS achieves significant system capacity gains over other SINR-target-based power allocation techniques, while maximising coverage in dense mobile environments. Furthermore, substantial power savings can be achieved.**

I. Introduction

For future wireless networks, there is an increasing demand for higher user and system throughput, along with growing expectation for all MSs in a cell to be available to multimedia and Internet services. This is especially difficult to maintain at the cell-edge. Furthermore, the necessity for more energy efficient, or "green," technologies is growing. Increasing traffic load is expected to double network energy consumption within the next ten years [1]. Inter-cell interference coordination (ICIC) mechanisms attempt to manage interference in order to maintain sufficient spectral efficiency for the users in the network. In this paper, a scheduling and power control technique that produces large energy savings while maintaining system capacity is developed.

Studies indicate that a substantial portion of wireless traffic originates indoors [2]. Poor signal reception through walls severely inhibits the operation of indoor data services, attracting considerable interest in the concept of femto-cells [3]. FBSs are low-cost, low-power, short range, plug-and-play base stations (BSs) which aim to extend and enhance macro-cell indoor coverage. While abundant research on femto-to-macro interference has been carried out [4, 5], few techniques have been considered to manage the interference between several densely deployed FBSs. In this paper, a power control scheme for such interference coordination is developed.

Initial work on power control for orthogonal frequency division multiple access (OFDMA) networks is presented in [6], where fractional power control (FPC) offers a modification to conventional power control to control the tradeoff between system capacity and cell-edge rate. Due to this, however, many users will not achieve their SINR targets, and hence user throughput can suffer. An extension to FPC is developed in [7], where the power control mechanism takes interference caused to neighbouring cells into account. While this achieves a modest capacity increase, only the variance of interference to other cells, rather than the mean, is reduced. Finally, in [8] a computationally efficient power control technique is introduced, where minimisation of transmit power is the main goal. However, by splitting the joint subcarrier and power allocation into two stages, the dependence between the two is disregarded, yielding suboptimal performance.

In this paper, a novel technique combining scheduling and power control for densely deployed femto-cells is considered, to not only minimise power consumption but also satisfy MS throughput requirements through fair interference management. The rest of the paper is structured as follows, Section II describes the system environment for this paper, and Section III describes the analytic basis and implementation of PFCS. Sections IV describes the simulation and results, and Section V offers a conclusion.

II. System Model

For this paper, a 5×5 apartment grid is considered for the femto-cell environment, where the probability p_{act} describes the likelihood of a given apartment containing an active FBS. In each active femto-cell, both the MS and FBS are uniformly distributed within the apartment. Due to the private deployment of femto-cells a closed-access system is assumed [9], and so each MS is assigned to the FBS in its apartment, even if a foreign femto-cell exhibits superior link conditions.

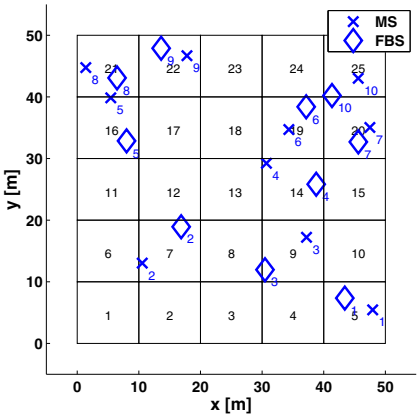

Fig. 1. Apartment block scenario with $p_{\mathrm{act}} = 0.4$, where each apartment is $R = 10\,\mathrm{m} \times 10\,\mathrm{m}$.

978-1-4673-1881-5/12/$31.00 ©2012 IEEE

A. Channel Model

In general, the channel gain, $G_{k,l}$, between a transmitter k and receiver l separated by d m is calculated as

$$G_{k,l} = |H_{k,l}|^2 \, 10^{\frac{-L(d)+X_\sigma}{10}}, \tag{1}$$

where $H_{k,l}$ describes the channel transfer function between transmitter k and receiver l, $L(d)$ is the distance-dependent path loss (in dB) and X_σ is the log-normal shadowing value (in dB) with standard deviation σ.

The path loss model used to calculate $L(d)$ is for a purely indoor link [10], *i.e.*, the link (desired or interfering) between a FBS and an indoor MS, and calculates the path loss as

$$L(d) = 127 + 30 \log_{10}(d_{\mathrm{km}}) \quad [\mathrm{dB}]\,. \tag{2}$$

where d_{km} is the distance d in km.

III. Pareto Optimal SINR Scheduling

For future wireless networks, ICIC plays an important role in not only satisfying individual MS requirements, but also maintaining system performance. An interference coordination technique is introduced that schedules MSs based on path gains such that POPC can be applied, and co-channel users can achieve their SINR targets with minimum transmit power.

A. Pareto Optimal Power Control

In POPC [11], given each link is assigned a SINR target, γ_i^*, the Pareto optimum transmit powers $\mathbf{P}^*=(P_1^*,\ldots,P_K^*)^T$ for a set of K interfering users (*i.e.*, in OFDMA, on the same resource blocks (RBs) in K different cells) are given by

$$\mathbf{P}^* = (\mathbf{I}-\mathbf{F})^{-1}\mathbf{u}, \qquad \text{iff} \quad \rho_F < 1\,, \tag{3}$$

where $\rho_F = \max_i |\lambda_i^{\mathbf{F}}|$ is the Perron-Frobenius eigenvalue of $\mathbf{F}$, $\mathbf{I}$ is the identity matrix,

$$\mathbf{u} = \left(\frac{(I_1+\eta)\gamma_1^*}{G_{1,v_1}}, \cdots, \frac{(I_K+\eta)\gamma_K^*}{G_{K,v_K}} \right)^T, \tag{4}$$

is the vector of interference (I_i) plus noise power scaled by the SINR targets and channel gains G_{i,v_j} from MS_i to FBS_{v_j}, and $\mathbf{F}$ is the interference matrix where

$$F_{ij} = \begin{cases} 0, & \text{if } i=j \\ \frac{\gamma_i^* G_{j,v_i}}{G_{i,v_i}}, & \text{if } i \neq j \end{cases} \tag{5}$$

with $i,j=1,\ldots,K$. $\mathbf{F}$ is non-negative and irreducible [11]. Hence, when POPC is applied, users can meet their γ_i^* with minimal transmit power.

B. Stepwise Removal (SR)

In POPC, if $\rho_F \not< 1$, no solution is available, and hence $\mathbf{P} \to \mathbf{0}$. A better way to address this problem is to successively remove single links from the group of interfering MSs, until an $\mathbf{F}$ is achieved with $\rho_F<1$. It makes sense to remove the link that is causing the most interference to the other users. It is clear, however, that turning off one of the links will harm the system spectral efficiency. Hence, for each link removal, the SINR target for the remaining links must be updated.

$$\gamma^*_{(1),\mathrm{up}} = \frac{\prod_j^K \left(1+\gamma_j^*\right)}{1+\gamma^*_{(2),\mathrm{up}}} - 1\,, \tag{6}$$

where $\gamma^*_{(i),\mathrm{up}}$ represents the updated SINR target of the ith *remaining* link. Since (6) has infinite solutions, an additional condition on $\gamma^*_{(1),\mathrm{up}}$ and $\gamma^*_{(2),\mathrm{up}}$ such as a power minimisation

$$\text{Solve (6) s.t.} \qquad \min\left\{\gamma^*_{(1),\mathrm{up}} + \gamma^*_{(2),\mathrm{up}}\right\}, \tag{7}$$

or an equal absolute SINR increase

$$\text{Solve (6) s.t.} \qquad \gamma^*_{(1),\mathrm{up}} - \gamma^*_{(1)} = \gamma^*_{(2),\mathrm{up}} - \gamma^*_{(2)}\,, \tag{8}$$

is necessary.

C. Pareto Optimal Scheduling (POS)

As can be seen, POPC is dependent on $\rho_F<1$, *i.e.*, on $\mathbf{F}$, and hence on the positions/gains/SINRs of the interfering MSs. Therefore, by preemptively scheduling users specifically such that $\rho_F<1$, POPC can be applied to most, if not all, MSs in the system. This is the aim of Pareto Optimal Scheduling (POS).

Since for a particular grouping of MSs to be feasible $\rho_F<1$, it follows the modulus of all eigenvalues λ_i of $\mathbf{F}$ must also be less than unity, *i.e.*, $|\lambda_i|<1$, $\forall i=1,\ldots,K$. In other words, all eigenvalues must lie within the unit circle. In [12], Jury provides a simplified analytic test of stability of linear discrete systems, *i.e.*, the necessary and sufficient conditions for any real polynomial to have all its roots inside the unit circle. Hence, this test can be directly applied to the characteristic function $f_{\mathbf{F}}(\lambda)$ of the matrix $\mathbf{F}$, whose roots are the eigenvalues of $\mathbf{F}$. The characteristic function of $\mathbf{F}$ can be expressed as follows:

$$\begin{aligned} \text{Given} \qquad f_{\mathbf{F}_3}(\lambda) &= \det(\mathbf{F}-\lambda\mathbf{I}) \\ &= -\lambda^3 + \lambda(F_{12}F_{21}+F_{13}F_{31}+F_{23}F_{32}) \\ &\quad + F_{12}F_{23}F_{31} + F_{13}F_{21}F_{32} \qquad (9) \\ &= \lambda^3 + c\lambda + d \qquad (10) \\ \text{Hence} \qquad c &= -F_{12}F_{21} - F_{13}F_{31} - F_{23}F_{32} \\ d &= -F_{12}F_{23}F_{31} - F_{13}F_{21}F_{32} \end{aligned}$$

In [12], the stability constraints for a polynomial of order $K=3$ are given[1]. Applying these to the characteristic function yields that for $f_{\mathbf{F}_3}(\lambda)$ to be "stable,"

$$\begin{aligned} & f_{\mathbf{F}_3}(\lambda) = \lambda^3 + c\lambda + d \\ & \quad a_3 = 1,\ a_2 = 0,\ a_1 = c,\ a_0 = d, \\ & \quad 1)\ \ |d| < 1 \\ & \quad 2)\ \ d^2 - 1 < c \ \rightarrow\ c > 1 - d^2 \\ & \quad 3)\ \ d + c + 1 > 0 \ \rightarrow\ c > -d - 1, \\ & \quad\quad d - c - 1 < 0 \ \rightarrow\ c > d - 1 \end{aligned} \tag{11}$$

which describes the ranges of c and d for which $\mathbf{F}$ is feasible. However, since from (5) $F_{ij}\geq 0$, $\forall i,j$, it is clear that both $c,d\leq 0$, and the constraints are reduced to only a single one, such that the **feasibility condition** becomes:

$$\begin{aligned} & 3)\quad c > -d - 1 \\ & \textbf{So, } \rho_F<1 \textbf{ if:} \\ & F_{12}F_{21} + F_{13}F_{31} + F_{23}F_{32} + F_{12}F_{23}F_{31} + F_{13}F_{21}F_{32} < 1\,. \end{aligned} \tag{12}$$

[1] $K=3$ cells are chosen for complexity reasons. For $K>3$, the stability conditions and hence the derivation of POS become highly complex, and is practically intractable.

So, a group of MSs, one in each cell (in the three-cell scenario), is feasible iff the condition in (12) is fulfilled. This is clearly dependent on the individual desired and interfering path gains, along with the SINR targets of the users.

1) Feasibility for $K-1=2$: In the case that the scheduler is unable to find feasible groups for particular MSs (due to *e.g.*, location at cell-edge), the SR algorithm from Section III-B would turn off one of the links in a group of MSs, resulting in a feasibility matrix $\mathbf{F}$ of size $K-1\times K-1$, in the three-cell case 2×2. Using the stability conditions from [12], the **feasibility condition** for two links is given by

$$\rho_F<1 \quad \text{if} \quad F_{12}F_{21}<1\,. \tag{13}$$

D. Pareto Femto-Cell Scheduling (PFCS)

POS is dependent on many users per cell to be able to iterate over multiple path gain combinations and, hence, find feasible MS-groups in these cells. In the femto-cell environment considered here, however, each cell contains only a single user, and hence in any grouping of three cells the users in these cells will directly form a MS-group. Now if this group is infeasible, then there is no possibility of a different (feasible) group being formed, and at least one link must be removed. Therefore, the SINR targets of the individual users must be varied such that $\mathbf{F}$ becomes feasible.

1) SINR Variation: In PFCS, the same feasibility conditions for $\mathbf{F}$ still apply, *i.e.*, (12) and (13). Hence, an intelligent mechanism for the variation of the individual SINRs must be formulated. This is done using the feasibility condition (12) for the case where all three MSs (*i.e.*, one in each cell) transmit:

$$\begin{aligned} f(\mathbf{F}) =& F_{12}F_{21}+F_{13}F_{31}+F_{23}F_{32}+F_{12}F_{23}F_{31}+F_{13}F_{21}F_{32} \\ =& \gamma_1^*\gamma_2^*\left(\rho^2\frac{G_{1,v_2}G_{2,v_1}}{G_{1,v_1}G_{2,v_2}}\right)+\gamma_1^*\gamma_3^*\left(\rho^2\frac{G_{1,v_3}G_{3,v_1}}{G_{1,v_1}G_{3,v_3}}\right)+ \\ &+\gamma_2^*\gamma_3^*\left(\rho^2\frac{G_{2,v_3}G_{3,v_2}}{G_{2,v_2}G_{3,v_3}}\right)+ \\ &+\gamma_1^*\gamma_2^*\gamma_3^*\left(\rho^3\frac{G_{1,v_2}G_{2,v_3}G_{3,v_1}+G_{1,v_3}G_{2,v_1}G_{3,v_2}}{G_{1,v_1}G_{2,v_2}G_{3,v_3}}\right) \\ =& \gamma_1^*\gamma_2^*A_{12}+\gamma_1^*\gamma_3^*A_{13}+\gamma_2^*\gamma_3^*A_{23}+\gamma_1^*\gamma_2^*\gamma_3^*A_{123} \end{aligned} \tag{14}$$

where $\mathcal{A}=\{A_{12},A_{13},A_{23},A_{123}\}$ is the set of coefficients of f that are constant throughout the SINR variation. Therefore if $f(\mathbf{F})>1$, by finding $\max\{\mathcal{A}\}$ the largest coefficient can be found, and hence the SINR targets preceding the coefficient can be reduced to ultimately decrease $f(\mathbf{F})$.

Given $f(\mathbf{F})>1$ and $\max\{\mathcal{A}\}=A_{ij}$, it is clear that γ_i^* and γ_j^* need to be reduced such that $f(\mathbf{F})<1$. The reduction is performed as follows:

$$\begin{aligned} r &= \frac{1}{10n_r}\left\lceil 10\left(1-\frac{1}{f(\mathbf{F})}\right)\right\rceil \\ \gamma_i^* &\leftarrow \gamma_i^*(1-r) \\ \gamma_j^* &\leftarrow \gamma_j^*(1-r) \end{aligned} \tag{15}$$

where r in (15) represents the SINR reduction factor rounded[2] up to a factor of .1, and n_r denotes the number of MSs whose SINR targets are being reduced (in the above case, $n_r=2$). To maintain the desired system spectral efficiency however, the remaining user's SINR target must be increased

$$\gamma_{k\neq\{i,j\}}^* = \frac{(1+\gamma_1^*)(1+\gamma_2^*)(1+\gamma_3^*)}{(1+\gamma_i^*(1-r))(1+\gamma_j^*(1-r))}-1\,. \tag{16}$$

Hence, the system spectral efficiency is maintained while the value of $f(\mathbf{F})$ is decreased. Although this procedure may achieve the desired SINR target constellation in the first step, is repeated until either $\gamma_i^*,\gamma_j^*<\gamma_{\min}$, or $f(\mathbf{F})<1$.

For the (rather unlikely) case that $\max\{\mathcal{A}\}=A_{123}$, the strongest interferer MS_i is found, and the same reduction is performed except $n_r=1$ in (15). The SINR target increase of the remaining MSs is

$$\gamma_{\{j,k\}\neq i}^* = \sqrt{\frac{(1+\gamma_1^*)(1+\gamma_2^*)(1+\gamma_3^*)}{(1+\gamma_i^*(1-r))}}-1\,. \tag{17}$$

a) Feasibility for $K-1=2$: For the occasion that the scheduler is unable to find a set of $\{\gamma_1^*,\gamma_2^*,\gamma_3^*\}\geq\gamma_{\min}$ such that $\mathbf{F}$ becomes feasible (*i.e.*, $f(\mathbf{F})<1$), the link causing the most interference is removed, and the SINR targets of the two remaining users are updated according to the SR algorithm.

If, now, the feasibility condition (13) is not satisfied, the SINR target of the MS_i with the weaker desired channel gain must be reduced according to (15) with $n_r=1$, while MS_j with the stronger desired link receives a SINR target boost according to

$$\gamma_j^* = \frac{(1+\gamma_i^*)(1+\gamma_j^*)}{1+\gamma_i^*(1-r)}-1\,, \tag{18}$$

to maintain the system spectral efficiency[3]. This is again repeated until either $\gamma_i^*<\gamma_{\min}$, or $f(\mathbf{F})<1$.

Finally, if the scheduler is unable to find $\{\gamma_i^*,\gamma_j^*\}\geq\gamma_{\min}$ such that $\mathbf{F}$ is feasible, the MS with the weaker desired link is removed, and the target of the remaining user is again updated.

2) Scheduling: While it is clear from Section III-D1 how an infeasible grouping of MSs can be made feasible, these groups must still be found. In a randomly deployed femto-cell environment, this can be a challenging task as there is no pre-existing infrastructure to guide grouping mechanisms. Here, the cell-grouping part of PFCS is described.

a) Interference Graphs: To find groups of femto-cells suitable for POPC, an interference graph [13] for the network instance is constructed, through which the strongest interfering cells can be grouped together. An interference graph is constructed by evaluating the interference users in the system cause to each other. For each MS, the strongest interferers are removed (and consequently considered as interfering neighbours) until the minimum signal-to-interference ratio (SIR), γ^*, at the MS is achieved.

Assuming each MS will transmit at maximum power, $P=P_{\max}$, each user will achieve a certain SIR. If the SIR

[2]The need for this rounding is two-fold; first, since $f(\mathbf{F})$ must be <1, without the rounding it would be steered towards 1 and not below, and second, because the SINR boost of the third MS will again slightly increase $f(\mathbf{F})$.

[3]The MS with the stronger desired link is chosen for the SINR target boost as it will require less power than the weaker MS to achieve it due to its enhanced desired channel gain, and hence cause less interference. This slightly reduces the fairness over a single slot, however through scheduling over multiple slots this is equalised

of MS_k, $\gamma_k < \gamma_k^*$, the strongest interferers are removed until

$$\gamma_k = \frac{S_k}{\sum_{l \in \mathcal{I}_k \setminus \mathcal{W}_k} I_{l,k}} \geq \gamma_k^* \,, \tag{19}$$

where S_k is the desired received signal strength of MS_k, $I_{l,k}$ the interference caused by MS_l at MS_k's BS, $\mathcal{I}_k$ all its interferers, and $\mathcal{W}_k$ the removed interferers, *i.e.*, neighbours. Hence, each user will have a list of strongly interfering neighbours based on its interference environment, and if MS_l is a neighbour of MS_k, the vice versa is also true.

Once this procedure has been done for all MSs in the system, the interference graph can be constructed, an example of which is shown in Fig. 2. From this, groups of (up to) three femto-

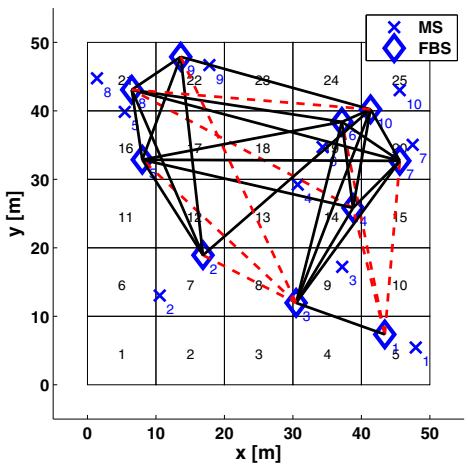

Fig. 2. Interference graphs for the (in Fig. 1) given 5×5 grid femto-cell scenario for various SINR targets. The solid lines indicate neighbours for $\gamma^* = 0$ dB, the dashed lines indicate the additional neighbours when $\gamma^* = 8$ dB.

cells (and hence the three MSs in these cells) are formed by collecting the three strongest interfering and neighbouring cells together, and then the next, and so on. For cells with fewer than two neighbours, smaller groups are formed.

b) SINR and Power Allocation: As a result of the interference graph grouping, each MS will be able to remove two of its strongest interferers through POPC and SINR variation, if necessary. The SINR target and transmit power allocation for each group is performed as follows:

1) If (12) is satisfied, then (3) (POPC) can be performed and each MS should achieve its SINR target.
2) If (12) fails, then $\max\{\mathcal{A}\}$ is found, and the γ_k^* are modified by (15) and (16) (or (17) if $\max\{\mathcal{A}\} = A_{123}$) until (12) is satisfied and (3) can be used.
3) If this is not possible, the strongest interfering link is removed, and (13) must be satisfied (with updated γ_k^* due to SR) in order for (3) to be applied.
4) If (13) fails, then the γ_k^* are adjusted through (15) and (18) until (13) is satisfied and (3) can be utilised.
5) If this is again not possible, then a second link is removed, and (3) (which converges to conventional power control for a single user) is performed for updated γ_k^*.

Through this power allocation, the number of simultaneously serviced (*i.e.*, $\gamma_k \geq \gamma_k^*$) MSs in the system will be maximised, along with the achievable throughput.

IV. Simulation and Results

Monte Carlo simulations are used to provide mean performance statistics of the achieved capacities of the system with and without the use of PFCS.

A. Simulation

The system and channel model for the simulation are detailed in Section II; multiple randomly deployed femto-cell networks are generated such that precise performance statistics can be acquired.

1) Scheduling and Power Allocation: For this study, each MS in a cell is assigned the full bandwidth (*i.e.*, all RBs), as only a single MS per cell is considered. For PFCS, the cell-grouping and allocation of power to the users is performed as described in Section III-D2. Furthermore, the simulation is run over multiple time slots, such that removed links can be scheduled in later slots and achieve capacity.

2) Performance Statistics: After the power allocation in each cell, the performance statistics can be gathered. These are composed of two values: the system throughput and power usage. First, the SINR, γ_u, of MS_u is calculated as

$$\gamma_u = \frac{P_u G_{u,v_u}}{\sum_k P_k G_{k,v_u} + \eta} \,, \tag{20}$$

where P_u and P_k are the transmit powers of MS_u and interfering MSs, respectively. Given the SINR, the throughput C_u of MS_u, using adaptive modulation and coding, is calculated

$$C_u(\gamma_u) = n_u^{\mathrm{RB}} k_{\mathrm{sc}} \varrho_{\mathrm{s}} \varepsilon_{\mathrm{s}}(\gamma_u) \,, \tag{21}$$

where n_u^{RB} is the number of RBs assigned to MS_u, k_{sc} the number of subcarriers per RB, ϱ_{s} the symbol rate per subcarrier, and $\varepsilon_{\mathrm{s}}(\gamma_u)$ the symbol efficiency[4].

The total system transmit power is calculated as a sum of the individual MS transmit powers.

B. Results and Discussion

The general simulation parameters are shown in Table I. In

TABLE I
Simulation Parameters

Parameter	Value
Apartment width, R	10 m
FBS probability, p_{act}	0.5
Number of available RBs, M	50
RB bandwidth, B_{RB}	180 kHz
Subcarriers per RB, k_{sc}	12
Symbol rate per subcarrier, ϱ_{s}	15 ksps
Time slots	6
Minimum SINR, $\gamma_{\min}$	-6 dB
Thermal noise, η	-174 dBm/Hz
Total MS transmit power	10 dBm
Shadowing Std. Dev., σ	10 dB
Auto-correlation distance	50 m

Fig. 3, the system throughputs for maximum power, PFCS, and LTE FPC [6] are shown. Here PFCS produces large gains over conventional power control ($\alpha = 1$), but does not achieve quite the system capacities of the other systems. It should be

[4]The modulation and coding is taken from Long-Term Evolution (LTE) [14], and the SINR ranges from [15]. The downlink is used because no uplink implementation was found, as these values are operator specific.

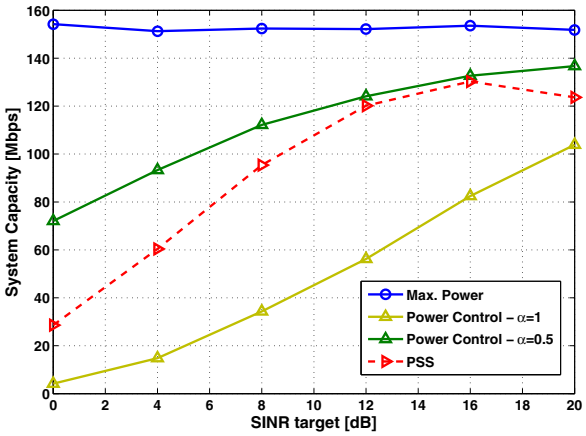

Fig. 3. System capacity results for the various power control techniques over a range of SINR targets.

mentioned here that the comparisons to both maximum power transmission and $\text{FPC}_{\alpha=0.5}$ are rather unfair, as these are based much less on the actual SINR targets of the users (in the case of max. power not at all), and hence use significantly more power to achieve their larger system throughputs.

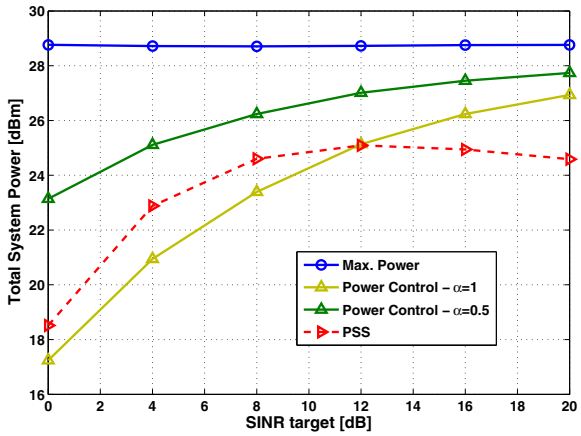

Fig. 4. System power results for the various power control techniques.

This is very clear in Fig. 4, where both maximum power and $\text{FPC}_{\alpha=0.5}$ consume considerably more power in the network than PFCS. Furthermore, while for low SINRs $\text{FPC}_{\alpha=1}$ shows some power savings (which is expected due to the low capacity achieved), for the higher SINR targets PFCS utilises the least amount of system power. This is mainly because less links are transmitting in each time slot (due to SR), and hence less power is spent while still achieving respectable system throughputs, an encouraging result. For the other systems, it is clear that $\text{FPC}_{\alpha=0.5}$ achieves a balance between max. power and $\text{FPC}_{\alpha=1}$ in all of the performance statistics. All in all, PFCS provides significant throughputs for almost all MSs in the system while minimising the necessary transmit power.

V. Conclusion

In this paper, PFCS, a scheduling technique designed to maximise the application of POPC in femto-cells, is developed. POS, the basis of PFCS, schedules users according to path gains such that POPC can be directly applied. As only a single MS per femto-cell is assumed, the path gains cannot be modified, and hence a technique to adapt the SINR targets of the users was developed to make infeasible groupings feasible. Through this, MSs are allocated Pareto optimal transmit powers while limited losses in spectral efficiency are incurred.

It is quite clear from the simulation results that PFCS provides substantial throughputs over a wide range of SINR targets, and significantly outperforms the purely target-based power control technique. Both max. power transmission and $\text{FPC}_{\alpha=0.5}$ are not strictly bound by SINR targets, and hence are able to transmit with higher power and achieve larger throughputs. On the other hand, it is evident that PFCS provides a low-power solution, significantly reducing the necessary MS transmit powers, creating a "greener" system.

References

[1] B. Badic, T. O'Farrell, P. Loskot, and J. He, "Energy Efficient Radio Access Architectures for Green Radio: Large versus Small Cell Size Deployment," in *Proc. of the 70th Vehicular Technology Conference*, Anchorage, Sep. 2009.

[2] V. Chandrasekhar, J. Andrews, and A. Gatherer, "Femtocell Networks: A Survey," *IEEE Communications Magazine*, vol. 46, no. 9, pp. 59–67, 2008.

[3] H. Claussen, "Performance of Macro- and Co-Channel Femtocells in a Hierarchical Cell Structure," in *Proc. of the 18th IEEE International Symposium on Personal, Indoor and Mobile Radio Communications (PIMRC)*, Athens, Greece, Sep. 3–7 2007, pp. 1–5.

[4] H. Haas and G. J. R. Povey, "The effect of adjacent channel interference on capacity in a hybrid TDMA/CDMA-TDD system using UTRA-TDD parameters," in *Proc. of the 50th IEEE Vehicular Technology Conference (VTC)*, vol. 2, Amsterdam, Sep. 1999, pp. 1086–1090.

[5] Z. Bharucha, A. Saul, G. Auer, and H. Haas, "Dynamic Resource Partitioning for Downlink Femto-to-Macro-Cell Interference Avoidance," *EURASIP Journal on Wireless Communications and Networking (special issue on Femtocell Networks)*, vol. 2010, no. Article ID 143413, pp. 1–12, May 2010. [Online]. Available: http://www.hindawi.com/journals/wcn/2010/143413.html

[6] A. Rao, "Reverse Link Power Control for Managing Inter-Cell Interference in Orthogonal Multiple Access Systems," in *Proc of. Vehicular Technology Conference (VTC)*, Oct. 2007, pp. 1837 –1841.

[7] Z. Li, Y. Wang, and D. Yang, "A Novel Power Control Scheme in OFDMA Uplink," in *Proc. of International Conference on Signal Processing (ICSP)*, 2008, pp. 2880 –2883.

[8] D. Kivanc, G. Li, and H. Liu, "Computationally Efficient Bandwidth Allocation and Power Control for OFDMA," *IEEE Transactions on Wireless Communications*, vol. 2, no. 6, pp. 1150 – 1158, 2003.

[9] Z. Bharucha, H. Haas, A. Saul, and G. Auer, "Throughput Enhancement through Femto-Cell Deployment," *European Transactions on Telecommunications*, vol. 21, no. 4, pp. 469–477, Mar. 31 2010, (invited). [Online]. Available: http://www.interscience.wiley.com

[10] *Channel Models for Femtocell*, retrieved May 2010, from: www.3gpp.org/ftp/Specs/, 3GPP TSG RAN1 WG1 Std. 59, Rev. R1-100560.

[11] A. Goldsmith, *Wireless Communications*. Cambridge University Press, 2005.

[12] E. Jury, "A simplified stability criterion for linear discrete systems," *Proceedings of the IRE*, vol. 50, no. 6, pp. 1493 –1500, 1962.

[13] M. Necker, "A graph-based scheme for distributed interference coordination in cellular ofdma networks," in *Vehicular Technology Conference, 2008. VTC Spring 2008. IEEE*, may 2008, pp. 713 –718.

[14] S. Sesia, I. Toufik, and M. Baker, *LTE - The UMTS Long Term Evolution: From Theory to Practice*, 1st ed., S. Sesia, I. Toufik, and M. Baker, Eds. Wiley, 2009.

[15] EDX Wireless, "Designing an LTE network using EDX SignalPro," Technical white paper, march 2010, retrieved Jan. 17 2011. [Online]. Available: http://www.edx.com/resources/documents/

Distributed and Autonomous Resource Allocation for Femto-Cellular Networks

Harald Burchardt*, Zubin Bharucha† and Harald Haas*

*Institute for Digital Communications, Joint Research Institute for Signal and Image Processing,
The University of Edinburgh, EH9 3JL, Edinburgh, UK
Email: {h.burchardt, h.haas}@ed.ac.uk

†DOCOMO Euro-Labs, 80687 Munich, Germany,
Email: bharucha@docomolab-euro.com

***Abstract*—A distributed and autonomous technique for resource and power allocation in femto-cell networks is presented. Resource blocks (RBs) are assigned to the user(s) in each cell individually without coordination between base stations (BSs). The allocatability of each resource is determined using only local information:**

- **the user's required rate;**
- **the quality of the desired signal;**
- **the level of interference incident on each RB; and**
- **the frequency-selective fading on each RB.**

Using fuzzy logic, these inputs are combined to determine which RBs are most suitable for allocation in a particular cell. A comprehensive study of this system yields a staggering system performance improvement over state-of-the-art interference coordination techniques.

I. Introduction

Future wireless communications systems are moving towards heterogeneous architectures, where within a cell there may be many different access points (APs) (*e.g.*, macro-, pico-, femto-cells, and/or relays) [1]. Intuitively, this has many positive effects for a mobile station (MS), which can now choose among several connections to find the most suitable. However, pico/femto-cellular overlays also create many challenges, *e.g.*, cell-organisation/optimisation, resource assignment, and especially interference coordination between APs [1–3]. Furthermore, due to unplanned deployment, closed-subscriber access, and backhaul difficulties, traditional inter-cell interference coordination (ICIC) techniques only go so far in dealing with these new challenges. These issues motivate the need for ***decentralised, autonomous*** interference coordination operating independently on each cell, utilising only local information, yet achieving an efficient/near-optimal solution for the entire network.

II. System Model

A 5×5 apartment grid models the femto-cell environment, where p_{act} describes the probability of a given apartment containing an active femto-base station (FBS). In each active femto-cell, the MS and FBS are uniformly distributed within the apartment. Moreover, a closed-access system is assumed [4], and so each MS is assigned to the FBS in its apartment, even if a foreign femto-cell exhibits superior link conditions.

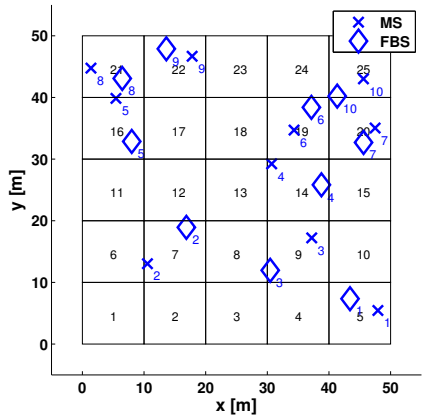

Fig. 1. Apartment block scenario with $p_{\text{act}} = 0.4$, where each apartment is $10\,\text{m}\times10\,\text{m}$.

III. Distributed and Autonomous Resource Allocation

Due to the customer-side random deployment of femto-cells, and the resulting lack of fixed connective infrastructure, there is no guarantee FBSs can communicate over a wired backbone. Hence, FBSs must perform resource and power allocation utilising locally available information only. To maximise cell performance, an FBS must allocate RBs such that the desired signal is maximised, while the interference incident from neighbouring cells is minimal. Furthermore, the BS must allocate enough resources to fulfil the rate requirements of its user(s). The necessary information is therefore clearly determined:

- the required rate of the user determines the number of RBs that need to be assigned;
- the quality (*i.e.*, strength) of the desired signal dictates the necessary transmit power;
- the level of interference incident on the RBs strongly influences the allocatability of each RB; and
- the frequency-selective fading profile also affects a RB's preferability.

These variables are locally available at the FBS in the reverse link, and at the MS(s) in the forward link, necessitating no extra information exchange between BSs.

A. Fuzzy Logic ICIC

The decision system is shown in Fig. 2. A fuzzy logic system evaluates which RB(s) are most suitable to be allocated to the MS, and determines the transmit power(s) needed to generate the required signal-to-interference-plus-noise ratio (SINR) such that the user's rate can be met. Obviously, an RB receiving little or no interference situated in a fading peak is most suitable for allocation, whereas any RB(s) experiencing high interference, or deep fades, are much less appropriate.

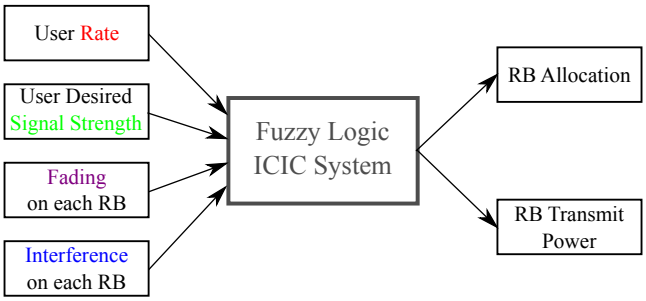

Fig. 2. Simplified graphical representation of the fuzzy logic autonomous resource and power allocation technique.

In fuzzy logic, an input range is divided into "membership functions" which give a coarse evaluation of the variable. For example, the level of interference can be qualified as "high," "low," or "medium" (shown in Fig. 3), which are determined through analysis of the input distribution[1]. By combining the membership values of the inputs through various rules, the allocatability of each RB is determined. The output is also "fuzzy," indicating how suitable an RB is to be allocated, avoiding a hard yes/no decision. Through this, a scheduler can allocate the "most appropriate" RBs.

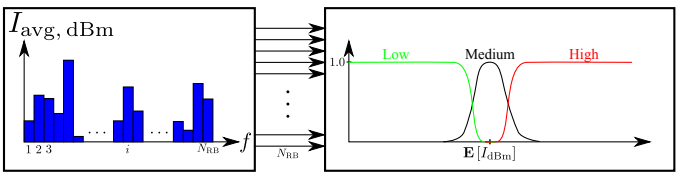

(a) RB Interference

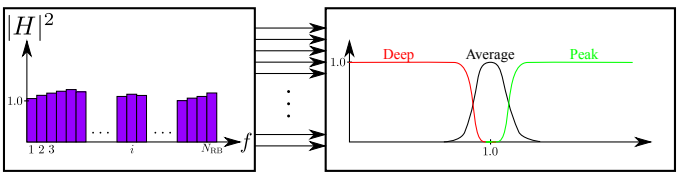

(b) RB Fading

Fig. 3. Examples of fuzzification and membership functions of two system inputs.

In each time slot, the FBS allocates the most applicable RBs to the MS. After data transmission is performed, the BS updates its information to more accurately represent the long-term communication environment of its cell. This is then used in the next time slot to, hopefully, improve the resource allocation. The same operation is performed in all femto-cells, and the RB allocations are individually optimised until the system converges to a stable solution.

[1]Details of the membership function assignment will be provided in the full paper.

IV. Simulation and Results

A. Simulation

Monte Carlo simulations are used to provide mean performance statistics of the system with and without the use of fuzzy logic ICIC.

1) User Requirements: Each MS is assigned a desired throughput requirement. The user's desired rate r_u^* is drawn from a random distribution[2] with mean $\bar{R}$, hence each MS_u requires a different number of RBs n_u^{RB}. Thus, the system will function best when strongly interfering FBSs are assigned orthogonal resources.

2) Performance Statistics: These are composed of two values: the system throughput and energy efficiency. The MS throughput C_u is calculated as the data transmitted on the assigned RBs that have achieved their SINR target γ_u^*. The system throughput is the sum of user throughputs. The energy efficiency β measures the data sent in the system per unit of energy expended.

3) Benchmarks: The performance benchmarks for the fuzzy logic system are *random almost-blank subframe (ABS) transmission* and *maximum power transmission*.

B. Results and Discussion

The simulation parameters are shown in Table I. It is clear

TABLE I
SIMULATION PARAMETERS

Parameter	Value
Apartment width, W	10 m
FBS probability, p_{act}	0.5
Number of available RBs, N_{RB}	50
RB bandwidth, B_{RB}	180 kHz
Average rate, $\bar{R}$	1.25 Mbps
Subcarriers per RB, k_{sc}	12
Symbol rate per subcarrier, ϱ_{s}	15 ksps
Time slots	25
Modulation orders, ε_{s}	$\{1, 2, 3, 4\}$ bits/sym
Target SINR, γ^*	$\{1, 8, 12, 15\}$ dB
ABS prob., Γ_{ABS}	0.1
Thermal noise, η	-174 dBm/Hz
Total MS transmit power	10 dBm
Shadowing Std. Dev., σ	10 dB
Auto-correlation distance	50 m

from Fig. 4 that fuzzy logic ICIC provides substantially improved system throughput performance over both benchmarks. It is the only technique which achieves the overall desired rate (*i.e.*, sum of individual desired rates), and provides 21% and 31% gains over maximum power and ABS transmission, respectively. These gains arise from fuzzy logic applying dynamic spatial reuse of resources, minimising interference and maximising signal strength in each cell, resulting in

[2]The distribution can be selected depending on the scenario and traffic/applications (*i.e.*, internet, mobile TV, etc.) desired by the users. This will be described in more detail in the full paper.

MSs transmitting on interference-free RBs. After multiple time slots, fuzzy logic reaches the maximum achievable rate, indicating a system-optimal solution.

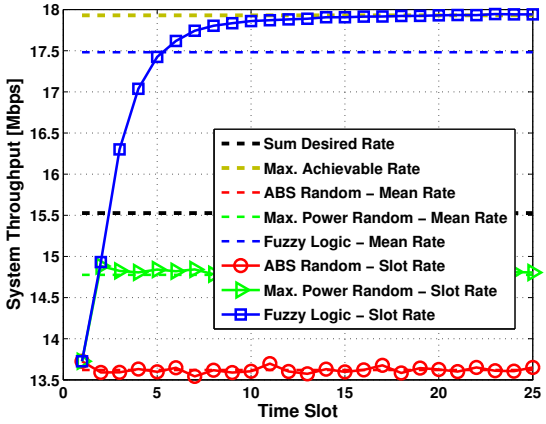

Fig. 4. System throughput results of fuzzy logic ICIC and the benchmarks.

Fig. 5 displays the energy efficiency of the simulated scenario, yielding again very dominant results of the fuzzy logic system, showing gains of $\approx 13\%$ over both benchmarks. Furthermore, the high energy efficiency is achieved quite rapidly, an encouraging result.

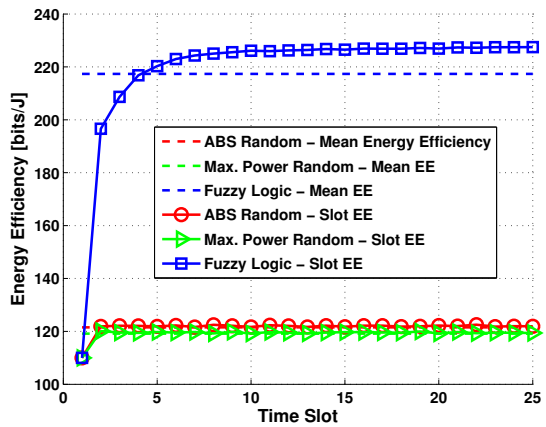

Fig. 5. System energy efficiency results of fuzzy logic ICIC and the benchmarks.

V. Conclusion

In this paper, a distributed and autonomous ICIC technique for femto-femto interference management and resource allocation is presented. At each FBS, local information is utilised to evaluate the allocatability of available RBs, taking into account the interference neighbourhood, user rates, and own-cell signal and fading environments. Fuzzy logic combines these inputs based on RB allocation rules, and submits to the BS the most suitable resources and transmit powers for successful communication. After several time slots, the locally optimised resource allocations form a near-optimal global solution, without any explicit communication between BSs.

References

[1] D. Lopez-Perez, I. Guvenc, G. de la Roche, M. Kountouris, T. Quek, and J. Zhang, "Enhanced intercell interference coordination challenges in heterogeneous networks," *Wireless Communications, IEEE*, vol. 18, no. 3, pp. 22 –30, june 2011.

[2] R. Madan, J. Borran, A. Sampath, N. Bhushan, A. Khandekar, and T. Ji, "Cell association and interference coordination in heterogeneous lte-a cellular networks," *Selected Areas in Communications, IEEE Journal on*, vol. 28, no. 9, pp. 1479 –1489, december 2010.

[3] S.-M. Cheng, S.-Y. Lien, F.-S. Chu, and K.-C. Chen, "On exploiting cognitive radio to mitigate interference in macro/femto heterogeneous networks," *Wireless Communications, IEEE*, vol. 18, no. 3, pp. 40 –47, june 2011.

[4] Z. Bharucha, H. Haas, A. Saul, and G. Auer, "Throughput Enhancement through Femto-Cell Deployment," *European Transactions on Telecommunications*, vol. 21, no. 4, pp. 469–477, Mar. 31 2010, (invited). [Online]. Available: http://www.interscience.wiley.com

Multi-Cell Cooperation: Evolution of Coordination and Cooperation in Large-Scale Cellular Networks

Harald Burchardt* and Harald Haas*
*University of Edinburgh

May 25, 2012

Abstract

Due to the large growth of mobile communications over the past two decades, the supporting cellular systems have continuously needed to expand and evolve in order to meet the ever-increasing demand of wireless connections. While simple frequency reuse and power control were enough to manage the demand of these networks at first, multicellular cooperation and coordination have become paramount to the operation of larger and more highly utilised communication systems. This article discusses the development of different techniques for cooperation in large cellular networks, and offers insights into the need for such an evolution. We investigate various branches of multi-cell cooperation, including user-based cooperation, system-wide optimisation, and the opportunity of multiple base station (BS) transmission. Furthermore, we offer an example of a recently proposed technique designed for multi-cell cooperation in full frequency reuse orthogonal frequency division multiple access (OFDMA) networks.

1 Introduction

Since the introduction of mobile technologies over two decades ago, wireless communication has evolved into a utility similar to water and electricity, needed by almost all people of todays modern society. To support the ever-growing demand for mobile communications, cellular networks have had to evolve from simple local service providers, to massively complex cooperative systems. While on the one hand the underlying transmission methods have been systematically advanced with each generation of wireless technologies, *i.e.*, :

- time-frequency division multiple access (T/FDMA) in 2nd generation (2G) networks;
- code division multiple access (CDMA) in 3G; and
- orthogonal frequency division multiple access (OFDMA) in 4G,

to improve the capacity and availability of these networks; on the other hand, the inherently enhanced complexity of these transmission schemes necessitates more intelligent methods of cooperation and system coordination. Ultimately, the dramatically increasing demand for mobile communications [1] requires more and more intelligent utilisation of the radio frequency (RF) spectrum, and enhanced cooperation between cells.

Before we begin, the ultimate goals of multi-cell cooperation must be introduced. By coordinating resource and power allocation over multiple cells (or indeed a whole network), the system is able to provide simultaneous service to thousands of users. Thus, the main goals of cooperation can be compiled as:

- the optimal utilisation of radio resources within a cellular network;
- the minimisation of interference to neighbouring cells; and hence
- the maximisation of the number of simultaneously transmitting users.

In the rest of this introduction, we will describe the most basic forms of network management without cooperation, and hence highlight the need for more advanced coordination techniques. Following this, we will investigate three areas of multi-cell cooperation, and how they intend to solve the problem of increased throughput demands for the limited bandwidth available for wireless systems. Finally, we will conclude with a performance analysis of an example of such techniques, and the envisioned further evolution to future mobile networks.

1.1 Frequency Reuse

The most basic form of interference mitigation utilised in wireless networks is that of frequency reuse. Consider two mobile stations (MSs) in neighbouring cells transmitting on the same band of frequencies, these will surely interfere with each other and, consequently, degrade each others signal. Hence, the logical conclusion would be to allocate orthogonal bandwidths to avoid interference. However, due to the quantity of MSs requesting resources, and the limited bandwidth available, it is clear that not all users can be allocated different frequencies, *i.e.*, the frequencies must be reused. Utilising the same frequency bands in neighbouring cells can be detrimental to the achievable throughputs in each cell (as stated in the example), however as the wireless signal attenuates directly as a function of the distance from the transmitter, a frequency band may be reused in cells that are sufficiently far away from each other. Thus, a frequency reuse scheme results (shown in the left of Fig. 1) where two neighbouring cells never share the same set of transmission frequencies, and MSs can transmit virtually interference-free.

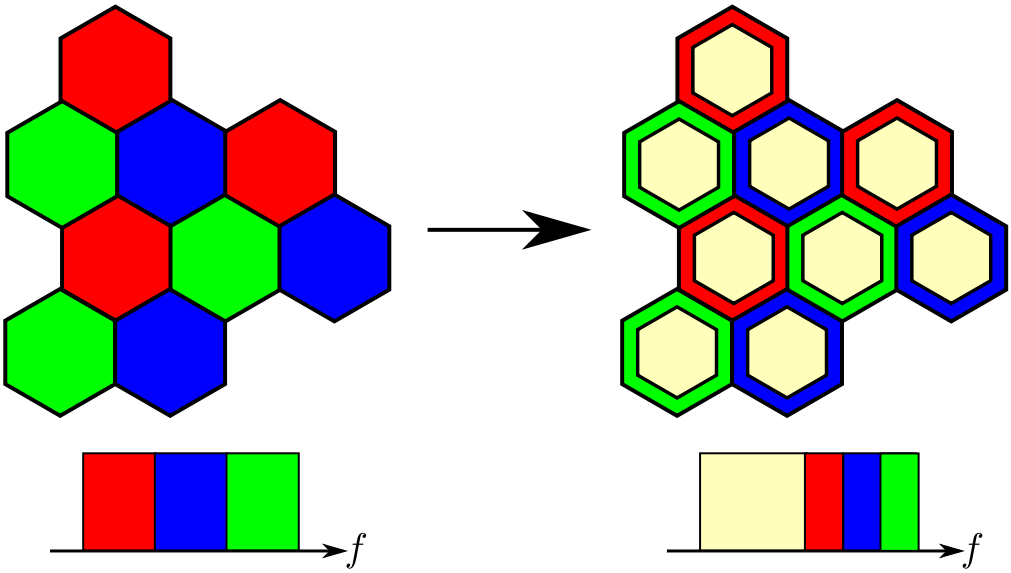

Fig. 1: On the left, the most basic from of frequency reuse, where the available bandwidth is divided in to three equal bands, and distributed such that no neighbouring cells utilise the same band. On the right, Fractional frequency reuse (FFR) improves the spatial reuse of resources by reusing the same band in the centre of the cell, and protecting the edges through standard frequency reuse.

FFR: While MSs in neighbouring cells do not interfere with each other, it is clear that only a portion (1/3 in example in Fig. 1) of the already limited system bandwidth is available in each cell, and therefore the number of users servable by the system is dramatically reduced. Therefore, FFR is adopted in more modern wireless systems [2], where the centre of all cells utilise the same frequency band, and only the cell-edges (which are more vulnerable to interference from other cells as they are closer) employ frequency reuse. An example of this is shown in the right of Fig. 1, and it is clear that the bandwidth available in each cell has doubled in comparison to traditional frequency reuse. However, in future systems where full frequency reuse (*i.e.*, the full bandwidth is used in all cells) is planned, cells will most certainly need to cooperate in order to ensure interference mitigation for their users.

1.2 Power Control

In general, a wireless base station (BS) will transmit at maximum power in the downlink in order to serve the MSs connected to it. However, in the uplink this can cause substantial difficulties such as large interference at a neighbouring BS, or massive received signal differences (from different users) at the same BS, referred to as the *near-far problem*. Therefore, transmit power control (TPC) is utilised in the uplink of most mobile communications systems to balance the signal-to-noise ratios (SNRs) of the MSs in a cell at the BS, and hence ease simultaneous reception and create a fairer system. In TPC, each MS transmits at a power level that is just large enough to overcome the path loss, or signal attenuation, from itself to its serving BS. Through this, nearby users will transmit with much lower power than users at the cell-edge, as a high-power user near to the BS would essentially drown out the farther users. Furthermore, due to the significantly reduced transmit powers, the interference to neighbouring cells is limited, additionally easing simultaneous transmission of users throughout the network. This will be essential for full frequency reuse networks.

While these basic forms of coordination were able to satisfy early networks demand of service, the vast increase in cellular activity cannot be compensated by these single-cell-management techniques. Hence, multi-cell cooperation has become more than necessary.

2 User-based Cooperation

Due to the ever increasing complexity and utilisation of modern mobile communications networks, it has become more and more difficult to serve the large number of MSs requesting service. Furthermore, resource allocation on a single-cell basis is no longer able to sustain the demands of these networks, and hence users often fall into outage. In this section, a class of techniques that utilise individual users' transmission requirements to perform multi-cell resource allocation is discussed. Here, cells adjust their resource selection and scheduling based on the MSs in neighbouring cells already transmitting. A few examples of such techniques are discussed below.

2.1 Dynamic Frequency Reuse (DFR)

The main drawback of static FFR is the inability to adapt to an ever-changing environment, and the consequent waste of wireless resources. Therefore, in DFR [3, 4] the allocation of frequency subbands to different cells is determined based on the contemporary resource allocation and consequent immediate interference environment in the cellular system. Ideally, we would prefer all frequencies to be available in all cells, so at minimum an FFR scheme with a common frequency band in the cell-centres is applied. Subsequently, the frequencies allocated to the cell-edge may be adapted based on the use of specific frequency bands in the neighbouring cells, and the interference incident from these to the cell of interest. Clearly, this necessitates some signalling between BSs, such that the possibility of close frequency reuse can be determined in each cell. Therefore, the frequency and consequent resource allocation in each cell is adapted dynamically to the behaviour of the cellular system.

DFR may be implemented by a central or distributed approach. In centralised approaches, resources are assigned to BSs by means of a central controller, which generally achieves more efficient resource utilisation, at the expense of additional signalling and higher complexity of the network infrastructure. In a distributed approach, each BS autonomously carries out the resource allocation, attempting to individually react to the interference environment. In distributed DFR methods, however, BSs generally may access only a predefined number of subbands, so these approaches provide little flexibility in subband reassignment when interference conditions change.

2.2 Successive Interference Cancellation (SIC)

While frequency reuse schemes help protect cells from interference, they are unable to actively eliminate co-channel interference (CCI) at the MS. This challenge, however, can be met through *interference cancellation*. To accurately define SIC, we use a definition given in [5], stating that

"interference cancellation should be interpreted to mean the class of techniques that demodulate and/or decode desired information, and then use this information along with the channel estimates to cancel received interference from the received signal." In other words, signal processing is utilised after reception to improve the quality of the desired information, while removing the interference from the received signal. An example of a simple implementation of SIC is shown in Fig. 2. In SIC, the strongest signal (it has, inevitably, the highest signal-to-noise-plus-interference

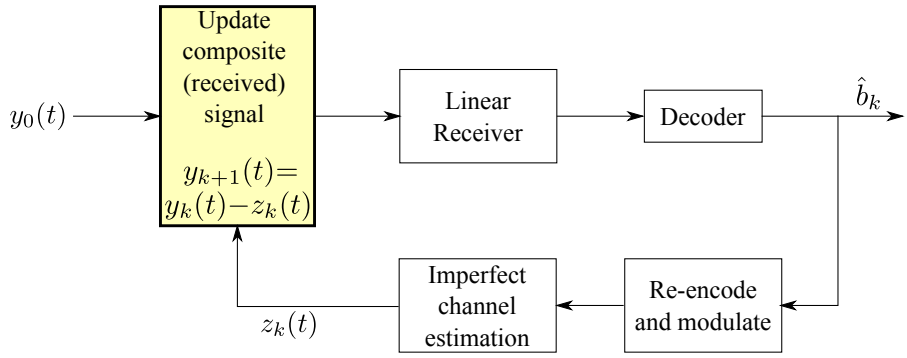

Fig. 2: An example of SIC, where the quality of the desired signal is improved by successively removing the detected interfering signals from the received signal.

ratio (SINR)) is detected and decoded first, then the next strongest, and so on. After the received signals have been reconstructed (through the respective channel estimations), these can be subtracted/cancelled from the composite received signal to improve the performance of the remaining MSs (*i.e.*, their signal detection). Thus, with each removed signal, the interference in the composite received signal is reduced, and the remaining signal SINRs consequently enhanced.

It has been shown that SIC can nearly achieve the Shannon capacity for multi-user additive white Gaussian noise channels [5]. Many well-known examples of interference cancellation are utilised today, such as the decision feedback equaliser (DFE) and the original Bell Labs layered space-time (BLAST) system. In the DFE, previously decoded symbols are utilised to cancel inter-symbol interference (ISI) of future received symbols, given that the channel is known. In BLAST decoding, spatial interference in multiple-input multiple-output (MIMO) systems can be removed in order to separate spatially multiplexed streams of data. Overall, there are many similarities [5] between the elimination of:

- ISI (equalisers);
- spatial interference (MIMO receivers);

and, consequently,

- multi-user interference cancellation.

Hence, while SIC for multi-cell cooperation may be rather novel, the idea of interference cancellation has been well proven over the years.

Of course, the great benefits that come from SIC in multi-user environments come at a price, which is not always satisfiable. In general, the concept of interference cancellation relies on the premise that the received signal can be reliably estimated. This means that not only can the desired signal be decoded, but also the received interfering signals. For this, a receiver must know both what was transmitted by an interferer (*i.e.*, what data was sent with which modulation and coding scheme (MCS)) and the channel over which it was sent (*i.e.*, how it has been modified). On the one hand, the system may signal amongst the BSs the MCS of all users simultaneously transmitting on the same frequencies such that this interference can be cancelled; this would however drastically increase the signalling burden on the network (*e.g.*, in comparison to frequency reuse techniques). On the other hand, even if this information is known, the receiver must perfectly estimate the interfering channel to be able to decode the signal, which is highly improbable. Hence, while SIC provides great promise for multi-cell coordination, its requirements are very difficult to fulfil.

2.3 Uplink Interference Protection (ULIP)

It is clear that the high complexity of SIC, and its heavy reliance on channel estimation, make it difficult to implement in cellular communication networks. In addition, multi-cell cooperation and coordination is more difficult to achieve in the uplink, however here is where it is usually most needed. Because each MS has a much more limited power budget than any BS, reducing interference in the uplink is paramount to modern mobile communications. Therefore, much work (such as TPC, briefly discussed in Section 1.2) is dedicated to alleviating the interference incident on especially cell-edge users in the reverse link. One such technique recently proposed is ULIP, and will be summarised here.

Whereas TPC determines MS transmit power based on local information, ULIP is a technique that actively combats CCI in the uplink of a cellular system [6]. The level of uplink interference originating from neighbouring cells (affecting co-channel MSs in the cell of interest) can be effectively controlled by reducing the transmit power of the interfering MSs (*i.e.*, rather than attempting to cancel the signal entirely). This is done based on the target SINR and tolerable interference of the vulnerable link. Bands are prioritised in order to differentiate those (vulnerable/victim) MSs that are to be protected from interference and those (aggressor/interfering MSs) that are required to sacrifice transmission power to facilitate the protection. Furthermore, MSs are scheduled such that those users with poorer transmission conditions receive the highest interference protection, thus balancing the areal SINR distribution and creating a fairer allocation of the available resources. In addition to interference protection, the individual power reductions also serve to decrease the total system uplink power, resulting in a greener system.

However, while ULIP significantly protects cell-edge users from uplink interference, it is clear that a substantial amount of signalling is necessary to facilitate this protection. Not only must the tolerable interference of each user be calculated and sent to its interferers, the interfering channel to that user must also be estimated. Fortunately, this can be done at the interfering MS using the reference signal received power (RSRP) of the cell it is interfering with, and thus does not add any signalling complexity to the network.

3 System-wide Optimisation

In the user-target-based cooperation techniques discussed above, it is clear that a significant amount of information must be signalled between BSs and MSs in order to facilitate successful simultaneous transmission in multicellular systems. Furthermore, because these techniques rely on individual users requirements, it is clear that they very rarely result in a system-optimal solution. Therefore, another class of techniques is considered, where assuming a central controller with all necessary information, the multi-cell cooperation and resource allocation problem can be expressed as an optimisation problem. Through this, such techniques attempt to reach globally optimum solutions for a system, at the cost of near unlimited knowledge at the controller. Some examples of these techniques will be discussed here.

3.1 Capacity Maximisation

In wireless networks, the resource and power allocation problem of the system as a whole is often posed as an optimisation problem where the objective is the maximisation of the achievable throughput (*i.e.*, sum rate) of the system [7]. Of course, individual user requirements must also be met, constraining the set of solutions to the problem. Therefore, a system optimisation problem

is generally constructed as follows:

$$\text{Objective: } \max \sum_i \text{UserRate}_i \qquad i = 1, 2, \ldots, N \text{ users}$$

$$\text{subject to:}$$

$$\text{Constraints: } \begin{cases} \text{UserRate}_i \geq \text{RateReq}_i & \forall i \\ \text{UserDelay}_i \leq \text{MaxDelay}_i & \forall i \\ \sum \text{UserPower}_i \leq \text{TotalPower} & \\ \vdots & \end{cases}$$

where the most common constraints posed are the user rate requirements and transmit power limitations. However, these may be extended to more detailed QoS requirements such as delay, buffer length, priority, etc. By solving the above problem, a system-wide optimal resource allocation for the network can be found.

Although such a method seems preferable to any individual-user-driven cooperation techniques, there are two significant drawbacks of system optimisation that greatly reduce its applicability to wireless cellular networks. First of all, the biggest difficulty of such an optimisation problem is that in almost all cases this problem becomes $\mathcal{NP}$-hard, and is therefore practically unsolvable using standard optimisation techniques. In most cases, the scheduling problem is then broken down into multiple optimisation problems, separating the resource allocation and transmit power determination, resulting in ultimately suboptimal solutions. Furthermore, because of the interdependency of, *e.g.*, subcarrier allocation and transmit power, solving the resource allocation does not guarantee a solution to the transmit power problem. Therefore, the optimality of these techniques is hardly ever achieved.

Secondly, not only is there a massive computational complexity involved, but also the large amount of system information that is required by the central controller to solve these system-wide problems must be communicated from each BS, implying a tremendous signalling burden on the network. Not only must the individual user requirements be signalled, but also the desired and interfering path gains of each MS in the system must be known at the central controller in order for an optimal resource and power allocation to be formed. Therefore, while in theory these problems present optimal network solutions, they are in practice almost impossible to implement.

3.2 Power Minimisation

Another form of the above optimisation problem is to, rather than maximise the sum rate, to minimise the total transmit power utilised in the wireless network [8]. Here, clearly, the power constraint falls away as it implies the maximisation of network performance with maximum power. On the other hand, the individual user requirements are the main constraints, where especially the rate of each user must be maintained, otherwise a system without any transmission would result. This form of optimisation is beneficial in two main ways:

- the minimisation of interference to other cells eases power and resource allocation over the network; and
- the minimisation of transmit power results in much greener networks, a topic of fervent discussion for future wireless communications.

However, the same difficulties apply to this problem as to the rate maximisation variation, and hence the practical implementation of such a system is highly complex.

4 Large-Scale Multiple Antenna Systems (LSMAS)

In the previous sections, we have discussed two contrasting forms of multi-cell cooperation and coordination: lower complexity user-based cooperation, and substantially complex system optimisation. Furthermore, in a network with thousands of BSs and antennas, the signalling burden

required by both of these coordination dogmas becomes immense. While this cannot necessarily be avoided, a new class of multicellular coordination which exploits this abundance of transmission elements is investigated, utilising multiple antennas cooperatively to achieve not only spectral but also energy efficiency gains. This is discussed here.

The recently proposed concept of LSMAS is a radical step towards a new way of conceiving MIMO systems for energy efficiency optimisation [9]. LSMASs are extended MIMO systems with tens or hundreds of radiating elements, each one consuming a small amount of energy, which may be co-located at a BS, spread out on the face of a building, or geographically distributed over an entire network. LSMASs provide a plethora of advantages over conventional MIMO systems. In particular, these large-scale systems offer higher data rates, increased link reliability, and potential energy savings through the exploitation of the many degrees of freedom offered by the many antenna elements. Meanwhile, random impairments such as thermal noise and other-cell interference, can be averaged out. While in the past multiple-antenna systems have been used to provide capacity gains through spatial diversity, energy efficient networks can be achieved by using massive multi-antenna systems where the many antennas are used to form and focus directed beams to a multiplicity of terminals on the forward link, and selectively collect signals from these terminals on the reverse link. Furthermore, the proposed approach is scalable with the number of antennas, and it provides energy savings that increase with the number of radiating elements. On the other hand, there are several theoretical (*e.g.*, capacity limits, power allocation strategies, signal transmission, channel estimation, amount of feedback, etc.) and practical (*e.g.*, antenna design, compensation of mutual coupling and spatial correlation, etc.) issues that need to be addressed. Overall, however, LSMASs offer a radical new direction in multicellular cooperation to improve not only the spectral efficiency of wireless communications networks, but also generate large power savings on the existing infrastructure.

4.1 Coordinated Multi-Point (CoMP) Transmission

One of the most fervently discussed topics for cooperative multicellular communication in future network is that of CoMP [10], where neighbouring BSs transmit together to multiple users in their cells. In CoMP, MSs in neighbouring cells are grouped based on the received pilot signal strength from the surrounding BSs, *i.e.*, users are grouped if the strongest BSs they see are identical. Once these groups are formed, each of the MSs in each group is served simultaneously by the BSs which provide the strongest signal strengths for that group (see Fig. 3). Consequently, these BSs jointly pre-code their transmissions to the user group such that the combined received signal from the set of BSs at each MS provides the user with its desired signal (*i.e.*, that would have been transmitted from its serving BS), without receiving any interference from the other cells in its set of strongest BSs. In [11], the combination mechanisms of such pre-processing

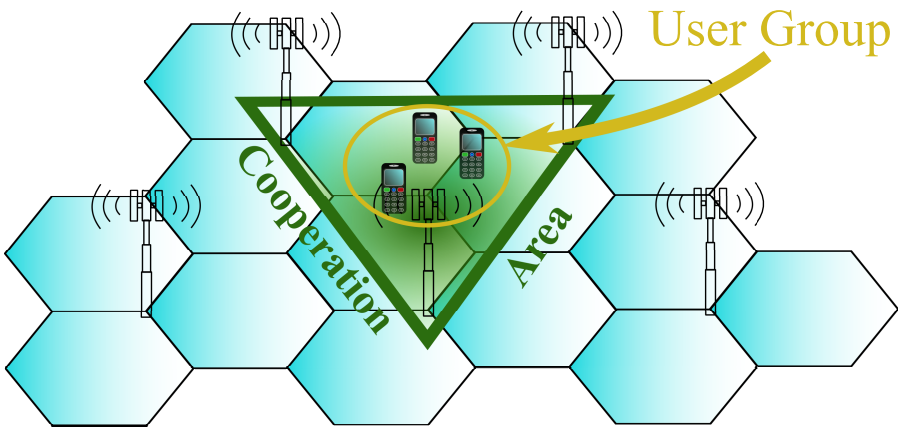

Fig. 3: A visualisation of CoMP, where the users within neighbouring cells, that experience identical sets of strongest BSs, can be served simultaneously and cooperatively by this set of BSs, eliminating interference from what would be the strongest interfering cells.

techniques are described and compared:

- **Joint TDMA (J-TDMA)** - Only one MS in the user group is served in each time slot. Thus, transmission is automatically CCI-free, at the cost of reduced spectral efficiency.

- **Joint zero-forcing (J-ZF)** - The joint pre-processing matrix $\mathbf{F}=\mathbf{H}^H\left(\mathbf{H}\mathbf{H}^H\right)^{-1}$ is the pseudo-inverse of the aggregate channel matrix $\mathbf{H}$ such that each user only receives a noisy version of its intended data. However, just as ZF receivers amplify noise, J-ZF pre-coding generally increases the average transmit power.

- **Joint minimum mean-square error (J-MMSE)** - This pre-processing achieves a compromise between CCI cancellation and transmitter power efficiency. Based on the MMSE criterion, the pre-coding matrix is given by $\mathbf{F}=\mathbf{H}^H\left(\mathbf{H}\mathbf{H}^H+\left({}^{N_0}/_{\rho}\right)\mathbf{I}\right)^{-1}$, where ${}^{N_0}/_{\rho}$ is a scaled version of the noise.

Essentially, CoMP eliminates the interference from what would normally be the most strongly interfering BSs, consequently enhancing SINR and thus throughput at each MS.

A common problem in the CoMP concept is that the gain strongly relies on ideal "user centric" clustering and assignment, meaning all MSs should be served by their individual set of strongest cells. In a large network with irregularly distributed MSs in the cells, the difficulty is to find sufficient users with these sets being identical, since due to shadowing the signal strength of BSs might be widely distributed. Thus, the typical penetration rate of MSs that might be served by such a single specific set of cells is often very small, causing many users to be denied service. In [12] partial CoMP, where shifted coverage areas increase the probability of MSs sharing a set of strongest cells, is suggested to alleviate this problem. While the performance gains of partial CoMP reach similar levels as those achievable via full CoMP, the additional signalling and complexity must be compensated by limiting transmission of reference signals by the MSs. Although, it is clear that large SINR and throughput gains are achieved.

While CoMP does not achieve the performance of system optimisation (*i.e.*, albeit at significantly reduced complexity), it is able to provide large gains over user-based cooperation schemes. In general, a substantial increase in signalling over traditional inter-cell cooperation techniques is necessary to facilitate CoMP. However, this is true for most of the recent multi-cell cooperation techniques, as the 'simple' solutions are no longer sufficient to provide the large throughput demands of todays networks. Furthermore, it is evident that joint processing and cooperative transmission techniques are necessary for future networks, implying that also user clustering techniques will need to be optimised to improve system performance. In general, however, it is clear that multicellular cooperation, and specifically LSMAS will be paramount to the performance and development of future wireless communications networks. A performance comparison of the discussed cooperation techniques is shown in Table 1. Pareto optimal scheduling (POS), which combines aspects from user-based cooperation and CoMP, will be described in Section 5.

5 Pareto-based Optimal Transmission Scheduling

In our final section, we would like to introduce a recently proposed OFDMA resource allocation and power control method [13] based on Pareto optimal power control (POPC) [14], which combines some of the aspects of user-based cooperation and CoMP. In POPC, given a feasible link allocation (*i.e.*, a group of users in neighbouring cells allocated the same resource block (RB)(s)), a transmit power vector $\mathbf{P}$ can be found such that all users achieve their SINR requirements with minimal power. This is of course a highly desirable result which, depending on the location and service requirements of the interfering MSs, is clearly not always possible. Hence, by scheduling users in such a manner to maximise the number of feasible user groupings (in principle, there can be as many user groups as there are (orthogonal) RBs in the system), the system spectral efficiency can be maximised.

However, scheduling users in such a manner is not a trivial task. In POPC, the desired and interfering path gains of users in neighbouring cells allocated the same frequency resource(s) are

Method	Objective	Complexity	Signalling	Optimality	Spec. Eff.	Energy Eff.
FFR	Interference Mitigation	++	++	−−	−−	−−
TPC	Uplink Fairness	++	+	−−	−−	+
DFR	Interference Management	+	+	−	−	−−
SIC	Interference Cancellation	−	−−	−	+	−
ULIP	Interference Mitigation	+	−	+	+	++
Sys. Opt.	Objective Optimisation	−−	−−	++	++	++
LSMAS	Efficient Transmission	−	−	+	+	++
CoMP	Cooperative Transmission	−	−	+	++	++
POS	Interference Management	+	−	−	+	++

Table 1: Technique Performance Comparison: Scores ranging over {−−, −, +, ++} are given in each performance area. '−−' indicates terrible performance, and '++' indicates superior performance (*i.e.*, '++' in *Complexity* means very low complexity, whereas in *Spec. Eff.* it signifies very high spectral efficiency). The general trend is evident that the more optimal and efficient the system is, the more complex it becomes.

combined in a matrix $\mathbf{F}$ where

$$F_{ij} = \begin{cases} 0, & \text{if } i = j \\ \frac{\gamma_i^* G_{j,i}}{G_{i,i}}, & \text{if } i \neq j \end{cases},$$

the SINR target of user i is γ_i^*, and $G_{j,i}$ is the path gain from the MS j in cell j to the BS in cell i. From this, the optimum transmit power vector $\mathbf{P}^* = (\mathbf{I} - \mathbf{F})^{-1}\mathbf{u}$, where $\mathbf{u}$ signifies the SNR of each user, can be calculated if the largest eigenvalue of $\mathbf{F}$ is shown to be less than 1. Effectively, this constraint establishes the stability (*i.e.*, feasibility) of the POPC system of equations. The largest eigenvalue is found via an eigenvalue decomposition, which can be highly computationally complex even for small matrices. Thus, in order for a group of users in neighbouring cells to be purposely scheduled onto the same RB, a simple expression for the allocatability of such a group must be developed.

In [13] the authors, through analytic derivation, have found that for three neighbouring cells (for any number of cells greater the complexity increases exponentially) that if three MSs i, j, and k, one in each cell, satisfy the condition

$$F_{ij}F_{ji} + F_{ik}F_{ki} + F_{jk}F_{kj} + F_{ij}F_{jk}F_{ki} + F_{ik}F_{ji}F_{kj} < 1\,, \tag{1}$$

they may be allocated the same resources in each cell, and POPC can be applied. This is clearly dependent on the individual desired and interfering path gains, along with the SINR targets of the users. Therefore, a scheduler might make use of this condition to schedule users such that the number of feasible groups of MSs is maximised, hence also maximising the spectral efficiency of these three cells; this is called POS. Of course, in a large network with hundreds of cells, this is not so useful. As indicated in Fig. 4, three neighbouring cells may be grouped in the network. By grouping three cells with coinciding beam patterns (see shaded cells in Fig. 4), POS can be applied to these three cells, and the cluster will be relatively shielded from neighbouring sectors interference due to the nature of the beam patterns. This clustering is then tessellated over the network, such that POS can be applied separately in each of these clusters without overly excessive CCI from the surrounding cells, allowing the MSs to achieve their transmission requirements. Thus, this form of POS combines the user-based cooperation methods of individual service requirements with the grouping of users that is so essential in CoMP.

In Fig. 5, a performance comparison to maximum power transmission (utilised in downlink transmission) and standard TPC (utilised in system uplink), in terms of spectral and energy efficiency is shown, displaying the potential of POS for future wireless communication networks.

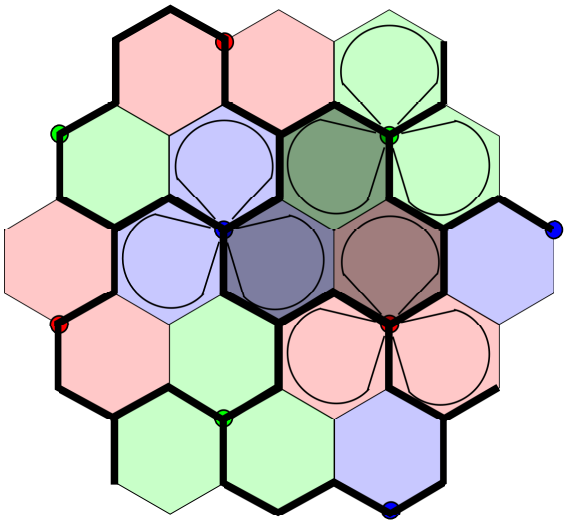

Fig. 4: Extension of three-cell POS to larger multi-cellular networks [13]. Universal frequency reuse is applied, and the differing colouration of the cells simply demarks which BS is serving them.

In general, POS has a performance advantage over power control over all SINR targets (except $\gamma_i^* = 20\,\text{dB}$), whereas also substantial gains over 13% are seen over max. power transmission in the mid-SINR (typically the operational) range. The POS performance begins to suffer for higher SINRs as not enough feasible MS groupings can be found. However, on average the POS spectral efficiency is equivalent to that of max. power transmission.

This becomes even more significant when considered together with the energy efficiency (calculated as data rate per unit of transmitted power $\left[\frac{\text{bits/s}}{\text{W}}\right] \equiv \left[\frac{\text{bits}}{\text{J}}\right]$) results shown in Fig. 5. As expected, maximum power transmission is the least energy efficient of the three considered techniques. POS, on the other hand, provides massive energy efficiency benefits for the system, even when compared to power control, with gains of up to 5 dB for higher SINRs. Hence, it is quite clear that POS drastically reduces the transmit power consumption in a macro-cellular network. Considering this together with the spectral efficiency results, it is evident that POS provides overall superior system performance over the standard resource and power allocation techniques.

6 Conclusions

Throughout this article, we have discussed the evolution of multi-cell cooperation from more simple user-requirements-driven cooperation techniques, over system-wide optimisation-based methods, to coordination in LSMAS and cooperative transmission. Clearly, techniques optimising the resource and power allocation for individual users do not always strike system optimum decisions, and hence from this research moved on to optimisation methods. While, if solvable, these techniques can provide system-optimal resource and power allocations by coordinating over all cells in a network, it was explained that these methods are highly intractable, and in most situations must be broken down into multiple subproblems, yielding suboptimal solutions. Finally, the most recent research has considered the opportunity of LSMAS, and cooperative transmission from multiple BSs in a network. CoMP provides large throughput gains for users in the network, but at the cost of additional complexity and rather unreliable scheduling. However, it is clear that for future networks to deliver the increasing service demands [1], such cooperation over multiple BSs is more than necessary.

We have concluded our paper by introducing a recently proposed technique that combines some of the aspects of user-based cooperation and CoMP scheduling. In POS, users in neighbouring cells are grouped based on their desired and interfering path gains, at which point POPC can be applied and large energy savings can be achieved without sacrificing spectral efficiency. And, although a large amount of information is needed to determine the feasibility of a group

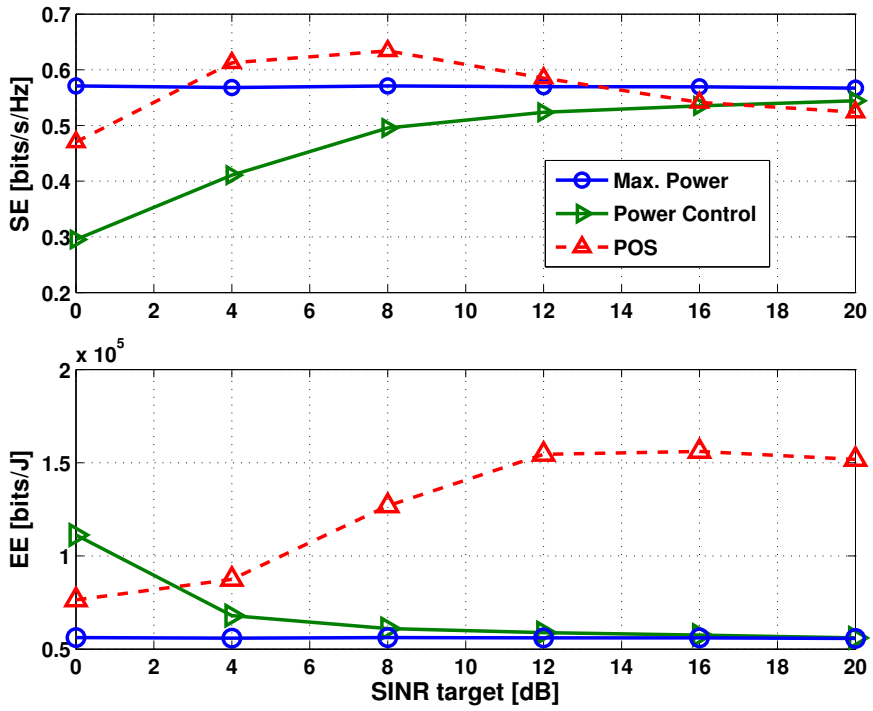

Fig. 5: System spectral efficiency (SE) and energy efficiency (EE) results for the various power control techniques in a multi-cellular network. In modern cellular systems, full frequency reuse is applied, utilising maximum power transmission in the forward link, and power control in the reverse link.

of MSs, since this procedure is performed on a three-cell basis, BSs need only the information from their immediate neighbours, limiting the additional complexity and signalling implied. The POS results, combined with the given comprehensive research review, thoroughly show the immense importance of multi-cell cooperation in todays, and more significantly for future wireless networks.

References

[1] Cisco Visual Networking Index, "Global Mobile Data Traffc Forecast Update, 2011-2016," Cisco, White Paper, Feb. 2012.

[2] A. Molisch, *Multiple Access and the Cellular Principle*. Wiley-IEEE Press, 2011.

[3] S. Ali and V. Leung, "Dynamic Frequency Allocation in Fractional Frequency Reused OFDMA Networks," *IEEE Trans. on Wireless Communications*, vol. 8, no. 8, Aug. 2009, pp. 4286–4295.

[4] M. Wang and T. Ji "Dynamic Resource Allocation for Interference Management in Orthogonal Frequency Division Multiple Access Cellular Communications," *IET Communications*, vol. 4, no. 6, Apr. 2010, pp. 675–682.

[5] J. G. Andrews"Interference Cancellation for Cellular Systems: A Contemporary Overview," *IEEE Wireless Communications Mag.*, vol. 12, no. 2, Apr. 2005, pp. 19–29.

[6] H. Burchardt, Z. Bharucha, G. Auer, and H. Haas, "Uplink Interference Protection and Scheduling for Energy Efficient OFDMA Networks," *EURASIP Journal on Wireless Communications and Networking*, May 2012.

[7] Y. Ma and D. Kim, "Rate-Maximization Scheduling Schemes for Uplink OFDMA," *IEEE Trans. on Wireless Communications*, vol. 8, no. 6, Jun. 2009, pp. 3193–3205.

[8] D. Kivanc, G. Li, and H. Liu, "Computationally Efficient Bandwidth Allocation and Power Control for OFDMA," *IEEE Trans. on Wireless Communications*, vol. 2, no. 6, Nov. 2003, pp. 1150–1158.

[9] G. Wright, "GreenTouch Initiative: Large Scale Antenna Systems," Spring meeting, Seoul, South Korea, 2011. [Online], Available: http://www.greentouch.org/uploads/documents/pres_gregory_wright.pdf.

[10] M. Sawahashi, Y. Kishiyama, A. Morimoto, D. Nishikawa, and M. Tanno, "Coordinated Multipoint Transmission/Reception Techniques for LTE-Advanced [Coordinated and Distributed MIMO]," *IEEE Wireless Communications*, vol. 17, no. 3, Jun. 2010, pp. 26–34.

[11] J.-S. Sheu and C.-H. Hsieh, "Joint Preprocessing Techniques for Downlink CoMP transmission in Multipath Fading Channels," *IEEE 75th VTC, Spring*, May 2012, pp. 1–5.

[12] W. Mennerich and W. Zirwas, "User Centric Coordinated Multi Point Transmission," *IEEE 72th VTC, Fall*, Sep. 2010, pp. 1–5.

[13] H. Burchardt, S. Sinanović, G. Auer, and H. Haas, "Pareto Optimal Power Control Scheduling for OFDMA Networks," *IEEE 76th VTC, Fall*, Sep. 2012.

[14] A. Goldsmith, *Wireless Communications*. Cambridge University Press, 2005.

Harald Burchardt received his B.Sc. in Electrical Engineering and Computer Science in 2007 from Jacobs University Bremen, and his M.Sc. in Communications Engineering in 2009 from the Technical University Munich. He is currently working towards his Ph.D. degree at the Institute for Digital Communications at the University of Edinburgh.

Harald Haas holds the Chair of Mobile Communications at the University of Edinburgh. He is also part-time chief technical officer (CTO) of a university spin-out company pureVLC Ltd. His main research interests are interference management in wireless networks, multiple antenna concepts and optical wireless communication. He holds 23 patents, and has published more than 230 conference and journal papers. He was invited speaker at TED Global 2011. He currently holds a prestigious Established Career Fellowship of the Engineering and Physical Sciences Research Council (EPSRC) in the UK.

Distributed and Autonomous Resource and Power Allocation for Wireless Networks

Harald Burchardt*, Sinan Sinanovic*, Zubin Bharucha† and Harald Haas*

*Institute for Digital Communications
School of Engineering and Electronics
The University of Edinburgh
EH9 3JL, Edinburgh, UK
{h.burchardt, s.sinanovic, h.haas@ed.ac.uk}

†DOCOMO Euro-Labs
Landsbergerstr. 312
80687 Munich, Germany
bharucha@docomolab-euro.com

***Abstract*—In this paper, a distributed and autonomous technique for resource and power allocation in orthogonal frequency division multiple access (OFDMA) femto-cellular networks is presented. Here, resource blocks (RBs) and their corresponding transmit powers are assigned to the user(s) in each cell individually without explicit coordination between femto-base stations (FBSs). The "allocatability" of each resource is determined utilising only locally available information of the following quantities:**

- **the required rate of the user;**
- **the quality (*i.e.*, strength) of the desired signal;**
- **the frequency-selective fading on each RB; and**
- **the level of interference incident on each RB.**

Using a fuzzy logic system, the time-averaged values of each of these inputs are combined to determine which RBs are most suitable to be allocated in a particular cell, *i.e.*, which resources can be allocated such that the user requested rate(s) in that cell are satisfied. Fuzzy logic presents a completely novel, low-complexity methodology for inter-cell interference coordination (ICIC). A comprehensive study of this system in a femto-cell environment is performed, yielding system performance improvements in terms of throughput, energy efficiency and coverage over state-of-the-art ICIC techniques.

***Index Terms*—autonomous resource allocation, distributed ICIC, fuzzy logic, OFDMA, femto-cellular networks.**

I. Introduction

Future wireless networks are moving towards heterogeneous architectures, where in each cell a user may have available over four different types of access points (APs) (*e.g.*, macro-, pico-, femto-cells, relays and/or remote radio heads) [1]. Intuitively, this has many positive effects for a mobile station (MS) resulting from the enhanced spatial reuse of resources. However, pico- and femto-cellular overlays also imbue many difficulties, *e.g.*, cell-organisation/optimisation, resource assignment to users, and especially interference coordination between APs within the same and neighbouring cells. Standard inter-cell interference coordination (ICIC) techniques based on network architectures [2, 3] only go so far in dealing with these challenges, and hence a new approach is necessary.

A. Challenges in Heterogeneous Networks (HetNets)

Because of the various types, locations and dense deployment of APs, and the different transmission powers associated with them, numerous technical challenges are posed by femto/pico-cell overlays [1, 4, 5]. These fall into the following areas:

- **Network self-organisation** - Self-configuration and -optimisation are required of all cells. In cellular networks, such organisation can be performed via optimisation techniques [6], however these tasks become increasingly difficult given the additional APs and network parameters to be considered, motivating a *distributed* approach [7].
- **Backhauling** - Connecting the different base stations (BSs) to the core-network necessitates extra infrastructure [1]. In the femto-cell case, the long delay of connection via wired backhaul prevents macro-femto ICIC [5], necessitating *autonomous* interference management.
- **Interference** - Cross-tier interference created to/from the overlaid cells (*e.g.*, pico-/femto-cells) must be mitigated to maintain performance, especially if access to these cells is restricted. High intra-femto-tier interference due to dense deployment is also of concern. The handling of this interference is paramount to the performance of such future networks, of which the main sources in densely deployed femto-cell scenarios [1] can be given as
  - *Unplanned deployment*- Femto-cells are deployed by end-users at "random" locations, and can be active or inactive at any time, further randomising their interference. Continuous sensing and monitoring is required by cells to dynamically/adaptively mitigate interference from the other tiers [8].
  - *Closed-subscriber access* - Restricted access control of pico- and femto-cells leads to strong interference in downlink and uplink if users cannot handover.
  - *Node transmission power differences* - The lower power of nodes such as pico- and femto-cells can cause association and interference problems.

In general, these issues motivate the need for innovative ***decentralised*** and ***autonomous*** interference coordination that operates independently on each cell, utilising only local information, yet achieving near-optimal solutions for the network. By allowing BSs and MSs to individually optimise their resource allocations and transmission powers, a global optimum may be found without centralised algorithms governing the system. This would substantially reduce not only the signalling burden but also the operational complexity of the network.

B. Randomly and Densely Deployed Femto-cells

Here, we address the relatively unexplored topic of ICIC for randomly deployed femto-cells. Due to the relative modernity of the femto-cell concept, and the innate random deployment of femto-cells within a macro-cell, most interference coordi-

nation is utilised for interference reduction to the macro-cell, rather than interference protection between femto-cells.

The state-of-the-art interference coordination for Long-Term Evolution (LTE) HetNets is the Almost-blank Subframe (ABS): a time-domain ICIC technique where an aggressor BS creates "protected" subframes for a victim BS by reducing its transmission activity on these [9]; the occurrences of the ABSs are known *a priori* at the coordinating BSs. Thus, throughput improvements are induced via the provided interference protection [10]. However, the omitted transmission frames may have adverse affects on the data rates at the aggressor BS. Furthermore, without guaranteed backhaul connections, femto-base stations (FBSs) may not be able coordinate the ABS slots. In this paper, we provide resource and power allocation for femto-femto interference environments which requires no signalling between FBSs, and enhances the overall throughput, energy efficiency and fairness of the femto-network.

On another note, recent research has seen the emergence of autonomous coordination techniques for Self-Organising Networks (SONs) [11, 12], where transmit powers on subbands are adjusted independently in each cell via local and network utility optimisation. These utilities are based on the average rate in the cell, however do not consider user-specific resource allocation for additional interference coordination. Furthermore, the proposed strategies do not consider heterogeneous architectures that will inevitably describe future networks. Finally, the suggested algorithms assume still some signalling between neighbouring BSs, hence cannot be considered fully autonomous, and may also limit their applicability specifically for femto-cell networks.

Finally, the application of fuzzy logic in collaboration with reinforcement learning techniques is comprehensively studied in [13], in order to tune the outputs of fuzzy inference systems. The application to wireless network coordination is investigated in [14–16], where fuzzy logic reduces the complexity of the learning algorithms by providing coarse evaluations of the network state. On a cell-individual basis, by again adapting subband transmission powers [14], adjusting the antenna downtilt [15], or modifying the downlink relative narrowband transmit power (RNTP) thresholds [16] the interference on specific resources can be controlled or removed completely. On the other hand, QoS requirements of individual users are neglected, a perspective that we attempt to address here. In addition, we employ fuzzy logic directly to ICIC in a holistic approach by considering many key parameters to perform resource allocation (*i.e.*, frequency reuse) and power control in all cells individually.

In this paper, we introduce a novel, low-complexity, distributed and autonomous ICIC technique, that performs independent *close-to-optimal* resource and power allocation in each cell, eliminating explicit signalling between FBSs. The rest of the paper is structured as follows: Section II describes the system deployment scenario and channel environment, Section III explains the fuzzy logic ICIC protocol and its performance in femto-cellular networks is analysed in Section IV. In Section V the simulation is described, and Section VI portrays and discusses the simulation results. Finally, some concluding remarks are offered in Section VII.

II. System and Channel Model

An orthogonal frequency division multiple access (OFDMA) network is considered, where the system bandwidth B is divided into M resource blocks (RBs). A RB defines one basic time-frequency unit of bandwidth $B_{\mathrm{RB}}{=}B/M$. MSs can transmit up to a fixed maximum power $P_{\max}$. Perfect time and frequency synchronisation is assumed.

Universal frequency reuse is considered, such that each femto-cell utilises the entire system bandwidth B. The set of RBs $\mathcal{M}$, where $|\mathcal{M}|{=}M$, is distributed by each BS to its associated MS(s). Throughout this paper, u defines an MS, and v_u the BS with which this MS is associated. The received signal observed by MS_u from BS_{v_u} on RB m is given by

$$Y_u^m = \underbrace{P_u^m G_{u,v_u}^m}_{S_u^m} + I_u^m + \eta\,, \tag{1}$$

where G_{u,v_u}^m signifies the channel gain between the MS_u and its serving BS_{v_u}, observed on RB m. Furthermore, P_u^m denotes the transmit power assigned to MS_u on RB m, S_u^m the desired received signal, $\eta{=}\eta_0 B_{\mathrm{RB}}$ the thermal noise, η_0 is the noise spectral density, and I_u^m the co-channel interference received on RB m from the BSs serving neighbouring cells. The interference I_u^m is defined by

$$I_u^m = \sum_{i\in\mathcal{I}} P_i^m G_{u,v_i}^m\,, \tag{2}$$

where $\mathcal{I}$ represents the set of interferers (*i.e.*, set of MSs in neighbouring cells that are also assigned RB m). Hence, the signal-to-interference-plus-noise ratio (SINR) observed at the MS_u on RB m is calculated by

$$\gamma_u^m = \frac{S_u^m}{I_u^m + \eta} = \frac{P_u^m G_{u,v_u}^m}{\sum\limits_{i\in\mathcal{I}} P_i^m G_{u,v_i}^m + \eta}\,. \tag{3}$$

Following this, the user throughput C_u is calculated as the data transmitted on the assigned RBs that have achieved their SINR target γ_u^*

$$C_u = \tilde{n}_u^{\mathrm{RB}} k_{\mathrm{sc}} s_{\mathrm{sc}} \varepsilon_{\mathrm{s}}\,, \tag{4}$$

where $\tilde{n}_u^{\mathrm{RB}}{=}\sum_{m=1}^{n_u^{\mathrm{RB}}} \mathbf{1}_{\gamma_u^m \geq \gamma_u^*}$ is the number of RBs assigned to MS_u achieving γ_u^*, n_u^{RB} is the total number of RBs allocated to MS_u, $\mathbf{1}_A$ the indicator function, k_{sc} the number of subcarriers per RB, s_{sc} the symbol rate per subcarrier, and ε_{s} the efficiency of the modulation and coding scheme (MCS) given in Table I. Finally, the system capacity is the sum throughput of all MSs in the network

$$C_{\mathrm{sys}} = \sum_u C_u\,. \tag{5}$$

The power efficiency β_u measures the data rate per unit of transmit power (or, alternatively, the data sent per unit of energy) of MS_u. This is defined as follows:

$$\beta_u = \frac{C_u}{P_u} = \frac{\tilde{n}_u^{\mathrm{RB}} k_{\mathrm{sc}} s_{\mathrm{sc}} \varepsilon_{\mathrm{s}}}{\sum_m^{n_u^{\mathrm{RB}}} P_u^m} \quad \left[\frac{\mathrm{bits/s}}{\mathrm{W}}\right] \equiv \left[\frac{\mathrm{bits}}{\mathrm{J}}\right], \tag{6}$$

where P_u is the transmit power of MS_u, and C_u the achievable capacity from (4). The availability χ is defined as the

TABLE I
MODULATION AND CODING TABLE

CQI index	min. SINR [dB]	Modulation	Code rate	Efficiency ε_s [bits/sym]
0	-	None	-	0
1	-6	QPSK	0.076	0.1523
2	-5	QPSK	0.12	0.2344
3	-3	QPSK	0.19	0.3770
4	-1	QPSK	0.3	0.6016
5	1	QPSK	0.44	0.8770
6	3	QPSK	0.59	1.1758
7	5	16QAM	0.37	1.4766
8	8	16QAM	0.48	1.9141
9	9	16QAM	0.6	2.4063
10	11	64QAM	0.45	2.7305
11	12	64QAM	0.55	3.3223
12	14	64QAM	0.65	3.9023
13	16	64QAM	0.75	4.5234
14	18	64QAM	0.85	5.1152
15	20	64QAM	0.93	5.5547

In Table I, the modulation and coding orders are taken from LTE [17], and the SINR ranges from [18]. In general, these values are operator specific, and hence are not standardised.

proportion of MSs that have acquired their desired rate, *i.e.*,

$$\chi = \frac{1}{n_{\text{usr}}} \sum_{u=1}^{n_{\text{usr}}} \mathbf{1}_{C_u \geq C_u^*} \,, \tag{7}$$

where n_{usr} is a random variable denoting the number of MSs in the scenario and C_u^* is the desired rate of MS_u. Lastly, Jain's Fairness Index [19] is used to calculate the throughput fairness of the system in each time slot

$$f(\mathbf{C}) = \frac{\left[\sum_u C_u\right]^2}{n_{\text{usr}} \sum_u C_u^2} \,, \tag{8}$$

where $\mathbf{C}$ denotes the throughputs of all MSs in the system.

A. Scenario Construction

A 5×5 apartment grid is considered for the femto-cell scenario, where the probability p_{act} describes the likelihood of an active FBS in a given apartment. Furthermore, we assume that multiple MSs may be present in an apartment. As it is unlikely all cells will have the same number of MSs, the user generation is implemented via probability table, where depending on the maximum number of users $\tilde{\mu}(u)$ allowed per cell, the number of MSs $n_c(u) \in \{1, \ldots, \tilde{\mu}(u)\}$ present in cell c is randomly chosen. Table II gives two examples of probability tables, where *(a)* equal probabilities are given to all $n(u)$, or *(b)* the probability reduces with each additional MS. Here, we utilise $\tilde{\mu}(u)$=3. An example of such a scenario is shown in Fig. 1. In each active femto-cell, both the MSs and FBS are uniformly distributed in the apartment. Due to the private deployment of femto-cells a closed-access system is assumed [20], so each FBS is assigned the MSs in its apartment, even if a foreign cell exhibits superior link conditions.

TABLE II
PROBABILITY TABLES FOR THE NUMBER OF USERS ALLOCATED IN A SINGLE FEMTO-CELL.

$\tilde{\mu}(u)$	1	2	3	4
$p_{n(u)=1}$	1	1/2	1/3	1/4
$p_{n(u)=2}$	0	1/2	1/3	1/4
$p_{n(u)=3}$	0	0	1/3	1/4
$p_{n(u)=4}$	0	0	0	1/4

(a)

or

$\tilde{\mu}(u)$	1	2	3	4
$p_{n(u)=1}$	1	2/3	4/7	8/15
$p_{n(u)=2}$	0	1/3	2/7	4/15
$p_{n(u)=3}$	0	0	1/7	2/15
$p_{n(u)=4}$	0	0	0	1/15

(b)

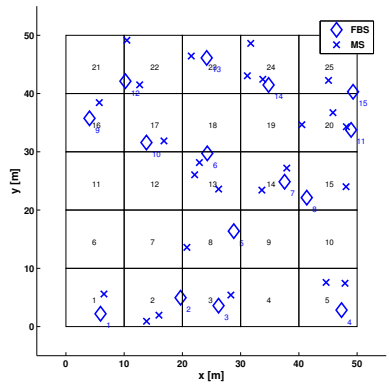

Fig. 1. Apartment block scenario with $p_{\text{act}} = 0.5$, where each apartment is $10\,\text{m}\times10\,\text{m}$, with $\tilde{\mu}(u)$=3 and equal user number probabilities. There are $N_{\text{app}}=5^2=25$ apartments in the scenario.

B. Channel Model

In general, the channel gain, $G_{k,l}^m$, between a transmitter l and receiver k, observed on RB m and separated by a distance d is determined by the path loss, log-normal shadowing, and channel variations caused by frequency-selective fading:

$$G_{k,l}^m = \left|H_{k,l}^m\right|^2 10^{\frac{-L_d(d)+X_\sigma}{10}} \,, \tag{9}$$

where $H_{k,l}^m$ describes the channel transfer function between transmitter l and receiver k on RB m, $L_d(d)$ is the distance-dependent path loss (in dB) and X_σ is the log-normal shadowing value (in dB) with standard deviation σ, as described in [21]. The channel response exhibits time and frequency dispersions, however channel fluctuations within a RB are not considered as the RB dimensions are significantly smaller than the coherence time and bandwidth of the channel [22]. Furthermore, the path loss $L_d(d)$ is identical on all RBs assigned to the MS. Finally, the delay profiles used to generate the frequency-selective fading channel transfer factor $H_{k,l}^m$ are taken from applicable propagation scenarios in [21], [23].

The path loss model used to calculate $L_d(d)$ is for indoor links [24], *i.e.*, the link (desired or interfering) between a FBS and an indoor MS, and calculates the path loss as

$$L_d(d) = \alpha + \beta \log_{10}(d) \quad [\text{dB}] \,. \tag{10}$$

where d is the distance between transmitter and receiver, and α, β are the channel parameters.

Log-normal shadowing is added to all links through correlated shadowing maps. These are generated such that the correlation in shadowing values of two points is distance-dependent. Table IV shows the shadowing standard deviation σ and auto-correlation distances considered, and all other simulation parameter values [24].

III. Distributed and Autonomous Resource Allocation

Due to the customer-side random deployment of femto-cells, and the resulting lack of fixed connective infrastructure, FBSs must perform resource and power allocation utilising locally available information only. To maximise performance in its own cell, a FBS must attempt to allocate RBs such that the desired signal on these is maximised, while the interference incident from neighbouring cells is minimal. Furthermore, the BS must allocate enough resources such that the rate requirements of the user(s) in the cell are fulfilled. The necessary, and locally available, information is therefore clearly determined:

- the required rate of a user determines the number of RBs that need to be assigned;
- the quality (*i.e.*, strength) of the desired signal dictates the necessary transmit power;
- the frequency-selective fading profile also affects the preferable RBs to be allocated; and
- the level of interference incident on the RBs strongly influences their allocatability.

All of these variables are locally available at the FBS in the reverse link, and at the MS(s) in the forward link, necessitating no extra information to be exchanged between BSs.

A. Fuzzy Logic for Autonomous Interference Coordination

In general, the resource and power allocation problem for a multi-cellular wireless network belongs to the class of mixed-integer non-linear programming (MINLP) problems; obtaining the solutions to these is known to be $\mathcal{NP}$-hard [25, 26]. Therefore, it is clear that a heuristic for local, autonomous resource management is required to solve this problem. A machine learning approach where FBSs acquire information about their transmission conditions over time would be such a viable solution, however can prove complex without the availability of training data. Therefore, we introduce fuzzy logic as our heuristic, through which "expert knowledge" is incorporated in the RB allocation decision process.

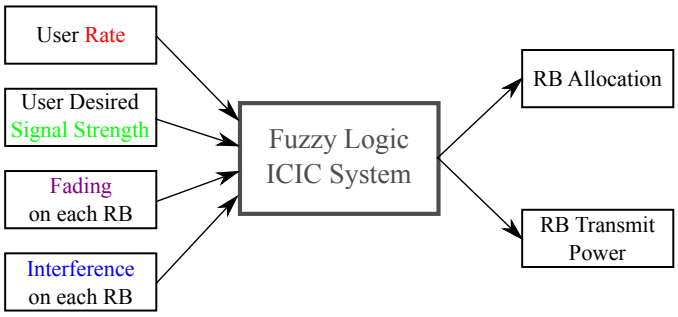

Fig. 2. Simplified graphical representation of our autonomous resource and power allocation technique.

The decision system, in its most simplified form, is represented in Fig. 2. In broad terms, the system evaluates which RB(s) are most suitable to be allocated to the MS in a given time slot, and determines the transmit power on these RBs to generate the required SINR such that the user's rate can be met. Obviously, an RB receiving little or no interference situated in a fading peak is most suitable for allocation to the femto-user, whereas any RB(s) receiving high interference, or experiencing deep fades, are much less appropriate.

In fuzzy logic, an input range is divided into multiple "membership functions" which give a coarse evaluation of the variable. These functions can have different shapes depending on the desired continuity between membership values. Here, the triangular (TRIMF), sigmoidal (SIGMF), and sigmoidal product (PSIGMF) membership functions are utilised, described by

$$f_{\mathrm{TRI}}(x;a,b,c) = \begin{cases} 0\,, & x \le a \\ \frac{x-a}{b-a}\,, & a \le x \le b \\ \frac{c-x}{c-b}\,, & b \le x \le c \\ 0\,, & c \le x \end{cases},$$

$$f_{\mathrm{SIG}}(x;a,c) = \frac{1}{1+e^{-a(x-c)}}\,,$$

$$f_{\mathrm{PSIG}}(x;a_1,c_1,a_2,c_2) = f_{\mathrm{SIG}}(x;a_1,c_1)f_{\mathrm{SIG}}(x;a_2,c_2)\,,$$

respectively. By combining the membership values of the inputs through various rules, the allocatability of each RB is determined. The output is also "fuzzy," indicating how suitable (or unsuitable) an RB is, avoiding a hard yes/no decision.

In each time slot, the FBS allocates the most applicable RBs to each MS, and data transmission is performed. Based on the received signal levels from the desired user and interfering MSs, the BS updates its information to more accurately represent the long-term interference and fading environments of its cell. This updated information is utilised in the next time slot to again carry out the, ideally improved, resource and power allocation. The same operation is performed in all femto-cells in the scenario, and the RB allocations are continuously individually optimised until the system converges to a stable solution, where the user(s) in each cell are satisfied.

1) Inputs: The input variables of the fuzzy logic system are:

- The **required rate** C^* of the MS is defined by the service being demanded by the user. The values

  Low: $f_{\mathrm{TRI}}(C^*;0,0,{}^3\!/\!_4\bar{C})$,
  Low-medium: $f_{\mathrm{TRI}}(C^*;{}^1\!/\!_2\bar{C},\bar{C},{}^3\!/\!_2\bar{C})$,
  Medium-high: $f_{\mathrm{TRI}}(C^*;{}^5\!/\!_4\bar{C},{}^7\!/\!_4\bar{C},{}^9\!/\!_4\bar{C})$, and
  High: $f_{\mathrm{TRI}}(C^*;2\bar{C},4\bar{C},4\bar{C})$,

  are used to categorise the rate requested by the user, where $\bar{C}$ is the average user desired rate. The ranges of these are dependent on the user scenario (*e.g.*, in femto-cells, a higher rate can be requested due to the superior channel conditions). This is a per-user requirement, and thus is equivalent for all RBs.
- The **desired signal level** S describes the transmission conditions from transmitter to receiver, *i.e.*, the stronger the desired signal, the better the channel between the two. The signal power domain is divided into thirds,

  Low: $f_{\mathrm{SIG}}(S;-2,F_{S,\mathrm{dB}}(0.4))$,
  Medium: $f_{\mathrm{PSIG}}(S;-2,F_{S,\mathrm{dB}}(0.6),2,F_{S,\mathrm{dB}}(0.4))$, and
  High: $f_{\mathrm{SIG}}(S;2,F_{S,\mathrm{dB}}(0.6))$,

  to sort users depending on their useful channels, where $F_{S,\mathrm{dB}}(s)$ is the cumulative distribution function (CDF) of the logarithmic desired signal. Since we consider the fast fading as a separate input, the desired signal level is

described per MS, and is thus equivalent over all RBs.

- The **fast fading component** $|H|$ for each RB may not always be readily available, however can become accessible via sounding or pilot/data transmission. Users' frequency selective fading profiles extend over the whole available bandwidth, and hence certain RBs are more suitable to an MS than others; or than to other MSs. The fast fading domain is split into

$$\begin{aligned} &\text{Deep:} && f_{\mathrm{SIG}}(S;-50,0.9),\\ &\text{Average:} && f_{\mathrm{PSIG}}(S;-50,1.1,50,0.9),\ \text{and}\\ &\text{Medium:} && f_{\mathrm{SIG}}(S;50,1.1), \end{aligned}$$

  centred around the mean fading level 1. In general, MSs should avoid RBs with "Deep" fades and try to acquire RBs with "Peak" fading values.
- The **level of interference** I illustrates the immediate interference environment for each MS on each RB. RBs with strong interference may indicate a close neighbouring cell currently utilising them, or even multiple interfering cells. Low or zero interference RBs would obviously be very attractive to a MS. The interference power domain is divided into thirds,

$$\begin{aligned} &\text{Low:} && f_{\mathrm{SIG}}(S;-2,F_{I,\mathrm{dB}}(0.4)),\\ &\text{Medium:} && f_{\mathrm{PSIG}}(S;-2,F_{I,\mathrm{dB}}(0.6),2,F_{I,\mathrm{dB}}(0.4)),\ \text{and}\\ &\text{High:} && f_{\mathrm{SIG}}(S;2,F_{I,\mathrm{dB}}(0.6)), \end{aligned}$$

  to categorise RBs by the amount of interference they suffer, where $F_{I,\mathrm{dB}}(i)$ is the CDF of the logarithmic interfering signal.

2) Fuzzy System: The fuzzy logic system is responsible for determining the allocatability of each RB in the cell, and the corresponding transmit powers. This is performed in three stages, as can be seen in Fig. 4. First, the fuzzified values of the inputs (see. Fig. 4) are fed into the **rule evaluation** stage, where these are combined to determine the "scores" of the membership functions of the outputs. These **rules** are defined in Table III. Most of these rules are self-explanatory. In essence, they are intuitive guidelines as to why a specific RB should be assigned to the MS or not, *e.g.*, allocating an RB that is receiving high interference (3. and 6.) is not beneficial except in certain cases; or allocating a medium-interference RB should not be done if the required rate is too high or the signal level is too low (4. and 5.). Finally, almost any RB with low interference can be allocated and be transmitted on with half power to achieve its rate (1.).

In the **rule output aggregation** stage, the results of all rules are combined for each RB to yield a fuzzy set representing *how much* an RB *should or should not* be allocated, and *how much* it *should or should not* transmit at half power (*i.e.*, if the majority of the rules yield "Yes" for RB allocation, then the RB *should* be allocated *more* than it *should not* be).

Finally, in the **defuzzification** stage, the *centre of gravity* (which is calculated using the integral-quotient in the Defuzzification box in Fig. 4) of the fuzzy set of each output is calculated to give a "score" for each RB. In essence, this stage determines finally the RB allocation (Yes/No) and the RB transmit power (Half/Max.), *e.g.*, an RB allocation score of 0.25 indicates a "Yes," and an RB transmit power score of 0.6 recommends maximum power transmission. Clearly, an RB with an allocation score of 0.1 is more allocatable than one with a score of 0.4.

3) Outputs: Finally, the outputs of fuzzy logic ICIC are:

- The **RB allocation** of the MS. The allocatability of each RB is calculated by fuzzy logic depending on the inputs. In the end, the BS assigns the required number of RBs to the MSs, choosing those that are most suitable for each. The lower the score, the better.
- The **transmit powers** of the RBs assigned to the MS. Each RB can transmit with either half or full (*i.e.*, maximum) power, depending on the inputs. For example, an RB with low interference may transmit at half power, whereas if the MS's desired signal is low or the fading on that RB is deep, full power should be utilised.

B. SINR-dependent Link Adaptation

In general, a wireless channel can change quite rapidly given alterations to its immediate environment, and hence there may be situations where a MS's desired link quality is much better/worse than necessary for its MCS. Alternatively, the scenario may arise when the BS/MS receives high interference from a nearby transmitter, and hence the user's SINR may fall below its target. Therefore, it is imperative that a MS can modify its MCS depending on the channel conditions. In Fig. 3, such an ability is added to the fuzzy logic ICIC system.

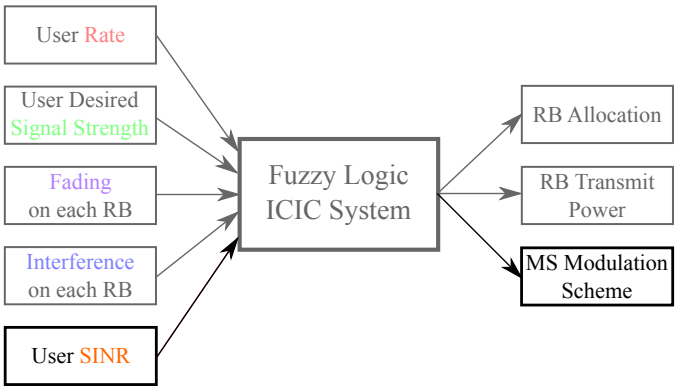

Fig. 3. Simplified graphical representation of our autonomous resource and power allocation technique with the opportunity for modulation scheme adaptation.

Since the success/failure of transmission on a given RB is mainly dependent on the SINR achieved on it, the MS SINR is utilised to directly modify the MS's MCS: this is called *link adaptation (LA)*. More specifically, the difference between the user's achieved average SINR $\bar{\gamma_u}$ and its target γ_u^*

$$\Delta_\gamma = \bar{\gamma_u} - \gamma_u^*\,, \tag{11}$$

is utilised. The membership functions for the SINR input and MCS output are shown in Fig. 4. It should be mentioned that only Δ_γ is used in the LA procedure, such that

- if $\Delta_\gamma > 3$ dB the input is "Better", and the MS modulation and coding order is "Increased by 1;"
- if $\Delta_\gamma > 5$ dB the input is "Marginally Better", and the MS modulation and coding order is "Increased by 2;"

TABLE III
FUZZY RULES

	Comb.	Des. Rate	Signal	Interference	Fading	SINR	RB Alloc.	Power	Modulation
1	AND	-	*not* Low	Low	-	-	Yes	Half	-
2	AND	Low	*not* Low	Med	Deep		Yes	Max.	-
3	AND	*not* Low	-	High	-	-	No	-	-
4	AND	Low-Med	*not* Low	Med	*not* Deep	-	Yes	Max.	-
5	AND	Med-High	*not* Low	Med	Peak	-	Yes	Max.	-
6	OR	-	-	High	Deep	-	No	-	-
7	AND	-	High	-	*not* Deep	-	Yes	Half	-
8	AND	-	Low	*not* Low	-	-	No	-	-
9	AND	Med-High	High	Med	Peak	-	Yes	Half	-
10	-	-	-	-	-	MuchWorse	-	-	Reduce3
11	-	-	-	-	-	Marg.Worse	-	-	Reduce2
12	-	-	-	-	-	Worse	-	-	Reduce1
13	-	-	-	-	-	Adequate	-	-	NoChange
14	-	-	-	-	-	Better	-	-	Increase1
15	-	-	-	-	-	Marg.Better	-	-	Increase2
16	-	-	-	-	-	MuchBetter	-	-	Increase3

- if $\Delta_\gamma > 7\,\text{dB}$ the input is "Much Better", and the MS modulation and coding order is "Increased by 3;"
- if $\Delta_\gamma < -3\,\text{dB}$ the input is "Worse", and the modulation and coding order is "Reduced by 1;"
- if $\Delta_\gamma < -5\,\text{dB}$ the input is "Marginally Worse", and the modulation and coding order is "Reduced by 2;"
- if $\Delta_\gamma < -7\,\text{dB}$ the input is "Much Worse", and the modulation and coding order is "Reduced by 3;" or lastly
- if $-3 < \Delta_\gamma < 3\,\text{dB}$ the input is "Adequate", and the modulation and coding order undergoes "No Change."

These rules are shown in Table III. Through this procedure, a user may fit its MCS to its transmission environment, and hence more easily achieve its target rate. Moreover, the average SINR $\bar{\gamma_u}$ is considered to prevent a MS from "ping-pong"-ing between MCSs, which may severely complicate the scheduling procedure. It should be noted that the input membership functions utilise the TRIMF over their respective ranges.

Finally, one might argue that given a user's signal strength and RB interference information, that a separate SINR input is unnecessary. However, because the MS can only receive interference information from other users transmitting on specific RBs, it is not guaranteed that it receives interfering signals on all RBs. Furthermore, the desired signal is also only measured on the allocated RBs, so a standard measure of the average SINR is the most precise description of an MS's overall transmission conditions.

A graphical representation of the fuzzy logic ICIC system and the input "fuzzification" is shown in Fig. 4.

C. Scheduling

Given the common assumption in femto-cell networks that only a single MS is present per cell, this user can be allocated the RBs with the best scores (as determined by the fuzzy logic system). In the reverse link, the contiguity constraint (specific to LTE) is fulfilled by allocating the required number of consecutive RBs with the least sum-score. With each FBS allocating the most suitable RBs in their cell, a natural frequency reuse will result. More specifically, it can be shown that neighbouring FBSs will allocate orthogonal sets of RBs, whereas femto-cells further from each other (*i.e.*, less interfering) may assign the same RBs without excessive interference.

There are, however, many possibilities to perform resource allocation in the presence of multiple users. For instance, in the forward link an FBS may simply assign RBs in the ascending order of scores calculated for all MSs. This is clearly a greedy approach, and may not be optimal in cases where MSs have vastly different channel conditions (not usually the case in femto-cells, but possible). Another possibility, then, for resource allocation may be a proportional fair scheduler (PFS), where the RB scores for each user are scaled by the ratio of achieved and desired rates. Here, an MS that strongly underachieved its rate would be allocated RBs before an MS that was closer to its target. Lastly, a "priority" scheduler may be utilised to give precedence to users with higher required rates/modulation orders, to more likely fulfil their QoS requirements.

D. Signal Statistics

In Fig. 4, the membership functions of the desired and interfering signal inputs are determined via analysis of the signal statistics in the deployment environment. While these can be determined experimentally, we analytically derive here these statistics such that they can be expanded to other scenarios. Thus, we know the power of any received signal P_r is calculated as

$$\begin{aligned} P_r &= P_t G \\ P_{r,\text{dB}} &= P_{t,\text{dB}} + G_{\text{dB}} = P_{t,\text{dB}} - L_{\text{dB}} \end{aligned} \tag{12}$$

where $L_{\text{dB}} = L_{d,\text{dB}} + X_\sigma$ is the signal path loss, and L_d and X_σ are described in Section II-B. Hence, the probability distribution function (PDF) of P_r (in dB) is given by

$$f_{P_r,\text{dB}}(\varrho) = f_{P_t,\text{dB}}(\theta) \circledast f_{L,\text{dB}}(-l; D)\,, \tag{13}$$

where $\circledast$ denotes the convolution operator, and D denotes the spatial dimension(s) by which the loss (which is distance-dependent) is parametrised, *i.e.*, in this case the apartment block. And since

$$f_{L,\text{dB}}(l; D) = f_{L_d,\text{dB}}(l) \circledast f_{X_\sigma,\text{dB}}(x)\,, \tag{14}$$

by finding $f_{L_d,\text{dB}}(l)$ and $f_{P_t,\text{dB}}(\theta)$, $f_{P_r,\text{dB}}(\varrho)$ is derived for both desired and interfering signals.

Due to the random nature of the BS and MS positions,

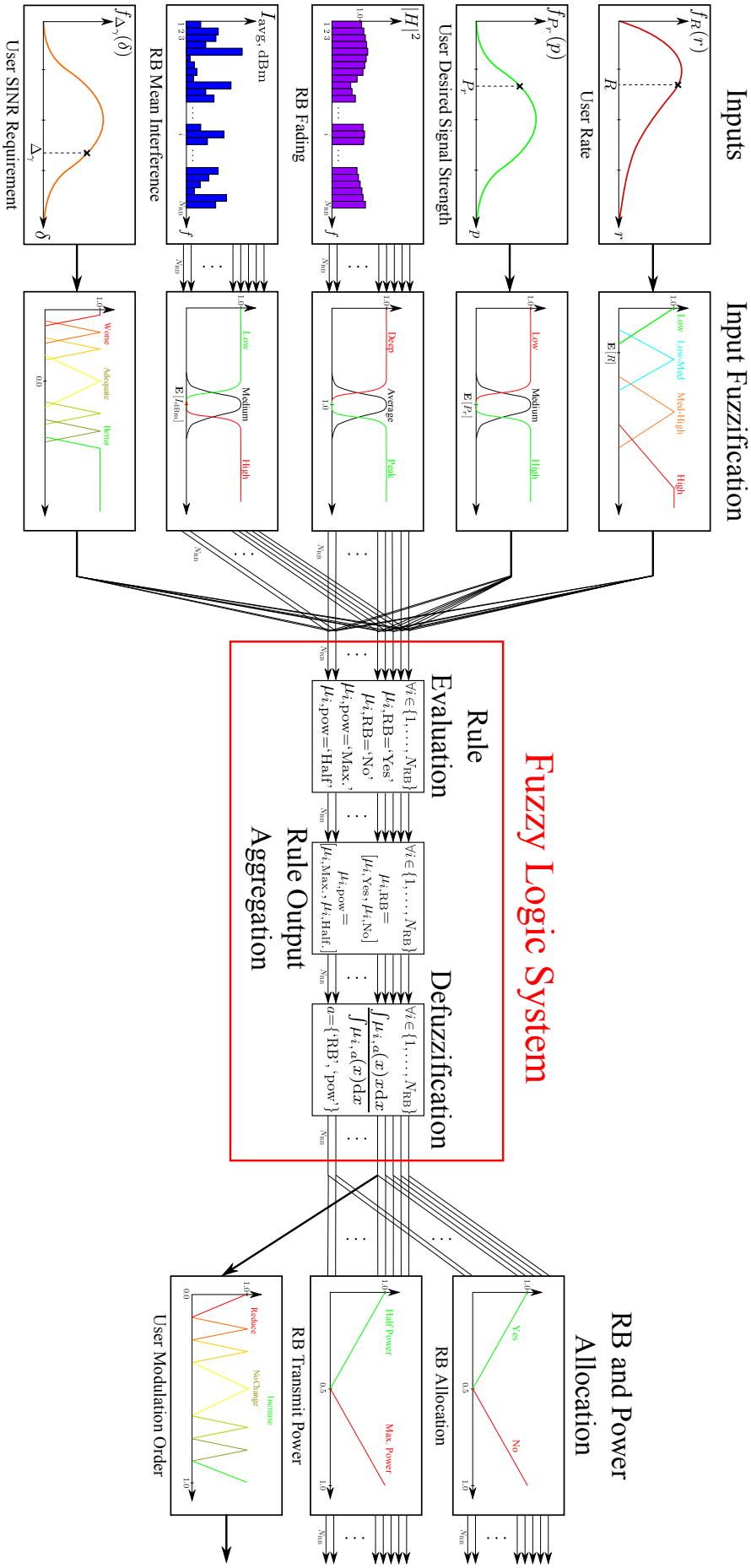

Fig. 4. Graphical representation of fuzzy logic resource and power allocation system.

the first step in analysing the signal PDFs is estimating the distribution of the path losses between transmitter (whether it is desired or interfering) and receiver. From (10) it is clear that the path loss l is proportional to the Tx-Rx distance d, and the inverse relationship is given by

$$\rho(l) = d = 10^{(l-\alpha)/\beta}\,. \tag{15}$$

Thus, the distance dependent loss PDF $f_{L_d,\mathrm{dB}}(l;D)$ is derived

$$f_{L_d,\mathrm{dB}}(l;D) = \left|\frac{\mathrm{d}\rho(l)}{\mathrm{d}l}\right| f_d(\rho(l);D) \tag{16}$$

$$\left|\frac{\mathrm{d}\rho(l)}{\mathrm{d}l}\right| = \frac{\ln 10}{\beta}10^{l-\alpha/\beta} = \frac{\ln 10}{\beta}\rho(l)$$

$$f_{L_d,\mathrm{dB}}(l;D) = \frac{\ln 10}{\beta}\rho(l) f_d(\rho(l);D)\,, \tag{17}$$

where $f_d(\rho(l);D)$ is the PDF of the Tx-Rx distance parametrised by D. This PDF is given in [27] by (18). Thus, by evaluating (17), the distance-dependent path loss PDF $f_{L_d,\mathrm{dB}}(l;D)$ becomes (19), where $\delta(l)=\rho(l)/D$. This PDF can be seen for both the desired signal (D=10m) and the interfering signal (D=50m, as interferer and receiver could be located in any two apartments in the scenario) in Fig. 5(a). Monte Carlo simulations that randomly place two nodes within the given dimensions $D\times D$, and calculate the resulting path loss, verify that the PDF given in (19) is indeed correct.

Referring back to (12), we have accurately described the path loss L_{dB}, and must now find the distribution of the RB transmit powers P_t. In our model, each MS transmits with a maximum *total* power $P_{\max}$ that is spread evenly over all RBs assigned to it. The number of RBs n^{RB} an MS is assigned is directly dependent on the required rate C^* of the user, thus P_t is defined by

$$P_t = \frac{P_{\max}}{n^{\mathrm{RB}}} \qquad \text{where } n^{\mathrm{RB}} = \left\lceil \frac{C^*}{k_{\mathrm{sc}} s_{\mathrm{sc}}} \right\rceil$$
$$= \frac{P_{\max} k_{\mathrm{sc}} s_{\mathrm{sc}}}{C^*} = \frac{A}{C^*}\,. \tag{20}$$

Here, the ceiling operation is removed for ease of derivation, however without loss of generality. Therefore, it is clear from (20) that P_t is inversely proportional to the rate r, which in our scenario is a random variable with distribution $f_{C^*}(r)$. Hence, the CDF of the transmit power $F_{P_t}(p)$ is given by

$$F_{P_t}(p) = \mathbf{P}\left[P_t \le p\right] = \mathbf{P}\left[\frac{A}{r} \le p\right] = \mathbf{P}\left[\frac{A}{p} \le r\right]$$
$$= 1 - \mathbf{P}\left[r \le \frac{A}{p}\right] = 1 - F_{C^*}\left(\frac{A}{p}\right)\,,$$

where $F_{C^*}(r)$ is the CDF of user desired rates, and therefore the PDF of the MS transmit power $f_{P_t}(p)$ is given by

$$f_{P_t}(p) = \frac{\mathrm{d}F_{P_t}(p)}{\mathrm{d}p} = \frac{A}{p^2} f_{C^*}\left(\frac{A}{p}\right) \tag{21}$$

The general expression is given in (21) for any rate PDF $f_{C^*}(r)$. Now, we need to perform a change of variable transform to determine the PDF of the transmit power in dB (refer to (12))

$$\theta = P_{t,\mathrm{dB}} = 10\log_{10}(P_t)\,, \tag{22}$$

and the inverse is given by

$$\varphi(\theta) = p = 10^{\theta/10}\,. \tag{23}$$

The PDF of MS transmit power $f_{P_t,\mathrm{dB}}(\theta)$ is calculated by

$$f_{P_t,\mathrm{dB}}(\theta) = \left|\frac{\mathrm{d}\varphi(\theta)}{\mathrm{d}\theta}\right| f_{P,\mathrm{dB}}(\varphi(\theta)) \tag{24}$$

$$\left|\frac{\mathrm{d}\varphi(\theta)}{\mathrm{d}\theta}\right| = \frac{\ln 10}{10}10^{\theta/10} = \frac{\ln 10}{10}\varphi(\theta)\,,$$

hence

$$f_{P_t,\mathrm{dB}}(\theta) = \frac{\ln 10}{10}\varphi(\theta) f_{P_t}(\varphi(\theta))$$
$$= \frac{\ln 10}{10}\frac{A}{\varphi(\theta)} f_{C^*}\left(\frac{A}{\varphi(\theta)}\right) \tag{25}$$

where (25) is the general expression for any rate distribution. Thus, the PDF of user transmit power has been derived, however under the assumption of transmission of a single bit per channel use. This is, of course, not a realistic assumption, and in our scenario we consider a user's ability to send with various MCSs (see Table I). Clearly, the MCS affects the number of RBs required by an MS, and thus also the MS transmit power. This is shown in (26)

$$P_t = \frac{P_{\max}}{n_{\mathrm{RB}}} \qquad \text{where } n_{\mathrm{RB}} = \left\lceil \frac{C^*}{k_{\mathrm{sc}} s_{\mathrm{sc}} \varepsilon_{\mathrm{s}}} \right\rceil$$
$$= \frac{P_{\max} k_{\mathrm{sc}} s_{\mathrm{sc}} \varepsilon_{\mathrm{s}}}{C^*} = \frac{A\varepsilon_{\mathrm{s}}}{C^*}\,. \tag{26}$$

Further, we assume each user is uniformly distributed a MCS[1], hence by replacing (20) with (26) and performing the same CDF transformation, the transmit power PDFs (*i.e.*, $f_{P_t}(p)$ and $f_{P_t,\mathrm{dB}}(\theta)$) are modified correspondingly as

$$f_{P_t}(p) \to \frac{1}{16}\sum_{\hat{m}=0}^{15} \frac{A\varepsilon_{\mathrm{s}}(\hat{m})}{p^2} f_{C^*}\left(\frac{A\varepsilon_{\mathrm{s}}(\hat{m})}{p}\right)\,,$$

$$f_{P_t,\mathrm{dB}}(\theta) \to \frac{\ln 10}{160}\sum_{\hat{m}=0}^{15} \frac{A\varepsilon_{\mathrm{s}}(\hat{m})}{\varphi(\theta)} f_{C^*}\left(\frac{A\varepsilon_{\mathrm{s}}(\hat{m})}{\varphi(\theta)}\right) \tag{27}$$

where $\hat{m}$ is the CQI index in Table I, and again, (27) is the general expression for any user rate distribution. Now, if we revisit that $n_{\mathrm{RB}}=\left\lceil \frac{C^*}{k_{\mathrm{sc}} s_{\mathrm{sc}} \varepsilon_{\mathrm{s}}} \right\rceil$, it is clear that only integer number of RBs can be assigned to each MS, and thus each user can only assume a transmit power from a discrete set of $P_t=\frac{P_{\max}}{n^{\mathrm{RB}}}$

$$P_t \in \left\{\frac{P_{\max}}{1}, \frac{P_{\max}}{2}, \cdots, \frac{P_{\max}}{M}\right\}\,, \tag{28}$$

where M denotes the total number of RBs available in each cell. Thus, $f_{P_t}(p)$ is evaluated at the powers in (28), as are the histogram bins in the Monte Carlo simulation, the results of which are presented in Fig. 5(a) for $C^*\sim\mathrm{Rayl}\left(\bar{C}\right)$, where $\bar{C}$ is the average rate. The close match of theoretical and empirical results confirms that the derivation for $f_{P_t,\mathrm{dB}}(\theta)$ is accurate.

Thus, we have now found accurate and precise analytical models for the distributions of the path losses and transmit

[1]This would be independent of its signal quality. This is not the best assumption, admittedly, however the reason is to further randomise the user requirements, and hence the necessary RB allocations. Through this, the allocation problem becomes more challenging for ICIC techniques, including our own.

$$f_d(d;D) = \begin{cases} 2\frac{d}{D}\left(\left(\frac{d}{D}\right)^2 - 4\frac{d}{D} + \pi\right) & 0 \le d \le D \\ 2\frac{d}{D}\left[4\sqrt{\left(\frac{d}{D}\right)^2 - 1} - \left(\left(\frac{d}{D}\right)^2 + 2 - \pi\right) - 4\tan^{-1}\left(\sqrt{\left(\frac{d}{D}\right)^2 - 1}\right)\right] & D < d \le \sqrt{2}D \end{cases} \tag{18}$$

$$f_{L_d,\mathrm{dB}}(l;D) = \frac{\ln 10}{\beta}\rho(l) \begin{cases} 2\delta(l)\left(\delta(l)^2 - 4\delta(l) + \pi\right) & \alpha \le l \le L(D) \\ 2\delta(l)\left[4\sqrt{\delta(l)^2 - 1} - \left(\delta(l)^2 + 2 - \pi\right) - 4\tan^{-1}\left(\sqrt{\delta(l)^2 - 1}\right)\right] & L(D) < l \le L\left(\sqrt{2}D\right) \end{cases} \tag{19}$$

powers, which are directly dependent on the network topology of the investigated scenario. From (12) it is clear that

$$f_{P_r,\mathrm{dB}}(\varrho) = f_{P_t,\mathrm{dB}}(\theta) \circledast f_{L,\mathrm{dB}}(-l;D)\,. \tag{29}$$

Hence, the desired and interfering signal PDFs are given in (30) and (31), respectively,

$$f_{S,\mathrm{dB}}(s) = f_{P_t,\mathrm{dB}}(\theta) \circledast f_{L,\mathrm{dB}}(-l;D{=}10) \tag{30}$$

$$f_{I,\mathrm{dB}}(i) = f_{P_t,\mathrm{dB}}(\theta) \circledast f_{L,\mathrm{dB}}(-l;D{=}50)\,. \tag{31}$$

In Fig. 5(b) a comparison to simulation results is drawn, where it is evident that the theoretical CDFs are slightly shifted from their experimental counterparts. The general shape (*i.e.*, variance) of the CDFs is accurate, and while there is a minor shift (1-2 dB) between simulation and theory, this difference is within the numerical margin of error, and thus acceptable.

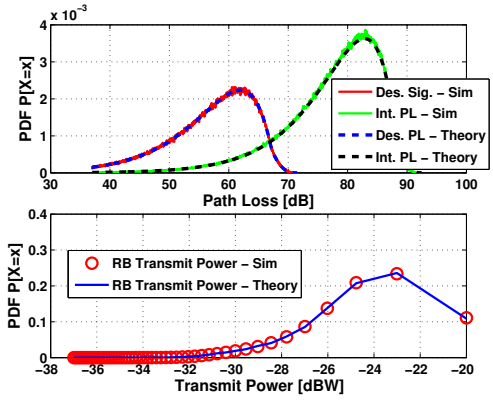

(a) Path Loss and Transmit Power PDFs

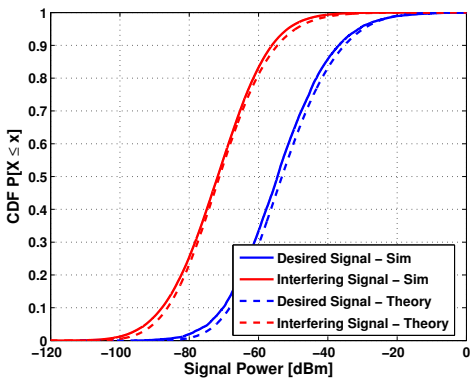

(b) Signal Energy CDFs

Fig. 5. Comparison of derived theoretical desired and interfering signal PDFs and CDFs to Monte Carlo simulation results, considering lognormal shadowing.

It is clear that the signal strength PDFs are mainly dependent on the distance between transmitter and receiver, and the transmit power. Therefore, extending fuzzy logic ICIC to other scenarios is straightforward, as simply the distance PDF $f_d(d;D)$ must be modified to fit the new environment, and the statistics can be found. Hence, not only have the received signals been derived for the femto-cell scenario, they are easily modified to other environments, thus expanding the applicability of fuzzy logic ICIC to virtually any wireless network.

IV. Optimality of Fuzzy Logic ICIC

Due to the heuristic nature and non-linearity of fuzzy logic, it is very difficult to perform a comprehensive theoretical analysis of the system performance of fuzzy logic ICIC. Therefore, to analyse the optimality of our technique, we experimentally compare fuzzy logic ICIC to the system-optimal performance, and a greedy heuristic of similar complexity. We demonstrate that fuzzy logic ICIC provides close-to-optimal throughput and coverage at significantly reduced complexity.

A. System Optimisation

The most obvious choice for performance comparison is that of posing the resource allocation as a system-wide optimisation problem. Since fuzzy logic is autonomous and, more importantly, distributed it *should*, on average, be suboptimal in terms of overall system performance. The optimal RB allocation of the system can be achieved by solving the problem posed in (32), and thus the aim of fuzzy logic is to as closely as possible approach the result of this problem. Given the definition for user throughput (4) and system sum throughput (5), we solve

$$\max \quad C_{\mathrm{sys}} = \sum_u C_u \qquad u{=}1,\,2,\,\ldots,\,n_{\mathrm{usr}}\,. \tag{32}$$

$$\text{s.t.} \quad \sum_{j=1}^{M} \mathbf{1}_{P_{u,j}>0} = n_u^{\mathrm{RB}} \qquad \forall u \tag{32a}$$

$$\sum_{j=1}^{M} P_{u,j} \le P_{\max} \qquad \forall u \tag{32b}$$

$$P_{u,j} \ge 0 \qquad \forall u, j \tag{32c}$$

in order to determine the maximum rate achievable in a given scenario. In the constructed MINLP [26] problem, (32b) and (32c) describe the restrictions on transmit power allocation at each MS: the sum of the allocated powers on all RBs cannot exceed $P_{\max}$, and the individual powers must be non-negative, respectively. The constraint (32a) limits the number of transmitting RBs at a single MS to the n_u^{RB} the user

needs to achieve its desired rate. This is necessary as since the objective is sum-rate-maximisation, the best solution is generally transmission on most, if not all RBs. However, since fuzzy logic ICIC only aims to satisfy user requirements, this would be an unfair comparison; hence the constraint (32a). It should be mentioned that a minimum rate constraint was originally considered. However, if a single MS cannot achieve its target rate, then no solution can be found by the problem, and hence this constraint was removed.

It is clear from C_u in (4) that (32) is non-linear, non-convex and, more significantly, *discrete*, which is further highlighted by the discrete set of constraints in (32a). In [28], the theory of Lagrange multipliers is extended to discrete space, utilising a *direction of maximum potential drop* to iterate through the solution space and optimise the objective function. We use this technique to find the system-optimal RB allocation.

B. Greedy Heuristic

While the comparison to the system-wide optimisation problem will demonstrate the optimality of fuzzy logic ICIC, it is important to note that we are comparing a centralised and a distributed approach. Therefore, we implement a commonly utilised distributed allocation technique, which "greedily" allocates the best RBs to the MS(s) in the cell [8]. Here, the potential SINR achievable on each RB is calculated using prior interference, signal, and transmit power information; and then the RBs with the strongest SINRs will be allocated to the user.

$$\begin{aligned} &\text{Given:} \quad P_u = {}^{P_{\max}}/_{n_u^{\mathrm{RB}}},\ I_u^m,\ G_{u,v_u}^m \quad m{=}1,\,2,\,\ldots\,,\,M\,, \\ &\text{Find:} \quad \gamma_u^m = \frac{P_u G_{u,v_u}^m}{I_u^m + \eta} \qquad \forall m\,. \end{aligned} \tag{33}$$

In (33), the same information is available as for fuzzy logic, and a greedy approach is utilised to allocate the RBs. This technique should maximise the throughput in each cell, however it does not take a system view as in (32), and hence will be suboptimal in terms of network throughput.

Therefore, we argue that the comparison to this greedy heuristic will show the optimality of fuzzy logic on a cell-individual basis, whereas the comparison to the optimisation problem shows the optimality achieved at the network level.

C. Results Comparison

To compare the performance of these two methods, fuzzy logic ICIC and a commonly utilised benchmark (proportional fair (PF) scheduling and maximum power transmission), a Monte Carlo simulation is run utilising the $5{\times}5$ apartment grid model described in Section II-A, with $\tilde{\mu}(u){=}1$ (*i.e.*, a single user per cell), and $\bar{C}{=}1.25$ Mbps. We utilise standard fuzzy logic ICIC without LA, as neither the optimisation technique nor the greedy heuristic employ LA. Fig. 6 shows the throughput and availability results for this scenario, where it is evident that the system-optimum solution cannot be reached by the distributed techniques. However, fuzzy logic is able to perform, on average, within 4% of the optimum throughput performance, and in fact the difference after 20 time slots (*i.e.*, two LTE frames) is less than 2%. Furthermore, it is clear that the average throughput of fuzzy logic is improved over the

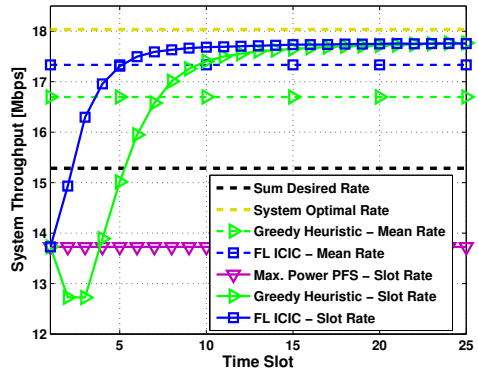

(a) Throughput

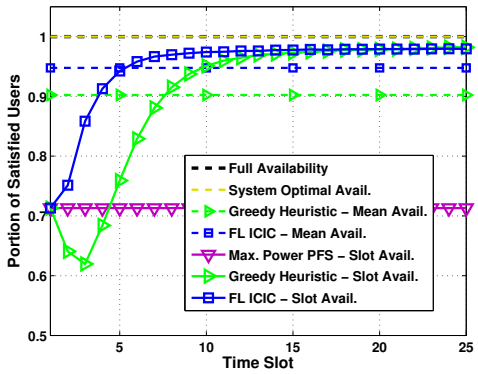

(b) Availability

Fig. 6. System performance comparison of fuzzy logic ICIC, the system-wide optimal solution, the proposed greedy heuristic and PFS maximum power transmission.

greedy heuristic (by 4%), even though after 15 time slots the performance is similar. This highlights that fuzzy logic ICIC is optimal on a cell-individual basis, and is able to (due to other inputs such as rate requirement and desired signal strength) converge to this optimum much quicker. On the other hand, the performance difference to the optimum is minute, and therefore fuzzy logic ICIC provides a "near-optimal" solution for the network as a whole.

The substantial decline in performance by the greedy heuristic in the first time slots results from the lack of interference information. The unused RBs with "zero" interference are allocated in all cells simultaneously, thus causing large outages in these slots. After more accurate statistics have been received, the performance improves as expected.

The same trends can be seen for the system availability, where while the optimum is clearly full availability (*i.e.*, $\chi{=}1$), fuzzy logic ICIC achieves 98% coverage, and hence produces almost negligible outage. Furthermore, it is able to reach this availability much faster than the greedy heuristic, indicating that fuzzy logic ICIC employs a balance between system-wide optimisation and cell-individual performance.

Finally, not only does the rapid convergence of fuzzy logic ICIC establish significant advantages over the greedy heuristic, it also demonstrates the operability of our technique in dynamic channel environments. While the considered femtocell scenario may not represent such an environment, the

achievement of average performance in 5 subframes, and peak performance in 10 indicates that fuzzy logic ICIC will achieve near-optimal solutions for even rapidly varying channel characteristics (*e.g.*, due to high mobility), as the convergence remains largely within the channel coherence times [17].

D. Complexity

To conclude our comparison, we analyse the complexities of the three schemes, to highlight the simplicity and efficiency of our fuzzy logic technique. In a cell where fuzzy logic ICIC is applied, $K{=}4$ inputs (see Fig. 2) are combined at each of M RBs available at the FBS, inducing a complexity of KM. Following this, the RBs are sorted according to their fuzzy score, in order to allocate the most appropriate to the MS. Since, in general, sorting algorithms demonstrate $O(N^2)$ complexity, the fuzzy logic complexity within a cell increases to $(KM)^2$. Furthermore, fuzzy logic ICIC requires multiple subframes $N_{\text{sf}}{\approx}10$ to converge to its operating performance. Finally, given a scenario with n_{usr} MSs, the system complexity of fuzzy logic ICIC is given by

$$O\left(n_{\text{usr}} N_{\text{sf}} (KM)^2\right) .$$

The greedy heuristic utilises a similar methodology as fuzzy logic, in that it also computes a "score" (in this case the instantaneous SINR) for each RB and then orders them for allocation. Hence, the evaluation complexity at each RB is KM (where in this case $K{=}2$ inputs), the sorting complexity is $(KM)^2$ in each of $N_{\text{sf}}{\approx}20$ time slots, and the overall complexity is given by

$$O\left(n_{\text{usr}} N_{\text{sf}} (KM)^2\right) .$$

For the optimisation problem (32), finding the solution complexity is more challenging than for the heuristics, as the problem is considered $\mathcal{NP}$-hard [26]. In general, $\mathcal{NP}$-hard problems are only solvable (if possible) in exponential time. Using [28], and defining a neighbour in the RB allocation space as having a Hamming distance of 2 (*i.e.*, a single RB re-allocation), there are $\sum_{u=1}^{n_{\text{usr}}} n_u^{\text{RB}} \left(M - n_u^{\text{RB}}\right)$ neighbours at each point in the search space. At each neighbour, the RB SINRs and consequent system throughput must be calculated, inducing a complexity of $O\left(M n_{\text{usr}} \left(1 + n_{\text{usr}}\right)\right)$. Finally, we determined experimentally that the algorithm needs $N_{\text{step}}{\approx}10$ steps to converge, and hence the overall complexity of (32) is

$$O\left(N_{\text{step}} \sum_{u=1}^{n_{\text{usr}}} n_u^{\text{RB}} \left(M - n_u^{\text{RB}}\right) M n_{\text{usr}} \left(1 + n_{\text{usr}}\right)\right) .$$

This is clearly much greater than the complexity of the two heuristics, which is expected. A comparison of the achieved throughputs and required complexities of the three techniques is shown in Fig. 7, where

$$\mu_{n_{\text{usr}}} = \frac{N_{\text{app}}}{2} p_{\text{act}} (\tilde{\mu}{+}1) = 12.5 ,$$
$$\sigma_{n_{\text{usr}}} = \sqrt{\frac{N_{\text{app}}}{2} p_{\text{act}} (\tilde{\mu}^2{-}1) + \frac{N_{\text{app}}}{4} p_{\text{act}} (1{-}p_{\text{act}}) (\tilde{\mu}{+}1)^2} = 2.5 ,$$

are the mean and standard deviation of n_{usr}, respectively (and given for the investigated scenario parameters $N_{\text{app}}{=}25$, $\tilde{\mu}{\equiv}\tilde{\mu}(u){=}1$, and $p_{\text{act}}{=}0.5$), and

$$\mu_{n_u^{\text{RB}}} = \frac{\bar{C}}{B_{\text{RB}}} \mathbf{E}\left[{}^1\!/_{\varepsilon_{\text{s}}}\right] = 9.41 ,$$
$$\sigma_{n_u^{\text{RB}}} \approx \sqrt{2 \frac{\bar{C}}{B_{\text{RB}}} \mathbf{E}\left[{}^1\!/_{\varepsilon_{\text{s}}^2}\right] - \mu_{n_u^{\text{RB}}}^2} = 14.76 \qquad (34)$$

are the mean and standard deviation of n_u^{RB}, respectively (and evaluated for $\bar{C}{=}1.25$ Mbps). Furthermore, n_{usr} is normally distributed (due to sufficient N_{app}), however the distribution of n_u^{RB} is dependent on the required rate distribution, which may vary (as indicated in Section V-B).

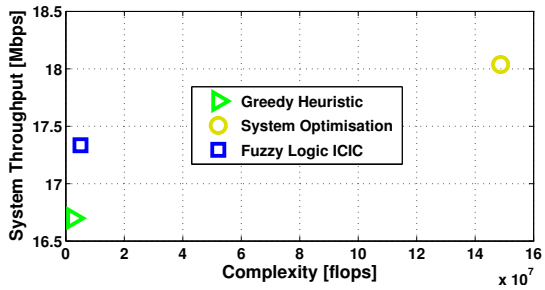

Fig. 7. System throughput versus required complexity for fuzzy logic ICIC, the system-wide optimal solution, and the proposed greedy heuristic.

It is evident that, while (32) provides the greatest system throughput, it is substantially more complex than both fuzzy logic and the SINR heuristic, which only suffer slightly in terms of achieved throughput. On the other hand, it is clear that fuzzy logic ICIC provides enhanced throughput and coverage for the system compared to the greedy heuristic, even though the complexities are very similar. Hence, we conclude that fuzzy logic provides low-complexity, near-optimal system performance in an autonomous and distributed manner.

V. Simulation

Monte Carlo simulations are used to provide performance statistics of the system with fuzzy logic ICIC and two benchmarks. The simulator is built following LTE specifications.

A. Scenario Construction and User Distribution

A $5{\times}5$ apartment grid is considered for the simulation environment with $\tilde{\mu}(u){=}3$ (see Fig. 1), and is constructed as described in Section II-A. In order to obtain statistically relevant results, the random effects from MS/BS placement, lognormal shadowing and frequency selective fading must be removed. Therefore, 2000 scenarios (with minimum three FBSs) are simulated and the results combined to acquire mean performance statistics of the system.

B. Resource Allocation

Each MS is assigned two transmission requirements: a desired throughput and MCS. The desired rate C_u^* of each user is drawn from a random distribution[2] with mean $\bar{C}$. Due to this, each MS_u will require a different number of RBs n_u^{RB}, and hence the system will function best when strongly interfering FBSs are assigned orthogonal resources.

[2]The distribution can be dependent on the scenario and traffic/applications (*i.e.*, internet, mobile TV, etc.) desired by the users.

The MCS is also assigned randomly, with equal probabilities for all available symbol efficiencies. While this is not the most realistic assumption, it has been applied here to further randomise the number of RBs each MS needs to achieve its rate. However, when LA is applied, the user's MCS will more accurately reflect its SINR conditions. Furthermore, the number of RBs requested will clearly change dependent on the modulation order selected.

Finally, RBs are allocated individually in each cell by the FBS. In the benchmarks, a PFS is used for RB assignment, which improves the frequency diversity relative to a random allocation. On the other hand, the fuzzy logic ICIC technique autonomously allocates RBs based on the local information available, in order to optimise the MS(s) performance in the cell. For our purposes, the allocation of RBs to MSs is performed greedily, as described in Section III-C.

C. Time Evolution

Each run of the Monte Carlo simulation is iterated over z=25 subframes, or, equivalently, 2.5 LTE frames, such that long-term SINR statistics can be gathered. Due to the random user and FBS distribution, plentiful runs with different network generations are considered in order to obtain statistically accurate results. At the start of each subframe, the scheduling and allocation of RBs is reperformed. The MSs are assumed to be quasi-static for the duration of a run.

The simulation is performed for a constant-traffic model, where each user requests the same number of RBs in each time slot (*i.e.*, subframe). Furthermore, the users are assumed to be static for the duration of a subframe, such that effects due to Doppler spread can be neglected. Perfect synchronisation in time and frequency is assumed, such that intra-cell interference is avoided. The simulation parameters are found in Table IV.

TABLE IV
SIMULATION PARAMETERS

Parameter	Value
Apartment width, W	10 m
FBS probability, p_{act}	0.5
System bandwidth, B	10 MHz
Number of available RBs, M	50
RB bandwidth, B_{RB}	180 kHz
Average rate, $\bar{C}$	1.25 Mbps
Subcarriers per RB, k_{sc}	12
Symbol rate per subcarrier, s_{sc}	15 ksps
Time slots	25
ABS prob., Γ_{ABS}	0.1
Spectral noise density, η_0	$-174\,\text{dBm/Hz}$
Total FBS transmit power	10 dBm
Channel parameters α, β	37, 30
Shadowing Std. Dev., σ	10 dB
Auto-correlation distance	50 m

D. Benchmarks

To evaluate the performance of fuzzy logic ICIC, two well-known benchmark systems have been implemented for comparison purposes. These are:

- **Maximum Power Transmission**: In the first benchmark, no power allocation is performed, and all MSs transmit at the maximum power on each RB.
- **Random ABS Transmission**: In the second benchmark, again all links transmit at full power, however, in each time slot a user transmits an ABS with probability Γ_{ABS}, where for this simulation Γ_{ABS}=0.1.

VI. RESULTS AND DISCUSSION

From the simulation, the statistics of the system throughput, energy efficiency, availability and fairness are generated for systems employing fuzzy logic ICIC and compared against the two benchmark systems. General simulation parameters are taken from Table IV and [29].

It is clear from Fig. 8 that fuzzy logic ICIC provides substantially improved system performance over both benchmark techniques. Especially in terms of system throughput, where the fuzzy logic schemes are the only techniques which achieve the overall desired rate (*i.e.*, sum of individual desired rates). In fact, fuzzy logic substantially overachieves the sum desired rate, indicating almost maximum coverage and all but negligible outage. The additional rate results from the discrete allocation of bandwidth (*i.e.*, RBs), and hence the achieved user rate is generally slightly greater than what was desired. With LA this becomes more apparent, as with higher spectral efficiency the throughput "overshoot" becomes even greater.

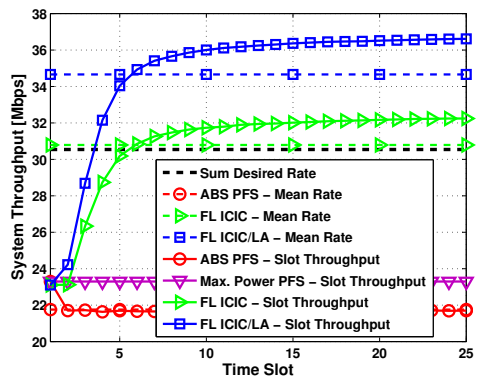

(a) Throughput

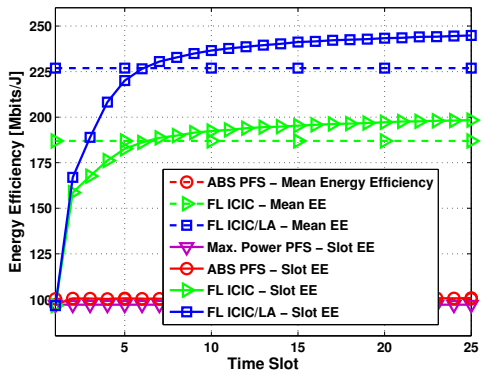

(b) Energy Efficiency

Fig. 8. System efficiency performance results of fuzzy logic ICIC, random ABSs transmission, and maximum power transmission.

The ABS performance is constant over all time slots (except the first), as the probability of ABS transmission(s) is identical in each slot. Hence, in each time slot 10%, on average, of the

users transmit an ABS, providing some interference mitigation for the remaining users. This abstinence of data transmission explains the throughput losses by the ABS system relative to full power transmission, as clearly the interference mitigation provided is less significant than the throughput sacrificed.

Fig. 8(b) displays the energy efficiency of the simulated scenario, yielding again very dominant results of the fuzzy logic systems. This is mainly due to the fact that fuzzy logic has the possibility of transmitting at half power, which is usually the case after multiple time slots and the achievement of a relatively orthogonal RB allocation. Furthermore, the high energy efficiency is achieved quite rapidly. The added energy efficiency due to LA is a direct result of the augmented throughputs (see (6)). It is shown that ABS transmission is slightly more energy efficient than maximum power, which is logical since on average 10% less power is used, but the loss in throughput is $<10\%$, thus enhancing the energy efficiency.

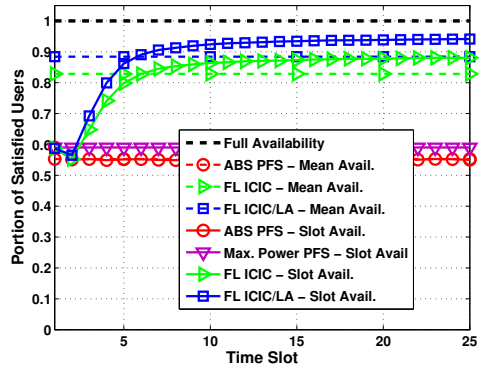

(a) Availability

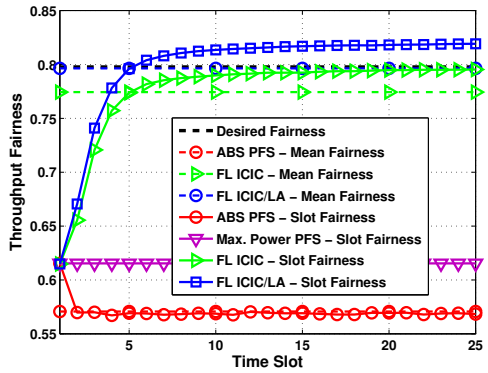

(b) Fairness

Fig. 9. System coverage results of fuzzy logic ICIC, random ABSs transmission, and maximum power transmission.

Lastly, the availability and throughput fairness in the system are investigated. As expected, fuzzy logic ICIC/LA provides by far the best MS availability, as can be seen from Fig. 9, achieving $\sim 94\%$ availability. This is expected as both the system throughputs are augmented, a direct result of the greater portion of satisfied MSs. Furthermore, it is clear that the fairness is greatly improved as well, especially when utilising LA. This is mainly due to the fact that users are (through LA) more adept to their transmission environments, and hence better achieve their desired rates. In fact, due to the reduced throughput granularity at higher MCSs, more MSs achieve the same throughput, and hence fuzzy logic ICIC/LA achieves a greater fairness than if all MSs would exactly achieve their targets. On another note, the max. power availability and fairness is boosted with regards to the ABS system, as all MSs can transmit without restrictions or abstinence, and hence even unsatisfied (in terms of rate) users achieve decent throughputs. A summary of the quantitative results is shown in Table V.

TABLE V
PERFORMANCE RESULTS

%-gain	vs.	C_{sys}	β_{sys}	χ_{sys}	$f(\text{C})$
FL ICIC/LA	Max. Pow.	57	151	59	33
FL ICIC	Max. Pow.	38	103	48	29
FL ICIC/LA	ABS	68	143	70	44
FL ICIC	ABS	48	97	59	40
FL ICIC/LA	FL. ICIC	14	24	7	3

VII. CONCLUSIONS

In this paper, a novel distributed and autonomous ICIC technique for femto-tier interference management and resource allocation is presented. Fuzzy logic generates broad evaluations of locally available inputs, combines them based on a defined set of RB allocation rules, and submits to the BS the most suitable resources and transmit powers for successful and efficient communication. After several time slots and more accurate average signal statistics, the locally optimised resource allocations converge to a stable system operating point.

By comparing fuzzy logic ICIC to a system-wide optimisation problem, it was shown that fuzzy logic provides close-to-optimal system performance with drastically reduced complexity. Furthermore, a comparison to a greedy heuristic of similar complexity shows faster convergence to cell-individual optimum resource allocation. Hence, fuzzy logic provides a low-complexity near-system-optimal solution of ICIC in femto-cell networks. This is confirmed in the simulation results, where fuzzy logic ICIC satisfies the system throughput requirements and significantly outperforms the given benchmarks. The addition of LA gives a further performance boost, achieving almost full availability along with enhanced throughput, energy efficiency, and fairness.

The main focus of the further development of fuzzy logic ICIC is the extension to HetNets, as highlighted in Section I. This will see macro-, pico- and femto-cells available in the same scenario, thus the MSs will not only need to perform resource and power allocation, but also determine which AP they desire to connect with. The autonomous and distributed nature of fuzzy logic ICIC should allow these networks to self-configure, and self-optimise, eliminating excessive signalling normally required in such networks. Furthermore, we seek to heuristically optimise the fuzzy logic system (*i.e.*, more specifically, the rules) by analysing the input-output characteristics, and tuning the system to make better decisions on each RB.

REFERENCES

[1] D. Lopez-Perez, I. Guvenc, G. de la Roche, M. Kountouris, T. Quek, and J. Zhang, "Enhanced intercell interference coordination challenges in heterogeneous networks," *IEEE Wireless Communications*, vol. 18, no. 3, pp. 22 –30, Jun. 2011.

[2] G. Boudreau, J. Panicker, N. Guo, R. Chang, N. Wang, and S. Vrzic, "Interference Coordination and Cancellation for 4G Networks," *IEEE Communications Magazine*, vol. 47, no. 4, pp. 74–81, 2009.

[3] D. Astely, E. Dahlman, A. Furuskar, Y. Jading, M. Lindstrom, and S. Parkvall, "LTE: The Evolution of Mobile Broadband," *IEEE Communications Magazine*, vol. 47, no. 4, pp. 44–51, 2009.

[4] R. Madan, J. Borran, A. Sampath, N. Bhushan, A. Khandekar, and T. Ji, "Cell association and interference coordination in heterogeneous lte-a cellular networks," *IEEE Journal on Selected Areas in Communications*, vol. 28, no. 9, pp. 1479 –1489, Dec. 2010.

[5] S.-M. Cheng, S.-Y. Lien, F.-S. Chu, and K.-C. Chen, "On exploiting cognitive radio to mitigate interference in macro/femto heterogeneous networks," *IEEE Wireless Communications*, vol. 18, no. 3, pp. 40 –47, Jun. 2011.

[6] P. Hasselbach, A. Klein, and I. Gaspard, "Transmit Power Allocation for Self-Organising Future Cellular Mobile Radio Networks," in *Proc. of IEEE 20th International Symposium on Personal, Indoor and Mobile Radio Communications (PIMRC)*, Sep. 2009, pp. 1342 –1346.

[7] D. Gesbert, S. G. Kiani, A. Gjendemsjø, and G. E. Øien, "Adaptation, Coordination, and Distributed Resource Allocation in Interference-Limited Wireless Networks," *Proc. of the 7th IEEE International Symposium on Wireless Communication Systems*, vol. 95, no. 12, pp. 2393–2409, Dec. 2007.

[8] Y.-Y. Li, M. Macuha, E. Sousa, T. Sato, and M. Nanri, "Cognitive interference management in 3g femtocells," in *Proc. of IEEE 20th International Symposium on Personal, Indoor and Mobile Radio Communications (PIMRC)*, Sep. 2009, pp. 1118 –1122.

[9] L. Lindbom, R. Love, S. Krishnamurthy, C. Yao, N. Miki, and V. Chandrasekhar, "Enhanced Inter-cell Interference Coordination for Heterogeneous Network in LTE-Advanced: A Survey," Tech. Rep., 2011.

[10] J. Pang, J. Wang, D. Wang, G. Shen, Q. Jiang, and J. Liu, "Optimized time-domain resource partitioning for enhanced inter-cell interference coordination in heterogeneous networks," in *Proc. of Wireless Communications and Networking Conference (WCNC)*, Apr. 2012, pp. 1613 –1617.

[11] A. Stolyar and H. Viswanathan, "Self-Organizing Dynamic Fractional Frequency Reuse for Best-Effort Traffic through Distributed Inter-Cell Coordination," in *Proc. of IEEE INFOCOM*, Apr. 2009, pp. 1287–1295.

[12] R. Combes, Z. Altman, M. Haddad, and E. Altman, "Self-Optimizing Strategies for Interference Coordination in OFDMA Networks," in *Proc. of IEEE International Conference on Communications (ICC) Workshops*, no. 1–5, Jun. 2011.

[13] L. Jouffe, "Fuzzy inference system learning by reinforcement methods," *IEEE Transactions on Systems, Man, and Cybernetics, Part C: Applications and Reviews*, vol. 28, pp. 338–355, Aug. 1998.

[14] M. Dirani and Z. Altman, "A cooperative Reinforcement Learning approach for Inter-Cell Interference Coordination in OFDMA cellular networks," in *Proc. of Modeling and Optimization in Mobile, Ad Hoc and Wireless Networks (WiOpt)*, May 2010, pp. 170–176.

[15] R. Razavi, S. Klein, and H. Claussen, "Self-optimization of capacity and coverage in LTE networks using a fuzzy reinforcement learning approach," in *Proc. of Personal Indoor and Mobile Radio Communications (PIMRC)*, Sep. 2010, pp. 1865–1870.

[16] P. Vlacheas, E. Thomatos, K. Tsagkaris, and P. Demestichas, "Autonomic downlink inter-cell interference coordination in LTE Self-Organizing Networks," in *Proc. of Network and Service Management (CNSM)*, Oct. 2011, pp. 1–5.

[17] S. Sesia, I. Toufik, and M. Baker, *LTE - The UMTS Long Term Evolution: From Theory to Practice*, 1st ed., S. Sesia, I. Toufik, and M. Baker, Eds. Wiley, 2009.

[18] EDX Wireless, "Designing an LTE network using EDX SignalPro," Technical white paper, march 2010, retrieved Jan. 17 2011. [Online]. Available: http://www.edx.com/resources/documents/

[19] R. Jain, D. Chiu, and W. Hawe., "A Quantitative Measure of Fairness and Discrimination for Resource Allocation in Shared Computer Systems," DEC Technical Report, Tech. Rep. 301, 1984.

[20] Z. Bharucha, H. Haas, A. Saul, and G. Auer, "Throughput Enhancement through Femto-Cell Deployment," *European Transactions on Telecommunications*, vol. 21, no. 4, pp. 469–477, Mar. 31 2010, (invited). [Online]. Available: http://www.interscience.wiley.com

[21] ITU-R Working Party 5D (WP5D) - IMT Systems, "Report 124, Report of correspondence group for IMT.EVAL," May 2008, United Arab Emirates.

[22] W. Wang, T. Ottosson, M. Sternad, A. Ahlen, and A. Svensson, "Impact of Multiuser Diversity and Channel Variability on Adaptive OFDM," in *Proc. of the 58th IEEE Vehicular Technology Conference (VTC-Fall)*, Orlando, USA, Oct. 6-9 2003, pp. 547–551.

[23] NTT DOCOMO, "New Evaluation Models (Micro Cell, Indoor, Rural/High-Speed)," 3GPP TSG RAN WG1 R1-082713, Jul. 2008. Retrieved Nov. 27, 2009 from www.3gpp.org/ftp/tsg_ran/WG1_RL1/TSGR1_53b/Docs/.

[24] 3GPP, "Simulation Assumptions and Parameters for FDD HeNB RF Requirements," 3GPP TSG RAN WG4 R4-092042, May 2008. Retrieved Sep. 1, 2009 from www.3gpp.org/ftp/Specs/.

[25] S. Almalfouh and G. Stuber, "Interference-Aware Radio Resource Allocation in OFDMA-Based Cognitive Radio Networks," *IEEE Transactions on Vehicular Technology*, vol. 60, no. 4, pp. 1699 –1713, May 2011.

[26] D. P. Bertsekas, *Nonlinear Programming*. Athena Scientific, 1999.

[27] M. Trott, "The Mathematica Guidebooks Additional Material: Average Distance Distribution," Oct. 2004.

[28] B. W. Wah and Z. Wu, "The Theory of Discrete Lagrange Multipliers for Nonlinear Discrete Optimization," in *Principles and Practice of Constraint Programming*, 1999, pp. 28–42.

[29] 3GPP, "X2 General Aspects and Principles (Release 8)," 3GPP TS 36.420 V8.0.0 (2007-12), Dec. 2007. Retrieved Sep. 1, 2009 from www.3gpp.org/ftp/Specs/.

Bibliography

[1] Z. R. Bharucha, "Ad Hoc Wireless Networks with Femto-Cell Deployment: A Study," Ph.D. dissertation, Univeristy of Edinburgh, 2010.

[2] *Measuring the Information Society*. International Telecommunication Union, 2012.

[3] M. Yun, Y. Rong, Y. Zhou, H.-A. Choi, J.-H. Kim, J. Sohn, and H.-I. Choi, "Analysis of Uplink Traffic Characteristics and Impact on Performance in Mobile Data Networks," in *Proc. of the IEEE International Conference on Communications (ICC)*, Beijing, China, 19–23 May 2008, pp. 4564 –4568.

[4] V. Chandrasekhar, J. Andrews, and A. Gatherer, "Femtocell Networks: A Survey," *IEEE Communications Magazine*, vol. 46, no. 9, pp. 59–67, 2008.

[5] H. Claussen, "Performance of Macro- and Co-Channel Femtocells in a Hierarchical Cell Structure," in *Proc. of the 18th IEEE International Symposium on Personal, Indoor and Mobile Radio Communications (PIMRC)*, Athens, Greece, Sep. 3–7 2007, pp. 1–5.

[6] D. Lopez-Perez, I. Guvenc, G. de la Roche, M. Kountouris, T. Quek, and J. Zhang, "Enhanced intercell interference coordination challenges in heterogeneous networks," *IEEE Wireless Communications*, vol. 18, no. 3, pp. 22 –30, Jun. 2011.

[7] "Visible Light Communication (VLC) - A Potential Solution to the Global Wireless Spectrum Shortage," GBI Research, Tech. Rep., 2011. [Online]. Available: http://www.gbiresearch.com/

[8] T. K. Srikantaiah and D. Xiaoying, "The Internet and its Impact on Developing Countries: Examples from China and India," *Asian Libraries*, vol. 7, no. 9, pp. 199–209, 1998.

[9] S. Sesia, I. Toufik, and M. Baker, *LTE - The UMTS Long Term Evolution: From Theory to Practice*, 1st ed., S. Sesia, I. Toufik, and M. Baker, Eds. Wiley, 2009.

[10] D. Mitra, "An asynchronous distributed algorithm for power control in cellular radio systems," in *Proc. of WINLAB Workshop*, 1993.

[11] J. Zander, "Performance of Optimum Transmitter Power Control in Cellular Radio Systems," *IEEE Transactions on Vehicular Technology*, vol. 41, no. 1, pp. 57–62, Feb. 1992.

[12] D. Kivanc, G. Li, and H. Liu, "Computationally Efficient Bandwidth Allocation and Power Control for OFDMA," *IEEE Transactions on Wireless Communications*, vol. 2, no. 6, pp. 1150 – 1158, 2003.

[13] L. Miao and C. G. Cassandras, "Optimal Transmission Scheduling for Energy-Efficient Wireless Networks," in *Proc. of IEEE INFOCOM*, apr 2006, pp. 1 –11.

[14] C. Li and M. J. Neely, "Energy-optimal scheduling with dynamic channel acquisition in wireless downlinks," *IEEE Transactions on Mobile Computing*, vol. 9, no. 4, pp. 527–539, Apr. 2010.

[15] A. Goldsmith, *Wireless Communications*. Cambridge University Press, 2005.

[16] S. Almalfouh and G. Stuber, "Interference-Aware Radio Resource Allocation in OFDMA-Based Cognitive Radio Networks," *IEEE Transactions on Vehicular Technology*, vol. 60, no. 4, pp. 1699 –1713, May 2011.

[17] D. P. Bertsekas, *Nonlinear Programming*. Athena Scientific, 1999.

[18] R. Madan, J. Borran, A. Sampath, N. Bhushan, A. Khandekar, and T. Ji, "Cell association and interference coordination in heterogeneous lte-a cellular networks," *IEEE Journal on Selected Areas in Communications*, vol. 28, no. 9, pp. 1479 –1489, Dec. 2010.

[19] S.-M. Cheng, S.-Y. Lien, F.-S. Chu, and K.-C. Chen, "On exploiting cognitive radio to mitigate interference in macro/femto heterogeneous networks," *IEEE Wireless Communications*, vol. 18, no. 3, pp. 40 –47, Jun. 2011.

[20] C. S. R. Murthy and B. S. Manoj, *Ad Hoc Wireless Networks: Architectures and Protocols*, 1st ed., ser. Prentice Hall Communications Engineering and Emerging Technologies, T. S. Rappaport, Ed. Prentice Hall, May 2004.

[21] T. S. Rappaport, *Wireless Communications: Principles and Practice*, 2nd ed. Prentice Hall PTR, 2002.

[22] A. J. Viterbi and R. Padovani, "Implications of Mobile Cellular CDMA," *IEEE Communications Magazine*, vol. 30, no. 12, pp. 38–41, Dec. 1992.

[23] J. D. Gibson, *The Mobile Communications Handbook*, J. D. Gibson, Ed. Springer/IEEE Press/CRC Press, Jun. 1996.

[24] 3GPP, "Requirements for Evolved UTRA (E-UTRA) and Evolved UTRAN (E-UTRAN)," 3GPP TS 25.913 V 8.0.0 (2008-12), Dec. 2008. Retrieved Oct. 10, 2009 from www.3gpp.org/ftp/Specs/.

[25] A. Ballard, "A new multiplex technique for communication systems," *IEEE Transactions on Power Apparatus and Systems*, vol. PAS-85, no. 10, pp. 1054 –1059, oct. 1966.

[26] 3GPP, *Base Station (BS) Radio Transmission and Reception (Release 8)*, 3GPP TS 36.104 V 8.2.0 (2008-05), Std., May 2008. Retrieved Aug. 1, 2008 from www.3gpp.org/ftp/Specs/. [Online]. Available: http://www.3gpp.org/ftp/Specs/html-info/36321.htm

[27] T. S. Rappaport, *Wireless Communications: Principles and Practice*, 2nd ed. Prentice Hall, ISBN: 0130422320, Dec. 2001.

[28] K. S. Gilhousen, I. M. Jacobs, R. Padovani, A. J. Viterbi, L. A. J. Weaver, and C. E. I. Wheatley, "On The Capacity of a Cellular CDMA System," *IEEE Transactions on Vehicular Technology*, vol. 40, no. 2, pp. 303–312, May 1991.

[29] R. W. Chang, "Synthesis of Band-Limited Orthogonal Signals for Multichannel Data Transmission," *Bell Systems Technical Journal*, vol. 45, pp. 1775–1796, Dec. 1966.

[30] B. Saltzberg, "Performance of an Efficient Parallel Data Transmission System," *IEEE Transactions on Communication Technology*, vol. 15, no. 6, pp. 805–811, Dec. 1967.

[31] S. Weinstein and P. Ebert, "Data Transmission by Frequency-Division Multiplexing Using the Discrete Fourier Transform," *IEEE Transactions on Communication Technology*, vol. 19, no. 5, pp. 628–634, Oct. 1971.

[32] A. Peled and A. Ruiz, "Frequency Domain Data Transmission Using Reduced Computational Complexity Algorithms," in *Proc. of the IEEE International Conference on Acoustics, Speech and Signal Processing (ICASSP)*, vol. 5, Denver, USA, Apr. 9–11 1980, pp. 964–967.

[33] L. J. Cimini, Jr., "Analysis and Simulation of a Digital Mobile Channel Using Orthogonal Frequency Division Multiplexing," *IEEE Transactions on Communications*, vol. 33, no. 7, pp. 665–675, Jul. 1985.

[34] M. Munster. (2008, Apr.) [Online]. Available: http://www-mobile.ecs.sotono.ac.uk/comms/ofdm_system.jpg.

[35] J. Heiskala and J. Terry, *OFDM Wireless LANs: A Theoretical and Practical Guide*, T. Reid and D. B. Williams, Eds. Sams Publishing, ISBN: 0672321572, 2002.

[36] D. N. C. Tse and S. V. Hanly, "Multiaccess Fading Channels. I. Polymatroid Structure, Optimal Resource Allocation and Throughput Capacities," *IEEE Transactions on Information Theory*, vol. 44, no. 7, pp. 2796–2815, Nov. 1998.

[37] R. Knopp and P. Humblet, "Information Capacity and Power Control in Single-Cell Multiuser Communications," in *Proc. of the IEEE International Conference on Communications (ICC)*, vol. 1, Seattle, USA, Jun. 18–22 1995, pp. 331–335.

[38] ——, "Multiple-Accessing over Frequency-Selective Fading Channels," in *Proc. of the IEEE International Symposium on Personal, Indoor and Mobile Radio Communications (PIMRC)akc10*, vol. 3, Toronto, Canada, Sep. 27-29 1995, pp. 1326–1330.

[39] S.-B. Lee, I. Pefkianakis, A. Meyerson, S. Xu, and S. Lu, "Proportional fair frequency-domain packet scheduling for 3gpp lte uplink," in *Proc. of IEEE INFOCOM*, Apr. 2009, pp. 2611 –2615.

[40] W. C. Y. Lee, *Mobile Cellular Telecommunications Systems*. McGraw-Hill Book Company, 1990, ISBN: 0071007903.

[41] V. H. MacDonald, "The Cellular Concept," *The Bell Systems Technical Journal*, vol. 58, no. 1, pp. 15–43, Jan. 1979.

[42] G. Calhoun, *Digital Cellular Radio*. Artech House, 1988.

[43] C. Shannon, "A Mathematical Theory of Communication," *Bell System Technical Journal*, vol. 27, pp. 379–423 & 623–656, Jul. & Oct. 1948.

[44] S.-E. Elayoubi, O. B. Haddada, and B. Fourestie, "Performance Evaluation of Frequency Planning Schemes in OFDMA-Based Networks," *IEEE Transactions on Wireless Communications*, vol. 7, pp. 1623–1633, May 2008.

[45] G. Boudreau, J. Panicker, N. Guo, R. Chang, N. Wang, and S. Vrzic, "Interference Coordination and Cancellation for 4G Networks," *IEEE Communications Magazine*, vol. 47, no. 4, pp. 74–81, 2009.

[46] S. Ali and V. Leung, "Dynamic frequency allocation in fractional frequency reused ofdma networks," *IEEE Transactions on Wireless Communications*, vol. 8, no. 8, pp. 4286 –4295, august 2009.

[47] M. Wang and T. Ji, "Dynamic resource allocation for interference management in orthogonal frequency division multiple access cellular communications," *IET Communications*, vol. 4, no. 6, pp. 675 –682, 16 2010.

[48] Y.-Y. Li, M. Macuha, E. Sousa, T. Sato, and M. Nanri, "Cognitive interference management in 3g femtocells," in *Proc. of IEEE International Symposium on Personal, Indoor and Mobile Radio Communications (PIMRC)*, Sep. 2009, pp. 1118 –1122.

[49] J. Ling, D. Chizhik, and R. Valenzuela, "On resource allocation in dense femto-deployments," in *Proc. of IEEE International Conference on Microwaves, Communications, Antennas and Electronics Systems (COMCAS)*, Nov. 2009, pp. 1 –6.

[50] J. Ellenbeck, C. Hartmann, and L. Berlemann, "Decentralized inter-cell interference coordination by autonomous spectral reuse decisions," in *Proc. of 14th European Wireless Conference*, june 2008, pp. 1 –7.

[51] 3rd Generation Partnership Project (3GPP), Technical Specification Group Radio Access Network, *Soft Frequency Reuse Scheme for UTRAN LTE*, 3GPP TSG RAN WG1 R1-050507, 3GPP Std., May 9–13, 2005.

[52] N. Himayat, S. Talwar, A. Rao, and R. Soni, "Interference management for 4g cellular standards [wimax/lte update]," *IEEE Communications Magazine*, vol. 48, no. 8, pp. 86 –92, august 2010.

[53] X. Mao, A. Maaref, and K. H. Teo, "Adaptive Soft Frequency Reuse for Inter-Cell Interference Coordination in SC-FDMA Based 3GPP LTE Uplinks," in *Proc. of the Global Telecommunications Conference*, New Orleans, Nov. 2008.

[54] V. Douros and G. Polyzos, "Review of Some Fundamental Approaches for Power Control in Wireless Networks," *Elsevier Computer Communications*, vol. 34, no. 13, pp. 1580–1592, Aug. 2011.

[55] R. Gejji, "Forward-link-power control in cdma cellular systems," *IEEE Transactions on Vehicular Technology*, vol. 41, no. 4, pp. 532 –536, Nov. 1992.

[56] A. Chockalingam, P. Dietrich, L. Milstein, and R. Rao, "Performance of closed-loop power control in ds-cdma cellular systems," *IEEE Transactions on Vehicular Technology*, vol. 47, no. 3, pp. 774 –789, aug 1998.

[57] F. Rashid-Farrokhi, L. Tassiulas, and K. Liu, "Joint optimal power control and beamforming in wireless networks using antenna arrays," *IEEE Transactions on Communications*, vol. 46, no. 10, pp. 1313 –1324, oct 1998.

[58] J. Rulnick and N. Bambos, "Mobile power management for maximum battery life in wireless communication networks," in *Proc. of IEEE INFOCOM*, vol. 2, mar 1996, pp. 443 –450 vol.2.

[59] J. Zander, "Distributed cochannel interference control in cellular radio systems," *IEEE Transactions on Vehicular Technology*, vol. 41, no. 3, pp. 305 –311, aug 1992.

[60] T.-H. Lee and J.-C. Lin, "A fully distributed power control algorithm for cellular mobile systems," *IEEE Journal on Selected Areas in Communications*, vol. 14, no. 4, pp. 692 –697, may 1996.

[61] Q. Wu, "Optimum transmitter power control in cellular systems with heterogeneous sir thresholds," *IEEE Transactions on Vehicular Technology*, vol. 49, no. 4, pp. 1424 –1429, jul 2000.

[62] G. J. Foschini and Z. Miljanic, "A Simple Distributed Autonomous Power Control Algorithm and Its Convergence," *IEEE Transactions on Vehicular Technology*, vol. 42, no. 4, pp. 641–646, Nov. 1993.

[63] N. Bambos, "Toward power-sensitive network architectures in wireless communications: concepts, issues, and design aspects," *IEEE Personal Communications*, vol. 5, no. 3, pp. 50 –59, jun 1998.

[64] U. M. Maurer, "Secret Key Agreement by Public Discussion from Common Information," *IEEE Transactions on Information Theory*, vol. 39, no. 3, pp. 733–742, May 1993.

[65] N. Bambos, S. Chen, and G. Pottie, "Channel access algorithms with active link protection for wireless communication networks with power control," *IEEE/ACM Transactions on Networking*, vol. 8, no. 5, pp. 583 –597, oct 2000.

[66] C. Saraydar, N. Mandayam, and D. Goodman, "Efficient power control via pricing in wireless data networks," *IEEE Transactions on Communications*, vol. 50, no. 2, pp. 291 –303, feb 2002.

[67] K.-K. Leung and C. W. Sung, "An opportunistic power control algorithm for cellular network," *IEEE/ACM Transactions on Networking*, vol. 14, no. 3, pp. 470 –478, june 2006.

[68] A. Rao, "Reverse Link Power Control for Managing Inter-Cell Interference in Orthogonal Multiple Access Systems," in *Proc of. IEEE Vehicular Technology Conference Fall (VTC-Fall)*, Oct. 2007, pp. 1837 –1841.

[69] F. Baccelli, M. Klein, M. Lebourges, and S. Zuyev, "Stochastic geometry and architecture of communication networks," *J. Telecommunication Systems*, vol. 7, pp. 209–227, 1995.

[70] F. Baccelli and S. Zuyev, "Stochastic geometry models of mobile communication networks," in *Frontiers in queueing: models and applications in science and engineering*. CRC Press, 1996, pp. 227–243.

[71] M. Haenggi, J. Andrews, F. Baccelli, O. Dousse, and M. Franceschetti, "Stochastic geometry and random graphs for the analysis and design of wireless networks," *IEEE Journal on Selected Areas in Communications*, vol. 27, no. 7, pp. 1029 –1046, september 2009.

[72] P. Pinto, A. Giorgetti, M. Win, and M. Chiani, "A stochastic geometry approach to coexistence in heterogeneous wireless networks," *IEEE Journal on Selected Areas in Communications*, vol. 27, no. 7, pp. 1268 –1282, september 2009.

[73] S. Akoum and R. Heath, "Multi-cell coordination: A stochastic geometry approach," in *Proc. of 13th International Workshop on Signal Processing Advances in Wireless Communications (SPAWC)*, june 2012, pp. 16 –20.

[74] Y. Shi, X. Dong, and K. Letaief, "Sum rate maximization in fading wireless networks using stochastic geometry," in *Proc. of IEEE International Conference on Communications (ICC)*, june 2012, pp. 5113 –5117.

[75] S. Jafar, *Interference Alignment – A New Look at Signal Dimensions in a Communication Network*. Now Publications, 2011.

[76] V. Cadambe and S. Jafar, "Interference alignment and degrees of freedom of the k -user interference channel," *IEEE Transactions on Information Theory*, vol. 54, no. 8, pp. 3425 –3441, aug. 2008.

[77] O. El Ayach, S. Peters, and R. Heath Jr., "The Practical Challenges of Interference Alignment," *IEEE Wireless Communications*, vol. 20, no. 1, pp. 35–42, Feb. 2013.

[78] M. Razaviyayn, G. Lyubeznik, and Z. Luo, "On the degrees of freedom achievable through interference alignment in a mimo interference channel," *IEEE Transactions on Signal Processing*, vol. 60, no. 2, pp. 812 –821, feb. 2012.

[79] M. Sawahashi, Y. Kishiyama, A. Morimoto, D. Nishikawa, and M. Tanno, "Coordinated multipoint transmission/reception techniques for lte-advanced [coordinated and distributed mimo]," *IEEE Wireless Communications*, vol. 17, no. 3, pp. 26 –34, june 2010.

[80] W. Mennerich and W. Zirwas, "User centric coordinated multi point transmission," in *Proc. of IEEE Vehicular Technology Conference Fall (VTC-Fall)*, sept. 2010, pp. 1 –5.

[81] J.-S. Sheu and C.-H. Hsieh, "Joint preprocessing techniques for downlink comp transmission in multipath fading channels," in *Proc. of IEEE Vehicular Technology Conference Spring (VTC-Spring)*, may 2012, pp. 1 –5.

[82] G. Klir and B. Yuan, *Fuzzy set and fuzzy logic: theory and applications*. Upper Saddle River, NJ: Prentice Hall, 1995.

[83] L. Jouffe, "Fuzzy inference system learning by reinforcement methods," *IEEE Transactions on Systems, Man, and Cybernetics, Part C: Applications and Reviews*, vol. 28, pp. 338–355, Aug. 1998.

[84] M. Dirani and Z. Altman, "A cooperative Reinforcement Learning approach for Inter-Cell Interference Coordination in OFDMA cellular networks," in *Proc. of Modeling and Optimization in Mobile, Ad Hoc and Wireless Networks (WiOpt)*, May 2010, pp. 170–176.

[85] R. Razavi, S. Klein, and H. Claussen, "Self-optimization of capacity and coverage in LTE networks using a fuzzy reinforcement learning approach," in *Proc. of IEEE International Symposium on Personal Indoor and Mobile Radio Communications (PIMRC)*, Sep. 2010, pp. 1865–1870.

[86] P. Vlacheas, E. Thomatos, K. Tsagkaris, and P. Demestichas, "Autonomic downlink inter-cell interference coordination in LTE Self-Organizing Networks," in *Proc. of Network and Service Management (CNSM)*, Oct. 2011, pp. 1–5.

[87] J. Predd, S. Kulkarni, and H. Poor, "Distributed learning in wireless sensor networks," *IEEE Signal Processing Magazine*, vol. 23, no. 4, pp. 56 – 69, Jul. 2006.

[88] A. Forster, "Machine Learning Techniques Applied to Wireless Ad-Hoc Networks: Guide and Survey," in *Proc. of Intelligent Sensors, Sensor Networks and Information (ISSNIP)*, Dec. 2007, pp. 365–370.

[89] Z. Yu and J. Tsai, "A framework of machine learning based intrusion detection for wireless sensor networks," in *Proc. of IEEE International Conference on Sensor Networks, Ubiquitous and Trustworthy Computing (SUTC)*, Jun. 2008, pp. 272 –279.

[90] Y. Kon, M. Ito, N. Hassel, M. Hasegawa, K. Ishizu, and H. Harada, "Autonomous parameter optimization of a heterogeneous wireless network aggregation system using machine learning algorithms," in *Proc. of IEEE Consumer Communications and Networking Conference (CCNC)*, Jan. 2012, pp. 894 –898.

[91] 3GPP, "Further Advancements for E-UTRA Physical Layer Aspects (Release 9)," 3GPP TR 36.814 V9.0.0 (2010-03), Sep. 2012. Retrieved Sep. 3, 2010 from www.3gpp.org/ftp/Specs/.

[92] L. Lindbom, R. Love, S. Krishnamurthy, C. Yao, N. Miki, and V. Chandrasekhar, "Enhanced Inter-cell Interference Coordination for Heterogeneous Network in LTE-Advanced: A Survey," Tech. Rep., 2011.

[93] J. Pang, J. Wang, D. Wang, G. Shen, Q. Jiang, and J. Liu, "Optimized time-domain resource partitioning for enhanced inter-cell interference coordination in heterogeneous networks," in *Proc. of IEEE Wireless Communications and Networking Conference (WCNC)*, Apr. 2012, pp. 1613 –1617.

[94] S. Ortiz, "The Wireless Industry Begins to Embrace Femtocells," *Computer*, vol. 41, no. 7, pp. 14–17, Jul. 2008.

[95] H. Claussen, L. Ho, and L. Samuel, "Self-Optimization of Coverage for Femtocell Deployments," in *Proc. of the Wireless Telecommunications Symposium (WTS)*, California, USA, Apr. 24–26 2008, pp. 278–285.

[96] W. Webb, *Wireless Communications: The Future*. John Wiley & Sons, 2007.

[97] C. Anderson, *The Long Tail: Why the Future of Business Is Selling Less of More*. Hyperion, 2006.

[98] S. Y. Hui and K. H. Yeung, "Challenges in the Migration to 4G Mobile Systems," *IEEE Communications Magazine*, vol. 41, no. 12, pp. 54–59, Dec. 2003.

[99] H. Claussen, L. T. W. Ho, and L. G. Samuel, "Financial Analysis of a Pico-Cellular Home Network Deployment," in *Proc. of the IEEE International Conference on Communications (ICC)*, Glasgow, Scotland, Jun. 24–28 2007, pp. 5604–5609.

[100] D. Knisely, T. Yoshizawa, and F. Favichia, "Standardization of Femtocells in 3GPP," *IEEE Communications Magazine*, vol. 47, no. 9, pp. 68–75, Sep. 2009.

[101] M. Alouini and A. Goldsmith, "Area Spectral Efficiency of Cellular Mobile Radio Systems," *IEEE Transactions on Vehicular Technology*, vol. 48, no. 4, pp. 1047–1066, 1999.

[102] G. Korinthios, E. Theodoropoulou, N. Marouda, I. Mesogiti, E. Nikolitsa, and G. Lyberopoulos, "Early Experiences and Lessons learned from Femtocells," *IEEE Communications Magazine*, vol. 47, no. 9, pp. 124–130, Sep. 2009.

[103] Analysys, "Picocells and Femtocells: Will indoor base-stations transform the telecoms industry?" [Online]. [Online]. Available: Available: http://research.analysys.com

[104] Z. Li, Y. Wang, and D. Yang, "A Novel Power Control Scheme in OFDMA Uplink," in *Proc. of International Conference on Signal Processing (ICSP)*, 2008, pp. 2880 –2883.

[105] E. Klerides and T. Charalambous, "Transmission Scheduling in Wireless Networks with SINR Constraints," in *Proc. of International Conference on Networking and Services ICNS*, Valencia, apr 2009, pp. 155–160.

[106] H. Haas and G. J. R. Povey, "The effect of adjacent channel interference on capacity in a hybrid TDMA/CDMA-TDD system using UTRA-TDD parameters," in *Proc. of the 50th IEEE Vehicular Technology Conference (VTC)*, vol. 2, Amsterdam, Sep. 1999, pp. 1086–1090.

[107] Z. Bharucha, A. Saul, G. Auer, and H. Haas, "Dynamic Resource Partitioning for Downlink Femto-to-Macro-Cell Interference Avoidance," *EURASIP Journal on Wireless Communications and Networking (special issue on Femtocell Networks)*,

vol. 2010, no. Article ID 143413, pp. 1–12, May 2010. [Online]. Available: http://www.hindawi.com/journals/wcn/2010/143413.html

[108] A. Stolyar and H. Viswanathan, "Self-Organizing Dynamic Fractional Frequency Reuse for Best-Effort Traffic through Distributed Inter-Cell Coordination," in *Proc. of IEEE INFOCOM*, Apr. 2009, pp. 1287–1295.

[109] R. Combes, Z. Altman, M. Haddad, and E. Altman, "Self-Optimizing Strategies for Interference Coordination in OFDMA Networks," in *Proc. of IEEE International Conference on Communications (ICC) Workshops*, no. 1–5, Jun. 2011.

[110] D. Gesbert, S. G. Kiani, A. Gjendemsjø, and G. E. Øien, "Adaptation, Coordination, and Distributed Resource Allocation in Interference-Limited Wireless Networks," *Proc. of the 7th IEEE International Symposium on Wireless Communication Systems*, vol. 95, no. 12, pp. 2393–2409, Dec. 2007.

[111] EDX Wireless, "Designing an LTE network using EDX SignalPro," Technical white paper, march 2010, retrieved Jan. 17 2011. [Online]. Available: http://www.edx.com/resources/documents/

[112] R. Jain, D. Chiu, and W. Hawe., "A Quantitative Measure of Fairness and Discrimination for Resource Allocation in Shared Computer Systems," DEC Technical Report, Tech. Rep. 301, 1984.

[113] J.-Y. Boudec, "Rate adaptation, congestion control and fairness: A tutorial," 2000.

[114] R. Jain, A. Durresi, and G. Babic, "Throughput Fairness Index: An Explanation," Online.

[115] ITU-R Working Party 5D (WP5D) - IMT Systems, "Report 124, Report of correspondence group for IMT.EVAL," May 2008, United Arab Emirates.

[116] W. Wang, T. Ottosson, M. Sternad, A. Ahlen, and A. Svensson, "Impact of Multiuser Diversity and Channel Variability on Adaptive OFDM," in *Proc. of the 58th IEEE Vehicular Technology Conference (VTC-Fall)*, Orlando, USA, Oct. 6-9 2003, pp. 547–551.

[117] NTT DOCOMO, "New Evaluation Models (Micro Cell, Indoor, Rural/High-Speed)," 3GPP TSG RAN WG1 R1-082713, Jul. 2008. Retrieved Nov. 27, 2009 from www.3gpp.org/ftp/tsg_ran/WG1_RL1/TSGR1_53b/Docs/.

[118] 3GPP, "Simulation Assumptions and Parameters for FDD HeNB RF Requirements," 3GPP TSG RAN WG4 R4-092042, May 2008. Retrieved Sep. 1, 2009 from www.3gpp.org/ftp/Specs/.

[119] S. McLaughlin, P. M. Grant, J. S. Thompson, H. Haas, D. I. Laurenson, C. Khirallah, Y. Hou, and R. Wang, "Techniques for Improving Cellular Radio Base Station Energy Efficiency," *IEEE Wireless Communications: Green Radio Special Issue*, 2011.

[120] D. Astely, E. Dahlman, A. Furuskar, Y. Jading, M. Lindstrom, and S. Parkvall, "LTE: The Evolution of Mobile Broadband," *IEEE Communications Magazine*, vol. 47, no. 4, pp. 44–51, 2009.

[121] P. Hosein, "On Uplink Interference Management for OFDMA Networks," in *Proc. of IEEE International Symposium on Personal, Indoor and Mobile Radio Communications (PIMRC)*, Athens, Greece, Sep. 2007.

[122] M. Al-Shalash, F. Khafizov, and Z. Chao, "Interference constrained soft frequency reuse for uplink ICIC in LTE networks," in *Proc. of IEEE International Symposium on Personal Indoor and Mobile Radio Communications (PIMRC)*, Sep. 2010, pp. 1882 –1887.

[123] M. Al-Rawi, R. Jantti, J. Torsner, and M. Sagfors, "Channel-aware inter-cell interference coordination for the uplink of 3G LTE networks," in *Proc. of the Wireless Telecommunications Symposium (WTS)*, Prague, Czech Republic, Apr. 2009, pp. 1–5.

[124] X. Zhang, C. He, L. Jiang, and J. Xu, "Inter-Cell Interference Coordination Based on Softer Frequency Reuse in OFDMA Cellular Systems," in *Proc. of International Conference on Neural Networks and Signal Processing*, Zhenjiang, China, June 2008, pp. 270–275.

[125] T. Zhang, Z. Zeng, C. Feng, J. Cheng, and L. Song, "Uplink Power Allocation for Interference Coordination in Multi-Cell OFDM Systems," in *Proc. of International Conference on Communications and Networking*, Hangzhou, China, Aug. 2008, pp. 716–720.

[126] A. Dejonghe, B. Bougard, S. Pollin, J. Craninckx, A. Bourdoux, L. V. der Perre, and F. Catthoor, "Green reconfigurable radio systems," *IEEE Signal Processing Magazine*, vol. 24, no. 3, pp. 90–101, May 2007.

[127] B. Badic, T. O'Farrrell, P. Loskot, and J. He, "Energy Efficient Radio Access Architectures for Green Radio: Large versus Small Cell Size Deployment," in *Proc. of the 70th Vehicular Technology Conference*, Anchorage, Sep. 2009.

[128] F. Meshkati, V. Poor, and S. Schwartz, "Energy-Efficient Resource Allocation in Wireless Networks: An Overview of Game Theoretic Approaches," *IEEE Signal Processing Magazine: Special Issue on Resource-Constrained Signal Processing, Communications and Networking*, May 2007.

[129] C. Xiong, G. Li, S. Zhang, Y. Chen, and S. Xu, "Energy- and Spectral-Efficiency Tradeoff in Downlink OFDMA Networks," in *IEEE International Conference on Communications (ICC)*, june 2011, pp. 1 –5.

[130] L. K. Tee, C. van Rensburg, and J.-A. Tsai, "Uplink Power Control for an OFDMA Mobile Cellular System," in *Proc. of IEEE Vehicular Technology Conference Fall (VTC-Fall)*, Baltimore, MD, Sep./Oct. 2007.

[131] 3GPP, "Physical Channels and Modulation (Release 8)," 3GPP TS 36.211 V 8.2.0 (2008-03), Mar. 2008. Retrieved Sep. 1, 2009 from www.3gpp.org/ftp/Specs/.

[132] T. M. Cover and J. A. Thomas, *Elements of Information Theory*, 1st ed., ser. Wiley Series in Telecommunications, D. L. Schilling, Ed. John Wiley & Sons, Sep. 1991.

[133] E. C. van der Meulen, "Some reflections on the interference channel," in *Communications and Cryptography: Two Sides of One Tapestry*, R. E. Blahut, D. J. C. Jr., and T. Mittelholzer, Eds. Springer, 1994, pp. 409–421.

[134] S. Shamai and A. Wyner, "Information-theoretic considerations for symmetric, cellular, multiple-access fading channels. i," *IEEE Transactions on Information Theory*, vol. 43, no. 6, pp. 1877 –1894, nov 1997.

[135] Y. Kim, T. Kwon, and D. Hong, "Area spectral efficiency of shared spectrum hierarchical cell structure networks," *IEEE Transactions on Vehicular Technology*, vol. 59, no. 8, pp. 4145 –4151, oct. 2010.

[136] Y. Ma and D. Kim, "Rate-maximization scheduling schemes for uplink OFDMA," *IEEE Transactions on Wireless Communications*, vol. 8, no. 6, pp. 3193–3205, jun 2009.

[137] C. Han, T. Harrold, S. Armour, I. Krikidis, S. Videv, P. Grant, H. Haas, J. Thompson, I. Ku, C.-X. Wang, T. A. Le, M. Nakhai, J. Zhang, and L. Hanzo, "Green Radio: Radio Techniques to Enable Energy-efficient Wireless Networks," *IEEE Communications Magazine*, vol. 49, no. 6, pp. 46–54, Jun. 2011.

[138] H. J. Kushner and P. Whiting, "Asymptotic properties of proportional-fair sharing algorithms," in *Allerton*, 2002.

[139] 3GPP, "X2 General Aspects and Principles (Release 8)," 3GPP TS 36.420 V8.0.0 (2007-12), Dec. 2007. Retrieved Sep. 1, 2009 from www.3gpp.org/ftp/Specs/.

[140] L. Gao and S. Cui, "Efficient Subcarrier, Power, and Rate Allocation with Fairness Consideration for OFDMA Uplink," *IEEE Transactions on Wireless Communications*, vol. 7, no. 5, pp. 1507–1511, May 2008.

[141] P. Hande, S. Rangan, M. Chiang, and X. Wu, "Distributed uplink power control for optimal sir assignment in cellular data networks," *IEEE/ACM Transactions on Networking*, vol. 16, no. 6, pp. 1420 –1433, Dec. 2008.

[142] C.-H. Lee and C.-J. Chang, "Performance Analysis of a Truncated Closed-loop Power-control Scheme for DS/CDMA Cellular Systems," *IEEE Transactions on Vehicular Technology*, vol. 53, no. 4, pp. 1149 – 1159, 2004.

[143] D. Ngo, L. Le, and T. Le-Ngoc, "Distributed Pareto-optimal power control in femtocell networks," in *Proc. of IEEE International Symposium on Personal Indoor and Mobile Radio Communications (PIMRC)*, Sep. 2011, pp. 222 –226.

[144] D. T. Ngo, L. B. Le, and T. Le-Ngoc, "Distributed pareto-optimal power control for utility maximization in femtocell networks," *IEEE Transactions on Wireless Communications*, vol. 11, no. 10, pp. 3434 –3446, Oct. 2012.

[145] S. Uygungelen, G. Auer, and Z. Bharucha, "Graph-based dynamic frequency reuse in femtocell networks," in *Proc. of IEEE Vehicular Technology Conference Spring (VTC-Spring)*, May 2011, pp. 1 –6.

[146] A. Ladanyi, D. Lopez-Perez, A. Juttner, X. Chu, and J. Zhang, "Distributed Resource Allocation for Femtocell Interference Coordination Via Power Minimisation," in *Proc. of Globecom Workshops*, Dec. 2011, pp. 744–749.

[147] S. Uygungelen, Z. Bharucha, and G. Auer, "Decentralized interference coordination via autonomous component carrier assignment," in *GLOBECOM Workshops (GC Wkshps), 2011 IEEE*, dec. 2011, pp. 219 –224.

[148] E. Jury, "A simplified stability criterion for linear discrete systems," *Proceedings of the IRE*, vol. 50, no. 6, pp. 1493 –1500, 1962.

[149] M. Necker, "A graph-based scheme for distributed interference coordination in cellular ofdma networks," in *Proc. of IEEE Vehicular Technology Conference Spring (VTC-Spring)*, may 2008, pp. 713 –718.

[150] H. Dhillon, R. Ganti, F. Baccelli, and J. Andrews, "Modeling and analysis of k-tier downlink heterogeneous cellular networks," *IEEE Journal on Selected Areas in Communications*, vol. 30, no. 3, pp. 550 –560, april 2012.

[151] S. Mukherjee, "Distribution of downlink sinr in heterogeneous cellular networks," *IEEE Journal on Selected Areas in Communcations*, vol. 30, no. 3, pp. 575 –585, april 2012.

[152] Z. Shi, H. Wang, M. Zhao, and M. C. Reed, "An uplink analytical model for two-tiered 3g femtocell networks," in *Proc. of International Symposium on Modeling and Optimization in Mobile, Ad Hoc and Wireless Networks (WiOpt)*, 31 2010-june 4 2010, pp. 367 –372.

[153] S. Bashar and Z. Ding, "Admission control and resource allocation in a heterogeneous ofdma wireless network," *IEEE Transactions on Wireless Communications*, vol. 8, no. 8, pp. 4200 –4210, august 2009.

[154] M. Trott, "The Mathematica Guidebooks Additional Material: Average Distance Distribution," Oct. 2004.

[155] B. W. Wah and Z. Wu, "The Theory of Discrete Lagrange Multipliers for Nonlinear Discrete Optimization," in *Principles and Practice of Constraint Programming*, 1999, pp. 28–42.

[156] R. Ganesh and K. Joseph, "Effect of Non-Uniform Traffic Distributions on Performance of a Cellular CDMA System," in *Proc. of the 6th IEEE International Conference on Universal Personal Communications*, vol. 2, San Diego, U.S.A., Oct. 1997, pp. 598–602.

[157] W. Mennerich and W. Zirwas, "User Centric Scheduling in Cooperative Networks," in *Proc of. Middle East Conference on Antennas and Propagation (MECAP)*, Cario, Egypt, Oct. 2010, pp. 1–5.

[158] Y. Jin and B. Sendhoff, "Pareto-Based Multiobjective Machine Learning: An Overview and Case Studies," *IEEE Transactions on Systems, Man, and Cybernetics–Part C: Applications and Reviews*, vol. 38, no. 3, pp. 397–415, May 2008.

[159] E. Weisstein, "Circle-Circle Intersection," Retrieved Jul. 02, 2012 from http://mathworld.wolfram.com/Circle-CircleIntersection.html.

[160] P. Omiyi, H. Haas, and G. Auer, "Analysis of TDD Cellular Interference Mitigation Using Busy-Bursts," *Trans. on Wireless Commun.*, vol. 6, no. 7, pp. 2721–2731, Jul. 2007.